Functional interrogations of Phospholipase C Gamma 1 (PLCG1) mutations in Sézary Syndrome

Patel, Varsha Maheshkumar

Awarding institution:
King's College London

Functional interrogations of

Phospholipase C Gamma 1 (*PLCG1*)

mutations in Sézary Syndrome

Varsha Maheshkumar Patel

Skin Tumour Unit,

St John's Institute of Dermatology,

School of Basic and Medical Biosciences,

King's College London.

PhD thesis submitted to King's College London for the degree of Doctor of Philosophy.

2019

Signed declaration

I declare that the work presented in this thesis is my own unless clearly stated otherwise.

Varsha M. Patel

Abstract

Sézary Syndrome (SS) is an aggressive leukaemic variant of cutaneous T-cell lymphoma (CTCL). After the tumour suppressor gene *TP53*, *PLCG1* is the most frequently mutated gene in CTCL. PLCγ1 (encoded by *PLCG1*) is fundamental in T-cell receptor (TCR) signalling as it hydrolyses a plasma membrane component to trigger pathways that induce NFκB, NFAT and AP-1 transcriptional activity. This thesis aimed to functionally interrogate nine PLCγ1 mutations (p.R48W, p.S312L, p.D342N, p.S345F, p.S520F, p.R1158H, p.E1163K, p.D1165H and the indel p.VYEEDM1161V) identified in SS. *PLCG1* mutations detected in diagnostic samples persisted in multiple tumour compartments several months after diagnosis, suggesting that these are likely driver gene mutations. A comprehensive analysis of whole-exome and targeted gene sequencing studies in addition to database interrogations revealed frequent *PLCG1* mutations in 7/10 different types of mature T-cell lymphomas and highlighted five hotspot mutations. In basal conditions, five mutant proteins directly increased PLCγ1 activity by elevating inositol phosphate production and significantly enhanced downstream NFκB and NFAT activity, demonstrating *bona fide* gain-of-function properties. The hotspot p.R48W protein required stimulation to significantly elevate NFκB activity. Four activating mutations mapped to the PLCγ2 protein surface that likely interacts with the plasma membrane. These four mutant proteins are hypothesised to have increased access to substrate, resulting in augmented TCR signalling. Abrogation of the key PLCγ1 phosphorylation residue did not influence the elevated NFκB, NFAT and AP-1 activity induced by gain-of-function proteins in basal conditions or NFκB activity in stimulated cells, suggesting that the mutant proteins act in a phosphorylation-independent manner. The indel in the C2 domain of PLCγ1 reduced total protein expression but importantly mediated gain-of-function, proposing a novel and critical role for this domain in regulating protein activity. An IKKβ inhibitor was ineffective at reducing PLCγ1-induced NFκB activity. In conclusion, *PLCG1* mutations frequently occur in mature T-cell lymphomas and persist in multiple tumour tissues throughout the course of disease in SS. Five mutant proteins potently activate proximal and distal signalling independently of extracellular stimuli and contribute to the dysregulated TCR signalling that is characteristic of CTCL. The data presented here provides compelling evidence for the development of novel mutation-specific PLCγ1 inhibitors.

Table of Contents

List of Figures

List of Tables

List of Appendices

Acknowledgements

I express my sincere gratitude to my supervisors Dr. Tracey Mitchell and Professor Sean Whittaker without whose valuable guidance and support this work would not have been possible. The mentoring I have received from both supervisors has enabled me to gain not only fundamental scientific knowledge but also essential transferable skills. I would like to thank our collaborator and my external thesis committee expert Professor Matilda Katan for her support and guidance throughout this project. I truly appreciate the advice provided by Dr. Francesca Capon and Dr. Susan John from my thesis committee, the guidance from Professor Maddy Parsons and assistance of members of the Nikon Imaging Centre. I would like to thank Dr. Marta Martins and Dr. Katy Everett for their collaborative contribution that has enriched this study.

I am grateful to the Biomedical Research Centre for awarding me this studentship. I owe a special thank you to my colleagues and members of the Skin Tumour Unit, including Dr. Wesley Woollard, Dr. Christine Jones, Rosie Butler, Charlotte Flanagan, Dr. Farrah Bakr, Dr. Vieri Grandi, Dr. Antoinette Yoxall, Dr. Nelema Begum, Silvia Ferreira, Carl Beyers, Dr. Maria Demontis, Vidhya Pararajasingam, Isabella Tosi and Samira Samuel for their help and advice and also for being great company over the years. In particular, I would like to thank Dr. Christine Jones for her help with data interpretation and analysis. I extend my gratitude to all my friends on the 9th floor and beyond for their support.

On a personal note, I cannot thank my parents Mahesh and Shushila enough for their never-ending support and encouragement and for always having faith in my ability to succeed. I am grateful to my husband Divyesh for being my greatest strength and biggest support and for always believing in me and guiding me. I thank my siblings, their partners and especially my wonderful nieces for their unconditional love and encouragement.

I now look forward to using the skills and knowledge I have gained throughout this PhD in my future endeavours.

Abbreviations

ABC DLBCL – Activated B-cell diffuse large B-cell lymphoma
AITL – Angioimmunoblastic T-cell lymphomas
AML – Acute myeloid leukaemia
Amp – Ampicillin
AP-1 – Activator protein-1
APC – Antigen presenting cells
APLAID – Autoinflammation and PLCγ2-associated antibody deficiency and immune dysregulation
APS – Ammonium persulfate
ATF – Activating transcription factor
ATLL – Adult T-cell leukeamia/ lymphomas
bp – base pairs
BCR – B-cell receptor
BLNK – B-cell linker protein
BSA – Bovine serum albumin
BTK – Bruton's tyrosine kinase
CADD – Combined annotation dependent depletion
CD – Cluster of differentiation
cDNA – Complementary DNA
CGH – Comparative genomic hybridisation
CHOP – Combination chemotherapy
CLA – common leukocyte antigen
CLL – Chronic lymphocytic leukaemia
CMV – Cytomegalovirus
CNV – Copy number variations
COSMIC – Catalogue of Somatic Mutations in Cancer
CTCL – Cutaneous T-cell lymphoma
DAG – Diacylglycerol
DAPI – 4',6-Diamidino-2-phenylindole
DMEM – Dulbecco's modified eagle medium
DMSO – Dimethly sulfoxide
ECL – Enhanced chemiluminescence
ECP – Extracorporeal photopheresis
EGF – Epidermal growth factor
EORTC – European Organisation for Research and Treatment of Cancer
eGFP – enhanced Green Fluorescent Protein
EGFR – Epidermal growth factor receptor
ERK – Extracellular-signal-regulated kinase
FBS – Fetal bovine serum
FDA – Food and Drug Administration
FGFR – Fibroblast growth factor receptor
FISH – fluorescent *in situ* hybridisation
FL – Full length
FOXP3 – Forkhead box P3
gDNA – Genomic DNA
HDAC – Histone deacetylase
HGF – Hepatocyte growth factor receptor

HSTL – Hepatosplenic T-cell lymphoma
HTLV-1 – Human T-leukaemia virus type 1
IFN-α – Interferon-α
IFN-γ – Interferon-γ
IGV – Integrative genomics viewer
IKKα – IKB kinase α
IKKβ – IKB kinase β
IL – Interleukin
Indel – Insertion-deletion
IP – Inositol phosphate
IP_3 – Inositol 1,4,5-trisphosphate
ISCL – International Society for Cutaneous Lymphomas
ITAM – Immunoreceptor tyrosine-based activation motif
ITK – IL-2 inducible kinase
JAK – Janus kinase
Kan – Kanamycin
Kb – kilobase
kDa - kilodalton
LAT – Linker of activation of T-cells
LB – Luria–Bertani
LCK – Lymphocyte-specific protein-tyrosine kinase
MAF – Minor allele frequencies
MAPK – Mitogen-activated protein kinase
MF – Mycosis Fungoides
MM – Multiple myeloma
MMAE – Monomethyl auristatin E
NEMO – NFκB essential modulator
NFAT – Nuclear factor of activated T-cells
NFκB – Nuclear factor kappa B
NGFR – Nerve growth factor receptor
NGS – Next-generation sequencing
NLS – Nuclear localisation signal
nRTK – Non-receptor tyrosine kinases
ORF – Open reading frame
OSCC – Oral squamous cell carcinoma
PA – Phosphatidic acid
PBMC – Peripheral blood mononuclear cells
PBS – Phosphate buffered saline
PCR – Polymerase chain reaction
PD-1 – Programmed cell death-1
PDB – Protein data bank
PDGFR – Platelet-derived growth factor receptor
PD-L – Programmed death ligand
PFA – Paraformaldehyde
PI – Phosphoinositide
PIP_2 – Phosphatidylinositol 4,5-bisphosphate
PKCθ – Protein kinase C-theta
PLA – Phospholipase A
PLAID – PLCγ2-associated antibody deficiency and immune dysregulation

PLB – Passive Lysis Buffer
PLCG1 – Phospholipase C Gamma1 gene
PLCγ1 – Phospholipase C Gamma1 protein
PLCG2 – Phospholipase C Gamma2 gene
PLCγ2 – Phospholipase C Gamma2 protein
PMA – Phorbol 12-myristate 13-acetate
PMSF – Phenylmethylsulfonyl fluoride
PolyPhen2 – Polymorphism phenotyping
p-PLCγ1 – phosphorylated PLCγ1
Provean – Protein variation effect analyzer
PTCL – Peripheral T-cell lymphoma
PTCL-nos – Peripheral T-cell lymphoma-not otherwise specified
PUVA – Psoralen + UVA phototherapy
PVDF – Polyvinylidene difluoride
qRT-PCR – Quantitative reverse transcription-polymerase chain reaction
RIPA – Radioimmunoprecipitation assay
RL-TK – Renilla thymidine kinase luciferase reporter construct
RTK – Receptor tyrosine kinases
RT-PCR – Reverse transcription-polymerase chain reaction
SCC – Squamous cell carcinoma
SDS – Sodium dodecyl sulfate
SIFT – Sorting intolerant from tolerant
SNP – Single nucleotide polymorphism
SNV – Single nucleotide variant
SOC – Super optimal broth with catabolite repression
SS – Sézary Syndrome
STAT - Signal transducers and activators of transcription
TBE – Tris-Borate-EDTA
TBS-T – Tris-buffered saline-tween
TCR – T-cell receptor
TCS – Targeted capture sequencing
TEMED – Tetramethylethylenediamine
Th – Helper T-cell
TIM – Triosephosphate isomerase
T-MF – Transformed Mycosis Fungoides
TNFα – Tumor necrosis factor-alpha
TNFR – Tumor necrosis factor receptor
TNMB – Tumour-node-metastasis-blood
TPCA-1 – Inhibitor of IKKβ
TPLL – T-cell-prolymphocytic leukaemia
Treg – Regulatory T-cell
UV – Ultraviolet
VEGFR – Vascular endothelial growth factor receptor
WES – Whole-exome sequencing
WGS – Whole-genome sequencing
WHO – World Health Organization
WM – Waldenström macroglobulinemia
ZAP70 – Zeta-chain associated protein kinase-70
5-hmC5 – Hydroxymethylcytosine

Chapter 1 Introduction

1.1 Cutaneous T-cell lymphomas

Cutaneous T-cell lymphomas (CTCL) are a rare and heterogeneous group of non-Hodgkin lymphomas characterised by clonal proliferation of mature malignant skin-resident $CD4^+$ T-cells (1). Many clinical variants of CTCL have been reported with Mycosis Fungoides (MF) and Sézary syndrome (SS) being the most common and accounting for 54% of CTCL cases (2). MF is an indolent variant and SS is classed as an aggressive form of CTCL (3). MF normally affects older adults and SS exclusively affects adults (4). The age-adjusted incidence of MF and SS are 5.5 and 0.1 per million person years, respectively (5).

MF and SS, although considered sub-types of CTCL, are classified as distinct disease entities by the World Health Organisation (WHO) rather than conditions on a disease continuum (6). However, this is still contentious as a recent study demonstrates plasticity of T-cell differentiation markers from a clonal population of cells (7), supporting the disease continuum theory as will be discussed in section 1.6.1. MF and SS demonstrate variable clinical presentation, histopathology and immunopathology as will be discussed in this chapter.

1.2 Diagnosis of CTCL

The diagnosis of primary CTCL is based on multiple factors including examining clinical presentation, histological analysis of lesional skin biopsies and immunophenotypic characterisation of cells. Each diagnostic criterion will be described in this section.

1.2.1 Clinical manifestation

MF is localised to the skin and initially presents with erythematous patches, which can progress over many years or decades into plaques that can further develop into tumours (Figure 1. 1) (8). The patches and plaques occur in sun-protected areas including the trunk and buttocks (4). MF patches are flat and can be scaly compared to normal skin (9). In contrast, plaques are raised skin lesions that can be smooth, crusted or ulcerated (9). Tumour-stage MF patients typically present with patches, plaques and tumours

that are frequently ulcerated (4). In advanced stage MF, the lymph node and visceral organs may be involved (4). MF is an indolent form of CTCL and 71% of early stage patients have a median survival of 12.9 years, but disease progression slowly occurs in approximately 30% of cases (10, 11). The incidence of MF is greater in males compared to females and the age of clinical presentation varies greatly from 12 to 88 years, with a median age of 57 years (11, 12). The diagnosis of early stage MF can be challenging as the clinical presentation can mimic other dermatological conditions including psoriasis, eczema and atopic dermatitis (13, 14).

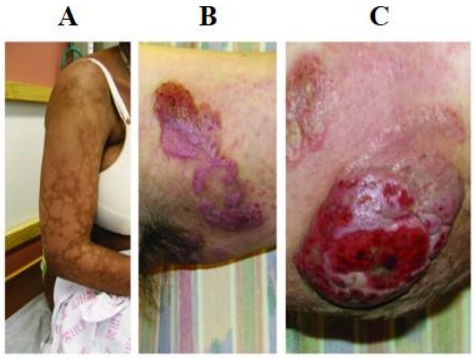

Figure 1. 1. Clinical presentation of MF. (A) MF initially presents with patches that can be hyper- or hypo-pigmented, the latter of which is shown. (B) The patches progress to form plaques. (C) The most advanced stage of MF presents with tumours. Images adapted from Kim *et al.* (2005) (1).

SS is an aggressive leukaemic variant of CTCL (3). SS is characterised by generalised erythroderma with at least 80% skin involvement (Figure 1. 2. A), lymphadenopathy and the spread of neoplastic T-cells known as Sézary cells in the peripheral blood, skin and lymph nodes (3). Sézary cells are enlarged malignant $CD4^+$ T-helper (Th) cells that have characteristic hyper-convoluted and cerebriform nuclei (Figure 1. 2. B) (15, 16). SS occurs more frequently in adult males than females (4, 12). SS patients have a poor prognosis due to rapid disease progression with a median survival of between 2 – 4 years (17, 18).

Patients with advanced stage CTCL characteristically have disease-associated immunosuppression (as discussed in section 1.6) and frequently die from opportunistic infections rather than from complications of a high tumour burden (19, 20).

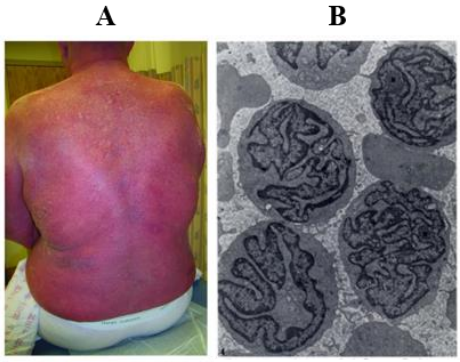

Figure 1. 2. Characteristic features of SS. (A) A SS patient with generalised erythroderma. (B) Sézary cells characterised by hyper-convoluted and cerebriform nuclei. Images adapted from Kim *et al.* (2005) and Lutzner and Jordan (1968) (1, 21).

1.2.2 Histological analysis

The histopathological features of early stage MF overlap with other inflammatory dermatoses and add to the challenge of achieving an early diagnosis (13). MF skin lesions have abnormal infiltration of neoplastic lymphocytes in the epidermis (epidermotropism), which form cellular clusters known as Pautrier microabscesses (Figure 1. 3) (22). Histological changes in the patch stages are subtle, however in MF plaques, infiltrates of small T-cells with abnormal cerebriform nuclei can be detected (23).

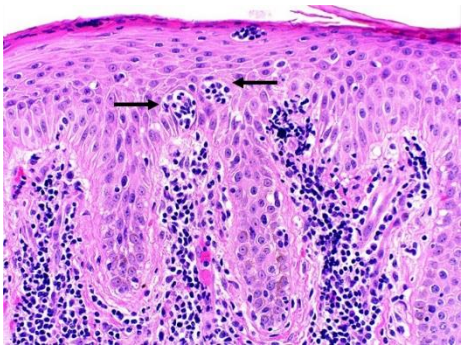

Figure 1. 3. Pautrier microabscesses in a MF skin section. Histological staining showing clusters of atypical cell infiltrates (Pautrier microabscesses), indicated by arrows. Image adapted from Kim *et al.* (2005) (1).

In SS, involved lymph nodes show a diffuse infiltrate of atypical cells that have cerebriform nuclei and disrupt the normal architecture of the nodes (Figure 1. 4) (24).

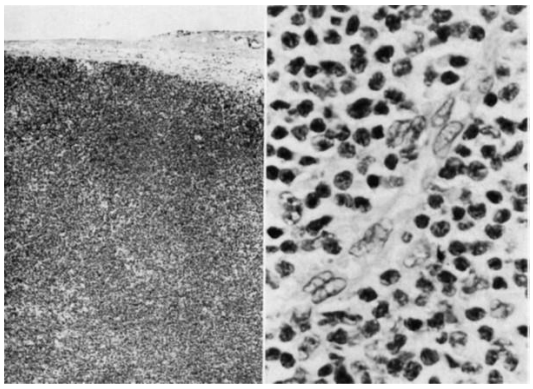

Figure 1. 4. Infiltration of cells with cerebriform nuclei in a SS lymph node section. The image on the left and right side were obtained with low and high magnification, respectively. Image adapted from Scheffer *et al.* (1986) (24).

1.2.3 Immunophenotypic characterisation

Immunophenotypic analysis of CTCL is required to confirm that the dominant cell population is composed of T cells and not B cells or other cell types. The following markers are used to confirm the T-cell phenotype by flow cytometry: $CD3^+$ (T-cell marker), $CD45^+$/common leukocyte antigen (CLA; bone-derived leukocyte marker) and $CD20^-$ (B-cell marker) (25). MF patients characteristically have monoclonal proliferation of atypical $CD2^+$, $CD3^+$, $CD4^+$, $CD5^+$, $CD45RO^+$, $CD8^-$ mature memory T-helper cells (26). As disease progresses, these neoplastic cells lose expression of CD2, CD5 and CD7 (26, 27). Atypical cells in SS have a $CD2^+$, $CD3^+$, $CD4^+$, $CD5^+$, $CD45RO^+$, $CD30^-$ mature memory T-helper cell phenotype (28). As with neoplastic cells in advanced stage MF, Sézary cells have loss of CD7 and also demonstrate loss of CD26 (29). Immunophenotypic analysis also includes analysis of the $CD4^+$:$CD8^+$ T-cell ratio, which normally occurs in a 2:1 proportion (25). In patch stage MF, an elevated CD4:CD8 ratio has been detected, which reduces with disease progression (25). In contrast, the ratio of $CD4^+$ cells is amplified over 10-fold compared to $CD8^+$ cells in SS (25).

1.3 CTCL staging

As described in section 1.2, the diagnosis of MF and SS depends on clinical, histological and immunophenotypical analyses. The tumour-node-metastasis-blood (TNMB) classification specified by the International Society for Cutaneous Lymphomas/ European Organisation for Research and Treatment of Cancer (ISCL/ EORTC) shown in Table 1. 1 is used to amalgamate the analyses and determine which compartments are involved (22).

Table 1. 1. ISCL/EORTC classification of tumour-node-metastasis-blood (TNMB) for MF and SS. Table adapted from Olsen *et al*. (2007) (22).

TNMB stages	
Skin	
T_1	Limited patches,* papules, and/or plaques† covering < 10% of the skin surface. May further stratify into T_{1a} (patch only) vs T_{1b} (plaque ± patch).
T_2	Patches, papules or plaques covering ≥ 10% of the skin surface. May further stratify into T_{2a} (patch only) vs T_{2b} (plaque ± patch).
T_3	One or more tumors‡ (≥ 1-cm diameter)
T_4	Confluence of erythema covering ≥ 80% body surface area
Node	
N_0	No clinically abnormal peripheral lymph nodes§; biopsy not required
N_1	Clinically abnormal peripheral lymph nodes; histopathology Dutch grade 1 or NCI LN_{0-2}
N_{1a}	Clone negative#
N_{1b}	Clone positive#
N_2	Clinically abnormal peripheral lymph nodes; histopathology Dutch grade 2 or NCI LN_3
N_{2a}	Clone negative#
N_{2b}	Clone positive#
N_3	Clinically abnormal peripheral lymph nodes; histopathology Dutch grades 3-4 or NCI LN_4; clone positive or negative
N_x	Clinically abnormal peripheral lymph nodes; no histologic confirmation
Visceral	
M_0	No visceral organ involvement
M_1	Visceral involvement (must have pathology confirmation¶ and organ involved should be specified)
Blood	
B0	Absence of significant blood involvement: ≤ 5% of peripheral blood lymphocytes are atypical (Sézary) cells‖
B_{0a}	Clone negative#
B_{0b}	Clone positive#
B1	Low blood tumor burden: > 5% of peripheral blood lymphocytes are atypical (Sézary) cells but does not meet the criteria of B_2
B_{1a}	Clone negative#
B_{1b}	Clone positive#
B2	High blood tumor burden: ≥ 1000/μL Sézary cells‖ with positive clone#

*For skin, patch indicates any size skin lesion without significant elevation or induration. Presence/absence of hypo- or hyperpigmentation, scale, crusting, and/or poikiloderma should be noted.

†For skin, plaque indicates any size skin lesion that is elevated or indurated. Presence or absence of scale, crusting, and/or poikiloderma should be noted. Histologic features such as folliculotropism or large-cell transformation (> 25% large cells), $CD30^+$ or $CD30^-$, and clinical features such as ulceration are important to document.

‡For skin, tumor indicates at least one 1-cm diameter solid or nodular lesion with evidence of depth and/or vertical growth. Note total number of lesions, total volume of lesions, largest size lesion, and region of body involved. Also note if histologic evidence of large-cell transformation has occurred. Phenotyping for CD30 is encouraged.

§For node, abnormal peripheral lymph node(s) indicates any palpable peripheral node that on physical examination is firm, irregular, clustered, fixed or 1.5 cm or larger in diameter. Node groups examined on physical examination include cervical, supraclavicular, epitrochlear, axillary, and inguinal. Central nodes, which are not generally amenable to pathologic assessment, are not currently considered in the nodal classification unless used to establish N_3 histopathologically.

¶For viscera, spleen and liver may be diagnosed by imaging criteria.

‖For blood, Sézary cells are defined as lymphocytes with hyperconvoluted cerebriform nuclei. If Sézary cells are not able to be used to determine tumor burden for B_2, then one of the following modified ISCL criteria along with a positive clonal rearrangement of the TCR may be used instead: (1) expanded $CD4^+$ or $CD3^+$ cells with CD4/CD8 ratio of 10 or more, (2) expanded $CD4^+$ cells with abnormal immunophenotype including loss of CD7 or CD26.

#A T-cell clone is defined by PCR or Southern blot analysis of the T-cell receptor gene.

A key criterion for determining blood involvement and the stage of involvement is by quantifying circulating Sézary cells (Table 1. 1). Blood stage B0 is characterised by no significant blood involvement with ≤5% of peripheral blood lymphocytes being Sézary cells (22). Stage B1 is defined by a low blood tumour burden with greater than 5% of peripheral blood lymphocytes being Sézary cells (22). Stage B2 is classified by a high tumour burden with ≥1000 Sézary cells per microliter (22). Sézary cells are quantified by flow cytometric analysis of $CD4^{+}CD7^{-}$ or $CD4^{+}CD26^{-}$ T-cells (30).

Once patients have been classified using the TNMB classification, the disease stage is determined using the criteria shown in Table 1. 2 (22). Correct staging is crucial as it determines which therapeutic interventions should be administered and therefore impacts the prognosis and survival outcome of patients (31, 32).

Table 1. 2. ISCL/EORTC staging guidelines for TNMB involvement in MF and SS. Table adapted from Olsen *et al*. (2007) (22).

	T	N	M	B
IA	1	0	0	0,1
IB	2	0	0	0,1
II	1,2	1,2	0	0,1
IIB	3	0-2	0	0,1
III	4	0-2	0	0,1
IIIA	4	0-2	0	0
IIIB	4	0-2	0	1
IVA_1	1-4	0-2	0	2
IVA_2	1-4	3	0	0-2
IVB	1-4	0-3	1	0-2

1.4 Treatment modalities

Several treatment approaches are used to manage the symptoms of MF and SS. Early stage disease is treated with skin-directed therapies, whereas systemic therapies are used for advanced MF and SS cases.

1.4.1 Skin-directed therapies

The skin-directed therapies for early stage disease induce apoptosis of malignant cells (1, 33). Categories of skin-directed treatments include phototherapy, topical corticosteroids, topical retinoids, topical chemotherapy and radiotherapy, each of which will be described. Two forms of phototherapy are used: Psoralen+Ultraviolet A (PUVA) and Ultraviolet B (UVB). Early stage MF patients can benefit from Psoralen consumption followed by ultraviolet A phototherapy. Psoralen is a light-sensitive mutagen that incorporates into DNA and forms adducts that are activated by UVA radiation, leading to inhibition of cell proliferation and induction of apoptosis (32). UVB therapy does not require administration of Psoralen, making it an easier form of phototherapy for clearing skin patches in early MF (34). Topical corticosteroids are effective for treating patch stage MF and are available as creams and ointments (35). Carmustine and Nitrogen mustard are types of topical chemotherapy (36, 37). In addition to treating patch stage, Carmustine is also used for plaque stage MF (36). Nitrogen mustard ointment can clear skin lesions and re-pigment hypo-pigmented skin regions (38). Radiotherapy in the form of total-skin electron-beam therapy targets the entire surface area of the skin and effectively eliminates malignant cells (39). Superficial X-irradiation is another form of radiotherapy also used to treat early stage MF (40).

1.4.2 Systemic therapies

Systemic treatments for advanced stage (IVA2 and IVB) disease include biologics or immune-regulators such as Interferon-γ (IFN-γ) and IFN-α or the retinoid Bexarotene and rexinoid Isotretinoin (1). Patients who do not benefit from skin-directed therapies should also be considered for treatment with single agent systemic therapy (41).

1.4.2.1 Current systemic therapies

IFN-γ and IFN-α inhibit production of the Interleukin (IL)-4 and IL-5 cytokines, which are characteristically elevated in CTCL and contribute to disease pathogenesis (41). Retinoids and rexinoids bind to retinoid x receptors and activate transcription factors that regulate cell proliferation and differentiation gene expression (42). Although effective treatments in some CTCL cases, the specific mechanism by which retinoid and rexinoids elicit their effects remains to be determined (42). Histone deacetylase (HDAC) inhibitors are used as systemic therapies to induce cellular growth arrest and apoptosis (43). HDAC enzymes remove acetyl groups from lysine bases on histones, enabling DNA to wrap around the histones to prevent transcription (44). Romidepsin is a HDAC inhibitor that is intravenously administered and works to epigenetically alter gene transcription and induces apoptosis (45). This inhibitor has been deemed safe and effective for CTCL patients that have previously received at least one systemic therapy (45). Vorinostat is an orally administered HDAC inhibitor also used to treat advanced stage CTCL (44).

Systemic phototherapy such as extracorporeal photopheresis (ECP) induces apoptosis of malignant cells in SS by treating peripheral blood *ex-vivo* with PUVA and infusing it back into the patient (1). Advanced stage disease may also benefit from combination therapies such as ECP with IFN-α or Bexarotene (46).

1.4.2.2 The emergence of monoclonal antibodies as immune checkpoint inhibitors

Immunotherapy, the use of monoclonal antibodies and drugs that suppress or stimulate the immune system, has emerged as an appealing strategy for CTCL. Immune checkpoint inhibitors are a form of immunotherapy currently undergoing investigation for use in CTCL, with programmed cell death-1 (PD-1) inhibitors being an important example. PD-1 is a member of the CD28 co-stimulatory receptor family of cell-surface proteins expressed on T-cells that provides immunosuppressive signals upon interaction with the PD-L1 or PD-L2 ligands (47). Interaction of PD-1 with its ligands maintains peripheral tolerance by preventing T-cells attacking host tissues in an autoimmune manner, making it a key immune checkpoint that can contribute to lymphomagenesis if dysregulated (47). Samimi *et al*. (2010) reported higher PD-1 expression on $CD4^+$ T cells from SS patients compared to MF and healthy individuals (48). Subsequently, frequent PD-1 expression has been reported in patch and plaque

stage MF, but greatly reduced expression in tumour stage CTCL samples and in patients with large cell transformation (49). PD-L1 expression has also been detected in the majority of atypical lymphocytes from all CTCL stages, which increased as disease progressed (49). Recently, Querfeld *et al*. (2018) performed a larger study and reported significantly increased PD-1 and PD-L1 expression in all stages of CTCL, with greater expression in advanced stage disease compared to patch and plaque stage (50). Overexpression of PD-1 in all stages of CTCL suggests that MF and SS are part of a disease continuum as opposed to separate disease entities. Immunosuppression is a key feature of CTCL and frequent expression of PD-1 and PD-L1 may be mechanisms by which immunosuppression develops (49). In light of the increased PD-1 and PD-L1 expression, antibodies targeting these cell surface molecules may be an effective therapeutic approach for CTCL. Pembrolizumab is an anti-PD-1 monoclonal antibody that has shown clinical efficacy and was well-tolerated by most MF and SS patients in a phase II trial (51). Another phase II trial (NCT02243579) with the same sample size of stage IB-IVB relapsed or refractory MF or SS patients treated with Pembrolizumab is currently underway (52, 53). Nivolumab is also a PD-1 blocking monoclonal antibody that has been shown to induce a partial response in 2/13 MF patients in a phase I trial with only mild side effects including fatigue (54). Nivolumab has also been shown to induce complete response in 1/11 diffuse large B-cell lymphoma cases, a disease in which increased PD-1^{+} tumour-infiltrating lymphocytes have been reported (54, 55).

Mogamulizumab is a further antibody under investigation as a therapy for CTCL (41). This antibody targets the CCR4 chemokine receptor that is expressed on neoplastic T-cells in approximately 40% of CTCL patients and has been approved as a therapeutic agent in Japan and the U.S.A. (41, 56). Alemtuzumab, a monoclonal antibody that targets CD52, which is highly expressed by malignant T-cells has been shown to be effective in SS patients but not advanced stage MF (41, 57). This suggests that Alemtuzumab binds to circulating malignant T lymphocytes more effectively than skin-resident neoplastic cells (57). Brentuximab vedotin is a monoclonal anti-CD30 antibody conjugated to monomethyl auristatin E (MMAE), a drug that inhibits tubulin polymerisation and thereby cell division (58). The antibody binds to cells expressing CD30 (which varies in CTCL) and enables the cells to endocytose MMAE, leading to cell cycle arrest and the induction of apoptosis (41). Brentuximab vedotin has proven

clinically effective in phase II studies of advanced stage or treatment-refractory MF or SS patients who had variable levels of CD30 expression (59, 60).

1.4.2.3 Challenges associated with immune checkpoint inhibitors

Although immune checkpoint inhibitors seem promising, there are challenges associated with these therapeutic approaches. The first challenge is that tumours harbour mutations in different genes with variable frequencies (61). This can influence the response patients have to immune checkpoint inhibitors as demonstrated by melanoma patients treated with CTLA-4 blockers (62, 63). CTLA-4 is a T-cell surface molecule that functions in a similar manner to PD-1, by providing negative signals to T-cells to prevent cells being activated against self-antigens (64). Melanoma patients with a high mutation burden of over 100 missense mutations responded better to anti-CTLA-4 antibodies compared to patients with a lower mutation burden who did not respond (62, 63). Therefore, patients being considered for CTLA-4 therapy should have their tumour mutation burden assessed by whole-exome sequencing to serve as a biomarker for clinical response to anti-CTLA-4 therapy (62, 63). The mutation burden in haematological malignancies including peripheral T-cell lymphomas-not otherwise specified (PTCL-nos) and angioimmunoblastic T-cell lymphoma (AITL) is significantly lower (approximately 25 mutations per tumour) than in solid tumours such as melanoma (65, 66). However, CTCL is an exception as the mutation burden ranges from an average of 50 – 100 missense mutations and some tumours have significantly higher rates of over 300 mutations per tumour (61, 67-71). Therefore, immune checkpoint inhibitors may be effective in CTCL due to the high mutation burden and PTCL-nos and AITL cases may not benefit from such inhibitors (61).

Another challenge of immune checkpoint inhibitors was demonstrated by Postow *et al*. (2015), who showed that melanoma patients with a diverse T-cell repertoire had a higher response rate to the anti-CTLA-4 monoclonal antibody, Ipilimumab, than patients with a restricted repertoire (72). This observation suggests that such inhibitors may be less effective in CTCL due to the loss of T-cell repertoire resulting from late-stage disease pathogenesis and immunosuppressive therapies commonly used in advanced stage disease (61).

1.4.2.4 Chemotherapy and haematopoietic stem cell transplantations

Single-agent chemotherapy with cytotoxic agents such as Methotrexate, Gemcitabine, Cyclophosphamide, Pentostatin and Temozolomide are used for advanced stage disease and for patients who have relapsed or refractory disease (32, 44). However, as chemotherapy is associated with poor survival outcomes it is not used as a first line therapy but is considered as a second line therapy for patients who do not respond to biological agents (41, 73).

Transformed MF (T-MF) is a rare and aggressive form of MF in which small neoplastic cells transform into large cells in 6% to 55% of MF patients (74-76). T-MF patients have a poor prognosis and reduced overall survival (74, 77). Systemic therapeutic interventions for T-MF include ECP, Bexarotene, IFNα, Vorinostat, low-dose Gemcitabine or Methotrexate or allogenic haematopoietic stem cell transplantation for non-responders (74, 77).

Combination chemotherapy (CHOP), a multi-agent chemotherapy regimen comprising of cyclophosphamide, doxorubicin, vincristine and prednisolone are reserved for advanced stage CTCLs including T-MF (78). However, such therapies are associated with high rates of rapid relapse compared to patients treated with IFNα and HDAC inhibitors, demonstrating that the aggressive treatment has no superior benefits to other non-chemotherapeutic systemic drugs (79). Furthermore, multi-agent therapies including total-skin electron-beam radiation and CHOP have comparable disease-free and overall survival outcomes for MF patients compared to topical treatment with mechlorethamine or topical mechlorethamine and oral methotrexate treatment for stage IVB disease, showing that combination therapies are not more effective than conventional skin-directed treatments (80).

Treatments currently aim to manage disease symptoms by clearing the skin, reducing tumour burden, preventing disease progression and improving the patient's quality of life (32). Investigations into autologous haematopoietic stem cell transplantations as a cure for advanced stage disease have not been promising (81). In contrast, allogeneic haematopoietic stem cell transplantations are currently the only effective cure that increase overall survival of advanced stage MF and SS patients (3, 82, 83). There are however major limitations in this therapeutic approach, the first being difficulty in identifying an HLA-matched donor and the second, patients succumbing to graft

versus host disease (3, 82). It is therefore pivotal to understand the genetic and molecular mechanisms causing advanced stage disease for the identification of novel therapeutic targets.

1.5 Differentiation of CD4$^+$ T-cells

CD4$^+$ T-cells have a fundamental role in maintaining a healthy adaptive immune system by protecting against pathogenic infections (84). Naïve CD4$^+$ T-cells differentiate into either effector T-helper (Th1, Th2, Th17 and Tfh) or regulatory T-cells (Tregs) (Figure 1. 5) (84, 85). Cell fate is determined by the cytokine milieu at the time of naïve T-cell activation by antigens presented from antigen presenting cells (APCs), such as dendritic cells (86). Transcription factors are also essential in determining cell fate as they control the expression of key cytokines that influence differentiation (87).

IL-12 induces Th1 cell differentiation and inhibits Th2 development, whereas IL-4 promotes Th2 cell fate and antagonises Th1 expansion (87). The transcription factors STAT4 and T-bet drive IL-12 production and promote Th1 differentiation (87). STAT6 and GATA-3 induce IL-4 expression to produce Th2 cells (87). Th1 cells produce IFNγ, which drives cell-mediated immunity and Th2 cells produce IL-4, IL-5 and IL-13, which promote a humoral response against allergens and parasitic infections including helminths (87). CTCLs have a Th2 predominant cytokine expression profile, which suppress anti-tumour Th1 cytokines as will be described in section 1.6.2.

TGFβ-1 in conjunction with the IL-6, IL-21 and IL-23 cytokines and the signal transducers and activators of transcription 3 (STAT3) and Rorγ transcription factors induces differentiation to Th17 cells (84). Th17 cells produce the pro-inflammatory IL-17 cytokine and also IL-22, which plays a key role in defending mucosal surfaces of organs and tissues from infections (84, 88).

IL-6, IL-21 and STAT3 induce differentiation to follicular helper T-cells (Tfh), which produce IL-21 that aids Tfh cells in providing help to B-lymphocytes to differentiate into memory B cells or high-affinity antibody-secreting plasma cells which clear

pathogens (89). Expression of Tfh markers have been reported in CTCL, suggesting a role for these cells in disease pathogenesis as will be described in section 1.6.4.

The STAT5 and Forkhead box P3 (FOXP3) transcription factors drive IL-2 production, which in combination with TGFβ-1 induces Treg differentiation (87). Tregs produce TGFβ-1, which inhibits differentiation of Th1 and Th2 cells and thereby suppresses immune responses as a regulatory mechanism (87). Tregs also play a fundamental role in maintaining tolerance to self-antigens (84). Dysregulated Treg expression is a key feature of CTCL as will be discussed in section 1.6.5.

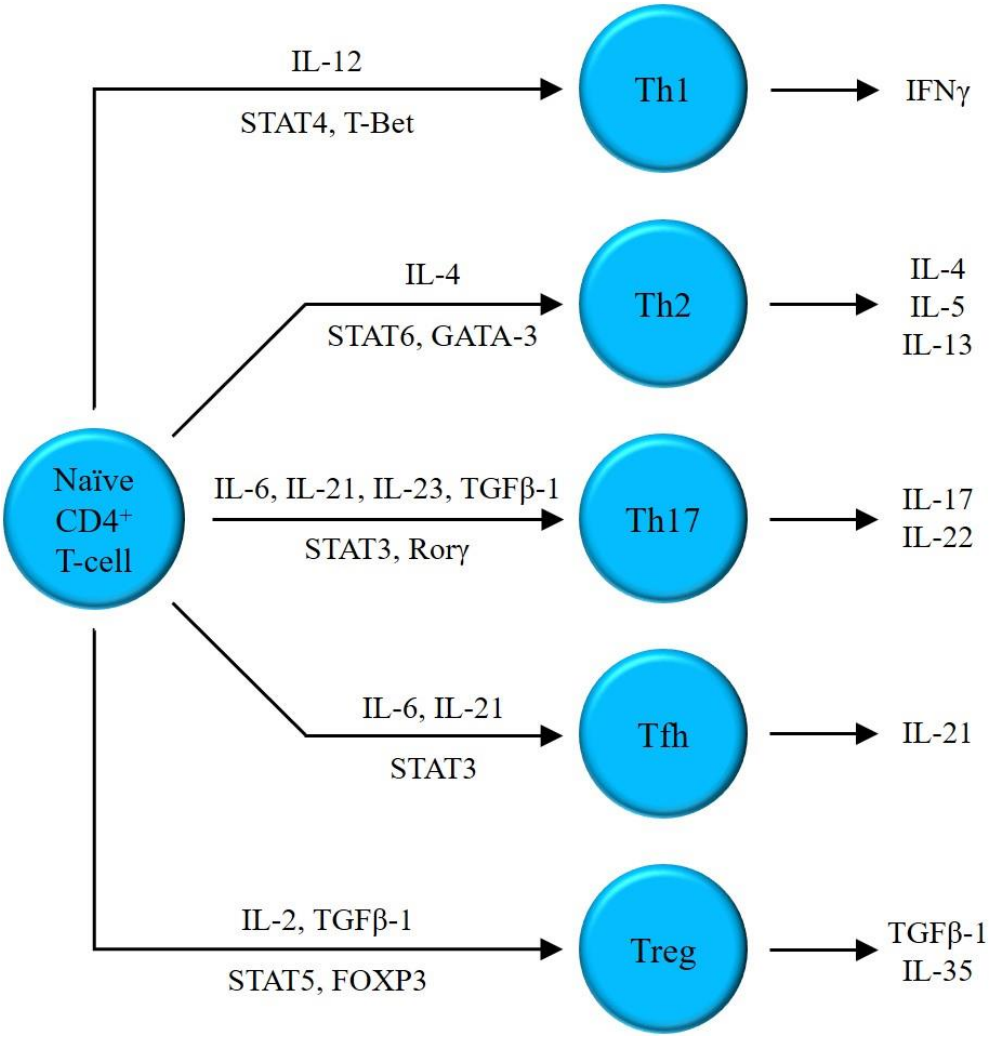

Figure 1. 5. Differentiation of naïve $CD4^+$ T-cells. Antigen presentation from APCs induces differentiation of naïve T-cells to effector T-helper cells (Th1, Th2, Th17 and Tfh) or regulatory T-cells (Treg). Figure adapted from O'Shea *et al*. (2013) (90).

Memory $CD4^+$ T-cells are sub-classified into central memory T-cells and effector memory T-cells (91). Central memory T-cells home to secondary lymphoid organs including lymph nodes as they express the lymph node homing CCR7 molecule (91). These cells have limited or no capability to remove antigen but can rapidly proliferate and differentiate to generate effector memory cells upon antigenic stimulation by mature dendritic cells (91). As will be described in section 1.6.1, malignant cells in SS express CCR7 and have a central memory T-cell immunophenotype.

Effector memory T-cells originate from naïve T-cells that have encountered antigen and undergone differentiation (92). These cells can migrate to peripheral tissues and therefore have a more rapid effector function than central memory cells at clearing pathogens (91). Effector memory T cells are characterised by lack of CCR7 expression and rapidly produce high levels of the effector cytokines IL-4, IL-5 and IFNγ upon antigen stimulation (92). Th1 (produce IFNγ) and Th2 (produce IL-4 and IL-5) cells are classed as effector memory T-cells (91). Neoplastic cells in MF lack CCR7 expression and have a skin-resident effector memory T-helper phenotype as will be discussed in section 1.6.1.

1.6 Immunopathogenesis of CTCL

Primary cells from MF and SS patients and CTCL cell lines have several abnormal characteristics that contribute to disease pathogenesis as will be described in this section.

1.6.1 Neoplastic cells in CTCL have central and effector memory T-cell immunophenotypes

Memory $CD4^+$ or $CD8^+$ T-cells are fundamental for mounting a rapid immune response when re-exposed to antigens (93). There are three types of memory T-cells: central memory cells that localise to lymph nodes, effector memory cells that circulate the body and resident memory cells which reside in peripheral tissues including the skin (94).

CTCL cells have memory cell phenotypes (95). Specifically, clonal malignant cells from the blood of SS patients demonstrate a central memory T-cell phenotype, characterised by expression of the lymph node homing molecules L-selectin and CCR7 in addition to CD27, a cell differentiation marker (95). Skin lesions from MF, on the other hand, display a skin-resident effector memory T-cell phenotype defined by the expression of CCR4 and CLA but lack L-selectin, CCR7 and CD27 expression (95). These distinct immunophenotypes support the classification of MF and SS as separate disease entities, however this is still contentious.

This theory has recently been challenged by a study in which mice immunised through the skin demonstrated identical T-cell receptor (TCR)-β chain sequences in abundant clones of both skin-resident memory cells and central memory T-cells in lymph nodes (7). This demonstrates the plasticity of T-cell differentiation marker expression and shows that skin-resident cells like those detected in MF and central memory cells such as those reported in SS can originate from a common clonal population of naïve T-cells (7). This suggests that neoplastic cells in MF and SS may have a common origin, making them part of a disease spectrum as opposed to separate disease entities.

1.6.2 Advanced stage CTCL has a Th2 predominant cytokine expression profile

SS and advanced stage MF highly express the Th2 cytokines IL-4, IL-5, IL-10 and IL-13 (96, 97). Importantly, expression of these cytokines is regulated by the nuclear

factor kappa B (NFκB), nuclear factor of activated T-cells (NFAT) and activator protein-1 (AP-1) transcription factors, of which NFκB is characteristically overexpressed in CTCL as discussed in section 1.6.6.

Elevated IL-4 levels produced by Th2 cells have been reported in the serum of SS patients, demonstrating a skew towards Th2 cytokine production (98). Furthermore, stimulated peripheral blood mononuclear cells (PBMCs) from SS patients produce higher levels of IL-4 and less of the Th1 cytokines IL-2 and IFNγ compared to healthy individuals (98). A reduction in the elevated IL-4 production was observed when PBMCs from these patients were co-cultured with IFNγ *in vitro,* demonstrating that the low level of IFNγ produced by SS patients is insufficient to maintain the balance of Th1-Th2 cytokine production (98). These data support the use of IFNγ as a form of systemic therapy in advanced stage CTCL as discussed in section 1.4.2. Expression of the IL-4 and IL-5 cytokines has also been detected at the transcriptional level in lesional skin from all stages of CTCL (96). Specifically, IL-4 and IL-5 mRNA were detected in skin biopsies of plaque and tumour stage CTCL but patch stage MF showed only expression of IL-5 (96). Targeting the elevated IL-4 levels with an anti-IL-4 antibody results in reduced proliferation of $CD4^+$ T-cells from SS patients *in vitro* (99).

The increasing expression of cutaneous IL-10 mRNA correlates with disease stage in MF (97). Wu *et al*. (2018) confirmed these findings and also showed that blocking IL-10 in a CTCL mouse model with a monoclonal anti-IL-10R antibody reduced tumour growth (100). These findings suggest that blockade of IL-10 signalling may be an effective therapeutic strategy for CTCL (100). Furthermore, IFNγ gene expression decreases in lesional skin as MF progresses from patch to plaque stage with no IFNγ detected in tumour lesions (97). Importantly, IL-10 is an immunosuppressive cytokine that contributes to the immunopathogenesis of CTCL by enabling immune evasion of tumour cells (97).

Immunohistochemical analysis has identified high expression of IL-13 and its receptors IL-13Rα1 and IL-13Rα2 in lesional skin of CTCL patients (99). Geskin *et al*. (2015) showed that culturing enriched $CD4^+$ T-cells from SS patients with IL-13 *in vitro* induced cell proliferation, demonstrating that this Th2 cytokine promotes

growth of neoplastic cells in SS (99). Blocking IL-13 signalling with an anti-IL-13 antibody greatly reduces the proliferation of SS cells *in vitro* (99).

Collectively, these data indicate that neoplastic T-cells have a Th2 helper cell phenotype characterised by elevated Th2 cytokines in the peripheral blood of SS patients and lesional skin from all stages of CTCL, which contributes to the disease pathogenesis. Furthermore, Guenova *et al*. (2013) show that both malignant and benign (non-clonal) T-cells from patients with leukaemic CTCL have a Th2 bias and produced more IL-4 and IL-13 than T-cells from healthy individuals and malignant cells also produced higher levels of IL-10 (101). IL-4 and IL-13 produced by malignant cells were shown to reduce production of the Th1 cytokine IFNγ from T-cells of healthy individuals, demonstrating the ability of cells to induce a Th2 microenvironment. (101). The elevated Th2 cytokine levels override the anti-tumour effects of the Th1 cytokine IL-2 in addition to IFNγ and thereby provide an advantageous microenvironment for tumour growth (102).

1.6.3 Activated T-cells in CTCL display an exhausted phenotype

$CD4^+$ T-cells in CTCL undergo clonal proliferation in a milieu of chronic inflammation (50). As a result, these cells are chronically activated leading to an exhausted phenotype that makes them unresponsive to antigens presented by cutaneous dendritic cells (50, 103). Exhausted T-cells contribute to immunosuppression as the cells do not effectively clear pathogenic infections, which are the leading cause for death in SS (104).

Exhausted $CD4^+$ T-cells from SS patients have increased PD-1 expression compared to MF patients and healthy controls (48, 103). A recent study confirmed and extended these findings by reporting significantly increased gene expression of PD-1, LAG-3 and CTLA-4 in all stages of CTCL compared to healthy skin, with greater expression in advanced stage disease than patch and plaque stage MF (50). PD-1, CTLA-4 and LAG-3 are suppressive immune checkpoints that negatively regulate TCR signalling, therefore overexpression of these inhibitory receptors may contribute to the characteristic immunosuppressive nature of CTCL cells (47, 48, 50).

Cytotoxic $CD8^+$ T-cells from CTCL patients also have increased CTLA-4 and LAG-3 expression compared to T-cells from healthy skin (50). Furthermore, tumour-

infiltrating $CD8^+$ cytotoxic T-cells have an exhausted phenotype and do not fully induce their anti-tumour effect to remove malignant $CD4^+$ T-cells from the skin (103). Thus, advanced stage disease is characteristically less cytotoxic and more immunosuppressive (1). Overexpression of the mentioned cell surface markers has made them prime therapeutic targets for immune check point inhibitors as discussed in section 1.4.2.2.

1.6.4 Neoplastic Tfh cells are detected in CTCL

PD-1 expression is a marker of not only activated T-cells but also of Tfh cells (105). To distinguish between the two cell types, co-expression of at least three Tfh markers including PD-1, ICOS, CXCL13, BCL-6, or CD10 is required to determine whether cells have a Tfh cell phenotype (105). Bosisio *et al*. (2015) have shown frequent expression of at least 3 of these markers in more than 10% of tumour cells in MF (106), suggesting a role for neoplastic Tfh cells in CTCL. Malignant cells in SS have also been reported to express PD-1, BCL6 and CXCL13 implicating a Tfh origin of the neoplastic cells (107). Another study reports 5 primary CTCLs which express Tfh markers and proposes that these cases are therefore referred to as primary cutaneous Tfh lymphomas (108). This suggests that a subset of CTCLs may arise from malignant Tfh cells and raises the question of whether such cases should be classed as a separate disease entity. The expression of PD-1, BCL-6, CXCL13, and CD10 on neoplastic cells is a characteristic feature of AITL, a lymphoma of Tfh cells (107).

1.6.5 Dysregulation of Tregs in CTCL

Tregs ($CD4^+CD25^+$) have immunosuppressive properties and play a key role in maintaining tolerance to self-antigens (20). MF skin lesions demonstrate high infiltration of Tregs, which reduces as disease progresses and lesional skin from SS show low Treg infiltration (109). An *ex vivo* study performed by our group identified no significant difference in Treg frequency in 10 SS patients compared to healthy control individuals (110). This study also showed that high burden CTCL tumours encompass dysfunctional Tregs that did not suppress T-cell proliferation and identified a significant association between these cells and elevated Sézary cell counts in four patients (110). The remaining six patients had functional Tregs that suppressed T-cell proliferation and had a relatively lower tumour burden (110). Reduced mRNA

expression of FOXP3, a transcription factor considered the master regulator of Tregs, was detected in patients with a high tumour burden and dysfunctional Tregs (110).

A subsequent study on a larger cohort of MF and unclassified CTCL patients also demonstrated no or very weak FOXP3 expression in tumour cell infiltrates from 85/86 cases (111). However, all cases demonstrated strong FOXP3 expression in tumour-infiltrating Tregs. Patch and plaque stage MF had a greater number of $FOXP3^+$ Treg cells than advanced stage disease, showing that expression is related to disease stage (111). Furthermore, an association between the high number of $FOXP3^+$ Tregs and improved survival was also demonstrated (111).

1.6.6 NFκB is constitutively active in CTCL

CTCL cell lines and primary cells from MF and SS patients characteristically have constitutive NFκB activity and overexpression of NFκB target genes. The HUT-78 cell line, which is derived from a SS patient, has constitutively active NFκB unlike the Jurkat cell line, which originates from an acute T-cell leukaemia patient (112, 113). HUT-78 cells were identified to produce high levels of tumour necrosis factor-α (TNFα), a pro-inflammatory cytokine that acts in an autocrine manner to constitutively activate NFκB, which further drives TNFα expression (112, 113). Treating HUT-78 cells with anti-TNFα antibodies drastically reduces NFκB activity, confirming that TNFα functions as a growth factor for this cell line (112, 113). HUT-78 cells, unlike Jurkat cells, are resistant to TNF-induced apoptosis which may be due to constitutive NFκB activity (113).

Immunohistochemical analysis has revealed that MF skin lesions have strong nuclear and cytoplasmic expression of the p65 NFκB subunit (114). Electrophoretic mobility shift assays and confocal microscopy have shown that in addition to HUT-78 cells, MyLa cells (MF cell line), SeAx cells (SS cell line) and peripheral blood cells from SS patients with a high proportion of tumour cells, all have constitutive NFκB activity (115). Treating SeAx and MyLa cells and tumour cells from SS patients with the proteasome inhibitor Bortezomib reduces NFκB activity and induces apoptosis, demonstrating that NFκB plays a key role in apoptosis resistance, a hallmark of CTCL cells (115). Inhibition of IKK2 (also known as IKKβ, a subunit of the IKK complex that regulates NFκB activity) also reduces nuclear localisation and activity of NFκB

and potently induces apoptosis of CTCL cell lines and tumour cells from SS patients (116).

An alternative mechanism of constitutive NFκB signalling is that of *NFKB2* gene rearrangements detected in CTCL cell lines and two CTCL patients (117). An *NFKB2* gene rearrangement identified in HUT-78 cells is likely to result in an abnormal truncated protein instead of the p100 NFκB subunit. High levels of this truncated protein have been detected in the nucleus of HUT-78 cells, suggesting that it may contribute to the constitutive NFκB activity observed in CTCL (117).

Recent deep sequencing studies on CTCL tumours have identified alternative mechanisms, namely several gene mutations and translocations that may contribute to constitutive NFκB activity as will be discussed in section 1.9.

The findings of the studies described provide evidence for the development of inhibitors specific to the NFκB signalling pathway as a therapeutic strategy for CTCL (116). Notably, elevated NFκB activity is also a key feature of other mature T-cell lymphomas including adult T-cell leukaemia/lymphomas (ATLL) and some subtypes of PTCL in addition to mature B-cell malignancies such as chronic lymphocytic leukaemia (CLL) and activated B-cell diffuse large B-cell lymphoma (ABC DLBCL) (118-120). This supports the pathogenic role of dysregulated NFκB expression and further supports the development of NFκB pathway inhibitors that can be used for multiple diseases.

1.6.7 Dysregulated expression of the AP-1 transcription factor family

Our group has shown increased copy number of JUNB, an AP-1 subunit and also demonstrated elevated mRNA and protein expression of this subunit in MF and SS patients (121). More than half of the SS patients that had elevated JUNB expression also demonstrated total and (activated) phosphorylated ERK1/2 protein expression implicating the ERK1/2-AP-1 signalling pathway in the pathogenesis of advanced stage CTCL (121). JUND protein expression, another AP-1 subunit, was detected in the majority of MF patients but only rarely in SS patients, suggesting that JUND dysregulation may contribute to early stage CTCL (121). Nakayama *et al*. (2012) confirmed the findings that JUND mRNA and protein expression is increased in skin lesions from MF patients (122).

1.6.8 CTCL cells are resistant to apoptosis

CTCL cells do not have a high replicative potential but are characteristically resistant to apoptosis, which results in tumour cell accumulation (33). Constitutive NFκB activity has been shown to contribute to apoptosis resistance in SS and CTCL cell lines as discussed in section 1.6.6. Furthermore, increased NFκB activation may be responsible for overexpression of its target anti-apoptotic genes *Bcl-2, cIAP1* and *cIAP2* in CTCL (123). In addition to NFκB, CTCL cells express constitutively activate STAT3, STAT5 and c-MYC transcription factors that also regulate *Bcl-2, cIAP1* and *cIAP2* expression (124-126).

Chromosomal loss of the 10q24 region that encodes the *FAS* gene has been identified in SS (127). *FAS* encodes the cell death receptor that induces apoptosis upon engagement with Fas ligand (FASL) (127). Therefore, lack of FAS expression on malignant SS cells is a potential mechanism by which the cells could resist apoptosis (127). Our group has shown reduced FAS expression on both the mRNA and protein level in SS and demonstrated that this reduction was associated with hypermethylation of the FAS CpG island (128).

1.6.9 Dysregulated JAK/STAT signalling

Chromosomal instabilities have been reported in SS including gain of the 17q22-25 region, which encodes the STAT3, STAT5A and STAT5B transcription factors (127, 129). These transcription factors are key components of the IL-2 cytokine signalling pathway that regulates the activation, proliferation and differentiation of T-cells (127). Regions encoding IL-2 and the IL-2 receptor chains (IL-2Rα and IL-2Rβ) are also gained in SS (127). These copy number gains would likely increase IL-2 signalling and contribute to oncogenesis in SS.

Constitutive activation of the STAT3 transcription factor has been reported in tumour stage MF, SS and in CTCL cell lines (130-132). Furthermore, overexpression of STAT3 protects CTCL cells from apoptosis (130). Constitutive STAT5 activity has been identified in all stages of CTCL (133, 134). In late stage disease, these transcription factors are activated by constitutive Janus Kinases-1 (JAK1) and JAK3 activity in a cytokine-independent manner (133).

The STAT3 and STAT5 transcription factors regulate the expression of Th2 cytokines, therefore copy number gains can contribute to the skewed Th2 cytokine profile that is characteristic of CTCL (133). Furthermore, chromosomal gains of components of the IL-2 signalling pathway are likely to increase the expression of target genes that regulate cellular growth and survival (127, 135).

1.6.10 Loss of cell cycle regulators

Deletion of the 9p21 region, which harbours the cyclin-dependent kinase inhibitor 2A and cyclin-dependent kinase 4 inhibitor B (*CDKN2A*/*CDKN2B*) loci has been identified in transformed MF and SS by array-comparative genomic hybridisation (CGH) and fluorescent *in situ* hybridisation (FISH) analyses (136, 137). The *CDKN2A*/*CDKN2B* genes encode the cell cycle progression regulators $p14^{ARF}$, $p15^{INK4b}$ and $p16^{INK4a}$, which function as tumour suppressors, therefore copy number loss can contribute to the pathogenesis of CTCL (136). An alternative mechanism of $p16^{INK4a}$ inactivation in MF is hypermethylation of the CpG island in the gene promoter reported in 11% (1/9) of plaque lesions that did not progress, 43% (3/7) of plaques which progressed and in a total of 71% (5/7) of tumour lesions (138). Importantly, deletion of the *CDKN2A*-*CDKN2B* locus is associated with reduced survival in CTCL (136).

1.6.11 Genomic instability is a key feature of CTCL

MF and SS are both associated with recurrent gross genomic rearrangements and chromosomal instabilities. Genomic aberrations that occur in both diseases have been identified as well as genomic losses and gains that are unique to the diseases. These findings add to the deliberation of whether MF and SS are separate diseases or part of a disease spectrum.

In addition to harbouring *CDKN2A*/*CDKN2B*, the deleted 9p21 region (see section 1.6.10) also harbours the methylthioadenosine phosphorylase (*MTAP*) gene, which encodes an enzyme important for the salvage of adenine and methionine (137). Our group has shown that copy number loss of *MTAP*, identified by quantitative reverse transcription-polymerase chain reactions (qRT-PCR), occurred more frequently than *CDKN2A* deletions in MF lesional skin and peripheral blood from SS patients (137). This copy number loss correlated with reduced MTAP mRNA expression in enriched

$CD4^+$ tumours cells from the peripheral blood of SS patients. *MTAP* loss was also identified to occur independently of *CDKN2A* loss in early stage MF (137).

In contrast to the deletion of the 9p21 region, there is a high level of genomic heterogeneity between MF and SS with distinct genomic aberrations identified in the two diseases. There is conflicting evidence of whether copy number gains or losses are more frequent in MF and SS. van Doorn *et al*. (2009) and Vermeer *et al*. (2008) used CGH analyses to identify more frequent chromosomal gains than losses in tumour-stage MF and SS, respectively (127, 129). However, Laharanne *et al*. (2010) used the same technique on a similar number of samples to show that chromosomal losses are more frequent than gains in transformed MF and SS (139).

In MF, loss of 5q13 and 9p21 and gain of 1p36.2 and 7q21-36 have been recurrently identified by array-based CGH (129). MF patients with loss of 9p21 or gain of 8q24 (encoding the proto-oncogene *cMYC*) or 1q21-1q22 have significantly reduced survival and poor prognosis compared to patients not harbouring these copy number variations (CNVs) (129).

Genomic instabilities are also frequent in SS and CGH analysis has identified loss of the 10q25-q26, 13q21-q22 and 17p13.1 regions (127, 129, 140). The most frequent chromosomal gains in SS are those of the 8q24.1–8q24.3 and 17q23–17q25 regions (127, 129). Gain of c-MYC (8q24.1–8q24.3) and loss of the tumour suppressor gene *TP53* encoded by the 17p13.2 region are likely to contribute to the pathogenesis of SS (127). Loss of the FAS cell death receptor encoded in the 10q24 region has also been identified in SS and may contribute to apoptosis resistance as discussed in section 1.6.8 (127).

Low resolution techniques including array-based CGH, FISH, RT-PCR, qRT-PCR and microarray analyses have discovered gross genomic instabilities in CTCL and have also identified dysregulated expression of genes involved in immunopathogenesis including *CDKN2A*/*CDKN2B*, *MTAP*, *FAS*, *cMYC*, *TP53*, *STAT3*, *STAT5A* and *STAT5B*. Point mutations in genes have also been reported in CTCL. The first missense mutations were identified in the cancer-associated *NRAS* and *KRAS* genes (components of the RAS/RAF/MEK/ERK signalling pathway) in SS and MF, respectively using a mass-spectrometry based genotyping approach (141). More recently, deep sequencing techniques, which have superior resolution have

detected single nucleotide variants (SNVs), insertions, deletions and insertion-deletions (indels) in a vast number of genes that were not previously implicated in CTCL, as will be discussed in section 1.9.

1.7 Characteristic features of cancer cells

Cancer can affect any organ but most malignancies regardless of the site of tumour have common features that arise from disrupted regulation of cell proliferation and apoptosis (142). The disrupted regulatory processes that lead to neoplastic growth have been classed into six key features by Hanahan *et al*. (2000) (142) who further review two emerging hallmarks identified by more recent research (143).

The first characteristic feature is self-sufficiency to growth signals. Normal cells depend on growth signals such as cytokines or growth factors to enter an active proliferative state, however cancer cells can proliferate in a stimuli-independent manner due to oncogenic perturbations that activate signalling pathways.

The second hallmark is insensitivity to inhibitory anti-growth signals. To maintain homeostasis, normal cells receive anti-proliferative signals to regulate the cell cycle. Cancer cells become insensitive to such signals and proliferate in an unregulated manner.

The third feature is evading programmed cell death (apoptosis). Cell numbers are regulated by a balance between cell proliferation and apoptosis to maintain homeostasis. Cancer cells become resistant to apoptosis and lead to an expansion of tumour cells.

The fourth capability is limitless replicative potential. Cells have a regulatory mechanism that defines a finite number of cell divisions based on the length of telomeres in a process called senescence. Cancer cells evade senescence and result in chromosomal instabilities.

The fifth alteration is sustained angiogenesis. Blood vessels are essential for supplying oxygen and nutrients to tissues. When organs are generated, new blood vessels grow in a process known as angiogenesis, which is tightly regulated once the tissue has fully

formed. In solid cancers, angiogenesis lacks regulation and becomes sustained, resulting in a constant supply of nutrients that promote tumour growth.

The sixth hallmark is tissue invasion and metastasis. In the advanced stages of most types of cancer, tumour cells migrate (metastasise) from the primary tumour and invade other tissues.

The first emerging hallmark is avoiding immune attack and destruction by T- and B-cells, natural killer cells and macrophages. These cell types are fundamental in immune surveillance and clearing emerging cancer cells, however tumours cells can avoid eradication by mechanisms which currently remain unclear and require further investigations.

The second emerging characteristic is deregulated cellular energetics. This capability enables the tumour cells to change the cellular metabolism to allow constant growth and proliferation.

1.8 Driver and passenger mutations and tumour mutation burden

1.8.1 Driver and passenger mutations

With each mitoses from the stage of fertilisation, somatic DNA replication errors known as mutations are acquired and accumulate in cells (Figure 1. 6) (144). The errors can be passenger or driver mutations. Passenger mutations are present in both normal and tumour (transformed) cells but do not alter cellular growth, proliferation or survival and therefore do not contribute to tumourigenesis (145). Driver genes however, are only identified in tumour cells as they provide a selective growth and survival advantage and contribute to oncogenesis (145). Metastatic and advanced stage tumours can harbour multiple driver gene mutations that further amplify the growth advantage and make the malignancy more aggressive (145). Driver mutations arise due to intrinsic DNA replication errors, lifestyle and environmental factors and as chemotherapy-resistant mutations (144). Chemotherapy-resistant mutations are acquired in patients who achieve clinical remission but then relapse due to the emergence of new drug-associated driver mutations that induce resistance to the specific therapeutic agent (144). As a result, tumour cells continue to grow faster and

survive longer than non-transformed cells (144). Examples of chemotherapy-resistant mutations will be discussed in section 1.16.2.

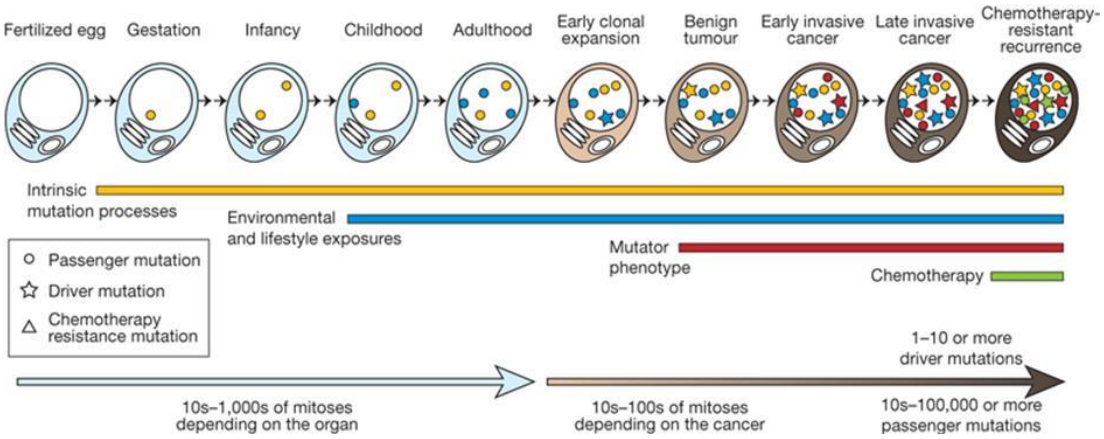

Figure 1. 6. The accumulation of somatic passenger and driver gene mutations in cells. Passenger mutations are acquired from intrinsic DNA replication errors and exposure to mutagens but do not confer cellular growth advantages. The acquisition of driver mutations provides a selective growth advantage to transformed cells, leading to clonal expansion and oncogenesis. Multiple driver gene mutations are identified in advanced stage cancer and chemotherapy-resistant mutations can arise in response to therapeutic agents. Image adapted from Stratton *et al*. (2009) (144).

1.8.2 Tumour mutation burden

The tumour mutation burden is defined as the number of somatic mutations within a tumour (146). The tumour mutation burden varies between different cancer types and between patients with the same malignancy. Alexandrov *et al*. (2013) show that the frequency of somatic mutations varies more than 1,000 fold in 7,042 primary tumours (507 analysed by whole-genome sequencing (WGS) and 6,535 by whole-exome sequencing (WES)) from 30 types of cancers (Figure 1. 7) (146). Pilocytic astrocytoma tumours (a paediatric malignancy) have the fewest mutations and Melanoma had the greatest median number of somatic mutations (146). Haematological and paediatric malignancies harboured fewer somatic mutations (Figure 1. 7; left of the graph) compared to solid tumours induced by carcinogens including UV radiation (Melanoma) and tobacco smoke (malignancies affecting the lungs) (Figure 1. 7; right of the graph) (146). In contrast to other haematological

malignancies that have low mutation frequencies, CTCL tumours have a high mutation rate that is comparable to mutagen-associated solid tumours including lung cancers and melanoma (70, 147, 148).

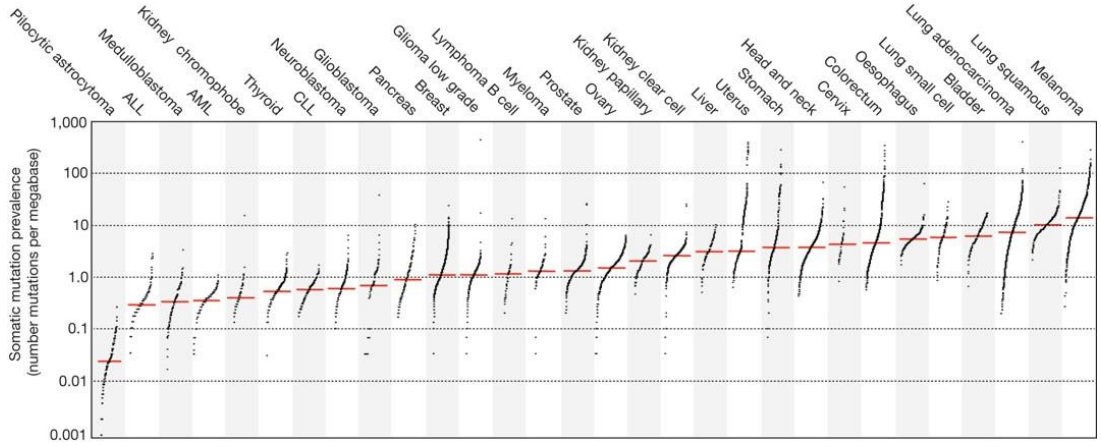

Figure 1. 7. The intra- and inter-variation of somatic tumour mutation burden in different malignancies. Mutation frequencies identified from whole-genomes and whole-exomes of 7,042 tumours from 30 solid and haematological malignancies. The number of mutations per megabase are shown on a logarithmic scale with dots representing individual samples and red lines representing the median number of mutations. ALL: acute lymphoblastic leukaemia, AML: acute myeloid leukaemia, CLL: chronic lymphocytic leukaemia. Figure adapted from Alexandrov *et al*. (2013) (146).

Solid tumours can harbour hundreds or even thousands of genetic variations, however only a few of these are driver mutations, which promote oncogenesis and the remaining are passenger mutations (149). A prominent example of a driver gene mutation is observed in advanced melanoma in which half of the patients have mutations in the *BRAF* gene, with p.V600E being the most frequent mutation (150). In contrast, no single gene mutation has been associated with such a high number of CTCL cases. The identification of somatic driver gene mutations amongst the vast number of passenger mutations detected by next-generation sequencing (NGS) is particularly challenging as CTCL tumours are genetically heterogeneous with SNVs identified in many different genes within one tumour. The first step in identifying somatic mutations is to sequence matched non-tumour DNA from patients to enable germline mutations to be filtered out. Thereafter, multiple bioinformatic

methodologies developed to aid the distinction of driver from passenger gene mutations can be applied. The first approach is frequency based and includes filtering out genes previously identified to be false positives by exome sequencing and then prioritising genes mutated in more than 5% of tumours (151). The second approach includes applying the "20/20 rule" proposed by Vogelstein *et al*. (2013) (149). This rule suggests that if more than 20% of the variants are recurrent missense mutations, then the gene is likely to be an oncogene, whereas genes with more than 20% of the mutations being truncations (and predicted to be inactivating) are probable tumour suppressor genes (Figure 1. 8) (149).

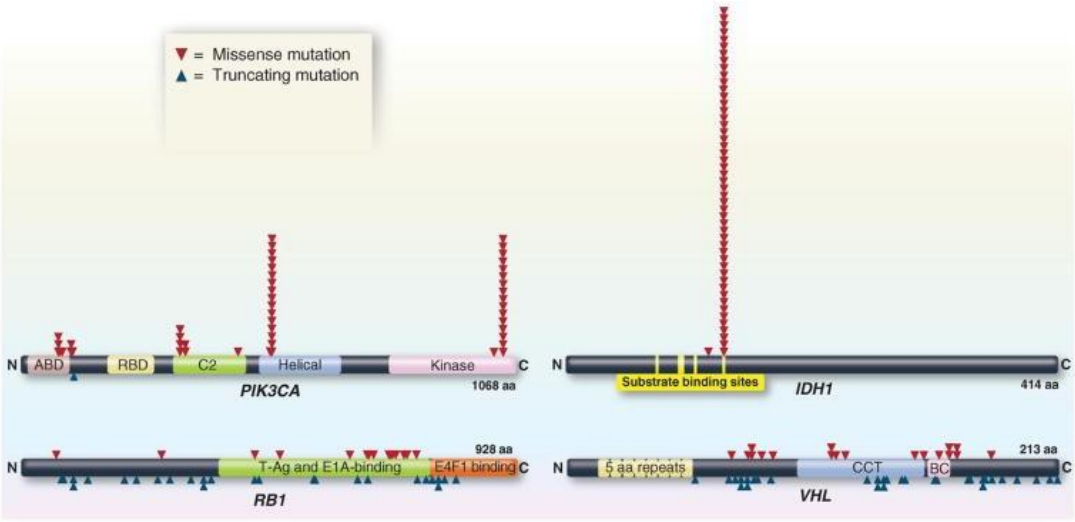

Figure 1. 8. Mutation distribution in oncogenes and tumour suppressor genes. The *PIK3CA* and *IDH1* oncogenes harbour recurrent missense mutations (red inverted triangles) in their functional protein domains. The tumour suppressor genes *RB1* and *VHL* harbour truncating mutations (blue triangles) throughout the genes. Figure adapted from Vogelstein *et al*. (2013) who analysed data from all cancer types using the Catalogue of Somatic Mutations in Cancer (COSMIC) database (149).

The third approach to identify driver mutations is by using the MutSigCV algorithm to determine which genes are mutated at a significantly higher rate than background gene mutations (152). Once the genes that potentially harbour driver mutations have been short-listed, pathogenicity prediction algorithms such as SIFT, Provean, PolyPhen2, Mutation Taster, MutPred2 and CADD can be used to predict the likely effect of mutations on the structure and/ or function of the encoded protein to enable

further prioritisation of which mutations may be drivers (153-158). These bioinformatic approaches can help filter out likely passenger mutations and generate a short-list of candidate driver mutations, but only functional analyses can confirm whether a variant is indeed a true driver gene mutation.

1.9 Genetic landscape of CTCL

Numerous studies including our own (147), have used NGS including WGS, WES, targeted capture sequencing (TCS), CNV analysis and whole-transcriptome analysis to investigate the genetic architecture of SS and advanced stage MF (Appendix Table 1). This section will highlight the findings and limitations of these studies.

1.9.1 CTCLs have prevalent UV signature mutations

Transition mutations, C>T or G>A, have been frequently identified in CTCL tumours by NGS studies (67, 69, 70, 147, 148). Such mutations are commonly induced by mutagenic UV exposure (159). CC>TT transitions of dinucleotide variants are also a UV mutation signature that have been highly detected in MF and SS tumours (67, 70, 148, 159). Such high rates of CC>TT dinucleotide transitions are also observed in the solid malignancy melanoma, in which UV exposure is a risk factor (148). Interestingly, the frequency of mutations with a UVB signature in SS is elevated compared to the other haematological malignancies including acute lymphoblastic leukaemia and acute myeloid leukaemia (AML) and is comparable to the frequency observed in non-melanoma cancers, namely squamous cell carcinomas (SCC) (70). This suggests that UV exposure may be causative in generating the CC>TT dinucleotide variants in SS (148). The high UVB signature suggests that neoplastic cells originate in the skin and then spread to peripheral blood in SS and supports the theory that MF and SS are part of the same disease spectrum.

CC>TT dinucleotide variants are rare occurrences in non-haematological malignancies including breast cancer, colon and rectal cancers, ovarian cancer, squamous cell lung cancer and lung adenocarcinoma (70, 148). In contrast to the frequent transitions detected in CTCL, B-cell cancers including CLL and malignant B-cell lymphomas have frequent T>G transversions and solid malignancies including

breast, colorectal, liver cancers and neuroblastomas are characterised by C>A transversions (146).

1.9.2 CTCLs harbour mutations in genes that alter key cellular processes and pathways

NGS studies performed on CTCL tumours have identified several signalling pathways and cellular processes to harbour mutations in genes involved in T-cell activation: *PLCG1*, *CD28*, *CARD11*, *VAV1*, *MALT1*, *NFAT5* and *NFKB2*; IL-2 signalling: *JAK1*, *JAK3*, *STAT3* and *STAT5*; epigenetic modification and chromatin remodelling: *ZEB1*, *ARID1A*, *TET2*, *DNMT3A*, *MLL2*, *MLL3* and *SETD1A*; genome maintenance: *POT1*, *ATM* and cell cycle regulation: *TP53* and *CDKN2A* (67-71, 147, 148, 160, 161). Pathways and processes identified to harbour gene mutations by NGS studies are schematically represented in Figure 1. 9.

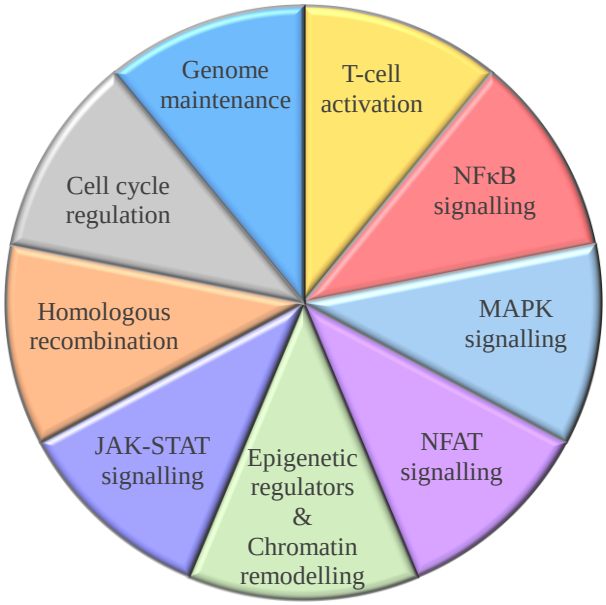

Figure 1. 9. Signalling pathways and processes identified to harbour gene mutations in CTCL by NGS studies. The size of each segment is not representative of the proportion of genes affected per pathway or process.

Different studies have identified identical gene mutations leading to the discovery of hotspot mutations, for example the *PLCG1* c.C1034T (p.S345F) mutation has been detected by all sequencing studies on CTCL samples, except by da Silva Almeida *et al*. (2015), who nevertheless identified other mutations in this gene (69). A meta-analysis of 220 CTCL samples analysed by nine NGS studies revealed that the most frequently mutated genes are the cell cycle regulation gene *TP53* and the TCR signalling gene *PLCG1* (162). Our NGS study also identified *PLCG1* to be frequently mutated in 11% (11/101) of SS tumours (147). Dysregulated TCR signalling is a key feature of CTCL that has been well established prior to NGS studies using array-based CGH, FISH, RT-PCR, qRT-PCR and microarray analyses. However, specific gene mutations were not identified by these techniques and deep sequencing studies have revealed a wealth of data on mutations of numerous genes involved in T-cell activation, proliferation, differentiation and death.

Functional interrogations of some of the identified mutations have been performed. McGirt *et al*. (2015) showed that HUT-78 cells, which harbour the activating JAK3 p.A573V mutation reported in MF, have increased downstream signalling as determined by elevated phosphorylated STAT5 (p-STAT5) expression (148). The authors further showed that treating three CTCL cell lines, HUT-78, HH and MyLa with the JAK3 inhibitor Tofacitinib reduced cell numbers and also reduced p-STAT5 expression in HUT-78 and Myla cells (148). These data support the use of JAK3 inhibitors for CTCL patients with *JAK3* mutations and in patients with elevated JAK3/STAT5 signalling (148). Notably, Tofacitinib is a Food and Drug Administration (FDA) approved drug that is already used to inhibit proliferation of activated T-cells in rheumatoid arthritis (148). Kiel *et al*. (2015) have shown that primary cells from SS patients harbouring the JAK1 p.Y654F and p.L710V mutations had reduced proliferation and inhibited phosphorylation of STAT1, STAT3 and STAT5 when treated with JAK inhibitor I (68). The JAK inhibitor I potently inhibits JAK2 and JAK3 in addition to JAK1. Ruxolitinib, a JAK1 and JAK2 inhibitor has been shown to decrease proliferation and induce moderate levels of apoptosis in MyLa, HUT-78 and HH cells (163). Ruxolitinib treatment also induced a strong reduction in DNA synthesis in all three cell lines, suggesting that the JAK inhibitor interferes with this process to inhibit cell growth rather than inducing apoptosis (163). Furthermore, the inhibitor reduces STAT3 and STAT5 activation in all three cell lines,

particularly in HUT-78 cells, which harbour the JAK1 p.Y654F mutation, demonstrating that JAK signalling is more sensitive to inhibition in the presence of JAK mutations (163). The gain-of-function mutations identified by NGS studies present an additional mechanism to copy number gains that can lead to constitutive JAK-STAT signalling in CTCL.

CARD11 is key TCR signalling protein. The CARD11 mutations p.S615F and p.E626K have been shown to significantly increase NFκB luciferase reporter activity in HEK293T and Jurkat cells (69). Furthermore, these mutations increase JNK phosphorylation after stimulation of Jurkat cells with phorbol 12-myristate 13-acetate (PMA), demonstrating that the mutations activate the mitogen-activated protein kinase (MAPK) pathway (69).

Wang *et al*. (2015) identified a significant difference in the elevated expression of the *CARD11*, *CCR4* and *PLCG1* genes in SS patients with mutations compared to healthy controls (70). However, no significant difference in gene expression was detected in patients with and without mutations in the three genes suggesting that patients without mutations in these genes may have other perturbations that increase the expression of these genes (70).

Choi *et al*. (2015) showed that the CD28 p.F51V mutation increases IL-2 expression in stimulated Jurkat cells but not in basal conditions, demonstrating that this mutation requires stimulation to induce its potential and is therefore not a true gain-of-function mutation that can trigger oncogenesis (67).

RLTPR is a scaffold protein that is involved in CD28 signalling (164). The RLTPR p.Q575E mutation has been shown to elevate IL-2 mRNA production in Jurkat cells upon stimulation with the CD86 ligand of the CD28 receptor, but not in basal conditions demonstrating that this mutation cannot drive tumourigenesis in a stimulation-independent manner (162).

Vaqué *et al*. (2014) have shown that the PLCγ1 p.S345F and p.S520F mutations significantly elevated NFAT-luciferase reporter activity in HEK293T cells, which can be reduced by treatment with the calcineurin inhibitor FK-506 and the PLC inhibitor U73122 (160). Treating the CTCL cell lines, MyLa and HUT-78, with FK-506 reduced cell proliferation, viability and also NFAT activity (160). Of note, these cells do not harbour *PLCG1* mutations (160), therefore it remains to be determined whether

cells harbouring gain-of-function *PLCG1* mutations are sensitive to FK-506 and U73122. Immunohistochemical analysis of skin samples from MF patients harbouring the p.S345F mutation show nuclear localisation of NFAT, suggesting constitutive transcriptional activity (160). No such difference was detected in nuclear expression of the NFκB subunits p50 and p52 in MF patients with the p.S345F or p.S520F mutations (160).

Although many gene mutations identified in CTCL have been functionally interrogated, a vast number of variants remain to be investigated to determine whether they are driver gene mutations.

1.9.3 Copy number alterations frequently occur in CTCL

CNV analysis performed using SNP arrays, WGS, WES and TCS data have confirmed the CNVs identified using array-based CGH, FISH, RT-PCR, qRT-PCR and microarray analysis including amplification of *STAT3* and *STAT5B* (67, 147) and loss of *CDKN2A*, *FAS* and *TP53* (67). As discussed in section 1.6, gain of *STAT3* and *STAT5B* is likely to elevate the expression of cytokines that contribute to the Th2 predominant microenvironment in CTCL. Loss of the tumour suppressor *TP53*, cell cycle regulator *CDKN2A* and the *FAS* cell death receptor also likely contribute to the immunopathogenesis of CTCL (0). Notably, NGS has identified that genes affected by CNVs also harbour point mutations with *TP53* being a prominent example (67, 69, 70, 147, 160, 161).

NGS sequencing has revealed copy number alterations of genes not previously implicated in CTCL (67-69, 71, 147, 161). Copy number loss has been reported in genes involved in chromatin remodelling: *ARID1A*, *ARID5B*, *SMARCC1* and *ZEB1*; histone methyl transferases: *MLL2*, *MLL3*, *MLL4*, *SETD1A*, *SETD1B*, *SETDB2* and *SETD6*; epigenetic modulator: *NCOR1*; DNA methyltransferases: *DNMT3A*, *DNMT3B*, *TET1* and *TET2*; cell cycle regulators: *CDKN1B* and *RB1*; T-cell activation: *JAK2*; homologous recombination: *BRCA2* and telomere maintenance: *ATM* (67, 68, 147). Copy number gains were identified in genes involved in T-cell activation *PRKCQ*, homologous recombination *RAD51C*, tumour suppressor regulation *PREX2* and STAT3 regulation *SOCS7* (67, 147).

CTCL has a higher number of CNVs compared to other malignancies reported in The Cancer Genome Atlas database as demonstrated by Choi *et al*. (2015) (67). The authors firstly showed that CTCL has an elevated ratio of somatic CNVs to SNVs in *TP53* compared to solid cancers and in *DNMT3A* compared to the haematological malignancy AML (Figure 1. 10. A) (67). Furthermore, deletions in CTCL were identified to be more prevalent than SNVs and amplifications combined, compared to other solid and liquid tumours (Figure 1. 10. B) (67). The prevalence of CNVs in CTCL may be attributable to mutations in key genome maintenance genes including *POT1* and *ATM*, as identified by our NGS study (147).

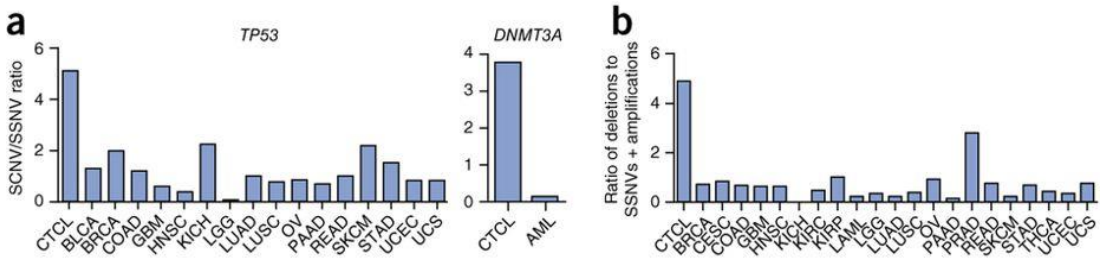

Figure 1. 10. The ratio of somatic CNVs to SNVs is amplified in CTCL. (A) CTCL has a higher proportion of somatic CNVs to SNVs in *TP53* and *DNMT3A* compared to solid cancers and the haematological malignancy AML, respectively. (B) Deletions are more prevalent than SNVs and amplifications in CTCL compared to other cancers. BLCA: bladder cancer, BRCA: breast cancer, COAD: colon cancer, GBM: glioblastoma multiforme, HNSC: head and neck squamous cell carcinoma, KICH: chromophobe renal cell carcinoma, LGG: lower grade glioma, LUAD: lung adenocarcinoma, LUSC: lung squamous cell carcinoma, OV: ovarian serous cystadenocarcinoma, PAAD: pancreatic ductal adenocarcinoma, READ: rectum adenocarcinoma, SKCM: cutaneous melanoma, STAD: stomach adenocarcinoma, UCEC: uterine corpus endometrial carcinoma, UCS: uterine carcinosarcoma, AML/LAML: acute myeloid leukaemia, CESC: cervical cancer, KIRC: clear cell kidney carcinoma, KIRP: papillary kidney carcinoma, PRAD: prostate adenocarcinoma, THCA: papillary thyroid carcinoma. Figure adapted from Choi *et al*. (2015) (67).

The CNVs reported in CTCL are likely to disrupt multiple signalling pathways and cellular processes in tumours. Loss of one copy (loss of heterozygosity) of the *ZEB1* and *ARID1A* genes and a homozygous deletion of *CDKN2A* have been shown to significantly correlate with reduced gene expression in SS (70). The functional consequences of the large number of genes affected by CNVs remain to be investigated.

1.9.4 Chromosomal translocations are infrequent in CTCL

WGS and RNA sequencing studies have reported chromosomal translocations in CTCL tumours (67, 68, 70, 161). The translocations result in the abnormal fusion genes *CARD11-PIK3R3*, *CD28-CTLA4*, *IKZF2-GLI2*, *FASN-SGMS1*, *SGMS1-ZEB1*, *TYK2-UPF1*, *COL25A1-NFKB2*, *SPATA21-RASA2*, *TPR-MET* and *MYBL1-TOX*. Furthermore, Ungewickell *et al*. (2015) used a software based approach to detect structural variations in MF and SS and identified gain of *TNFRSF1B*, *NFKB2* truncations and the *CTLA4-CD28* and *CD274-RAD51B* (PD1-RAD51B) fusion genes (71). Copy number gain of *TNFRSF1B* correlates with increased gene expression levels in MF and SS tumours and with TNFR2 (encoded by *TNFRSF1B*) protein expression in the HH cell line, which harbours this copy number gain (71). The CTLA4-CD28 fusion results from a deletion on chromosome 2 that juxtaposes the extracellular portion of CTLA-4, a negative regulator of TCR signalling, with the activating cytoplasmic tail of CD28, a co-stimulatory protein for T-cell activation. Jurkat cells overexpressing the CTLA4-CD28 fusion demonstrated increased cell proliferation compared to cells transfected with CTLA-4 alone, implicating the oncogenic potential of the fusion protein in CTCL (71).

In comparison to the 218 CTCL tumours analysed by WES (67-71, 147, 161), only 13 have been investigated by WGS (67, 68, 148). The structural rearrangements including translocations and gene fusions reported are therefore unlikely to be fully exhaustive. WGS analyses on a greater number of samples would also provide information on aberrations in gene regulatory regions that may contribute to pathogenesis.

Despite the low number of WGS studies performed on SS tumours, the occurrence of translocations is notably rare compared to other haematological malignancies. A prime

example is the balanced *BCR-ABL* translocation reported in around 90% of chronic myeloid leukaemia cases and encodes a constitutively active tyrosine kinase (165).

1.9.5 Frequently perturbed pathways in CTCL

The complex heterogeneity of CTCL tumours, harbouring an admixture of SNVs, CNVs and structural alterations can alter multiple signalling pathways. As described in this section, the NGS studies have identified perturbations of genes involved in several signalling pathways and cellular processes including T-cell activation via the MAPK, NFκB and NFAT pathways and the TNFR2, CD28 and CTLA-4 receptors; IL-2-JAK-STAT pathway, epigenetic regulators and chromatin remodelling, genome maintenance, cell cycle regulation and homologous recombination (67-71, 147, 148, 160, 161). A meta-analysis of 220 CTCL tumours identified genes that were not implicated by the smaller individual studies including genes involved in signalling via the TCR (*PTPRN2* and *RLTPR*), NFκB (*PRKCB* and *CSNK1A1*), MAPK (*MAP2K1* and *NF1*) and cellular processes including immune surveillance (*CD58* and *RFXAP*) and chromatin remodelling (*BCOR*, *KDM6A*, *SMARCB1* and *TRRAP*) (162). The pathways and cellular processes predicted to be affected by SNVs and CNVs identified in CTCL tumours are schematically represented in Figure 1. 11.

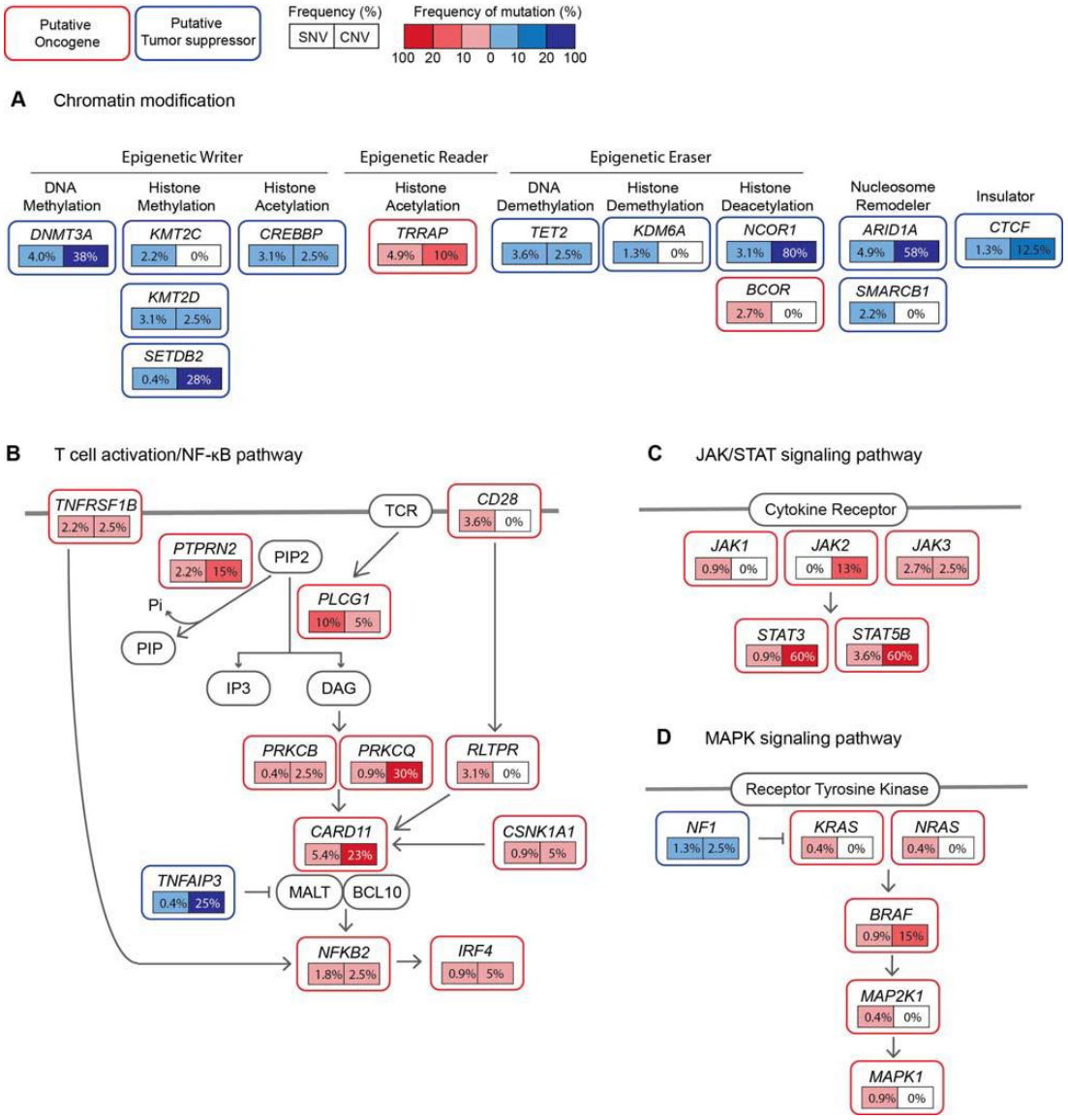

Figure 1. 11. Pathways affected by recurrent mutations in CTCL. The frequency of SNVs (left box) and CNVs (right box) per gene involved in (A) chromatin modification processes, (B) T-cell activation and NFκB signalling, (C) JAK/STAT signalling and (D) MAPK signalling are represented. Potential oncogenes and tumour suppressor genes are highlighted in red and blue, respectively and darker shades indicate a higher aberration frequency. The SNV frequencies were determined by Park *et al*. (2017) and CNV frequencies by Choi *et al*. (2015) (67, 162). Figure adapted from Park *et al*. (2017) (162).

As mentioned, the DNA damage response and T-cell activation pathways were the most frequently perturbed in CTCL and *TP53* (14%) and *PLCG1* (9%) were the most frequently mutated genes in these pathways, respectively (162). This finding was confirmed by Chang *et al*. (2018) who analysed 139 CTCL tumours from seven NGS studies and identified that 19% of tumours harboured *TP53* mutations and 10% had *PLCG1* mutations (166). Importantly, this meta-analysis identified that mutations of the NFκB signalling genes *PLCG1*, *TNFRSF1B* and *CARD11* were mutually exclusive, suggesting that mutations in any one of these genes is adequate to disrupt signalling and induce oncogenesis in SS (166). *PLCG1* mutations have been identified in CTCL by several NGS studies and the encoded protein (PLCγ1) plays a pivotal role in TCR signalling (as will be discussed in section 1.13). This thesis will therefore focus on functionally interrogating *PLCG1* mutations to determine their effect on TCR signalling components.

NGS studies have collectively identified frequent aberrations in key pathways and some SNVs, CNVs and structural rearrangements increase T-cell signalling, gene expression, proliferation and survival *in vitro,* demonstrating the ability to drive lymphomagenesis. Thus, the perturbed pathways and particularly the mutated genes highlight key therapeutic targets and provide evidence for the development of novel mutation-specific inhibitors.

1.9.6 Limitations of NGS analyses in CTCL

Although NGS studies have uncovered a wealth of information on the genetic architecture of CTCL these studies have limitations. Deep sequencing studies have all analysed advanced stage CTCL, specifically tumour stage MF and SS, therefore the genetic events that occur in early stage MF remain to be identified. This can prove challenging as the neoplastic cells in patch and plaque stage MF are sparse in comparison to normal cells, making it difficult to identify low frequency somatic mutations by NGS.

The approach of using small discovery cohorts to identify mutated genes for targeted deep sequencing introduces a bias in the selection of genes analysed. For example, our study performed WES on 10 SS tumours and identified 549 genes to harbour somatic mutations (147). These genes were deep sequenced in 91 more patients. The mutations

identified in our discovery cohort therefore defined the genes that were selected for further analyses. The *CARD11* gene, identified to be frequently mutated in CTCL, was not mutated in our discovery patients and was therefore not deep sequenced in a larger cohort of patients (147). However, as shown by Park *et al*. (2017) and Chang *et al*. (2018), meta-analyses of NGS studies have increased statistical power to identify genes implicated in disease pathogenesis (162, 166).

NGS techniques cannot identify epigenetic changes in CTCL tumours. Immunohistochemical analysis of lesional biopsies from MF patients has identified a loss of 5-Hydroxymethylcytosine (5-hmC), an important epigenetic regulator (167). 5-hmC levels decrease as disease progresses and correlate with poor overall survival (167). Increasing the levels of 5-hmC using vitamin C in PBMCs from patients with leukaemic CTCL and nine CTCL cell lines increased apoptosis, suggesting that restoring 5-hmC in patients may have therapeutic benefits (167). This demonstrates how NGS studies alone cannot define the pathogenesis of CTCL and the perturbations identified need to be analysed in the context of epigenetic changes within the tumours.

1.10 Phospholipases

The plasma membrane is composed of a bilayer of phospholipids including phosphoinositides (PIs) (168). PIs reside in the inner leaflet/ cytosolic face of cells and make up less than 1% of the plasma membrane with phosphatidylinositol-(4,5)-bisphosphate (PIP_2) being one of the predominant cellular PIs (168). Despite being a minor component of the plasma membrane, PIP_2 has a major role in biological functions (169).

Phospholipases are fundamental enzymes that transduce inter- and intra-cellular signals by hydrolysing phospholipids, including PIP_2, to generate secondary messengers (170). Phospholipases are categorised into three major classes, PLA, PLC and PLD, based on the site these enzymes cleave phospholipids (Figure 1. 12) (170). The PLA1 and PLA2 enzymes hydrolyse phospholipids to produce saturated and unsaturated fatty acids, respectively. PLC cleaves phospholipids to produce inositol 1,4,5-trisphosphate (IP_3) and diacylglycerol (DAG) and hydrolysis of phospholipids by PLD generates phosphatidic acid (PA). The secondary messengers produced by the three phospholipase classes have diverse cellular functions, which initiate signalling cascades that promote cell survival, proliferation, differentiation, migration and apoptosis (170). Thus, dysregulated phospholipase activity is highly likely to contribute to tumorigenesis.

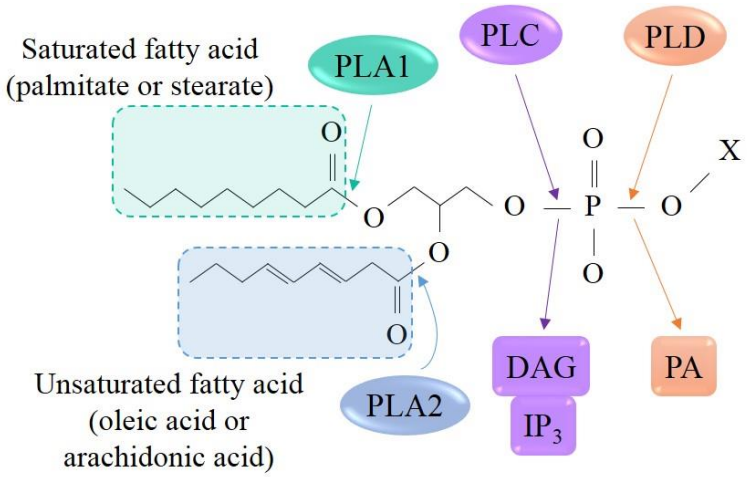

Figure 1. 12. Cleavage sites of phospholipases. The three major classes of phospholipases, PLA, PLC and PLD, are categorised by the position they cleave phospholipids, to generate secondary messengers that have diverse cellular functions. Figure adapted and modified from Park *et al*. (2012) (170).

1.11 The Phospholipase C family

Thirteen phospholipase C (PLC) enzymes have been described in mammals and are categorised into six families (PLCβ1-4, PLCγ1-2, PLCδ1, PLCδ3-4, PLCε, PLCζ and PLCη1-2) (Figure 1. 13) (170). Phospholipases are inactive in resting cells but mediate inter- and intra-cellular signalling when cells are activated (170). Therefore, the regulation of phospholipase activity is fundamental and PLC enzymes regulate their own activity by auto-inhibition (171).

The PLCγ isozymes have a unique protein domain arrangement known as the γ-specific array, which comprises of the split PH, nSH2, cSH2, SH3 domains located between the catalytic X-Y domains (Figure 1. 13) (172). In contrast, the other five PLC families have a linker between the X-Y domains (Figure 1. 13) (172). The γ-specific array in the PLCγ isozymes interacts with the X-Y catalytic domains and blocks substrate accessing the active site as a means of protein auto-inhibition (172) as described in detail in section 1.13.3. The linker between the X and Y catalytic domains in the PLCβ, PLCδ, and PLCε isoforms mediates auto-inhibition, facilitated by the negative charged residues in the linker repelling the enzymes from the negatively charged plasma membrane (171). This repulsion prevents substrate accessing the active site of these phospholipases (171). Upon interaction of upstream signalling proteins such as Rac, the negative residues in the X-Y linkers are repositioned, enabling PIP_2 to access the active site (171).

The function and regulation of the PLCη isozymes is not well characterised and requires further investigations (173). The PLCζ isozyme is expressed in sperm unlike the other PLCs, which are expressed in somatic cells (174). The X-Y linker of PLCζ contains positively charged residues and does not mediate auto-inhibition but increases protein activity, suggesting a unique function of the gamete-specific PLCζ X-Y linker (174).

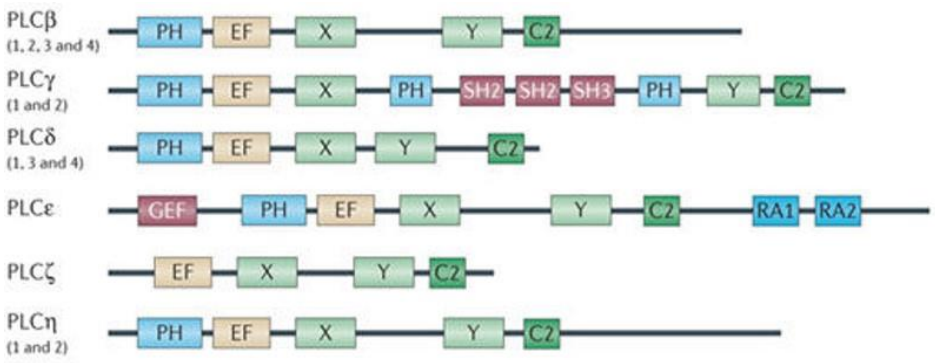

Figure 1. 13. The protein domain organisation of six PLC families. Thirteen PLC isozymes are categorised into six families. Figure adapted from Park *et al*. (2012) (170).

1.12 An introduction to PLCγ1 and PLCγ2

PLCγ1 is ubiquitously expressed in all tissues and is encoded by the *PLCG1* gene (175). PLCγ2 is a closely related isozyme that is encoded by the *PLCG2* gene on chromosome 16, whilst *PLCG1* is located on chromosome 20 (176). Both isoforms have an identical protein domain arrangement encoded by 32 exons. PLCγ1 and PLCγ2 have high sequence homology across key functional domains (Figure 1. 14) (175, 176).

The PLCγ isozymes comprise of five core domains (PH, EF, X, Y and C2) and four domains in the γ-specific array that mediates auto-inhibition (Figure 1. 14. A). When the protein adopts its 3D folded conformation, the core domains interact to form the PLCγ catalytic core (Figure 1. 14. B). The cSH2 domain in the γ-specific array forms an auto-inhibitory interaction with the triosephosphate isomerase (TIM) barrel of the catalytic X-Y domains and is therefore fundamental for regulating protein activity and maintaining PLCγ in an inactive state (172).

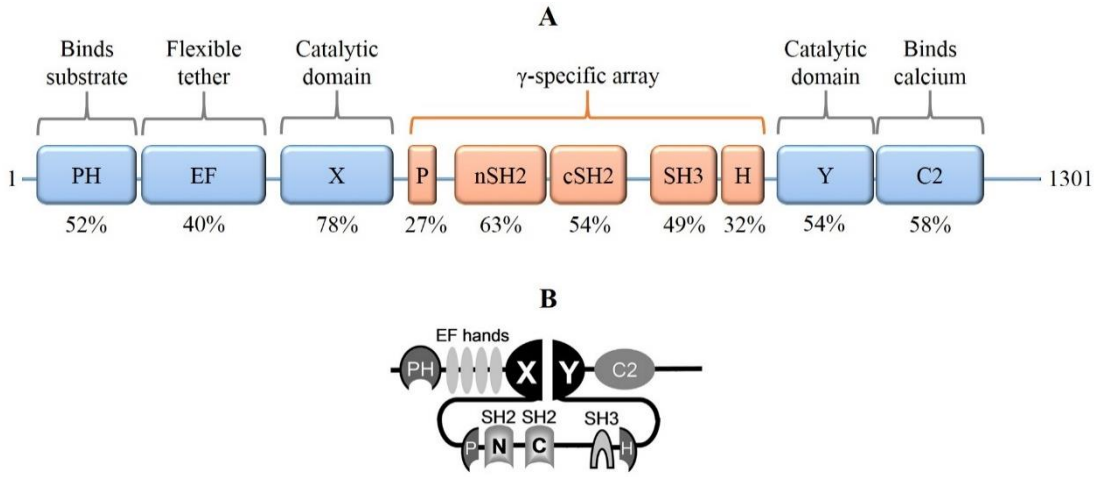

Figure 1. 14. Schematic representation of PLCγ (1 and 2) protein domain organisation. (A) PLCγ1 and PLCγ2 have high sequence homology in most functional protein domains as represented by the percentages. Figure adapted and modified from Koss *et al*. (2014) (175). (B) In the 3D protein conformation, the catalytic X-Y domains interact to form the TIM-barrel, which interacts with the cSH2 domain of the γ-specific array to regulate protein activity by auto-inhibition. Figure adapted and modified from Poulin *et al*. (2005) (177).

The PH domain mediates phospholipid substrate binding and stabilises PLCγ at the membrane (170, 178). The EF domain forms a flexible tether between the PH and X domain (170). The C2 domain binds calcium ions and mediates interactions with the membrane (170). The split PH domain defines the n- and c-terminals of the γ-specific array. The n-terminal SH2 (nSH2) domain is essential for mediating interactions of PLCγ with receptor tyrosine kinases (RTK) and non-receptor tyrosine kinases (nRTK) (170). The SH3 domain is a protein-protein interaction domain, which binds proline-rich motifs on adapter proteins that are involved in signal transduction (170).

PLCγ1 transduces signals from numerous cell surface receptors including the TCR, vascular endothelial growth factor receptor (VEGFR), hepatocyte growth factor receptor (HGF), platelet-derived growth factor receptor (PDGFR), epidermal growth factor receptor (EGFR), fibroblast growth factor receptor (FGFR) and nerve growth factor receptor (NGFR) (Figure 1. 15) (179). Engagement of these receptors by antigens or growth factors activates PLCγ1, which triggers extensive signalling cascades to activate the NFκB, NFAT and AP-1 transcription factor families (180).

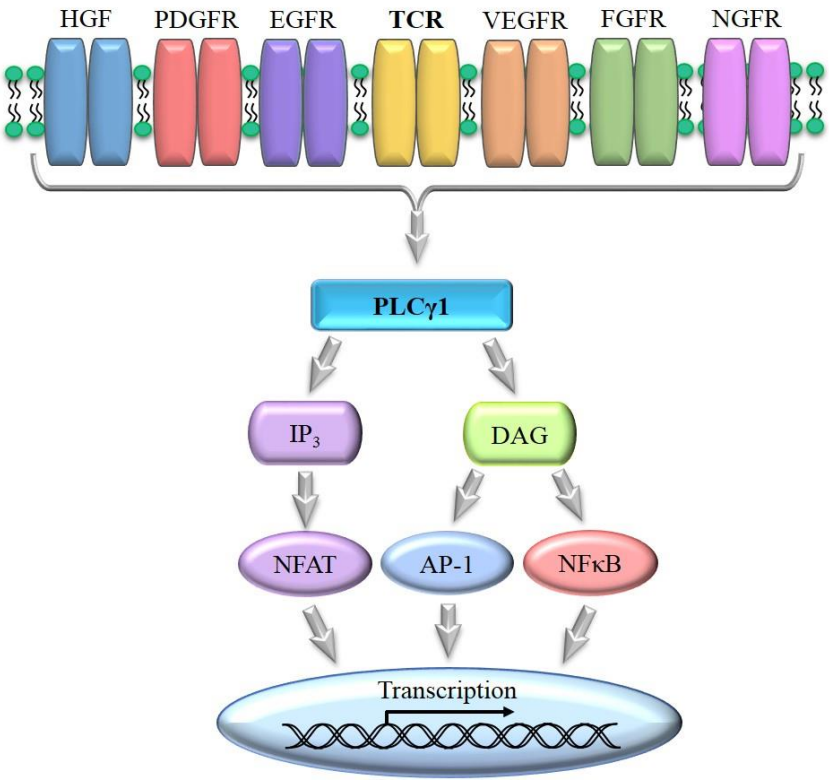

Figure 1. 15. PLCγ1 mediates signalling from several cell surface receptors to key transcription factors that regulate gene expression.

Unlike PLCγ1, PLCγ2 is mainly expressed in cells of a haematopoietic lineage, including B lymphocytes, mast cells, natural killer cells and platelets but is also expressed at lower levels in T-cells (181). PLCγ2 has an analogous role to PLCγ1 in mediating B-cell receptor (BCR) and TCR signalling, respectively (Figure 1. 16) and like PLCγ1, PLCγ2 is also activated by growth factors (175). Notably, PLCγ1 is also expressed in B-cells (182). PLCγ2 has been reported to be expressed in primary T-cells and plays a role in TCR signalling and T-cell selection when PLCγ1 is depleted in mice, demonstrating functional redundancy between PLCγ1 and PLCγ2 (181). On the contrary, expression of basal levels of PLCγ1 were not sufficient to restore platelet activation in PLCγ2-deficient mice unless PLCγ1 expression levels were increased to those of PLCγ2 in platelets (183).

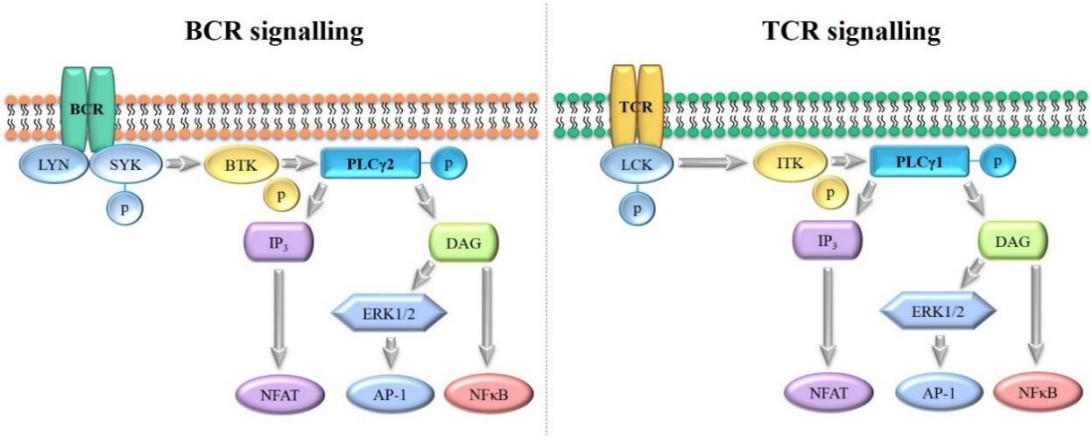

Figure 1. 16. PLCγ2 and PLCγ1 have analogous roles in BCR and TCR signalling. The enzymes trigger signalling cascades to activate the NFAT, AP-1 and NFκB transcription factor families in B- and T-lymphocytes.

1.13 The pivotal role of PLCγ1 in TCR signalling

1.13.1 The T-cell receptor

The TCR on the majority of T-cells is formed of an α and β chain heterodimer, whilst in 5-10% of T-cells the receptor is a heterodimer composed of a γ and δ chain (184). The αβ-TCR has short intra-cytoplasmic regions which lack signalling domains (185). The TCR is therefore non-covalently linked to the CD3 complex (which comprises of the γε and εδ heterodimers) and the TCR ζ chains (Figure 1. 17) (185). The TCR, CD3 complex and the ζ chains form the TCR-CD3 complex. The CD3 molecules and ζ chains encompass immunoreceptor tyrosine-based activation motifs (ITAMs), which harbour tyrosine phosphorylation residues that are fundamental for signal transduction from the TCR (Figure 1. 17).

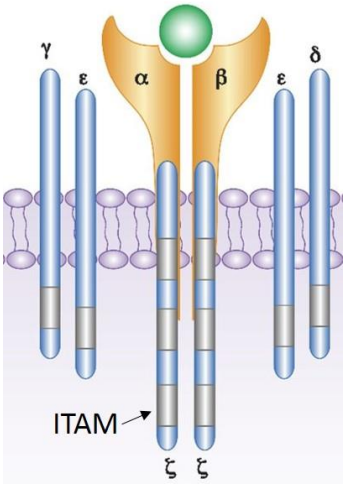

Figure 1. 17. The TCR structure. The TCR is composed of an α and β heterodimer that associates with the γε and εδ CD3 heterodimers and two ζ chains. The CD3 dimers and ζ chains harbour ITAMs, which are phosphorylated during T-cell activation to mediate signal transduction. Figure adapted and modified from Jahan *et al*. (2016) (186).

1.13.2 TCR activation and signalling to PLCγ1

A schematic representation of the TCR signalling pathway that will be described in the rest of section 1.13 is shown in Figure 1. 18. The TCR is activated by antigen peptide molecules presented by major histocompatibility complexes on the surface of APCs (187). CD4 is a co-receptor that assists in strengthening the interaction between the TCR and APCs (187). TCR activation triggers serial phosphorylation cascades by RTKs and nRTKs (187). The SRC-family tyrosine kinase lymphocyte-specific protein-tyrosine kinase (LCK), binds to the cytoplasmic tail of CD4 (187). LCK and the other SRC-family tyrosine kinase FYN phosphorylate the ITAMs on the CD3-γ, -δ, -ε and the -ζ chains, leading to the recruitment of the zeta-chain associated protein kinase-70 (ZAP70) (187). LCK then phosphorylates and activates ZAP70, which phosphorylates the scaffold proteins linker of activation of T cells (LAT) and SLP-76 (39, 188).

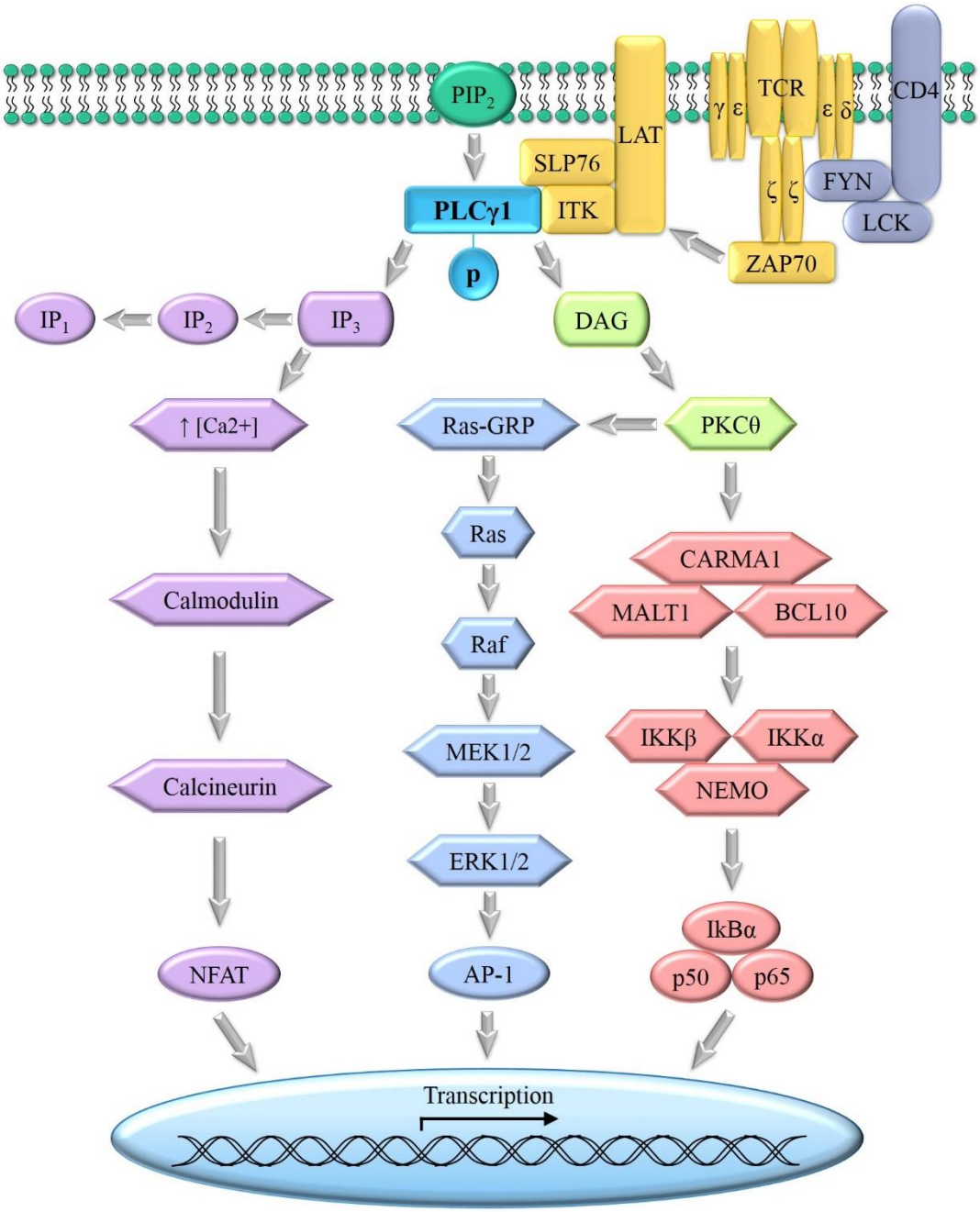

Figure 1. 18. The TCR signalling pathway. PLCγ1 is a fundamental signal transducer of TCR signalling via the secondary messengers IP_3 (metabolised to IP_2 and IP_1) and DAG, which activate the NFAT, AP-1 and NFκB transcription factors.

1.13.3 PLCγ1 auto-inhibition and activation by tyrosine phosphorylation

In resting cells, PLCγ1 localises to the cytosol (178). PLCγ1 is maintained in an inactive state by auto-inhibition to regulate the enzymes' activity. Interaction of the cSH2 domain with the catalytic X-Y domains forms the auto-inhibitory interface that blocks substrate accessing the active site and represses PLCγ1 activity (Figure 1. 19. A). The phosphorylated residues on LAT act as docking sites for the nSH2 domain of PLCγ1 and induce translocation of PLCγ1 from the cytosol to the plasma membrane, bringing the enzyme in close proximity to its substrate, PIP_2 (178, 189). The PLCγ1 PH domain stabilises the enzyme at the membrane, where PLCγ1 interacts with SLP-76 via its SH3 domain (178, 190). LCK phosphorylates and activates IL-2 inducible kinase (ITK), which phosphorylates the p.Y783 tyrosine residue on PLCγ1 and activates the enzyme (191). The phosphorylated p.Y783 residue forms a high affinity interaction with the PLCγ1 cSH2 domain and leads to a conformational shift that disrupts the auto-inhibitory interface between the catalytic X-Y and cSH2 domains (Figure 1. 19. B, C) (172). Thus, the active site of PLCγ1 is available to hydrolyse PIP_2 into the secondary messengers IP_3 and DAG (Figure 1. 20).

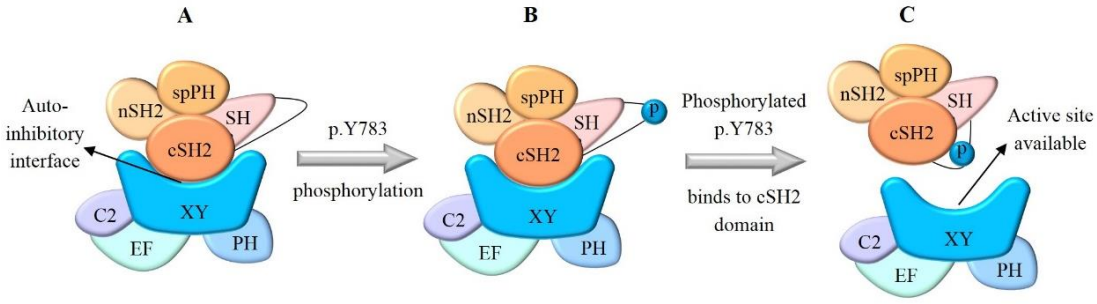

Figure 1. 19. PLCγ1 activity is regulated by auto-inhibition. (A) PLCγ1 is maintained in an inactive state by an auto-inhibitory interaction between the catalytic X-Y domains and the cSH2 domain, blocking substrate accessing the active site. (B, C) Receptor and non-receptor tyrosine kinases phosphorylate the p.Y783 residue, which then interacts with the cSH2 domain and disrupts the auto-inhibitory interface, making the active site available for substrate hydrolysis. Figure adapted and modified from Koss *et al*. (2014) (175).

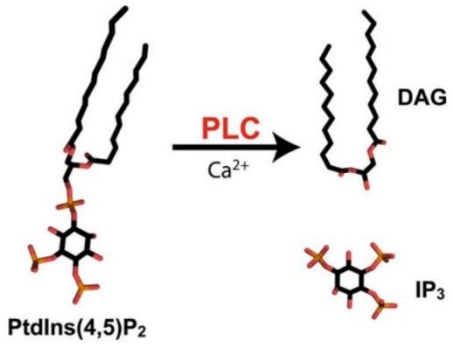

Figure 1. 20. Hydrolysis of PIP_2 by PLC isozymes. The PLC family of enzymes hydrolyse the minor plasma membrane phospholipid component PtdIns(4,5)P_2 (PIP_2) to produce the secondary messengers DAG and IP_3. Figure adapted from Gresset *et al*. (2012) (192).

ITK also phosphorylates the PLCγ1 p.Y775 residue, which contributes to activating the enzyme to a lesser extent than the p.Y783 residue (191). PLCγ1 is phosphorylated at three additional tyrosine residues (p.Y472, p.Y771 and p.Y1253) by RTKs and nRTKs, however phosphorylation of these residues does not significantly contribute to PLCγ1 activation (177, 193). Therefore, phosphorylation of the p.Y775 and p.Y783 residues are necessary and sufficient to activate PLCγ1.

1.13.4 Activation of secondary messengers and downstream signalling by PLCγ1

Activated PLCγ1 is fundamental in TCR signalling as the secondary messengers, IP_3 and DAG, produced by PIP_2 hydrolysis transduce signals down three major signalling cascades to activate the NFκB, NFAT and AP-1 transcription factors (Figure 1. 18). Notably, the PLCγ1 p.Y783 residue has been shown to be critical for proximal TCR signalling measured by inositol phosphate (IP) production *in vitro* (177, 194). The p.Y775 and p.Y783 residues are required to induce NFAT and AP-1 reporter activity *in vitro* (193). Importantly, the phosphorylated p.Y783 residue induces transcriptional activity more potently than p.Y775, making the former residue fundamental for PLCγ1 activity (193).

The secondary messenger IP_3 binds to IP_3 receptors on the endoplasmic reticulum and triggers the release of calcium from intra-cellular stores (Figure 1. 18) (195). IP_3 is

rapidly metabolised to inositol-1,4-bisphosphate (IP_2), which is metabolised to inositol-1-phosphate (IP_1) (Figure 1. 18). The rise in intra-cellular calcium levels activates the calcium-binding protein calmodulin, which in turn activates calcineurin, a serine phosphatase (195). In resting cells, constitutively active kinases phosphorylate serine residues on the NFAT transcription factor family and maintain the transcription factors in inactive forms in the cytoplasm (196). Fourteen serine residues on NFAT family members are phosphorylated, of which 13 are dephosphorylated by calcineurin in activated cells (196). Dephosphorylation of NFAT unveils the nuclear localisation signal (NLS) and concomitantly masks the nuclear export signal, enabling the transcription factors to enter the nucleus (196). The transcription factors bind to NFAT-specific response elements in the regulatory regions of target genes (Appendix Table 2) and initiate transcription (196). The NFAT family comprises of five members: NFAT1 – NFAT5. Of the five members, NFAT1-NFAT4 are activated by increased intra-cellular calcium levels and dephosphorylation by calcineurin activity, whilst NFAT5 is activated by osmotic stress and integrin activation (195).

The other secondary messenger, DAG, activates protein kinase C-theta (PKCθ), which initiates signalling cascades to stimulate two fundamental transcription factor families: AP-1 and NFκB (Figure 1. 18). PKCθ activates the MAPK pathway that triggers phosphorylation cascades via RAS/ RAF/ MEK1/2 and ERK1/2 to activate the AP-1 transcription factors (197). AP-1 comprises of homo- or hetero-dimers composed of the Fos (cFos, FosB, Fra1 and Fra2), Jun (cJun, JunB and JunD) or activating transcription factor (ATF) subunits that bind to the AP-1 binding site in the regulatory regions of target genes (Appendix Table 3) (196, 198). ERK1/2 can also activate other transcription factors including c-MYC and NFκB (197).

DAG-induced PKCθ activity also activates the canonical NFκB pathway by stimulating the CARMA/BCL10/MALT1 signalosome, which activates the IKK complex (Figure 1. 18) (199). The IKK complex comprises of two catalytic kinase subunits, IKKα and IKKβ and one regulatory subunit IKKγ (NFκB essential modulator; NEMO) (Figure 1. 18) (200). The activated IKK complex phosphorylates IκBα, the NFκB inhibitor. IκBα binds to NFκB (p50/p65 heterodimers) and masks the transcription factors' NLS, sequestering NFκB in its inactive state in the cytoplasm (201). When the IKK complex phosphorylates IκBα, the NFκB inhibitor is ubiquitinated and degraded by the proteasome (200). Dissociation of IκBα from

NFκB, unveils the NLS, allowing the transcription factor to translocate to the nucleus where it binds to κB sites in the regulatory regions of NFκB target genes (Appendix Table 4) and initiates transcription (200). The NFκB transcription factor family includes five proteins: p65 (RelA), RelB, c-Rel, p105/p50 (NF-κB1), and p100/52 (NF-κB2), which form homo- and hetero-dimers (200). All five NFκB proteins have a Rel homology domain that enables the proteins to dimerise, translocate to the nucleus and bind DNA in target genes (200).

1.13.5 Common target genes of the NFκB, NFAT and AP-1 transcription factor families

The regulatory regions of some target genes harbour composite binding sites for NFAT and AP-1, which bind co-operatively as transcriptional partners (195). NFAT dimers can also bind to NFκB binding sites as both transcription factors have Rel homology regions with high structural similarity that allow DNA binding (195). The NFAT, NFκB and AP-1 transcription factors have common target genes including those that encode FASL, IL-4 and IL-13 (Appendix Table 2 – Appendix Table 4). The overlap in target genes can be attributed to their regulatory regions harbouring binding sites for all three transcription factors, which can function in synergy (195).

Notably, all three transcription factors that are regulated by PLCγ1 have been implicated in the pathogenesis of CTCL. Specifically, NFκB is constitutively active in tumour cells from MF and SS patients and in CTCL cell lines and NFκB target genes including *IL-10*, *IL-13* and *BCL-2* are also characteristically overexpressed as discussed in section 1.6. AP-1 subunits have also been reported to be overexpressed in CTCL as have the target genes of this transcription factor: *BCL-2*, *cMYC*, *IL-4*, *IL-5* and *IL-13* (section 1.6). Furthermore, the NFAT transcription factor has recently been implicated in CTCL, with increased nuclear localisation detected in patients harbouring the activating PLCγ1 p.S345F mutation (section 1.9.2) (160). As PLCγ1 activates NFκB, NFAT and AP-1, mutations in *PLCG1* may contribute to the characteristic dysregulated expression and/ or activity of these transcription factors and their target genes in CTCL. One such example has been demonstrated by elevated NFAT-luciferase reporter activity induced by two PLCγ1 mutations, as discussed in section 1.9.2 (160).

1.14 The crucial role of PLCγ2 in BCR signalling

The BCR is composed of the membrane-bound heavy and light chain immunoglobulin IgM (Figure 1. 21. A) (202). When antigens bind to BCRs, the receptors aggregate and induce downstream signalling (Figure 1. 21. B). As with the TCR, the BCR is the antigen binding subunit that has short cytoplasmic tails and therefore relies on the ITAMs in the Igα and Igβ heterodimers to mediate signal transduction (Figure 1. 21. A) (202). The conformational change induced by BCR aggregation induces phosphorylation of ITAMs by the SRC-family of tyrosine kinases (Figure 1. 21. C) (203). The phosphorylated ITAMs act as docking sites for the spleen tyrosine kinase (SYK), which phosphorylates the B-cell linker protein (BLNK/ SLP-65), an adaptor that recruits Bruton's tyrosine kinase (BTK) and PLCγ2 (Figure 1. 21. C) (203). Several kinases including BTK, FYN and LCK phosphorylate PLCγ2. BTK phosphorylates the PLCγ2 p.Y753, p.Y759 and p.Y1197 tyrosine residues (204, 205). LCK also phosphorylates the PLCγ2 p.Y753 and p.Y759 residues and additionally phosphorylates p.Y743 (206). The p.Y1217 tyrosine base of PLCγ2 is phosphorylated in a BTK-independent manner (207). Phosphorylation of PLCγ2 activates the enzyme to hydrolyse PIP_2 into IP_3 and DAG. As with TCR signalling, these secondary messengers trigger multiple signalling cascades to activate the NFAT, NFκB and AP-1 transcription factors in B-lymphocytes (Figure 1. 16).

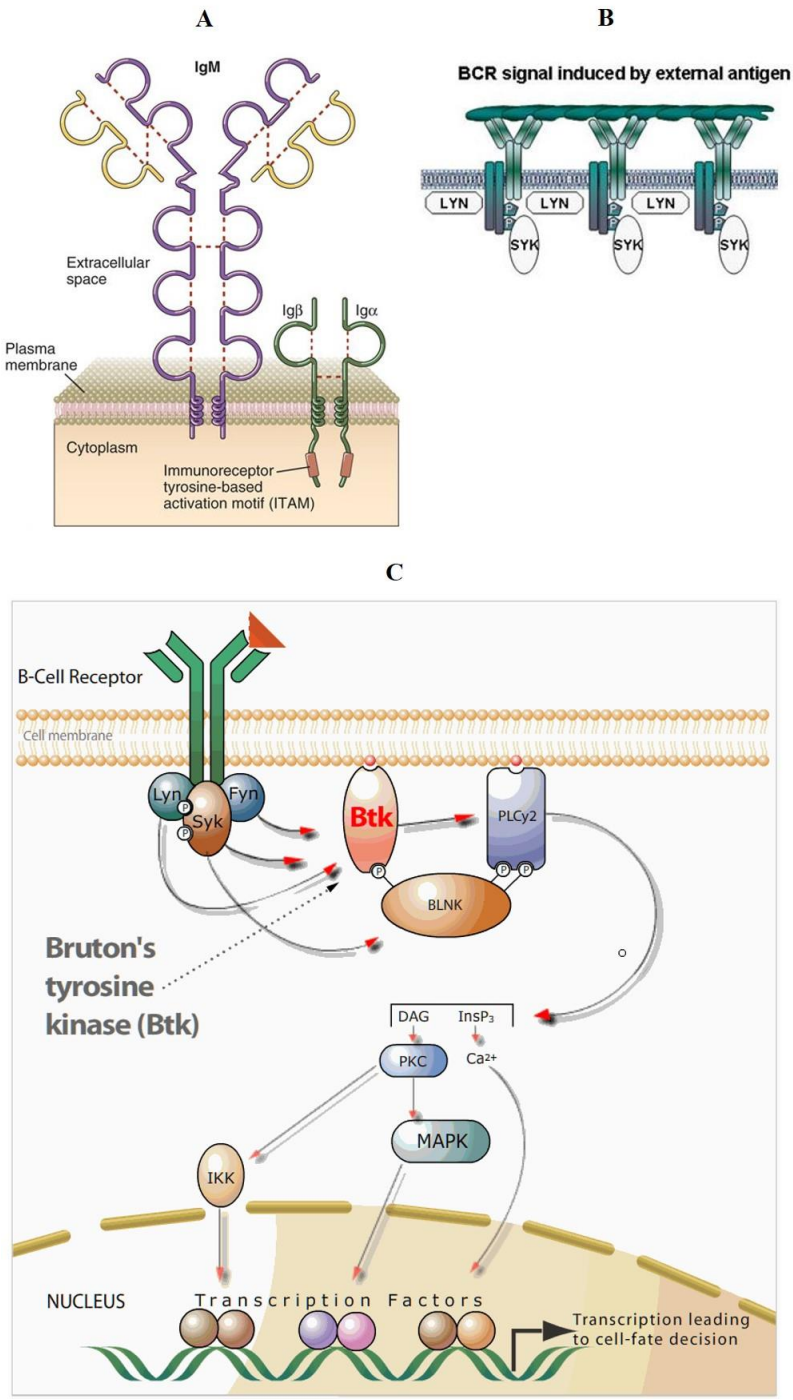

Figure 1. 21. The BCR structure and signalling pathway. (A) The BCR is composed of the immunoglobulin IgM, which interacts with Igα-Igβ heterodimers that harbour cytoplasmic ITAMs. (B, C) Antigens bind to the BCR and lead to receptor aggregation, which induces phosphorylation of ITAMs and recruitment of the LYN, FYN and SYK kinases to activate BTK. BTK phosphorylates and activates PLCγ2 to hydrolyse PIP_2 into IP_3 and DAG, which trigger pathways to activate the NFAT, NFκB and AP-1 transcription factors. Images adapted from Abbas *et al*. (2012), Efremov *et al*. (2012) and Kapoor *et al*. (2016) (208-210).

1.15 Mutations and overexpression of PLCγ1 in cancer

PLCγ1 is ubiquitously expressed in all tissues and is activated by the TCR and numerous growth factor receptors (179). Mutations in *PLCG1* and aberrant PLCγ1 expression levels have been detected in several haematological and solid malignancies, respectively and will be described in this section.

1.15.1 Somatic *PLCG1* mutations in cancer

A vast number of NGS studies have reported somatic *PLCG1* mutations in many types of mature T-cell lymphomas including advanced stage MF, SS, ATLL, PTCL-nos, AITL, Hepatosplenic T-cell lymphoma (HSTL) and T-cell-prolymphocytic leukaemia (TPLL) (Table 1. 3). Our deep sequencing study also identified *PLCG1* mutations in 11% of SS tumours (Table 1. 4) (147). Furthermore, advanced stage primary and secondary angiosarcomas also harbour *PLCG1* mutations (Table 1. 3). Angiosarcomas are rare neoplasms of endothelial cells that line blood and lymphatic vessels (211). Like SS, advanced stage angiosarcomas are aggressive diseases that have a poor prognosis and have been shown to be genetically heterogeneous by NGS sequencing studies (212-215).

A large deep sequencing study on 370 ATLL tumours identified that *PLCG1* was the most frequently mutated gene in 36.2% of cases (Table 1. 3). *PLCG1* mutations occur most frequently in ATLL compared to other malignancies (Table 1. 3). Notably, McGirt *et al*. (2015), Yoo *et al*. (2014), Wang *et al*. (2017), Kunze *et al*. (2014) and Vallois *et al.* (2016) also report a high *PLCG1* mutation frequency of between 20% - 30.8%, however this inflated frequency can be attributed to analyses of small sample sizes of 5-13 tumours (Table 1. 3).

Table 1. 3. Deep sequencing studies reporting *PLCG1* mutations in mature T-cell malignancies and angiosarcomas. ATLL: adult T-cell leukaemia/lymphoma, PTCL-nos: peripheral T-cell lymphomas-not otherwise specified, MF: Mycosis Fungoides, AITL: angioimmunoblastic T-cell lymphoma, SS: Sézary Syndrome, HSTL: hepatosplenic T-cell lymphoma, TPLL: T-cell-prolymphocytic leukaemia.

Malignancy	**Mutation frequency**	**Reference**
MF	**22.2%** (10/45) **2.7%** (1/37) **20%** (1/5) **9.8%** (4/41)	Vaqué *et al.* 2014 (160) Caumont *et al*. 2015 (216) McGirt *et al*. 2015 (148) Ungewickell *et al*. 2015 (71)
SS	**12.5%** (1/8) **5.1%** (2/39) **10%** (4/40) **9.1%** (6/66) **18.1%** (19/105) **12%** (3/25) **6.7%** (1/15) **10.9%** (11/101)	Vaqué *et al.* 2014 (160) Caumont *et al*. 2015 (216) Choi *et al*. 2015 (67) Kiel *et al.* 2015 (68) Wang *et al*. 2015 (70) da Silva Almeida *et al*. 2015 (69) Prasad *et al*. 2016 (161) Woollard *et al*. 2016 (147)
PTCL-nos	**14.6%** (6/41) **30.8%** (4/13) **14.6%** (6/41)	Manso *et al*. 2014 (217) Vallois *et al.* 2016 (218) Manso *et al*. 2018 (219)
AITL	**20%** (1/5) **11.7%** (7/60) **11.1%** (8/72) **22.2%** (2/9) **14.0%** (8/57)	Yoo *et al*. 2014 (65) Manso *et al*. 2014 (217) Vallois *et al.* 2016 (218) Wang *et al.* 2017 (220) Manso *et al*. 2018 (219)
ATLL	**36.2%** (134/370)	Kataoka *et al*. 2015 (221)
HSTL	**15%** (3/20)	McKinney *et al*. 2017 (222)
TPLL	**5.6%** (2/36)	Kiel *et al*. 2014 (223)
Primary angiosarcomas	**30%** (3/10) **5.2%** (6/116) **3%** (1/34)	Kunze *et al.* 2014 (213) Huang *et al.* 2016 (220) Murali *et al*. 2015 (215)
Secondary angiosarcomas	**8.8%** (3/34) **4.3%** (5/116)	Behjati *et al.* 2014 (212) Huang *et al.* 2016 (220)

Table 1. 4. *PLCG1* mutations identified by our TCS study of 101 SS tumours. Identical variants identified in more than one patient are highlighted in the same colour (147).

Patient I.D.	Patient DNA number	Nucleotide substitution	Amino acid change
1	6885B	c.C142T	p.R48W
2	8004B	c.C142T	p.R48W
3	L11_0158B	c.C935T	p.S312L
4	3297B	c.G1024A	p.D342N
5	8344B	c.G1024A	p.D342N
6	3451B	c.C1034T	p.S345F
7	9308B	c.C1034T	p.S345F
8	4736B	c.C1559T	p.S520F
9	L12_0697B	c.G3487A	p.E1163K
10	4142B	c.G3487A	p.E1163K
11	4346B	c.G3493C	p.D1165H

Point mutations, small deletions and indels occur throughout PLCγ1 in mature T-cell lymphomas (Figure 1. 22). In contrast, the disease-specific p.R707Q/L mutations only occur in primary and secondary angiosarcomas and would influence VEGFR signalling in endothelial cells (212-214). The p.R707Q mutation has been reported to be acquired after Sunitinib (tyrosine kinase inhibitor) therapy in one case of hepatic angiosarcoma (224). Further investigations including larger cohorts of relapsed patients are required to determine whether *PLCG1* acquires somatic mutations as resistance mechanisms to Sunitinib treatment. Notably, the p.S345F mutation has been reported in all the mature T-cell malignancies listed in Table 1. 3 and in primary angiosarcoma of the breast and spleen (214). Multiple *PLCG1* mutations per tumour have been identified in ATLL (221), but not in other mature T-cell lymphomas and angiosarcomas in which patients harbour a single *PLCG1* mutation. In secondary angiosarcomas, *PLCG1* mutations co-occur with *PTPRB* or *cMYC* mutations, an observation unique to this disease subtype (212, 214).

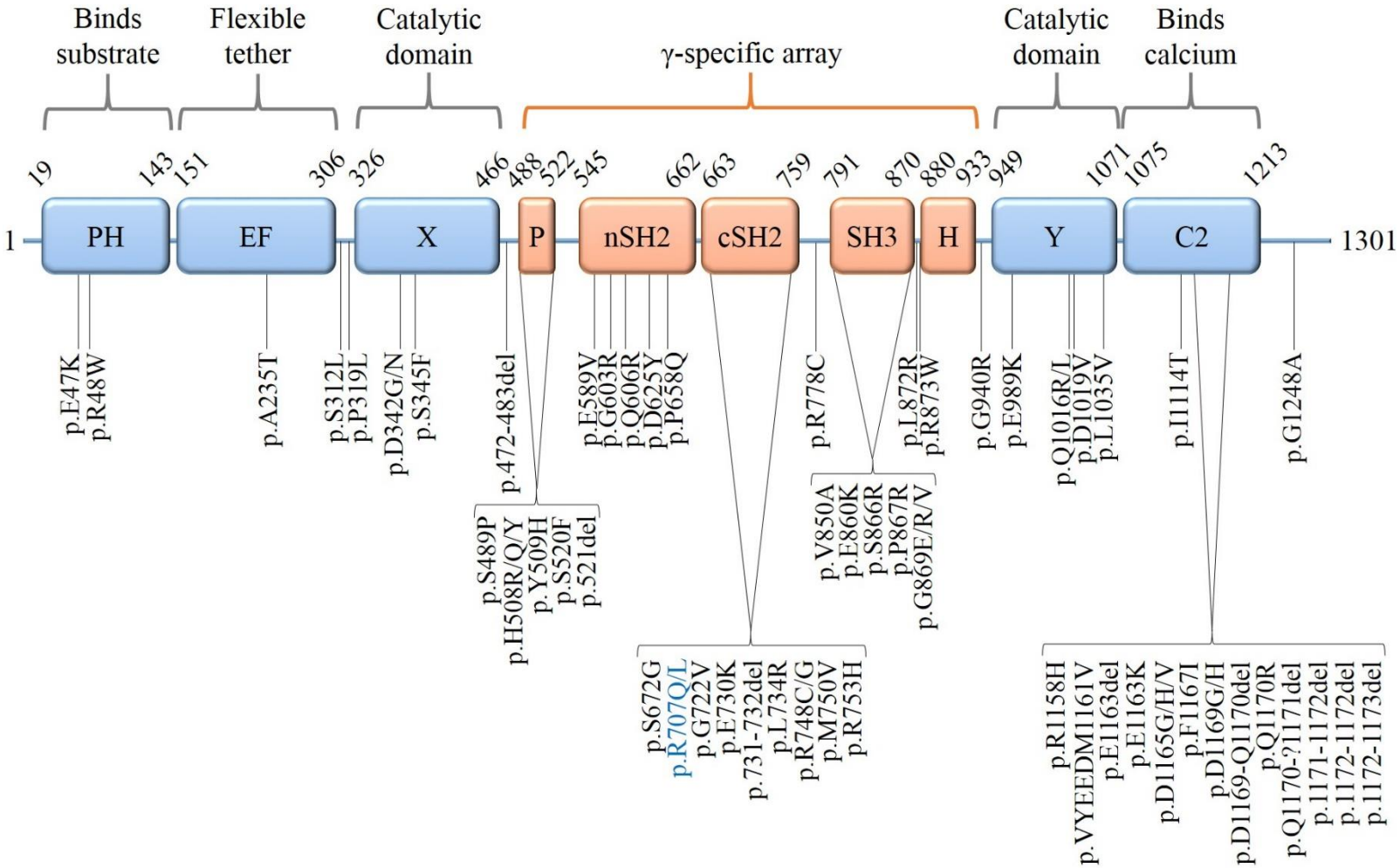

Figure 1. 22. PLCγ1 mutations reported in mature T-cell lymphomas and angiosarcomas. Mutations reported in angiosarcomas are shown in blue text. The p.S345F mutation occurs in T-cell malignancies and primary angiosarcomas. Refer to Table 1. 3 for references.

Eleven *PLCG1* mutations have been functionally characterised, nine of which occur solely in mature T-cell lymphomas, one in angiosarcomas (p.R707Q) and the p.S345F mutation in both (Table 1. 5). Nine of the ten mature T-cell lymphoma mutations increase NFAT activation and MALT1 activity in HEK293T cells (Table 1. 5) (160, 218). The p.R707Q mutation increases IP_1 production (in HEK293 cells), apoptosis resistance, cell migration and invasion in the endothelial HUVEC cell line (213). As discussed in section 1.9.2, the p.S345F mutation has been associated with increased nuclear expression of NFAT in lesional skin of MF patients.

Notably, there are no reports of disease-associated germline *PLCG1* mutations demonstrating that mutations are somatically acquired during oncogenesis. The prevalence of *PLCG1* mutations in many different malignancies strongly suggests that this gene harbours driver mutations, which play a key role in tumourigenesis. This is supported by the ability of the mutations to increase components of TCR or VEGFR signalling pathways, *in vitro* (Table 1. 5).

PLCγ1 plays a fundamental role in mediating TCR and VEGFR2 signalling to key transcription factors including NFκB. The TCR signalling pathway harbours mutations in many genes in CTCL (section 1.9.2), but importantly *PLCG1* is the most frequently mutated T-cell activation gene (162, 166). *PLCG1* mutations have been shown to occur in mutual exclusivity to other NFκB pathway genes in SS, suggesting that perturbation of one gene in this signalling cascade is sufficient to disrupt the pathway and lead to oncogenesis (166). This is significant as dysregulated TCR signalling, in particular constitutive NFκB activity, is a characteristic feature of neoplastic CTCL cells (section 1.6.6). As PLCγ1 induces the NFκB pathway, signalling from mutant PLCγ1 proteins may contribute to the dysregulated NFκB activity in mature T-cell lymphomas. Vallois *et al*. (2016) demonstrate that PLCγ1 mutations increase MALT1 activity (218), which is suggestive of increased NFκB activity but the effects of PLCγ1 mutations on NFκB activation remains to be directly assayed.

Table 1. 5. A summary of the functional interrogations performed on PLCγ1 mutations. Arrows denote an increase in the readout of the assays performed, dashes represent no change and n/a indicates assays not performed for the specified mutations.

Mutation	NFAT activation	MALT1 activity	IP-1 production	Apoptosis resistance	Migration	Invasion	References
p.E47K	↑	↑	n/a	n/a	n/a	n/a	(218)
p.R48W	-	-	n/a	n/a	n/a	n/a	(218)
p.D342G	↑	↑	n/a	n/a	n/a	n/a	(218)
p.S345F	↑ ↑	- ↑	n/a	n/a	n/a	n/a	(160) (218)
p.S520F	↑ ↑	- ↑	n/a	n/a	n/a	n/a	(160) (218)
p.R707Q	n/a	n/a	↑	↑	↑	↑	(213)
p.E730K	↑	↑	n/a	n/a	n/a	n/a	(218)
p.G869E	↑	↑	n/a	n/a	n/a	n/a	(218)
p.E1163K	↑	↑	n/a	n/a	n/a	n/a	(218)
p.D1165G	↑	↑	n/a	n/a	n/a	n/a	(218)
p.D1165H	↑	↑	n/a	n/a	n/a	n/a	(218)

1.15.2 CNV of *PLCG1*

Our TCS analysis identified a partial amplification of *PLCG1* in one patient who did not harbour any mutations in this gene. The amplification initiates in intron 21 of *PLCG1*, spans the *ZHX3*, *LPIN3*, *EMILIN3* genes and ends in intron 6 of the *CHD6* gene on chromosome 20 (co-ordinates: 39797710 – 40126876). The copy number gain would result in amplification of exon 22 – 32 of *PLCG1* and amino acid p.W828 in the PLCγ1 SH3 domain and beyond. The CNV could not be validated as the DNA sample in which it was identified had been depleted. No other CNVs of *PLCG1* have been reported in mature T-cell lymphomas. Copy number gain of *PLCG1* and other PLC isoforms including *PLCB1* and *PLCB4* have been detected in glioblastoma multiforme (225). It is likely that amplification of PLCγ1 would augment downstream signalling and contribute to tumourigenesis, however this remains to be functionally validated.

1.15.3 Overexpression of PLCγ1 in solid carcinomas

Many solid tissue carcinomas frequently demonstrate elevated PLCγ1 expression. Overexpression of PLCγ1 has been detected in breast cancer and in the majority of tumours the active phosphorylated form of PLCγ1 (p-PLCγ1) was also detected (226). Furthermore, breast tissues expressing p-PLCγ1 also expressed the EGFR or Human epidermal growth factor receptor-2 (HER2), known to activate PLCγ1 (226). These findings suggest that two consecutive steps of the epidermal cell signalling pathway are amplified and may contribute to carcinogenesis (226). A subsequent study identified variable PLCγ1 expression in the cytoplasm of breast tumour cells and importantly demonstrated p-PLCγ1 expression predominantly in the nucleus (227). Elevated expression of PLCγ1 and p-PLCγ1 are associated with unfavourable clinical outcomes including metastasis occurrence, therefore PLCγ1 overexpression is considered a marker for metastasis development in breast cancer (227).

Increased PLCγ1 expression has also been detected on both the mRNA and protein level in colon cancer (228). Treatment of the human colorectal cell line (LoVo) with the PLC inhibitor U73122 demonstrated decreased cell migration after stimulation, suggesting that PLCγ1 plays a key role in cell migration (229). LoVo cells were identified to have constitutive NFκB activity, which was enhanced by EGF stimulation

(via the EGFR-PLCγ1 pathway) and reduced by U73122, demonstrating that PLCγ1 signalling regulates NFκB activity (229). Notably, the PLC inhibitor has been shown to elevate PLCγ1 activity in cell-free systems and also has a broad range of cellular targets and therefore lacks specificity (230). The effect of PLCγ1 on regulating migration and NFκB activity in LoVo cells should be reviewed with more specific inhibitors. A recent study has reported a significant correlation between *PLCG1* copy number gain and increased PLCG1 RNA expression in colon cancer, demonstrating that CNVs can influence gene expression in tumours (231).

PLCγ1 overexpression has been detected in the basal layer of epidermal skin from SCC patients and cell lines (232). A correlation between lower PLCγ1 expression and significantly improved overall survival, disease-free survival, and a better clinical response to chemotherapy in locally advanced and surgically removable oral squamous cell carcinoma (OSCC) patients has also been reported (233). Therefore, PLCγ1 expression may serve as a prognostic marker for advanced OSCC (233). Furthermore, PLCγ1 expression is associated with a higher incidence of OSCC and increased expression correlates with disease progression of potentially malignant oral lesions to OSCC (234). Thus, PLCγ1 may also serve as a biomarker for the identification of high-risk patients that could progress to develop OSCC (234).

1.16 Disease-associated germline and somatic mutations in PLCG2

As described in section 1.12, PLCγ1 and PLCγ2 are closely related isozymes, which mediate TCR and BCR signalling, respectively. Germline *PLCG2* mutations have been reported in immune disorders and somatic mutations in drug-resistant mature B-cell malignancies as will be described in this section.

1.16.1 Germline *PLCG2* mutations in immune disorders

Linkage analysis of three families affected by a syndrome characterised by cold-induced urticaria, antibody deficiency and susceptibility to auto-immunity and infections, revealed a partial deletion of the n-terminus of the cSH2 domain (p.646-685) in two families and partial deletion of the c-terminus of the cSH2 and n-terminus of the SH3 domain (p.686-806) in the third family (Figure 1. 23) (235). *In vitro* analyses demonstrate that the deletions increase PLCγ2 activity by elevating IP

production. The increased activity is attributed to deletions of the cSH2 domain, which disrupt PLCγ2 auto-inhibition (235). This syndrome was therefore coined phospholipase Cγ2-associated antibody deficiency and immune dysregulation (PLAID) (235).

WES of a family with a dominantly inherited auto-inflammatory condition revealed the PLCγ2 p.S707Y mutation in both affected individuals (236). This mutation was shown to increase IP production and intra-cellular calcium levels *in vitro* (237). As with the deletions in PLAID, the p.S707Y mutation locates to the cSH2 domain and disrupts auto-inhibition to elevate PLCγ2 activity. This syndrome was therefore named autoinflammation and PLCγ2-associated antibody deficiency and immune dysregulation (APLAID) (236).

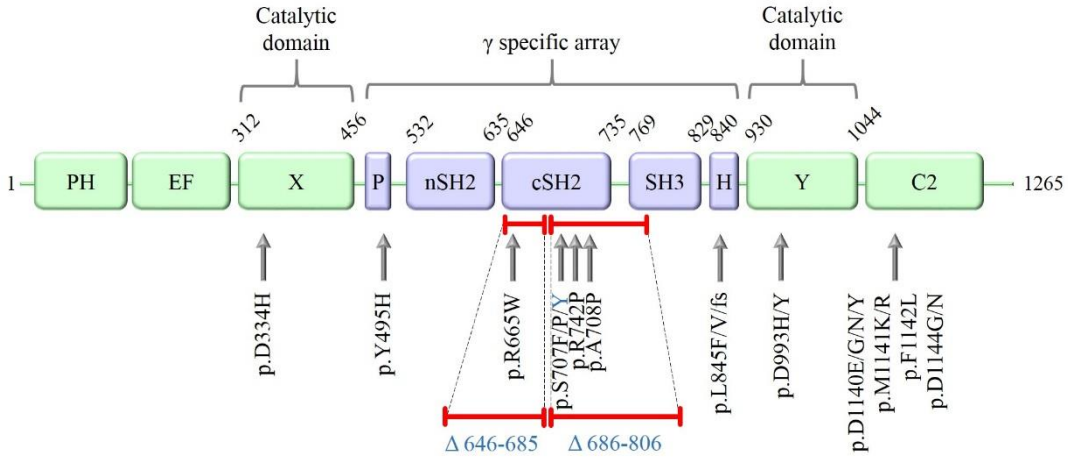

Figure 1. 23. Germline and somatic PLCγ2 mutations mapped to the functional protein domains. Germline mutations including two deletions identified in the auto-immune condition PLAID and the p.S707Y mutation in APLAID are denoted in blue. Somatic mutations identified in Ibrutinib-resistant CLL and Waldenström macroglobulinemia are shown in black. The p.S707Y mutation is also somatically acquired in Ibrutinib-resistant CLL (235, 236, 238-247).

1.16.2 Somatic *PLCG2* mutations in mature B-cell neoplasms

PLCG2 frequently harbours somatic mutations in Ibrutinib-resistant CLL. CLL is a mature B-cell malignancy in which BCR signalling is constitutively active, leading to apoptosis resistance of tumour cells (238, 248). CLL is the most common type of leukaemia in western countries and with the exception of allogenic stem cell

transplantation it is considered incurable (238, 249). The orally administered small molecule inhibitor Ibrutinib is the first BTK inhibitor that effectively brings CLL patients into remission (249). This inhibitor is also an effective treatment for other B-cell lymphomas including Waldenström macroglobulinemia (WM), mantle-cell lymphoma and ABC DLBCL (250-252), but resistance to this inhibitor has been reported in all three malignancies (218, 245, 253, 254). Notably, *PLCG2* mutations have also been identified in Ibrutinib-resistant WM (245).

RNA sequencing and deep DNA sequencing studies have demonstrated frequent mutations in the *PLCG2* and *BTK* genes in around 80-90% of Ibrutinib-resistant CLL patients (238-241, 243, 244, 246, 247, 255). Ibrutinib forms an irreversible covalent bond with the p.C481 residue of BTK, a key kinase that mediates BCR signalling (see section 1.14) and inhibits the elevated downstream BCR signalling observed in CLL (243, 249). The most frequent BTK mutation (p.C481S) occurs at the key Ibrutinib binding residue and results in reversible as opposed to irreversible binding of the drug, which decreases the inhibitor's ability to reduce elevated BCR signalling in CLL (239). The BTK p.C481S mutation therefore confers resistance to Ibrutinib in some relapsed patients (239).

The somatically acquired *PLCG2* mutations identified in Ibrutinib-resistant CLL and WM are shown in Figure 1. 23. Studies have revealed that Ibrutinib-resistant CLL patients can harbour (i) *BTK* mutations alone (238, 240, 241, 244, 247), (ii) *PLCG2* mutations alone (238, 240, 241, 243, 247), (iii) *BTK* and *PLCG2* mutations (238, 240, 243, 247) or (iv) multiple *PLCG2* mutations (238, 240, 241, 247). Highly sensitive sequencing techniques have enabled the identification of resistance-associated *BTK* and *PLCG2* mutations up to 15 months prior to disease progression from drug-induced relapse (256). The identification of multiple *PLCG2* mutations per patient strongly suggests that these are putative driver gene mutations that are positively selected during the development of drug resistance (240).

Of all the *PLCG2* mutations identified in Ibrutinib-relapsed CLL patients (Figure 1. 23) the p.R665W and p.L845F mutations have been functionally validated as gain-of-function mutations, which elevate intra-cellular calcium levels and IP production *in vitro* (239, 242, 243). Notably, the p.S707Y mutation is somatically acquired in Ibrutinib-resistant CLL and also inherited as a germline mutation in the immune

disorder APLAID (237). p.S707Y is an activating mutation that increases PLCγ2 activity and downstream signalling by elevating intra-cellular calcium levels (236). Thus, *PLCG2* mutations confer a BTK-independent resistance mechanism to Ibrutinib.

The BTK p.C481S mutation and PLCγ2 p.R665W, p.S707Y and p.L845F mutations mediate gain-of-function implicating their role as drug-induced driver gene mutations that confer resistance to Ibrutinib, however this remains to be proved by reversing the effects using mutation-specific inhibitors.

1.17 Hypothesis

PLCG1 mutations frequently occur in mature T-cell lymphomas including CTCL, in which this gene is the most frequently mutated amongst TCR activation genes. PLCγ1 plays a pivotal role in TCR signalling and activates key transcription factors including NFκB, which is constitutively active in CTCL. Therefore, this thesis hypothesises that PLCγ1 variants are true gain-of-function mutations that elevate TCR signalling and contribute to the molecular pathogenesis of SS.

1.18 Aims

To investigate the hypothesis that PLCγ1 variants are *bona fide* activating mutations that increase TCR signalling, this study aims to:

1. Prioritise which of the nine PLCγ1 mutations (p.R48W, p.S312L, p.D342N, p.S345F, p.S520F, p.R1158H*, p.E1163K, p.D1165H and the in-frame indel p.VYEEDM1161V*) identified in SS tumours by our deep sequencing study and Kiel *et al*. (2015)*, should be taken forward for functional analyses (68, 147).

2. Functionally interrogate the prioritised mutations to determine the influence on protein expression and activity by assaying proximal and downstream signalling and also investigate the efficacy of an IKKβ inhibitor to reduce NFκB activity.

3. Investigate where the mutations map onto a 3D protein model and to optimise an imaging system to enable the cellular localisation of mutant PLCγ1 proteins to be visualised.

Chapter 2 Materials and Methods

2.1 Materials

Table 2. 1. General reagents used for various techniques.

Item	Catalogue Number	Manufacturer
Ethanol absolute	20821.330	VWR Chemicals
β-mercaptoethanol	M3148	Sigma-Aldrich
Isopropanol	109634	Merck

Table 2. 2. DNA extraction kit for isolating DNA from frozen $CD4^+$ enriched T-cells.

Item	Catalogue Number	Manufacturer
QIAamp DNA Blood Mini Kit	51104	Qiagen

Table 2. 3. RNA extraction kit for isolating RNA from frozen $CD4^+$ enriched T-cells.

Item	Catalogue Number	Manufacturer
RNeasy Plus Mini Kit	74134	Qiagen
QIAshredder	79656	Qiagen

Table 2. 4. Reverse Transcription kit.

Item	Catalogue Number	Manufacturer
High Capacity cDNA Reverse Transcription Kit	4368814	Applied Biosystems

Table 2. 5. Agarose gel electrophoresis and polymerase chain reaction (PCR) product clean-up reagents.

Item	Catalogue Number	Manufacturer
Agarose powder	Bio-41025	Bioline reagents Limited
10x Tris-Borate-EDTA (TBE)	EC-860	National diagnostics
Ethidium Bromide	E1510	Sigma-Aldrich
100 bp ladder	CSL-MDNA-100BP	Cleaver Scientific Ltd
1 kb GeneRuler DNA ladder	SM0313	Thermo Fisher Scientific
ExoSAP-IT	USBM7825040UL	Affymetrix Incorporated

Table 2. 6. Ultracompetent bacterial culture reagents.

Item	Catalogue Number	Manufacturer
Sodium chloride	27810.295	VWR Chemicals
Bacto tryptone	211705	BD Biosciences
Bacto yeast extract	212750	BD Biosciences
Bacto agar	214010	BD Diagnostic Systems
Ampicillin sodium salt	A0166	Sigma-Aldrich
Kanamycin sulfate	K1377	Sigma-Aldrich
SOC Outgrowth Medium	B9020S	New England Biolabs UK Ltd
Glycerol	G7893	Sigma-Aldrich

Table 2. 7. Site-directed mutagenesis and plasmid DNA extraction kits used to isolate DNA from bacterial cultures.

Item	Catalogue Number	Manufacturer
QuikChange Lightning Site-Directed Mutagenesis Kit	210518	Agilent Technologies
QIAprep Spin Miniprep Kit	27106	Qiagen
HiSpeed Plasmid Midi Kit	12643	Qiagen
HiSpeed Plasmid Maxi Kit	12662	Qiagen

Table 2. 8. Cell culture reagents.

Item	Catalogue Number	Manufacturer
Dulbecco Modified Eagle Medium (DMEM), high glucose, GlutaMAX	61965026	Gibco
TrypLE™ Express Enzyme (1x), phenol red	12605010	Gibco
Fetal Bovine Serum (FBS)	51800-500	Biosera
Penicillin-Streptomycin (10,000 U/mL)	15140122	Gibco
Phosphate Buffered Saline (PBS), pH 7.2	20012-019	Gibco
Opti-MEM I Reduced Serum Medium	31985062	Gibco
Hydrogen Peroxide Aseptic (35%)	GPC2698	Atom Scientific
Sodium Orthovanadate (Vanadate)	P0758S	New England Biolabs UK Ltd
Dimethyl sulfoxide (DMSO)	sc-358801	Santa Cruz Biotechnology

Table 2. 9. Cytokines and growth factors for cell culture.

Item	Catalogue Number	Manufacturer
Recombinant Human epidermal growth factor (EGF) protein	PHG0314	Gibco
Recombinant Human tumour necrosis factor alpha (TNFα) protein	300-01A	Peprotech Corporation

Table 2. 10. Kits and reagents used to test cell cultures for Mycoplasma contamination.

Item	Catalogue Number	Manufacturer
PCR Master Mix	M7501	Promega Corporation
Mycoplasma Detection Kit - QuickTest	B39032	Biotool

Table 2. 11. Transfection reagents.

Item	Catalogue Number	Manufacturer
FuGENE HD Transfection Reagent	E2311	Promega Corporation
Lipofectamine™ LTX Reagent with PLUS™ Reagent	15338100	Invitrogen

Table 2. 12. Inhibitors used to treat cell cultures.

Item	Catalogue Number	Manufacturer
IKKβ inhibitor IV (TPCA-1)	sc-203083	Santa Cruz Biotechnology

Table 2. 13. Western blotting reagents.

Item	Catalogue Number	Manufacturer
Amersham enhanced chemiluminescence (ECL) prime western blot detection reagent	RPN2232	GE Healthcare Life Sciences
4x Laemmli sample buffer	161-0747	Bio-Rad Laboratories Incorporated
Radioimmunoprecipitation assay (RIPA) lysis buffer system	sc-24948	Santa Cruz Biotechnology
X-ray film RX NIF sheets	47410 19230	Fujifilm
Pierce BCA protein assay kit	23227	Thermo Scientific
Trizma Base	T1503-1kg	Sigma-Aldrich
Trizma HCl	T5941-500g	Sigma-Aldrich
Glycine	G7126-5kg	Sigma-Aldrich
0.1% ponceau S (w/v) in 5% acetic acid	P7170-IL	Sigma-Aldrich
Tween 20	P9416-100ml	Sigma-Aldrich
10% (w/v) Sodium dodecyl sulfate (SDS)	161-0416	Bio-Rad Laboratories Incorporated
Methanol	20847.307	VWR Chemicals
Polyvinylidene difluoride (PVDF) western blotting membrane	03010040001	Roche Applied Science
Bovine serum albumin (BSA; protease-free)	80400-100	Alpha Diagnostics International
Precision plus protein dual color standards	161-0374	Bio-Rad Laboratories Incorporated
30% Acrylamide	EC-201	National diagnostics
10% Ammonium persulfate (APS)	A3678	Sigma-Aldrich
Tetramethylethylenediamine (TEMED)	T9281	Sigma-Aldrich

Table 2. 14. Antibodies used for western blotting.

Item	Catalogue Number	Manufacturer
Rabbit monoclonal anti-PLCγ1 (D9H10) XP	5690	Cell Signaling Technology
Rabbit polyclonal anti-phospho-PLCγ1 (Tyr783)	2821	Cell Signaling Technology
Mouse monoclonal anti-Penta-His	34660	Qiagen
Rabbit anti-β-Actin	4967	Cell Signaling Technology
Goat anti-rabbit IgG H&L (HRP)	ab97051	Abcam
Goat anti-mouse IgG H&L (HRP)	ab6789	Abcam

Table 2. 15. Immunofluorescence reagents.

Item	Catalogue Number	Manufacturer
13 mm diameter, No #1 round cover slides	630-1597	VWR
Paraformaldehyde, 4% in PBS	15424389	Alfa Aesar
4',6-Diamidino-2-Phenylindole (DAPI)	D3571	Thermo Fisher Scientific
Phalloidin, CF568	00044-T	Biotium
SlowFade™ Diamond antifade mountant	S36967	Thermo Fisher Scientific
0.8 – 1.0 mm microscope slides	FB58626	Fisher Scientific

Table 2. 16. Recipe for 250 mL of 1.5 M Tris buffer (pH 8.8) for western blotting.

Reagent	Quantity	Final concentration
Tris base (Sigma-Aldrich)	45.41 g	1.5 M
MilliQ water	Dissolve in 200 ml	-
Adjust pH to 8.8		
MilliQ water	Up to 250 mL	-

Table 2. 17. Recipe for 250 mL of 1 M Tris buffer (pH 6.8) for western blotting.

Reagent	Quantity	Final concentration
Tris base (Sigma-Aldrich)	30.29 g	1.5 M
MilliQ water	Dissolve in 200 ml	-
Adjust pH to 6.8		
MilliQ water	Up to 250 mL	-

Table 2. 18. Recipe for 500 mL of 10x TBS buffer (pH 7.6) for western blotting.

Reagent	Quantity	Final concentration
Sodium chloride (VWR)	40 g	1.4 M
Trizma-Base (Sigma)	12.1 g	0.2 M
MilliQ water	Up to 500 mL	-
Adjust pH to 7.6		

Table 2. 19. Recipe for 400 mL of 1x TBS-Tween (TBS-T) buffer for western blotting.

Reagent	Quantity	Final concentration
10x TBS	40 mL	1x
MilliQ water	360 mL	-
Tween20 (Sigma)	0.4 mL	0.1% (v/v)

2.2 Methods

2.2.1 Patient samples

All SS patients participating in this study had a diagnosis of primary Sézary Syndrome (de novo) and fulfilled the WHO classification of tumours of haematopoietic lymphoid tissues (6). All patients demonstrated an identical T-cell clone in peripheral blood and lesional skin by TCR gene rearrangement studies and were classified as blood stage B2. None of the patients received PUVA therapy before diagnosis. Tumour samples were obtained with informed consent from a national approved research tissue bank and blood samples were obtained from healthy volunteers (IRAS Project ID: 238203). The clinical outcomes of all 11 patients harbouring *PLCG1* mutations are shown in Table 2. 20.

Table 2. 20. Clinical outcomes of 11 SS patients harbouring *PLCG1* mutations.

Patient I.D.	Date of diagnosis	Clinical outcome	Comments
1	18/02/2008	Deceased 24/04/2009	Death related to lymphoma
2	09/06/2009	Alive	Allogenic haematopoietic stem cell transplant received on 12/04/2012
3	22/08/2011	Deceased 01/04/2014	Death due to disease
4	30/05/2002	Deceased 22/08/2016	Death due to disease
5	01/03/2009	Unknown	Loss to follow up post diagnosis
6	06/10/2002	Deceased 23/10/2008	Death due to disease
7	01/04/2008	Deceased 29/01/2018	Unknow if related to CTCL
8	03/08/2001	Unknown	Loss to follow up since 2016
9	02/08/2012	Deceased 09/01/2013	Death due to disease
10	01/01/2000	Deceased 19/09/2004	Death due to disease
11	10/02/2004	Deceased 22/06/2004	Death due to disease

No association was found between the survival outcomes of patients harbouring *PLCG1* mutations compared to those without mutations in this gene in our NGS study of 101 SS tumours (147). This may be due to a lack of power from a small sample set and analysis of a larger cohort of patients whose clinical outcomes and *PLCG1* mutation status are known would be more insightful. In particular, expansion of the integrated database of CTCL cases generated by Chang *et al*. (2018) may serve as a useful tool for such analyses if the survival outcomes for the patients can be sourced (166).

2.2.2 DNA extraction from enriched $CD4^+$ T-cells

DNA was extracted from frozen enriched $CD4^+$ T-cells from SS patients using the QIAamp DNA Blood Mini Kit (Qiagen) as per the manufacturer's guidelines. DNA was eluted in 200 µL AE buffer and quantified using the Nanodrop ND-1000 spectrophotometer.

2.2.3 RNA extraction from enriched $CD4^+$ T-cells

RNA was extracted from frozen enriched $CD4^+$ T-cells from SS patients using the RNeasy Plus Mini Kit (Qiagen) as per the manufacturer's guidelines. RNA was eluted in 30 µL RNase-free water and quantified using the Nanodrop ND-1000 spectrophotometer.

2.2.4 Two-step Reverse Transcription-PCR

Total RNA was extracted from enriched $CD4^+$ T-cells as per section 2.2.3 and reverse transcribed to produce cDNA using the High Capacity cDNA Reverse Transcription Kit (Applied Biosystems). Twenty microliter reactions were prepared as per Table 2. 21 and subjected to the thermal conditions shown in Table 2. 22. cDNA was stored at -20°C.

Table 2. 21. Reverse transcription reaction composition.

Reagent	**Final concentration**	**Volume (20 µL reaction)**
10 x RT Buffer	1 x	2 µL
25 x dNTP mix (100mM)	1 x	0.8 µL
10 x RT Random primers	1 x	2 µL
MultiScribe Reverse Transcriptase	50 units	1 µL
Nuclease-free water	-	Variable
RNA	0.1 - 2 µg	Variable

Table 2. 22. Thermal cycling conditions for reverse transcription.

Temperature	Duration
25°C	10 minutes
37°C	120 minutes
85°C	5 minutes

2.2.5 Targeted Capture Sequence alignment analysis

Integrative Genomics Viewer (IGV) (257) was used to visualise and confirm the location of gene variants that had been detected by TCS and also to check the coverage of sequence reads at specified co-ordinates prior to validation by Sanger sequencing.

2.2.6 Primer design and optimisation

Genomic (g)DNA and complementary (c)DNA sequences were obtained from the genome browser Ensembl (176) and the Primer3 software (258) was used to design PCR and Sanger sequencing primers. The specificity of primers to amplify the region of interest was analysed *in silico* using the Primer-Blast tool (259). The optimal annealing temperatures for primer pairs (Eurofins MWG) was determined by performing PCRs at different annealing temperatures using 20 – 50 ng gDNA or 1 – 10 ng cDNA derived from the peripheral blood of healthy individuals or cell lines as a template. Five percent (v/v) DMSO (Agilent Technologies) was used in reactions containing GC-rich primers to prevent intra- and inter-strand re-annealing (260).

2.2.7 Polymerase Chain Reaction

Fifteen microliter PCRs were prepared as per Table 2. 23 and subjected to the thermal conditions shown in Table 2. 24, using the optimal annealing temperatures specified in Table 2. 25 - Table 2. 28. gDNA or cDNA from the peripheral blood of healthy individuals or cell lines and nuclease-free water (Ambion) were used in positive and negative control reactions respectively.

Table 2. 23. PCR composition.

Reagent	Manufacturer	Volume	Final concentration
10 x PCR Buffer II	Applied Biosystems	1.5 µL	1 x
25 mM MgCl2	Applied Biosystems	1.2 µL	2 mM
10 mM dNTP	VWR	0.3 µL	0.2 mM
10 µM Forward primer	Eurofins MWG	0.15 µL	0.1 µM
10 µM Reverse primer	Eurofins MWG	0.15 µL	0.1 µM
AmpliTaq Gold DNA polymerase	Applied Biosystems	0.075 µL	0.375 Units
Nuclease-free water	Ambion	Variable	-
DMSO	Agilent Technologies	0.75 µL	5% (v/v)
DNA/ cDNA	-	Variable	20-50 ng/ 1-10 ng

Table 2. 24. PCR thermal cycling conditions.

Step	Temperature	Duration	Cycles
Initial denaturation	95°C	10 minutes	1
Denaturation	94°C	30 seconds	25 – 35
Annealing	x°C	30 seconds	
Extension	72°C	1 minute	
Final extension	72°C	7 minutes	1

Table 2. 25. gDNA primers for PCR amplification and Sanger sequencing to validate *PLCG1* mutations.

Primer name	Sequence (5' to 3')	Target Variant(s)	Amino acid change	Amplicon size	Annealing Temperature
PLCG1_C142T_F	CCTCAGCCCCAACCTCAG	c.C142T	p.R48W	316 bp	60°C
PLCG1_C142T_R	GTGGGCGCACTTACTGGC				
PLCG1_C935T_F	AGCACTCTCTCTCCTACCCC	c.C935T	p.S312L	207 bp	64°C
PLCG1_C935T_R	TGTTGTGCGAGGAGGAGATC				
PLCG1_3_F	GATCTCCTCCTCGCACAACA	c.G1024A c.C1034T	p.D342N p.S345F	310 bp	59°C
PLCG1_3_R	CACACTCAATGCAGCGACAG				
PLCG1_C1559T_F	GACCCTGGCTCACAAGTCC	c.C1559T	p.S520F	227 bp	60°C
PLCG1_C1559T_R	CCTGTCAGGGGAAGGCAA				
PLCG1_Ex29_F	CACCAGTCATCCCATCCTCT	c.G3487A c.G3493C	p.E1163K p.D1165H	300 bp	62°C
PLCG1_Ex29_R	CACGAGGGACAGAGCAAG				

Table 2. 26. cDNA primers for PCR amplification and Sanger sequencing to validate *PLCG1* mutations.

Primer name	Sequence (5' to 3')	Target Variant(s)	Amino acid change	Amplicon size	Annealing Temperature
PLCG1_cDNA_C142T_F	CCTCAGCCCCAACCTCAG	c.C142T	p.R48W	379 bp	60°C
PLCG1_ cDNA_C142T_R	AGCTGGGTCCTCTTGATAGC				
PLCG1_ cDNA_C935T_F	GGAGCCATACTTCTTCCTGGA	c.C935T c.G1024A c.C1034T	p.S312L p.D342N p.S345F	243 bp	62°C
PLCG1_ cDNA_C935T_R	TCCCAGCAGTCCAACTCAAT				
PLCG1_cDNA_C1559T_F	ACTCTGAGAACGACATCAGCA	c.C1559T	p.S520F	219 bp	58°C
PLCG1_ cDNA_C1559T_R	TCCCATGGAACCACTTCTCA				
PLCG1_ cDNA_Ex29_F	AGCCCTTCCACTTCCAGATC	c.G3487A c.G3493C	p.E1163K p.D1165H	179 bp	61°C
PLCG1_ cDNA_Ex29_R	CAACTCCAGGTCCTCACTGT				

Table 2. 27. Sanger sequencing primers used to sequence the open reading frame (ORF) of PLCγ1 plasmids. These primers were also used to PCR amplify and sequence the *PLCG1* ORF from the SeAx, HUT-78, MyLa and Jurkat cell lines.

Primer name	Sequence (5' to 3')	Target exons	Amplicon size	Annealing Temperature
PLCG1_cDNA_1_F	CCTCAGCCCCAACCTCAG	1 – 3	493 bp	64°C
PLCG1_cDNA_1_R	GCCCTTGATCCACATGTTCA			
PLCG1_cDNA_2_F	CCTGAAAACGCTGAGCCTG	2 – 10	590 bp	65°C
PLCG1_cDNA_2_R	GCGAGTTCCACACACTGTTC			
PLCG1_cDNA_3_F	CTTCCTCCGAGACCCCTTAC	9 – 14	568 bp	55°C
PLCG1_cDNA_3_R	CTCAGCCAGCTTCTTGTGC			
PLCG1_cDNA_4_F	CCCTCACCCAACCAGCTTAA	13 – 17	600 bp	57°C
PLCG1_cDNA_4_R	AAACTCATTACAGCGCAGGG			
PLCG1_cDNA_5_F	GTATCCACTCCCGGCAAGAT	17 – 21	593 bp	55°C
PLCG1_cDNA_5_R	CCTCTGGGCCTTGTAGTCAA			
PLCG1_cDNA_6_F	ACGCAACCCTGGCTTCTAT	20 – 25	571 bp	57°C
PLCG1_cDNA_6_R	TTCATCAAAGGGAACAGGCC			
PLCG1_cDNA_7_F	CCCTGGAGCTCTCTGAACTT	25 – 29	599 bp	63°C
PLCG1_cDNA_7_R	GATCTGGAAGTGGAAGGGCT			
PLCG1_cDNA_8_F	GGAGATTGAGGTGGCTGGAG	28 – 32	600 bp	65°C
PLCG1_cDNA_8_R	CAGTTCGCGGCATTCTACAA			

Table 2. 28. PCR and Sanger sequencing primers used to sequence the *PLCG1* exons from gDNA of ATLL cell lines.

Primer name	Sequence (5' to 3')	Target exons	Amplicon size	Annealing Temperature
PLCG1_cDNA_C142T_F	CCTCAGCCCCAACCTCAG	1	379 bp	58°C
PLCG1_ cDNA_C142T_R	AGCTGGGTCCTCTTGATAGC			
PLCG1_Ex2-4_F	GAATGAGGAAACCAGGCTGC	2 – 4	695 bp	61°C
PLCG1_Ex2-4_R	CTGGCTAAGGTTCTGGATGC			
PLCG1_Ex5-7_F	CCACAGGTCAGAGGTCATGA	5 – 7	672 bp	61°C
PLCG1_Ex5-7_R	ATCAAGAATCGCCCAGTGGA			
PLCG1_Ex8-10_F	GGCAGTGGGAGTAGGGAAC	8 – 10	848 bp	61°C
PLCG1_Ex8-10_R	CTGGATAGGCAAGGAGAGGC			
PLCG1_Ex11-12_F	AGCACTCTCTCTCCTACCCC	11 – 12	655 bp	61°C
PLCG1_Ex11-12_R	AGTCTTTCTGCCCTCTGTCC			
PLCG1_Ex13-15_F	CACTGTGAGGGGCTACTTAGA	13 – 15	826 bp	61°C
PLCG1_Ex13-15_R	TCCCATGGAACCACTTCTCA			
PLCG1_Ex16-17_F	CAACGAGGATGAGGAGGAGC	16 – 17	982 bp	65°C
PLCG1_Ex16-17_R	TGTGCTCTGGTCAGGCTC			

Table 2. 28. Continued.

Primer name	Sequence (5' to 3')	Target exons	Amplicon size	Annealing Temperature
PLCG1_Ex18-19_F	AGCAAAGAGTGAGGGAAGGG	18 - 19	573 bp	61°C
PLCG1_Ex18-19_R	CAACACACCAGGTCTTGCTG			
PLCG1_Ex20_F	TCCAGAAACCAGTAGCTGCT	20	233 bp	61°C
PLCG1_Ex20_R	AGATGGCCCAGAACACAGAA			
PLCG1_Ex21-23_F	GCTCTGACTGGTGCTTCTCA	21 - 23	816 bp	61°C
PLCG1_Ex21-23_R	GGGCAAGAGAAACAGATGGG			
PLCG1_Ex24_F	TGAGATGTCTATTCCCAGCTGT	24	398 bp	61°C
PLCG1_Ex24_R	ACACAACCTAAACACACCACA			
PLCG1_Ex25-27_F	CTACAGGGCCTTGTGTGTGT	25 - 27	820 bp	61°C
PLCG1_Ex25-27_R	TGACCACCTTGATGCCTGAA			
PLCG1_Ex28-30_F	AATTGGAGGGAGCAGGAAGG	28 - 30	694 bp	61°C
PLCG1_Ex28-30_R	CTGGCTCTCCTCCCACCTA			
PLCG1_Ex31-32_F	AGAAGTGCAGAGGAGTCATTG	31 - 32	498 bp	61°C
PLCG1_Ex31-32_R	CAGTTCGCGGCATTCTACAA			

2.2.8 Agarose gel electrophoresis

Two percent and 0.8% (w/v) agarose gels were made by dissolving 2 g or 0.8 g agarose powder (VWR) in 100 mL 1x TBE buffer (National Diagnostics), respectively and supplemented with 0.5 µg/mL ethidium bromide (Sigma). PCR products (3 µL) or 100 ng plasmid DNA were mixed with 3 µL glycerol loading dye and analysed adjacent to 5 µL of 100 bp molecular weight marker (Cleaver Scientific Ltd) or 1 kb DNA ladder (Thermo Fisher Scientific), respectively. Gels were immersed in 1x TBE buffer and a voltage of 180 V was applied to separate DNA fragments by molecular weight. Gels were visualised with a UV transilluminator and the GelDoc-IT^{TM} imaging system (UVP).

2.2.9 Sanger sequencing

PCR products were purified using the ExoSAP-IT enzyme (Affymetrix) that was diluted in a 1:24 ratio with nuclease-free water (Ambion). Reactions were warmed to 37°C for 30 minutes to facilitate enzyme activity and then heated to 80°C for 15 minutes to inactivate the enzyme. Purified PCR products or 300 ng plasmid DNA were sent to Source Bioscience (Cambridge) for Sanger sequencing with aliquots of 3.2 µM forward and reverse primers (Table 2. 25 – Table 2. 28). Sequencing data files were analysed using the FinchTV software (version 1.4; Geospiza) or the Sequencher software (version 4.9; Gene Codes Corporation). PCR products of DNA amplified from the peripheral blood of a healthy control individual were used to obtain wild-type sequences for the chromatograms shown in Chapter 3.

2.2.10 Cell line DNA and cDNA

Stocks of cDNA from the SeAx, HUT-78, MyLa and Jurkat cells lines were available in our research group. gDNA from 19 ATLL cell lines (CY-6, USH'2, UR1, OGF20, MKI-1, KAW2, EE8, OKA3, YGS13, JSH4, HAM9, YK8, KOB, KKI, SO4, LMY1, LMY2, LMWT5 and HUT102) was kindly provided by Professor Matilda Katan (University College London; UCL). MT2 cell line gDNA was gifted by Professor Graham Taylor (Imperial College London).

2.2.11 Pathogenicity predictions

The pathogenicity prediction algorithms Sorting Intolerant from Tolerant (SIFT) (153), Protein Variation Effect Analyzer (Provean) (154), Polymorphism Phenotyping (PolyPhen2) (155), Mutation Taster (156), MutPred2 (157) and Combined Annotation Dependent Depletion (CADD) (158) were used to predict the potential effect of *PLCG1* variants on the protein level. Damaging, deleterious, probably damaging or disease-causing variants are predicted to affect the protein structure and/ or function, whereas neutral, benign or tolerated variants are unlikely to have an impact on the protein. A consensus conclusion was drawn from 5/6 algorithms for missense mutations. The PolyPhen2 and MutPred2 algorithms cannot predict the likely effect of indels on the protein, therefore a consensus was drawn for p.VYEEDM1161V from 3/4 of the remaining algorithms.

2.2.12 Mapping mutations to the functional protein domains

PLCG1 variants were mapped to the PLCγ1 and PLCγ2 protein domains based on the amino acid numbering and protein domain schematics published by Bunney *et al.* (2012) and Liu *et al*. (2015) respectively (194, 243).

2.2.13 Mapping mutations to the PLCγ2 crystal structure

Mapping of the PLCγ1 mutations onto a composite structure of the closely related PLCγ2 isozyme was performed by Dr. Katie Everett (University of Cambridge) as follows: The 3D model of the full length PLCγ protein was generated using the structure of PLCγ2 to represent the core of PLCγ. PLCγ2 structures were obtained from the Protein Data Bank (PDB) for the spPH (PDB: 2K2J), nSH2 (PDB: 2DX0), cSH2 (PDB: 2EOB) and SH3 (PDB: 2EQI) domains. The structure of the tandem SH2 domains from PLCγ1 (PDB: 3GQI) were used to arrange these domains relative to each other. Docking of the domains to the TIM barrel was carried out using the ClusPro web-server (261, 262). The two SH2 domains were docked with the catalytic domain and then the spPH domain was added to this complex, followed by the SH3 domain. At each stage the most likely conformation was chosen based on biochemical data. The models were analysed using DeepView-Swiss-PdbViewer and the Pymol molecular visualisation software (263, 264). PLCγ1 mutations were subsequently mapped to this model.

2.2.14 Phylogenetic conservation analysis

To determine whether the amino acids changed by the mutations are evolutionarily conserved, the PLCγ1 protein sequences from 12 vertebrate species (human, chimp, monkey, mouse, rabbit, dog, horse, elephant, chicken, lizard, frog and zebrafish) were obtained from the genome browser Ensembl and aligned using the multiple sequence alignment software Clustal Omega (265). The human PLCγ1 and PLCγ2 protein sequences were aligned with Clustal Omega to identify the PLCγ2 residues that correspond to the PLCγ1 amino acids altered by mutations. The conservation analysis was repeated for these PLCγ2 residues in the same vertebrate species.

2.2.15 Determining the *PLCG1* mutation frequency in mature T-cell lymphomas

The frequency of somatic *PLCG1* mutations in mature T-cell lymphomas was obtained by filtering for variants identified in haematopoetic and lymphoid tissue in the COSMIC database (Version 87).

The following analyses were performed by Dr. Christine Jones (KCL). To determine the frequency of *PLCG1* mutations per disease subtype, the PubMed database was searched to identify publications incorporating the WHO classification of T-cell lymphomas: adult T-cell leukaemia/lymphoma, anaplastic large cell lymphoma, angioimmunoblastic T-cell lymphoma, enteropathy-associated T-cell lymphoma, extra-nodal natural killer /T-cell lymphoma (nasal type), hepatosplenic T-cell lymphoma, lymphomatoid papulosis, Mycosis Fungoides / Sézary Syndrome, peripheral T-cell lymphoma-not otherwise specified, primary cutaneous anaplastic large cell lymphoma, primary cutaneous CD30-positive T cell lymphoproliferative disorders, T-cell large granular lymphocyte leukaemia or T-cell prolymphocytic leukaemia in combination with either the term “next generation sequencing” or “whole-exome sequencing”. The resulting publications and corresponding supplementary data were interrogated for *PLCG1* mutations.

2.2.16 Plasmids

The PLCγ1-pTriEx-4 and eGFP-PLCγ1 vectors, which encode the full length wild-type human *PLCG1* cDNA, with the latter containing a GFP tag, were kindly provided by Professor Matilda Katan (UCL). These vectors were used as templates to create mutant PLCγ1 constructs by site-directed mutagenesis. The pGL3-NFκB-firefly

luciferase reporter plasmid (which contains five NFκB response elements: GGGGACTTTCCC), the pGL3-AP-1-firefly luciferase construct (that encompasses three AP-1 binding motifs: TGACTCA) and the transfection control pRL-TK-renilla luciferase vector were a kind gift from Dr. Susan John (KCL). The pGL3-NFAT-firefly luciferase reporter construct that harbours three NFAT response elements (AGGAAAAACTGTTTCA) was purchased from the Addgene repository (#17870). The pBABE-EGFR construct was kindly provided by Professor Mahvash Tavassoli (KCL). Table 2. 29 lists all the plasmids used in this study. The primers used to sequence the regulatory regions of the plasmid including the cytomegalovirus (CMV) enhancer and promoter, T7 and P10 promoters and polyA tail are listed in Table 2. 30. The primers used to confirm the transcription factor binding sites in the reporter plasmids and the EGFR sequence in the pBABE-EGFR vector are listed in Table 2. 31. Plasmid features were visualised using the SnapGene Viewer software (version 2.7.2 from GSL Biotech; available at snapgene.com), as shown for the PLCγ1-pTriEx-4 and eGFP-PLCγ1 vectors in Figure 2. 1.

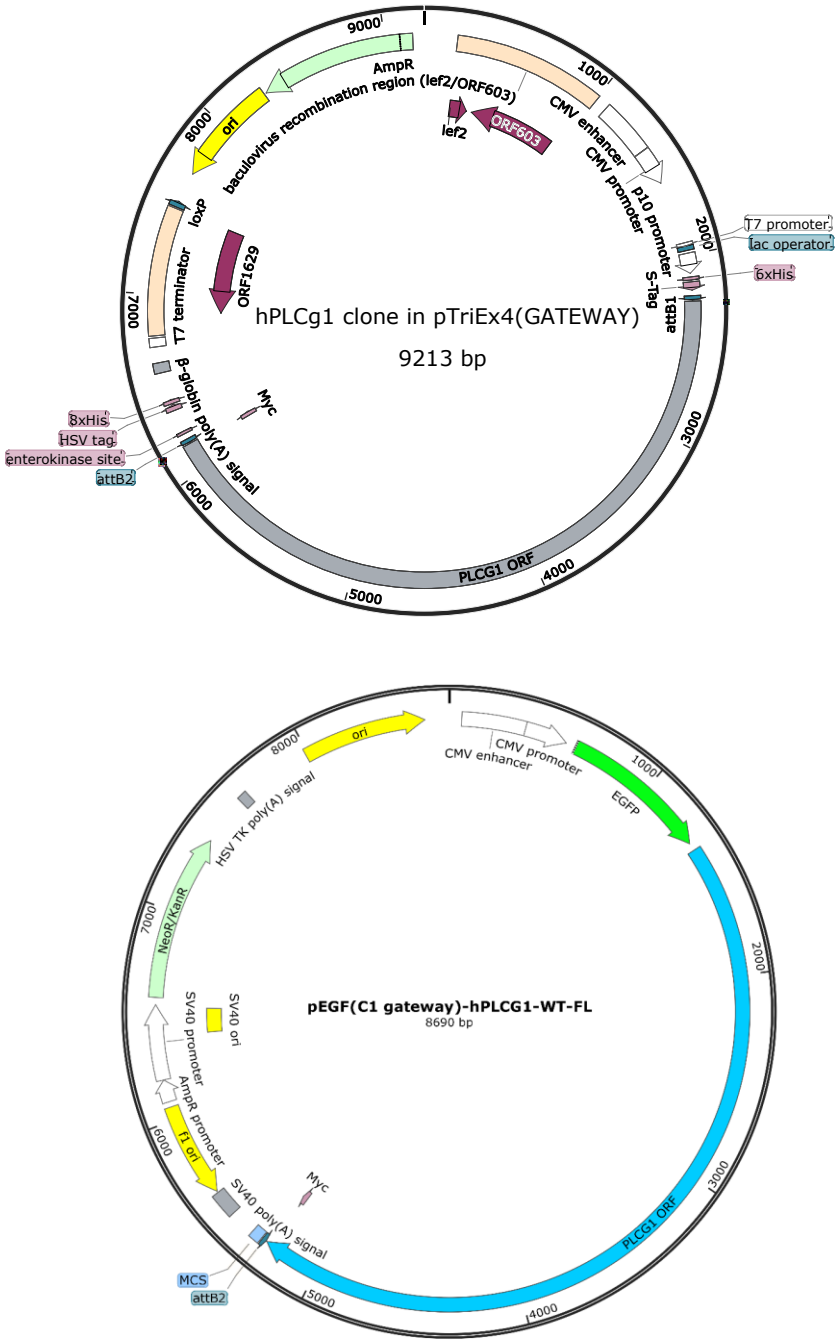

Figure 2. 1. Maps of the PLCγ1-pTriEx-4 and eGFP-PLCγ1 vectors.

Table 2. 29. Plasmids used in this study. Full Length (FL); human (h). Ampicillin (Amp), Kanamycin (Kan) Professor Matilda Katan (MK), Varsha M. Patel (VMP), Dr. Antoinette Yoxall (AY), Dr. Susan John (SJ) and Professor Mahvash Tavassoli (MT).

Plasmid name	Key property	Vector	Antibiotic resistance	Source
WT	FL hPLCG1 wild-type cDNA	pTriEx-4	Amp	MK
R48W	FL hPLCG1 cDNA: c.C142T mutant	pTriEx-4	Amp	VMP
S312L	FL hPLCG1 cDNA: c.C935T mutant	pTriEx-4	Amp	VMP
D342N	FL hPLCG1 cDNA: c.G1024A mutant	pTriEx-4	Amp	VMP
S345F	FL hPLCG1 cDNA: c.C1034T mutant	pTriEx-4	Amp	MK
S520F	FL hPLCG1 cDNA: c.C1559T mutant	pTriEx-4	Amp	MK
Y783F	FL hPLCG1 cDNA: c.A2348T mutant	pTriEx-4	Amp	MK
R1158H	FL hPLCG1 cDNA: c.G3473A mutant	pTriEx-4	Amp	AY
E1163K	FL hPLCG1 cDNA: c.G3487A mutant	pTriEx-4	Amp	VMP
D1165H	FL hPLCG1 cDNA: c.G3493C mutant	pTriEx-4	Amp	VMP
VYEEDM1161V	FL hPLCG1 cDNA: c.GTGTATGAGGAAGACAdelG mutant	pTriEx-4	Amp	AY
S345F-Y783F	FL hPLCG1 cDNA: c.C1034T & c.A2348T mutant	pTriEx-4	Amp	VMP
S520F-Y783F	FL hPLCG1 cDNA: c.C1559T & c.A2348T mutant	pTriEx-4	Amp	VMP
E1163K-Y783F	FL hPLCG1 cDNA: c.G3487A & c.A2348T mutant	pTriEx-4	Amp	VMP

Table 2. 29. Continued

Plasmid name	Key property	Vector	Antibiotic resistance	Source
eGFP-WT	FL hPLCG1 wild-type cDNA & GFP tag	pEGFP-C1 gateway	Kan	MK
eGFP-D342N	FL hPLCG1 cDNA: c.C1024T mutant; GFP tag	pEGFP-C1 gateway	Kan	VMP
eGFP-S345F	FL hPLCG1 cDNA: c.C1034T mutant; GFP tag	pEGFP-C1 gateway	Kan	VMP
eGFP-S520F	FL hPLCG1 cDNA: c.C1559T mutant; GFP tag	pEGFP-C1 gateway	Kan	VMP
eGFP-Y783F	FL hPLCG1 cDNA: c.A2348T mutant; GFP tag	pEGFP-C1 gateway	Kan	VMP
eGFP-E1163K	FL hPLCG1 cDNA: c.G3487A mutant; GFP tag	pEGFP-C1 gateway	Kan	VMP
eGFP-D1165H	FL hPLCG1 cDNA: c.G3493C mutant; GFP tag	pEGFP-C1 gateway	Kan	VMP
eGFP-VYEEDM1161V	FL hPLCG1 cDNA: c.GTGTATGAGGAAGACAdelG mutant; GFP tag	pEGFP-C1 gateway	Kan	VMP
pGL3-NFAT-luciferase	3x AGGAAAAACTGTTTCA NFAT response elements	pGL3	Amp	Addgene
pGL3-NFκB-luciferase	5x GGGGACTTTCCC NFκB response elements	pGL3 basic	Amp	SJ
pGL3-AP-1-luciferase	3x TGACTCA AP-1 response elements	pGL3 basic	Amp	SJ
pRL-TK-luciferase	Renilla Thymidine Kinase Luciferase Reporter	pRL-TK	Amp	SJ
pBABE-EGFR	EGF receptor	pBABE	Amp	MT

Table 2. 30. Sanger sequencing primers used to sequence the regulatory regions of plasmids. The CMV and polyA tails of the pTriEx4-PLCγ1 and eGFP-PLCγ1 plasmids were sequenced. The CMV promoter and enhancer sequences in all plasmids were verified using the pTriEx4_PLCG1_CMV primer pair. The T7 and P10 promoters were sequenced in the pTriEx4-PLCγ1 vectors and the GFP tag in the eGFP-PLCγ1 plasmids.

Primer name	Sequence (5' to 3')
pTriEx4_PLCG1_CMV_F	CGGGGTCATTAGTTCATAGCC
pTriEx4_PLCG1_CMV_R	AGCATCTAGTGATCTGACGGT
pTriEx4_PLCG1_polyA_F	TCACAAATACCACTGAGATCGAT
pTriEx4_PLCG1_polyA_R	CCAAGGGGTTATGCTAGTTACA
pTriEx4_PLCG1_T7_P10_F	TGCTGTCTCATCATTTTGGCA
pTriEx4_PLCG1_T7_P10_R	GTGATGGTGGTGATGGTGTG
eGFP_PolyA_F	GCCATACCACATTTGTAGAGGT
eGFP_PolyA_R	CAACACTCAACCCTATCTCGG
eGFP_1_F	GTGTACGGTGGGAGGTCTAT

Table 2. 31. Sanger sequencing primers used to confirm key characteristics in vectors. The sequence of transcription factor binding sites in the reporter plasmids, the chimeric intron in the Renilla transfection control plasmid and the EGFR sequence in the pBABE-EGFR vector were analysed.

Primer name	Plasmid	Sequence (5' to 3')
pGL3_MCS_Luc_F	pGL3-AP-1-luciferase	GGCATTCCGGTACTGTTGGT
pGL3_MCS_Luc_R	pGL3-NFκB-luciferase	TGTCCACCTCGATATGTGCA
pGL3_NFAT_Luc_F	pGL3-NFAT	GCTAGCCCCGATGTTTTCTG
pGL3_NFAT_Luc_R		GCCGGGCCTTTCTTTATGTT
pRLTK_C_intron_F	pRL-TK-luciferase	CTGCAGAAGTTGGTCGTGAG
pRLTK_C_intron_R		CTTTCGAAGTCATGGTGGCT
EGFR_RTPCR_2F	pBABE-EGFR	CCAAGGCACGAGTAACAAGC
EGFR_RTPCR_3R		ATTCGCTCCACTGTGTTGAG

2.2.17 Luria–Bertani (LB) medium and LB-agar plates

LB medium and LB-agar medium were made as per Table 2. 32 and Table 2. 33, respectively and sterilised by autoclaving at 121°C for 20 minutes. The LB-agar medium was cooled to approximately 50°C before an Ampicillin or Kanamycin solution (both Sigma-Aldrich) was added to a final concentration of 50 μg/mL. The LB-agar medium was poured into sterile petri dishes and allowed to set before storing at 4°C.

Table 2. 32. Recipe for 400 mL of LB medium for bacterial cultures.

Reagent	Quantity	Final concentration
Sodium chloride (VWR)	4 g	1% (w/v)
Bacto trypton (BD Biosciences)	4 g	1% (w/v)
Bacto yeast extract (BD Biosciences)	2 g	0.5% (w/v)
MilliQ water	Up to 400 mL	-

Table 2. 33. Recipe for 400 mL of LB-agar for bacterial culture plates.

Reagent	Quantity	Final concentration
Sodium chloride (VWR)	4 g	1% (w/v)
Bacto trypton (BD Biosciences)	4 g	1% (w/v)
Bacto yeast extract (BD Biosciences)	2 g	0.5% (w/v)
MilliQ water	Up to 400 mL	-
Bacto agar (BD Biosciences)	6 g	1.5% (w/v)

2.2.18 Site-directed mutagenesis

The PCR-based mutagenesis reactions were prepared as per Table 2. 34 using the QuikChange Lightning Site-Directed Mutagenesis Kit (Agilent Technologies). Salt-free mutagenesis primers (Eurofins MWG) used to introduce the nucleotide changes are listed in Table 2. 35 and the thermal cycling conditions shown in Table 2. 36. Mutagenesis reaction products were treated with 2 μL endonuclease *Dpn* I for 5 minutes at 37°C to digest methylated and hemimethylated wild-type template DNA.

XL-10 Gold Ultracompetent cells were transformed with the plasmids as per the mutagenesis kit manual. Fifty microliters of transformed cells were diluted in 200 µL nutrient-rich Super Optimal broth with Catabolite repression (SOC) medium (New England Biolabs) and spread on LB-agar plates that contained either 50 µg/mL Ampicillin or Kanamycin, to select for cells successfully transformed with the plasmids that encode antibiotic resistance genes. Plates were incubated at 37°C for 16 hours.

Table 2. 34. Site-directed mutagenesis reaction composition. Reactions were set up as per the QuikChange Lightning Site-Directed Mutagenesis Kit manual. *DMSO was added to the reactions that contained GC-rich primers, namely for the production of the PLCγ1-R48W, PLCγ1-S312L and PLCγ1-D342N plasmids.

Reagent	**Volume (51 µL reaction)**
10 x reaction buffer	5 µL
dNTP mix	1 µL
100 ng dsDNA template	Variable
Forward primer (125 ng/µL)	1
Reverse primer (125 ng/µL)	1
QuikSolution reagent	1.5 µL
DMSO*	2.5 µL
Nuclease-free water (Ambion)	Variable
QuikChange Lightening Enzyme	1 µL

Table 2. 35. Primers for site-directed mutagenesis. Underlined bases indicate mutant nucleotides introduced during the reaction.

Primer name	Sequence (5' to 3')	Target Variant	Amino acid change
C142T_F_MUT	CAGCGACCCGAGTGGAAGACCTTCC	c.C142T	p.R48W
C142T_R_MUT	GGAAGGTCTTCCACTCGGGTCGCTG		
C935T_F_MUT	CAAAGAGAACAGTGTGTGGAACTTGCAGCTGGATGC	c.C935T	p.S312L
C935T_R_MUT	GCATCCAGCTGCAAGTTCCACACACTGTTCTCTTTG		
G1024A_F_MUT	GTACCTGACCGGGAACCAGTTCTCCAG	c.G1024A	p.D342N
G1024A_R_MUT	CTGGAGAACTGGTTCCCGGTCAGGTAC		
C1034T_F_MUT	CGGGGACCAGTTCTTCAGTGAGTCCTCC	c.C1034T	p.S345F
C1034T_R_MUT	GGAGGACTCACTGAAGAACTGGTCCCCG		
C1559T_F_MUT	GCAGCAAGATCTACTACTTTGAGGAGACCAGCAGTG	c.C1559T	p. S520F
C1559T_R_MUT	CACTGCTGGTCTCCTCAAAGTAGTAGATCTTGCTGC		
Y783_F_MUT	ACGCAACCCTGGCTTCTTTGTAGAGGCAAACC	c.A2348T	p.Y783F
Y783_R_MUT	GGTTTGCCTCTACAAAGAAGCCAGGGTTGCGT		
G3473A_F_MUT	TGAATTTGCCTTTCTGCACTTCGTGGTGTATGAGG	c.G3473A	p.R1158H
G3473A_R_MUT	CCTCATACACCACGAAGTGCAGAAAGGCAAATTCA		
G3487A_F_MUT	CTGCGCTTCGTGGTGTATAAGGAAGACATGTTTAGTG	c.G3487A	p.E1163K
G3487A_R_MUT	CACTAAACATGTCTTCCTTATACACCACGAAGCGCAG		
G3493C_F_MUT	CTTCGTGGTGTATGAGGAACACATGTTTAGTGACC	c.G3493C	p.D1165H
G3493C_R_MUT	GGTCACTAAACATGTGTTCCTCATACACCACGAAG		
Del _F_MUT	CCTTTCTGCGCTTCGTGGTGTTTAGTGACCAGAATT	c.GTGTATGAGG AAGACAdel-insG	p.VYEEDM1161V
Del_R_MUT	AATTCTGGTCACTAAACACCACGAAGCGCAGAAAGG		

Table 2. 36. Thermal cycling conditions for site-directed mutagenesis reactions. The duration of the extension step varied based on the size of the vector and was calculated as per the manufacturer's protocol (30 seconds per kb of plasmid).

Step	Temperature	Duration	Cycles
Initial denaturation	95°C	2 minutes	1
Denaturation	95°C	20 seconds	18
Annealing	60°C	10 seconds	
Extension	68°C	4min 36sec for pTriEx-4 vector (9.2 kb) or 4min 21sec for eGFP- vector (8.69 kb)	
Final extension	68°C	5 minutes	1

2.2.19 Bacterial cultures

Individual bacterial colonies were inoculated in 5 mL LB medium supplemented with 50 µg/mL Ampicillin or Kanamycin for 16 hours at 37°C with shaking at 180 rpm. Bacterial cultures were centrifuged at 3,000 rpm for 10 minutes at 4°C and cell pellets were either frozen at -20°C or used immediately for plasmid DNA isolation. Alternatively, 5 mL starter cultures were incubated for 8 hours at 37°C with shaking at 180 rpm before adding a 1:100 dilution of the culture to 50 mL or 1:500 dilution to 150 mL LB medium supplemented with 50 µg/mL Ampicillin or Kanamycin. Cultures were grown for 16 hours at 37°C with shaking at 180 rpm. Cultures were centrifuged at 4,500 rpm for 15 minutes at 4°C and cell pellets were either frozen at -20°C or used immediately for plasmid DNA isolation

2.2.20 Glycerol stocks

Glycerol stocks of bacterial cultures were made by mixing 250 µL of 80% (v/v) sterile glycerol (Sigma-Aldrich) with 750 µL of bacterial culture and stored at -80°C.

2.2.21 Streaking glycerol stocks

To grow single colonies, 1 µL of bacterial glycerol stocks were diluted in 49 µL LB media and spread on LB-agar plates that contained the appropriate antibiotic.

2.2.22 Plasmid DNA isolation

Plasmid DNA was isolated from 5 mL, 50 mL and 150 mL bacterial cell pellets using the QIAprep Spin Miniprep Kit, the HiSpeed Plasmid Midi Kit and the HiSpeed Plasmid Maxi Kit, respectively according to the manufacturer's guidelines. Plasmid DNA was eluted in 30 µL EB buffer when isolated using the QIAprep Spin Miniprep Kit and in 1 mL TE buffer when extracted using the larger kits. DNA concentrations were quantified using the Nanodrop ND-1000 spectrophotometer and plasmids were stored at -20°C.

2.2.23 Cell line cultures

2.2.23.1. *Cell lines*

HEK293 cells, a Human embryonic kidney cell line, was kindly provided by Dr. Francesca Capon (KCL). COS-7 cells, a monkey fibroblast-like cell line was cultured and used for experiments by Dr. Marta Martins (Instituto de Medicina Molecular, Portugal). HeLa cells, a cervical cancer cell line was a kind gift from Professor Maddy Parsons (KCL). All cultures were maintained at 37°C, 5% CO_2 and 95% humidity in T75 flasks (Corning Incorporated).

2.2.23.2. *Reviving frozen cells and maintaining cell cultures*

Frozen cell lines were thawed at 37°C for 1 minute and then centrifuged at 1,500 rpm for 5 minutes at 22°C. After washing with 1 mL PBS (Gibco), cells were re-suspended in 10 mL complete DMEM medium (Gibco) composed of DMEM supplemented with 10% (v/v) FBS (Biosera), 100 Units/mL Penicillin and 100 µg/mL Streptomycin (Gibco). Cells were sub-cultured twice a week by washing with 5 mL PBS and dissociation with 2.5 mL Trypsin (Gibco).

2.2.23.3. *Freezing cell line cultures*

Cells in the log phase of growth were frozen at a density of 1 – 3 x 10^6 cells/mL in freezing medium composed of 90% (v/v) FBS supplemented with 10% (v/v) DMSO that was filter sterilised. Cells were stored in cryogenic vials at -80°C before being transferred to liquid nitrogen for long term storage.

2.2.24 Mycoplasma testing

Cell line cultures were routinely tested and confirmed to be free from Mycoplasma contamination using the techniques described in section 2.2.23.1 – 2.2.23.2.

2.2.23.1. *PCR-based Mycoplasma testing*

Cell supernatants were pre-heated at 95°C for 5 minutes and then added to PCRs prepared as per Table 2. 37 (266). Negative and positive control reactions contained 2.5 µL sterile water or Mycoplasma-containing supernatant, respectively. Reactions were subjected to the thermal conditions shown in Table 2. 38. PCR products were analysed by agarose gel electrophoresis as per section 2.2.8.

Table 2. 37. Mycoplasma PCR composition.

Reagent	**Volume**	**Final concentration**
2x PCR Master Mix (Promega Corporation)	6.25 µL	1 x
GPO-3 forward primer (Eurofins MWG) 5’ GGGAGCAAACAGGATTAGATACCCT 3’	0.25 µL	5 µM
MGSO reverse primer (Eurofins MWG) 5’ TGCACCATCTGTCACTCTGTTAACCTC 3’	0.25 µL	5 µM
Nuclease-free water	3.25 µL	-
Cell supernatant	2.5 µL	-

Table 2. 38. PCR thermal cycling conditions for Mycoplasma testing of cell lines.

Step	**Temperature**	**Duration**	**Cycles**
Initial denaturation	94°C	2 minutes	1
Denaturation	94°C	1 minute	40
Annealing	55°C	1 minute	
Extension	72°C	2 minutes	
Final extension	72°C	5 minutes	1

2.2.23.2. *Biotool Mycoplasma Detection QuickTest kit*

The Biotool Mycoplasma Detection QuickTest kit was used as per the manufacturer's guidelines. The kit indicates the presence of Mycoplasma metabolites based on a visual colourimetric analysis.

2.2.25 Transfection of HEK293 cells for western botting

HEK293 cells were seeded at a density of 4 x 10^5 cells in 2 mL complete DMEM in 6-well plates. After 24 hours, the FuGENE HD Transfection Reagent (Promega Corporation) and the PLCγ1-pTriEx-4 plasmids were diluted in a 1.5 µL:0.5 µg ratio in Opti-MEM I Reduced Serum Medium (Gibco) to a final volume of 100 µL. TE buffer was used as a vehicle control for transfections. FuGENE-DNA complexes were allowed to form during a 15 minute incubation at room temperature and then added dropwise to cells before incubating at 37°C.

2.2.26 Pervanadate treatment of HEK293 cells for western blotting

A 30mM stock of pervanadate, a protein-tyrosine phosphatase inhibitor, was made as per Table 2. 39. The stock was sterilised through a 0.2 micron filter and incubated at room temperature for 15 minutes in the dark. The stock was then diluted to 1 mM in serum-containing DMEM and added to cell cultures at a final concentration of 100 µM. Cells were treated with pervanadate 23 hours after transfection for 1 hour to stabilise PLCγ1 phosphorylation (213). Cells were immediately harvested by detachment with Trypsin and centrifugation at 6,000 rpm for 5 minutes at 22°C. Cell pellets were washed in 100 µL PBS and centrifuged again before storing at -80°C.

Table 2. 39. Recipe for 0.3 mL of 30 mM Pervanadate.

Reagent	**Quantity**	**Final concentration**
Sodium orthovanadate (New England Biolabs UK Ltd)	90 µL	30 mM
Hydrogen Peroxide (Atom Scientific)	1.54 µL	0.18% (w/w)
PBS (Gibco)	208.45 µL	1x

2.2.27 Co-transfection of HEK293 cells for luciferase reporter assays

HEK293 cells were co-transfected with PLCγ1-pTriEx-4 vectors, NFκB-, NFAT- or AP-1-firefly luciferase reporter plasmids and the Renilla transfection control construct as described by Vaqué *et al*. (2014) (160). Briefly, 8 x 10^4 cells were seeded in 0.5 mL complete DMEM medium in 24-well plates. After 24 hours, 50 ng pRL-TK, 100 ng firefly luciferase reporter constructs, 1 µg of PLCγ1-pTriEx-4 vectors or TE buffer (vehicle control), 3 µL Lipofectamine LTX and 1 µL Plus Reagent (Life Technologies) were diluted in Opti-MEM I Reduced Serum Medium to a final volume of 100 µL and incubated at room temperature for 10 minutes. The DNA-lipofectamine complexes were added drop-wise to cells and incubated at 37°C. After 4 hours, cells were starved in 0.5 mL serum- and antibiotic-free DMEM to remove any growth factors in the media that can activate PLCγ1. After 16 hours, cells were washed in 100 µL PBS and lysed in 100 µL passive lysis buffer (PLB) provided in the Dual-Luciferase Reporter Assay System kits (Promega Corporation). Lysates were used immediately to measure luminescence levels or stored at -80°C.

2.2.28 EGF stimulation of HEK293 cells for luciferase reporter assays

For cells to be analysed in stimulated conditions, HEK293 cells were additionally co-transfected with 0.75 µg of the pBABE-EGFR plasmid as the cells endogenously express the EGF receptor at low levels (267, 268). After serum starving for 16 hours, cells were stimulated with 100 ng/mL EGF for 8 hours, washed with PBS and lysed as described in section 2.2.27.

2.2.29 Extraction of whole-cell lysates for western blotting

Complete RIPA buffer (Santa Cruz Biotechnology) was prepared as per Table 2. 40 and used to lyse cell pellets that were either freshly harvested or stored at -80°C. Lysates were chilled on ice for 20 minutes and then centrifuged at 13,000 rpm for 10 minutes at 4°C. Protein-containing supernatants were stored at -80°C.

Table 2. 40. Recipe for 1 mL of complete RIPA buffer for whole-cell lysates. All reagents were purchased from Santa Cruz Biotechnology.

Reagent	Quantity	Final concentration
1x RIPA lysis buffer	0.96 mL	1x
Phenylmethylsulfonyl fluoride (PMSF)	0.01 mL	2 mM
Sodium othovanadate	0.01 mL	1 mM
Protease inhibitor cocktail	0.02 mL	2% (v/v)

2.2.30 Protein quantification

The protein concentration of whole-cell lysates was quantified using the Pierce BCA protein assay kit (Thermo Scientific) as per the manufacturer's guidelines. Briefly, BSA protein standards were diluted in complete RIPA buffer and the BCA working reagent was made by mixing reagent A and reagent B in a 50:1 ratio. Two hundred microliters of working reagent were added to 10 µL BSA protein standards or cell lysates, mixed thoroughly and incubated at 37°C for 30 minutes. BSA protein standards were quantified in triplicates to determine the mean absorbance at 562 nm using the FLUOstar Omega plate reader (BMG Labtech) and MARS data analysis software. Based on the absorbance and concentration of each protein standard, a standard curve was produced using linear regression. The standard curve was used to infer the concentration of each lysate, measured in duplicates.

2.2.31 Western blotting

Whole-cell lysates were mixed with 4x Laemmli sample buffer (Bio-Rad Laboratories Incorporated) that was supplemented with 10% (v/v) β-Mercaptoethanol (Sigma). Lysates were denatured at 95°C for 10 minutes. Protein extracts (10 µg) were loaded onto 10% gels made as per Table 2. 41 alongside 7 µL of the Precision plus protein dual color standard (Bio-Rad Laboratories Incorporated). Gels were immersed in 1x running buffer (25 mM Trizma-Base, 192 mM Glycine and 0.1% (v/v) SDS) that was made by diluting 10x buffer (made as per Table 2. 42) in a 1:9 ratio. A voltage of 135 V was applied for 2 hours to separate proteins by molecular weight. Proteins were electro-transferred onto methanol-primed 0.2 µm PVDF membranes (Roche Diagnostics Limited) at 90 V for 2.5 hours at 4°C. Transfer buffer was prepared as per

Table 2. 43. Membranes were blocked with 5% blocking buffer made as per Table 2. 44 for up to 2 hours. Membranes were incubated in the primary antibodies: rabbit monoclonal anti-PLCγ1 (1:20,000), mouse monoclonal anti-penta-His-tag (1:2,000 and 1:5,000), rabbit polyclonal anti-Tyr783-phospho-PLCγ1 (p-PLCγ1; 1:50,000) and rabbit polyclonal anti-β-Actin (1:10,000) at 4°C overnight or at room temperature for up to 2 hours. Antibodies detecting total or phosphorylated proteins were diluted in 5% milk or 5% BSA blocking buffer, respectively. After washing with TBS-T, membranes were incubated in HRP-linked goat anti-rabbit IgG H&L (1:5,000 – 1:10,000) or goat anti-mouse IgG H&L (HRP; 1:5,000) for up to 2 hours at room temperature. Membranes were washed and protein expression detected with The Amersham ECL Prime Western Blotting Detection Reagent (GE Healthcare Life Sciences). Membranes were exposed to X-ray films (Fujifilm) and chemiluminescent signals were developed with a medical film processor (SRX-101A, Konica Minolta).

Table 2. 41. Recipe for making 10% polyacrylamide gels for western blotting.

Reagent	**Separation gel Volume (mL)**	**Stacking gel Volume (mL)**
MilliQ water	4.0	2.1
30% (w/v) Acrylamide (National diagnostics)	3.3	0.5
1.5 M Tris-HCl pH 8.8	2.5	-
1 M Tris-HCl pH 6.8	-	0.38
10% (w/v) SDS (Bio-Rad Laboratories Incorporated)	0.10	0.03
10% (w/v) APS	0.10	0.03
TEMED (Sigma-Aldrich)	0.004	0.003

Table 2. 42. Recipe for 1 litre of 10x running buffer for western blotting.

Reagent	**Quantity**	**Final concentration**
Trizma-Base (Sigma)	30.2 g	250 mM
Glycine (Sigma)	144 g	1.92 M
10% (w/v) SDS	100 mL	1% (v/v)
MilliQ water	Up to 1 litre	-

Table 2. 43. Recipe for 1 litre of 1x transfer buffer for western blotting.

Reagent	Quantity	Final concentration
Trizma-Base (Sigma)	3 g	25 mM
Glycine (Sigma)	14.4 g	192 mM
MilliQ water	Up to 800 mL	-
Methanol (VWR)	200 mL	0.2% (v/v)

Table 2. 44. Recipe for 5% (w/v) of blocking buffer for western blotting.

Reagent	Quantity	Final concentration
1x TBS-T	40 mL	1x
Milk or BSA	2 g	5%

2.2.32 Optimisation of HEK293 transfection and antibody dilution for western blotting

To optimise the transfection of HEK293 cells, different ratios of the FuGENE reagent and DNA concentrations (3µL:1µg, 6µL:1µg, 3µL:2µg, 6µL:2µg, 6µL:3µg and 6µL:4µg) were tested. Whole-cell lysates were probed with 1:2,000 and 1:5,000 dilutions of a penta-His antibody and analysed by western blotting. The antibody binds to the 6-His tag epitope encoded upstream the *PLCG1* ORF in the pTriEx-4 vector (Figure 2. 1). The 6µL:2µg ratio produced the most intense and specific 150 kDa protein band (that corresponds to His-tagged PLCγ1) when probed with both antibody dilutions (Figure 2. 2). Therefore, the 6µL:2µg ratio of FuGENE reagent to DNA quantity was used for all subsequent cell transfections for western blotting analyses.

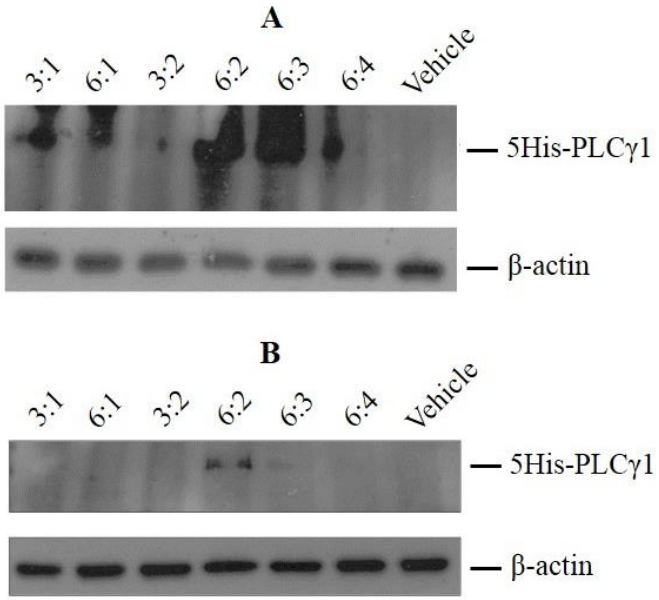

Figure 2. 2. Optimisation of HEK293 cell transfection and penta-His antibody dilution for western blotting. Cells were transfected with different ratios of FuGENE reagent (µL):DNA concentration (µg) and whole-cell lysates were probed with (A) 1:2,000 and (B) 1:5,000 dilutions of a penta-His antibody to detect the 6-His-tagged PLCγ1 protein (150 kDa). β-actin (45 kDa) expression was used as a loading control. The blots shown represent one experiment.

The penta-His antibody produced a high level of background and would not be ideal for comparing the expression of wild-type and mutant PLCγ1 proteins. Therefore, whole-cell lysates from HEK293 cells transfected with wild-type PLCγ1 or a vehicle control were probed with 1:8,000 and 1:20,000 dilutions of a monoclonal anti-PLCγ1 antibody. The 1:20,000 antibody dilution produced a more specific protein band corresponding to PLCγ1 than the 1:8,000 dilution, which resulted in a higher level of background binding (Figure 2. 3). Therefore, a 1:20,000 dilution of the anti-PLCγ1 antibody was determined to be optimal for subsequent analyses.

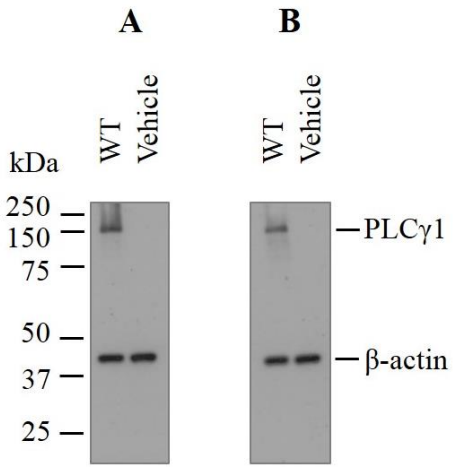

Figure 2. 3. Anti-PLCγ1 antibody dilution optimisation for western blotting. Whole-cell lysates from HEK293 cells transfected with the wild-type PLCγ1 vector or vehicle control were probed with (A) 1:8,000 or (B) 1:20,000 dilutions of the antibody. β-actin expression was used as a loading control. The blots shown represent one experiment.

To optimise the detection of phosphorylated PLCγ1 (p-PLCγ1) expression, whole-cell lysates of cells transfected with wild-type PLCγ1 or vehicle control were probed with increasing dilutions of an anti-p-PLCγ1 antibody. Cells were treated with the protein-tyrosine phosphatase inhibitor pervanadate for 1 hour before harvesting, to stabilise the phosphorylation signal as per Kunze *et al*. (2014) (213). Transfected cells that were not treated with pervanadate did not show a p-PLCγ1 signal (data not shown). Lysates were first probed with 1:1,000, 1:3,000 and 1:8,000 antibody dilutions, which resulted in intense non-specific signals (data not shown). The antibody was further diluted to 1:25,000, 1:30,000, 1:40,000, 1:45,000 and 1:50,000. In wild-type PLCγ1-transfected cells, all five dilutions produced a strong band with a molecular weight of over 150 kDa, which corresponds to the 155 kDa weight of p-PLCγ1 (Figure 2. 4). The 1:50,000 anti-p-PLCγ1 antibody dilution was determined to be optimal for analysing phosphorylated PLCγ1 expression in subsequent experiments.

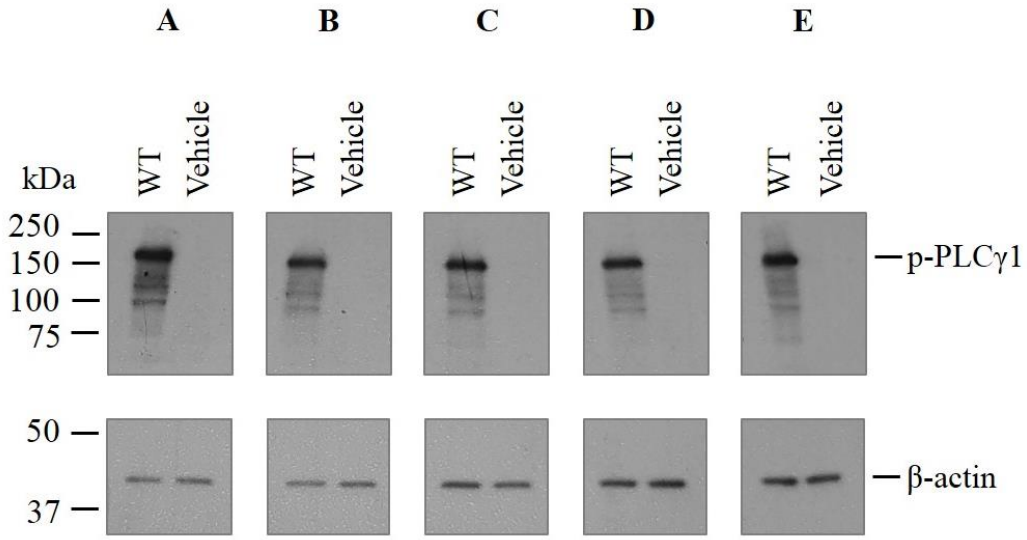

Figure 2. 4. Anti-p-PLCγ1 antibody dilution optimisation for western blotting. (A) 1:25,000, (B) 1:30,000, (C) 1:40,000, (D) 1:45,000 and (E) 1:50,000 dilutions of an anti-p-PLCγ1 antibody were used to probe whole-cell lysates from HEK293 cells transfected with wild-type PLCγ1 vector or vehicle control. β-actin was used as a loading control. The blots shown represent one experiment.

2.2.33 IP quantification

IP quantification experiments were performed by Dr. Marta Martins (Instituto de Medicina Molecular, Portugal). IP levels were quantified in COS-7 cells transfected with PLCγ1-pTriEx-4 vectors as per Everett *et al.* (2009) (269), with the exceptions of cells transfected with 2.5 µg of plasmid DNA and counts per minute quantified instead of disintegrations per minute. For stimulation experiments, cells were treated with 100 ng/mL EGF for 1 hour before quantifying IP production. All assays were performed in internal duplicates and repeated at least twice. IP levels were normalised to cells transfected with wild-type PLCγ1 but not subsequently stimulated.

2.2.34 IKKβ inhibitor treatment

HEK293 cells co-transfected with the wild-type or mutant PLCγ1-pTriEx-4 vectors, the NFκB-firefly luciferase plasmid and pRL-TK transfection control construct, were starved overnight as detailed in section 2.2.27. Cells were treated with increasing doses (10 nM – 10 µM) of the IKKβ inhibitor IV (TPCA-1; Santa Cruz Biotechnology) for 8 hours. For stimulation experiments cells were also co-transfected with 0.75 µg of

the pBABE-EGFR construct and stimulated with 100 ng/mL EGF for 8 hours, after 30 minutes of pre-treatment with TPCA-1 (total TPCA-1 treatment for 8.5 hours). The cells were washed in 100 µL PBS, lysed in 100 µL PLB and stored at -80°C.

Transfected cells were also stimulated with TNFα (Peprotech Incorporated) as follows. HEK293 cells were co-transfected with the NFκB-firefly luciferase plasmid and pRL-TK construct. After 24 hours, cells were pre-treated with TPCA-1 for 30 minutes before stimulation with 10 ng/mL TNFα for 5 hours (270). Cells were lysed as described above and stored at -80°C.

2.2.35 Dual-Luciferase Reporter Assays

The Dual-Luciferase Reporter Assay System (E1910; Promega Corporation) was used to quantify luciferase levels in co-transfected cells. Fifteen – twenty microliters of lysates from sections 2.2.27, 2.2.28 and 2.2.34 were analysed in duplicate or triplicate in white opaque 96-flat well bottom plates (Corning Incorporated) using the Orion II microplate luminometer (Berthold Detection Systems). The firefly luciferase reporter gene measurement was determined in relative light units by the addition of 100 µL Luciferase Assay Reagent II. Addition of 100 µL Stop & Glo Reagent quenched firefly luminescence and enabled quantification of Renilla luciferase levels, which were used as transfection controls. The mean ± standard deviation firefly and Renilla luciferase values were determined from the readings of each sample. The firefly values were normalised to the Renilla values (F÷R) for each sample to obtain a fold change for the transcription factor reporter genes. The activation fold change of cells expressing mutant proteins was normalised to that of cells expressing wild-type PLCγ1.

2.2.36 HeLa cell transfection and immunofluorescence analysis

Thirteen millimetre glass cover slips (VWR International) were placed into 24-well plates, onto which 1 x 10^4 HeLa cells were seeded in 0.5 mL complete DMEM medium. After 24 hours, 1.5 µL of the FuGENE HD Transfection Reagent and 350 ng of the eGFP-PLCγ1 plasmid DNA were diluted in Opti-MEM I Reduced Serum Medium to a final volume of 100 µL. DNA-FuGENE complexes were allowed to form during a 15 minute incubation at room temperature. Complexes were added dropwise to cells before incubating at 37°C. The following procedures of fixing, permeabilising and staining cells were performed at room temperature in a low light environment to

prevent photo-bleaching. Twenty-four hours after transfection, the cells were washed twice with PBS and fixed with 4% Paraformaldehyde (Alfa Aesar) for 10 minutes. The cells were washed twice and stored in PBS at 4°C for up to three days. Fixed cells were permeabilised with 0.2% (v/v) Triton-X (Sigma) for 10 minutes and then washed twice. The cells were stained with 4 units of Phalloidin (Biotium) for 20 minutes to enable visualisation of F-actin and cell structure. Cells were washed thrice and then incubated in 1 µM of 4′,6-Diamidino-2-phenylindole (DAPI) (Thermo Fisher Scientific) for 5 minutes to stain the nucleus. After washing three times with PBS and once with distilled water the cover slips were mounted onto microscope slides (Fisher scientific) using the SlowFade™ Diamond Antifade Mountant (Thermo Fisher Scientific). Slides were stored at 4°C and visualised with the A1 Inverted Confocal microscope at the Nikon Centre (KCL). Table 2. 45 details the excitation and emission maximum of each fluorophore.

Table 2. 45. The excitation and emission wavelengths of the fluorophores used for immunofluorescence.

Fluorophore	**Excitation maximum**	**Emission maximum**
Phalloidin	562 nm	583 nm
DAPI	358 nm	461 nm
eGFP	488 nm	509 nm

2.2.37 Statistical analysis

Two-tailed Student's t-tests were used to determine whether differences in transcriptional activity levels were statistically significant as per Vaqué *et al*. (2014), Kataoka *et al*. (2015) and Nagata *et al*. (2014), using the GraphPad QuickCalcs Web site (160, 221, 271).

Chapter 3 Identification of *PLCG1* mutations in Sézary Syndrome for functional analyses

3.1. Introduction

Mature T-cell lymphomas have been recurrently identified by deep sequencing studies to harbour somatic *PLCG1* mutations (Table 1. 3). To investigate the genetic architecture of SS, our group also performed deep sequencing on 101 tumours (147). The first phase of the study included identifying somatic mutations by WES of DNA extracted from $CD4^+$ enriched tumour cell populations from 10 discovery screen patients. This led to the identification of 549 genes harbouring at least one somatic mutation in the discovery cohort, including one patient harbouring the PLCγ1 p.S345F mutation (147). The 549 genes were subsequently included in a prevalence screen for TCS of DNA isolated from PBMCs of 91 SS patients (who had a high tumour burden) in addition to the 10 discovery screen patients (147). Our study identified that 11% (11/101) of SS tumours harboured seven *PLCG1* mutations and four of these (p.R48W, p.D342N, p.S345F and p.E1163K) were recurrently detected in individual tumours (Table 1. 4) (147). *PLCG1* encodes the PLCγ1 protein, a key mediator of TCR signalling, making mutations in this gene of particular interest in the context of mature T-cell lymphomas.

This chapter aims to prioritise which of nine PLCγ1 mutations (p.R48W, p.S312L, p.D342N, p.S345F, p.S520F, p.R1158H*, p.E1163K, p.D1165H and p.VYEEDM1161V*) identified in SS by our deep sequencing study and Kiel *et al.* (2015)* should be taken forward for functional analyses (68, 147). The first investigation aims to validate the seven mutations identified by our NGS study using Sanger sequencing. This technique will also be used to determine if the mutations persist in multiple tumour tissues obtained over extended periods of time. Mutations shown to persist over time and/ or in multiple tumour compartments are likely to be driver gene mutations that provide selective growth advantages to tumour cells. All nine mutations will be analysed using six pathogenicity prediction algorithms to determine their likely effect on protein structure and/or activity. Furthermore, conservation analysis will be used to investigate whether the amino acids altered by PLCγ1 mutations affect evolutionarily conserved residues. Finally, as *PLCG1* mutations recurrently occur in mature T-cell lymphomas, CTCL and ATLL cell lines

will be sequenced to determine if they have any of the nine mutations of interest. Cell lines harbouring these mutations could serve as models for functional assays.

The mutations that (i) persist over time and/ or in multiple tumour compartments, (ii) are predicted to be damaging on the protein level and (iii) alter evolutionarily conserved residues will be prioritised for functional analyses.

3.2. *PLCG1 mutations identified by deep sequencing of SS tumours*

The Integrative Genomics Viewer (257) was used to confirm the location of seven variants identified in 11 SS patients by our TCS study and to analyse the coverage of sequence reads. The number and percentage of reads that harboured the ancestral and minor/ mutant allele are shown in Table 3. 1. The coordinates that define the location of the variants had good coverage by 53 – 636 reads and 10% – 53% of the reads harboured the mutant alleles (Table 3. 1).

Table 3. 1. Mutant *PLCG1* alleles detected in 11 SS patients by targeted capture sequencing. The number and percentage of reads that detected the ancestral and minor/ mutant alleles were determined using the Integrative Genomics Viewer. Recurrent mutations identified in different patients are highlighted in the same colour.

Patient I.D.	DNA number	Nucleotide substitution	Amino acid change	Ancestral allele	Ancestral allele (No. reads)	Ancestral allele (% of reads)	Minor Allele	Minor Allele (No. reads)	Minor allele (% of reads)	Total No. reads
1	6885b	c.C142T	p.R48W	C	35	66	T	18	34	53
2	8004b	c.C142T	p.R48W	C	67	81	T	15	18	83
3	L11_0158b	c.C935T	p.S312L	C	93	47	T	105	53	198
4	3297b	c.G1024A	p.D342N	G	160	89	A	18	10	179
5	8344b	c.G1024A	p.D342N	G	222	86	A	36	14	258
6	3451b	c.C1034T	p.S345F	C	174	84	T	33	16	207
7	9308b	c.C1034T	p.S345F	C	172	66	T	88	34	260
8	4736b	c.C1559T	p.S520F	C	107	78	T	30	22	137
9	L12_0697b	c.G3487A	p.E1163K	G	393	62	A	242	38	636
10	4142b	c.G3487A	p.E1163K	G	347	72	A	142	27	517
11	4346b	c.G3493C	p.D1165H	G	336	70	C	135	28	478

3.3. Sanger sequencing validation of mutations

The DNA samples in which the mutations were originally identified by TCS were amplified by PCR and analysed by Sanger sequencing to confirm that the variants were true mutations and not sequencing artefacts.

Firstly, primers were designed to amplify the regions of interest using the *PLCG1* gDNA sequence from the genome browser Ensembl and the Primer3 software (176, 258). The annealing temperatures of all primer pairs were optimised by testing increasing temperatures in PCRs using DNA from healthy control individuals. PCR products were analysed on agarose gels and the temperature that yielded the most intense amplicon was selected as the optimal annealing temperature for each primer pair. For example, 59.5°C was the optimal annealing temperature for the PLCG1_C142T primer pair that was designed to validate the p.R48W mutation (Figure 3. 1. A). Using the optimised conditions, PCRs were performed on the diagnostic DNA samples that were used for TCS and identified to harbour *PLCG1* mutations. Nuclease-free water and DNA from a healthy control individual were used in negative and positive control reactions, respectively. The PCR products were analysed on agarose gels to confirm successful DNA amplification (Figure 3. 1. B) and subsequently treated with the ExoSAP-IT enzyme to hydrolyse excess nucleotides and primers.

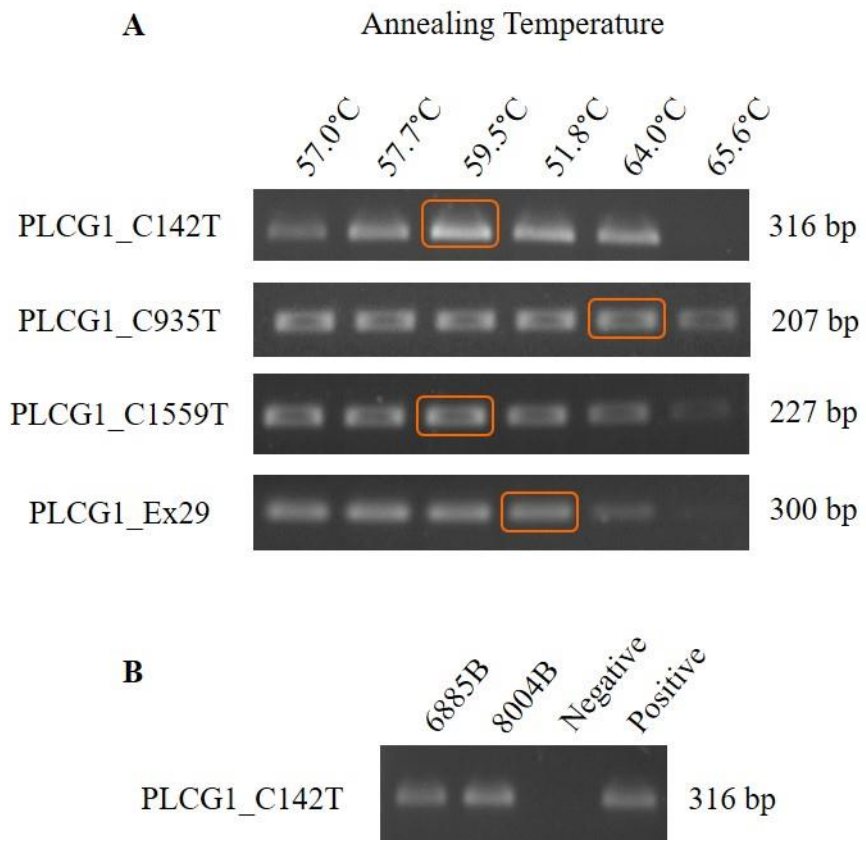

Figure 3. 1. PCR primer optimisation and patient DNA amplification. (A) Optimal conditions for four primer pairs were determined by performing PCRs at increasing annealing temperatures on healthy control DNA. The temperatures yielding the most intense amplicons (enclosed in orange) were determined to be optimal and used in subsequent PCRs. (B) Successful amplification of peripheral blood DNA from SS patient 1 and 2 with the PLCG1_C142T primer pair. Nuclease-free water and healthy control DNA were used in negative and positive control PCRs, respectively.

The PCR products were sent for Sanger sequencing (Source Bioscience, Cambridge) with aliquots of the primers used to amplify the region of interest. Sanger sequencing chromatogram analyses confirmed the presence of *PLCG1* mutations identified by TCS in all 11 patients. The PCR and Sanger sequencing reactions were performed once for each sample. A representative chromatogram of the p.R48W mutation in patient 1 is shown in Figure 3. 2. The validation chromatograms for the other 10 patients are shown in Appendix Figure 1 – Appendix Figure 10. The *PLCG1* mutations in patient 4 – 7 were validated by Dr. Nelema Begum during a summer research project in our group.

Sample	Sample no.	Chromatogram
Wild-type	-	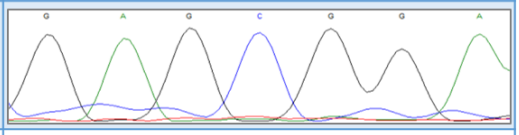
Blood	6885B	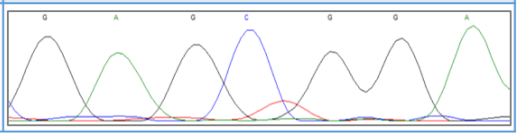

c.C142T; p.R48W

Figure 3. 2. The p.R48W mutation in the peripheral blood of SS patient 1.

3.4. PLCG1 mutations persist in multiple tumour compartments

Serial tumour samples from the peripheral blood, lesional skin, involved lymph nodes and enriched $CD4^+$ T-cells from patients harbouring *PLCG1* mutations were analysed by Sanger sequencing to determine if the mutations were present in different tumour tissues and over extended periods of time. DNA extracted from most serial tumour samples was available from the Skin Tumour Unit research tissue bank. Where unavailable, DNA and RNA were extracted from frozen $CD4^+$ enriched tumour cell populations from peripheral blood and the RNA was reverse transcribed into cDNA. The PCR primers used to validate the mutations were used to amplify the regions of interest in DNA from the serial samples. Primers were designed to specifically amplify cDNA and the annealing temperatures were optimised using healthy control cDNA as described in section 3.3. The optimised conditions were used to amplify cDNA synthesised from tumour cell RNA. Amplified PCR products were analysed by Sanger sequencing. The PCR and Sanger sequencing reactions were performed once.

Notably, nine of the 11 patients demonstrated persistence of the p.R48W, p.S312L, p.S345F, p.S520F, p.E1163K and p.D1165H mutations in more than one tumour compartment (Figure 3. 3 – Figure 3. 7, Appendix Figure 11, Appendix Figure 13 – Appendix Figure 15). No serial tumour samples were available for patient 5 due to loss at follow-up. The p.D342N mutation did not persist in serial tumour samples from patient 4 (Appendix Figure 12). This is likely due to a reduced tumour burden through multiple treatment regimens including chemotherapy, retinoids and Campath

monoclonal antibody therapy, which induced lymphopenia. The presence of mutations in cDNA synthesised from tumour cell RNA shows that the p.R48W, p.S312L, p.S345F, p.S520F and p.E1163K mutations are expressed on the transcriptional level in SS tumours.

Importantly, the p.R48W, p.S345F, p.S520F, p.E1163K and p.D1165H mutations persist up to 181 months after diagnosis in 6/8 patients for whom serial tumour samples were available (Figure 3. 5, Figure 3. 6, Appendix Figure 11, Appendix Figure 13 – Appendix Figure 15). No post-diagnostic samples were available for patient 3, 5 and 9.

The lack of mutation persistence in some patients may be attributable to therapeutic interventions that reduced tumour burden or a lack of detection sensitivity by Sanger sequencing for sparse tumour infiltrates in lesional skin. High sensitivity sequencing techniques such as locked nucleic acid-clamped real-time PCR, which can detect mutant alleles that are present at low frequencies in tumour samples are discussed on page 199. Patient 1 underwent an allogenic haematopoietic stem cell transplantation after which the p.R48W mutation could not be detected (Figure 3. 3). The p.S345F mutation persisted in the peripheral blood of patient 6 for 17 months but not after receiving triple therapy (Interferon-α, Photopheresis and Bexarotene) that resolved the leukaemic disease (Figure 3. 5). The mutation was subsequently detected in an involved lymph node at 72 months as the patient developed nodal progression (Figure 3. 5). The diagnostic sample for patient 7 was unavailable, however tumour samples obtained 4 months after diagnosis did not harbour the p.S345F mutation (Figure 3. 6). This is likely due to the patient receiving ECP therapy, which reduced the tumour burden. Diagnostic samples were also unavailable for patient 8, therefore peripheral blood DNA obtained 4 months after diagnosis was used to confirm the presence of the p.S520F mutation (Appendix Figure 13). A summary of the Sanger sequencing results of all tumour samples analysed is shown in Table 3. 2.

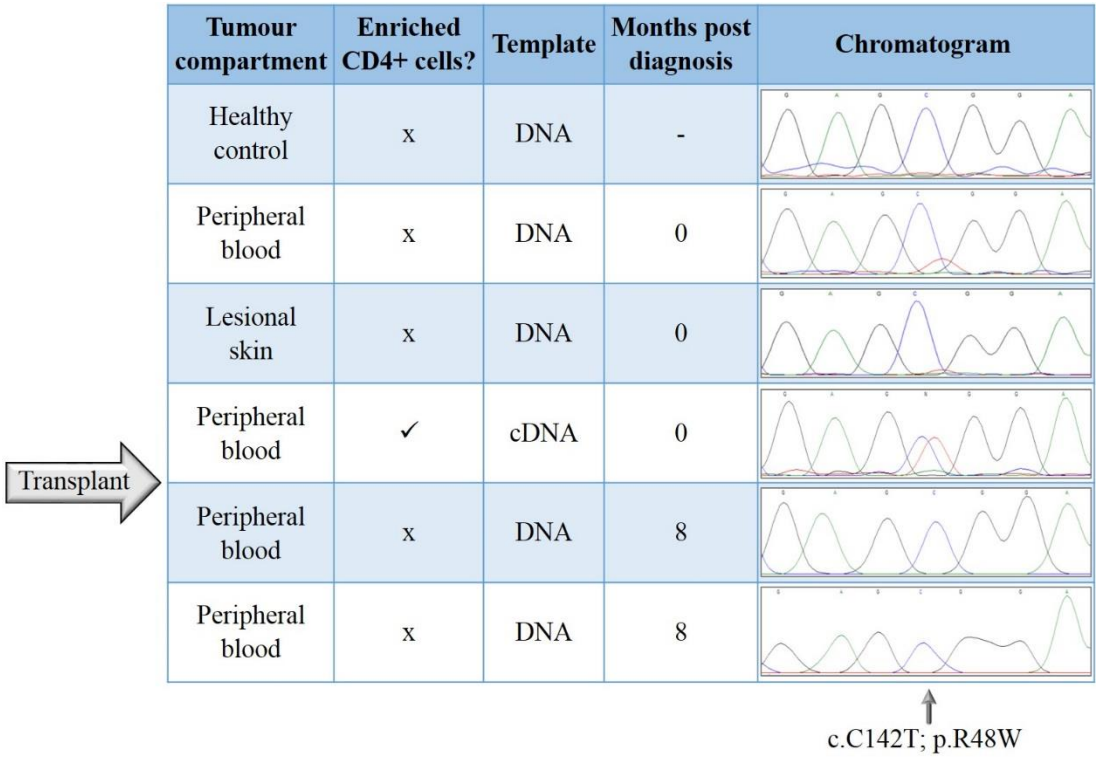

Figure 3. 3. The p.R48W mutation was detected in diagnostic tumour tissues in patient 1. The variant was absent after complete remission from an allogenic haematopoietic stem cell transplantation. DNA from a healthy control individual was sequenced to show the wild-type allele in the top panel.

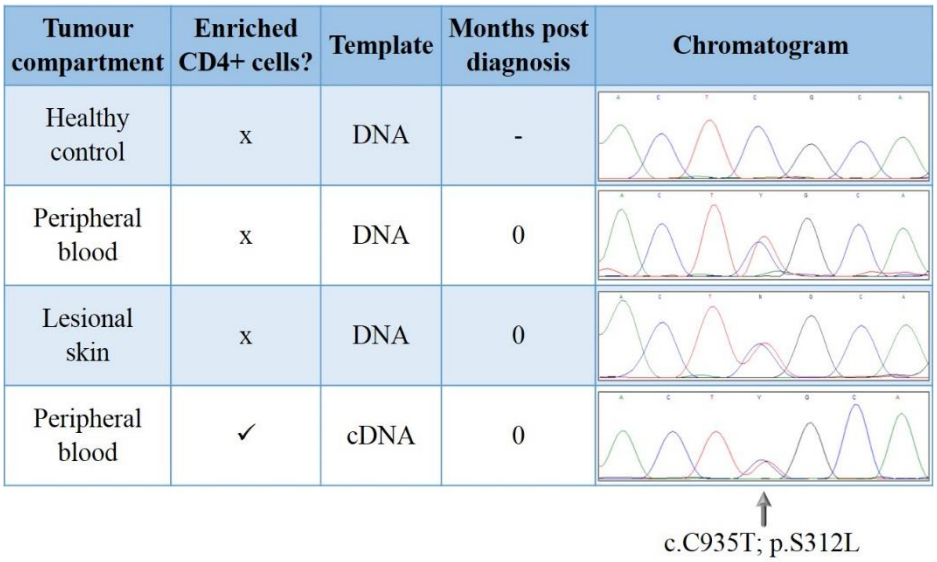

Figure 3. 4. The p.S312L mutation was present in multiple tumour compartments at diagnosis in patient 3. DNA from a healthy control individual was sequenced to show the wild-type allele in the top panel.

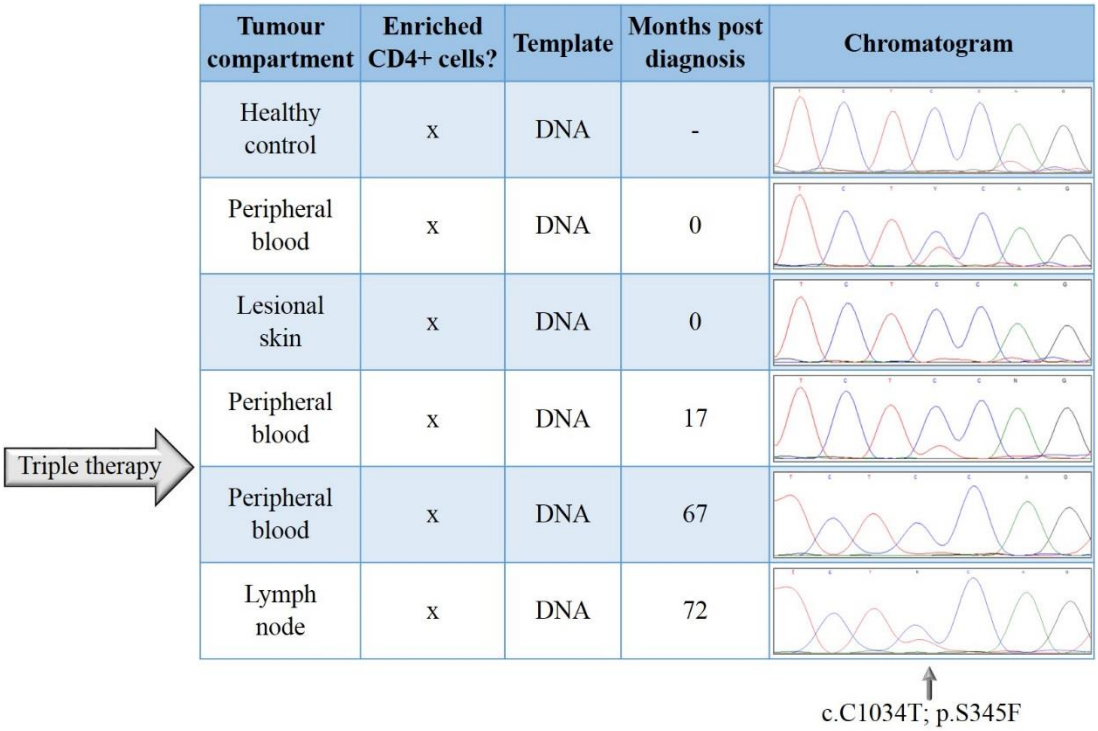

Figure 3. 5. The p.S345F mutation persists over time in the blood of patient 6. The mutant allele was absent in peripheral blood after triple therapy (Interferon-α, Photopheresis and Bexarotene) but was detected in an involved lymph node during nodal progression. DNA from a healthy control individual was sequenced to show the wild-type allele in the top panel.

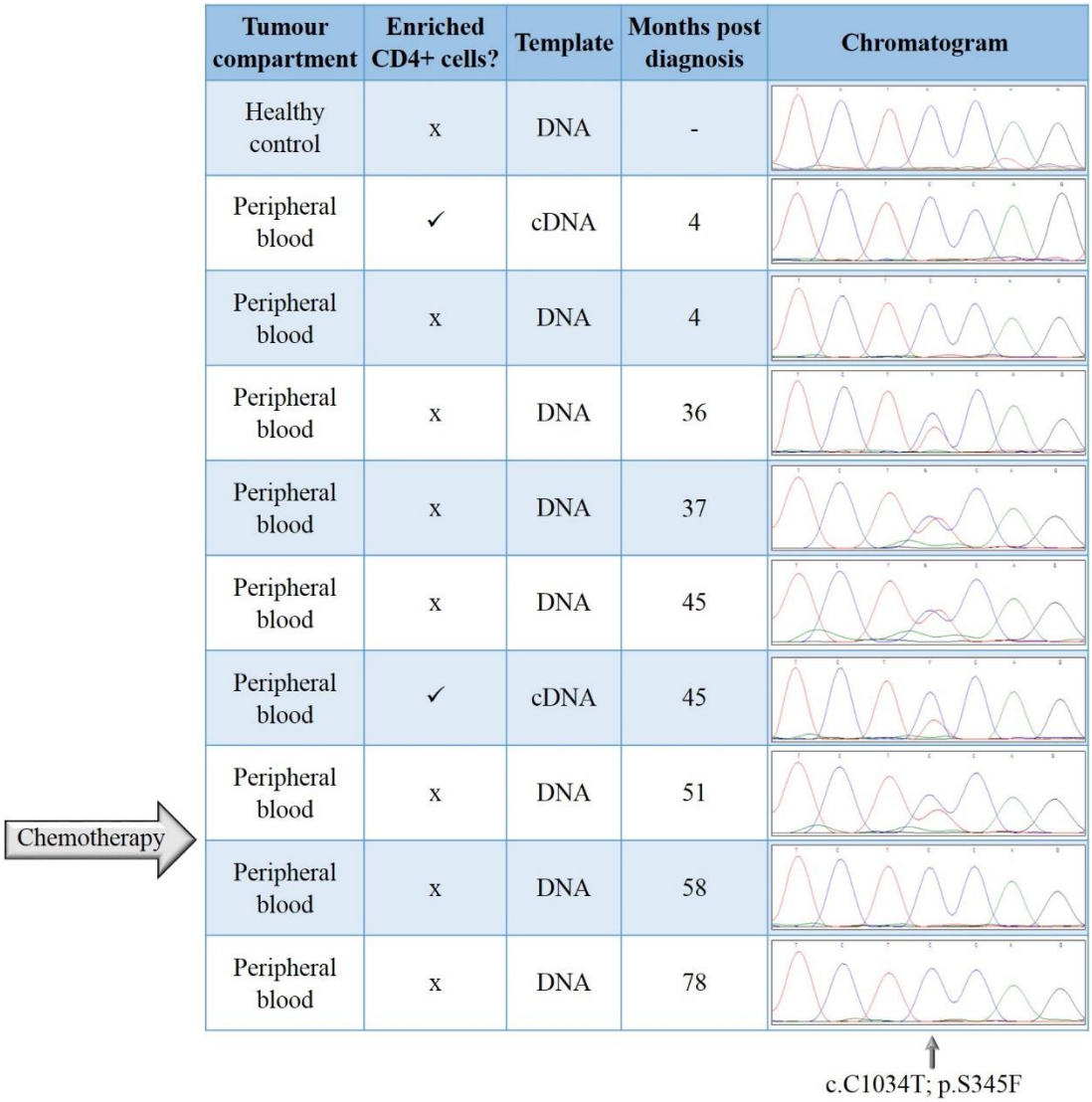

Figure 3. 6. The p.S345F mutation persists over time and in multiple tumour compartments in patient 7. The mutation was absent 4 months after diagnosis due to ECP treatment but was detected thereafter as the tumour burden increased. Chemotherapy effectively reduced the tumour burden and eliminated the mutant allele. DNA from a healthy control individual was sequenced to show the wild-type allele in the top panel.

Tumour compartment	Enriched CD4+ cells?	Template	Months post diagnosis	Chromatogram
Healthy control	x	DNA	-	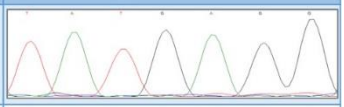
Lesional skin	x	DNA	0	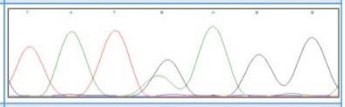
Peripheral blood	x	DNA	0	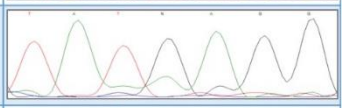
Peripheral blood	✓	cDNA	0	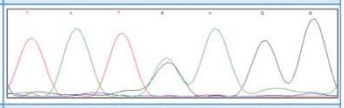
Peripheral blood	x	DNA	0	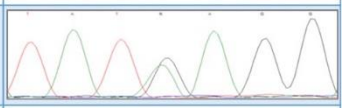
Lymph node	x	DNA	1	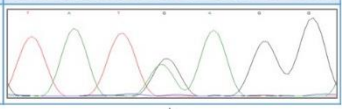

Figure 3. 7. The p.E1163K mutation is present in multiple tumour tissues at diagnosis in patient 9. DNA from a healthy control individual was sequenced to show the wild-type allele in the top panel.

Table 3. 2. *PLCG1* mutations persist over time and in multiple tumour compartments in SS. The mutations were validated by Sanger sequencing of peripheral blood DNA that was analysed by TCS. Serial DNA samples from peripheral blood, lesional skin, involved lymph nodes and tumour cell RNA were also screened for the mutations. Recurrent variants are highlighted in the same colour. ✓= variant validated, x = variant not validated, N/A = sample unavailable.

Patient I.D.	DNA number	Nucleotide substitution	Amino acid change	Mutation validated?	Detected in >1 sample?	Persists overtime?
1	6885B	c.C142T	p.R48W	✓	✓	x
2	8004B	c.C142T	p.R48W	✓	✓	✓
3	L11_0158B	c.C935T	p.S312L	✓	✓	N/A
4	3297B	c.G1024A	p.D342N	✓	x	x
5	8344B	c.G1024A	p.D342N	✓	N/A	N/A
6	3451B	c.C1034T	p.S345F	✓	✓	✓
7	9308B	c.C1034T	p.S345F	✓	✓	✓
8	4736B	c.C1559T	p.S520F	✓	✓	✓
9	L12_0697B	c.G3487A	p.E1163K	✓	✓	N/A
10	4142B	c.G3487A	p.E1163K	✓	✓	✓
11	4346B	c.G3493C	p.D1165H	✓	✓	✓

3.5. PLCγ1 mutations are predicted to be damaging

In addition to the seven PLCγ1 mutations (p.R48W, p.S312L, p.D342N, p.S345F, p.S520F, p.E1163K and p.D1165H) identified by our deep sequencing study, two further mutations (p.R1158H and the in-frame p.VYEEDM1161V indel) identified in SS tumours by Kiel *et al.* (2015) were also included for further analyses (68, 147). The pathogenicity prediction algorithms SIFT, Provean, PolyPhen2, Mutation Taster, MutPred2 and CADD were used to predict the effect of *PLCG1* mutations on the structure and/ or function of the PLCγ1 protein (153-158). The predictions from each algorithm are shown in Table 3. 3, with a consensus conclusion drawn based on 5/6 algorithms for missense mutations and 3/4 algorithms for the indel. The PolyPhen2 and MutPred2 algorithms only predict the likely effect of point mutations and were not applicable for the indel. Using the above defined criteria for a consensus, eight of nine mutations except p.S312L were predicted to be damaging to the PLCγ1 protein.

Table 3. 3. Pathogenicity predictions performed with multiple algorithms for nine PLCγ1 mutations identified in SS. Consensus criteria for missense mutations: 5/6 algorithms. Consensus criteria for indel: 3/4 algorithms.

Nucleotide substitution	Amino acid change	SIFT	Provean	PolyPhen2	Mutation Taster	MutPred2	CADD	Consensus
c.C142T	p.R48W	Damaging	Deleterious	Probably damaging	Disease causing	Damaging	Deleterious	**Damaging**
c.C935T	p.S312L	Tolerated	Deleterious	Benign	Disease causing	Neutral	Deleterious	Inconclusive
c.G1024A	p.D342N	Tolerated	Deleterious	Probably damaging	Disease causing	Damaging	Deleterious	**Damaging**
c.C1034T	p.S345F	Damaging	Deleterious	Probably damaging	Disease causing	Damaging	Deleterious	**Damaging**
c.C1559T	p.S520F	Damaging	Deleterious	Probably damaging	Disease causing	Damaging	Deleterious	**Damaging**
c.G3473A	p.R1158H	Damaging	Deleterious	Probably damaging	Disease causing	Damaging	Deleterious	**Damaging**
c.G3487A	p.E1163K	Damaging	Deleterious	Probably damaging	Disease causing	Damaging	Deleterious	**Damaging**
c.G3493C	p.D1165H	Damaging	Deleterious	Probably damaging	Disease causing	Damaging	Deleterious	**Damaging**
c.GTGTATGAGGAAGACAdelG	p.VYEEDM1161V	Damaging	Deleterious	N/A	Disease causing	N/A	Deleterious	**Damaging**

3.6. PLCγ1 mutations alter evolutionarily conserved residues.

The nine PLCγ1 mutations of interest were mapped to the functional protein domains (Figure 3. 8) based on the amino acid numbering and functional domains schematically represented by Bunney *et al.* (2012) (194). Eight mutations map to the protein core (blue domains), which mediates the catalytic activity of PLCγ1 in the 3D protein conformation. The p.S520F mutation is located in the split PH domain of the γ-specific array that mediates protein auto-inhibition.

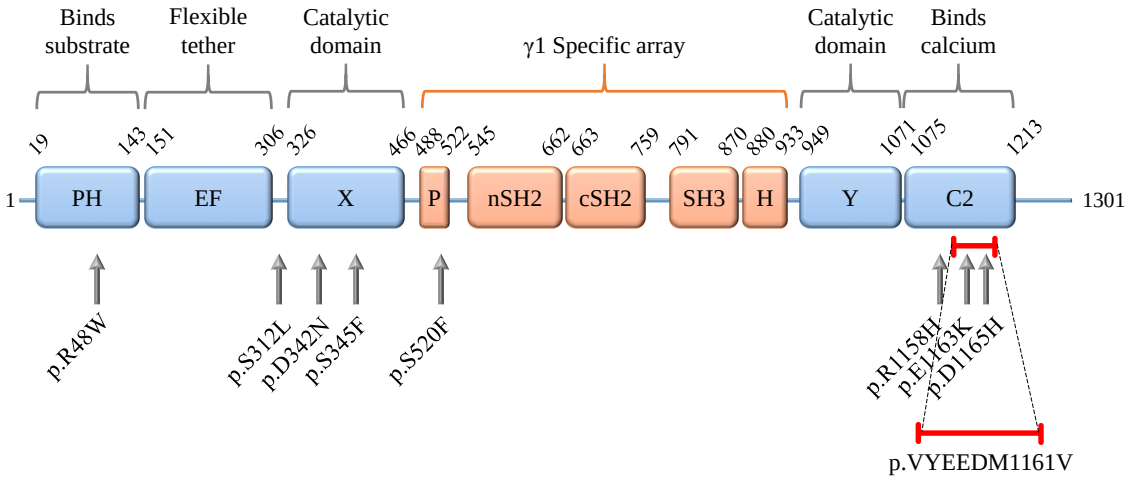

Figure 3. 8. PLCγ1 mutations mapped to the functional protein domains. Eight missense mutations and one in-frame indel were identified in SS tumours. Protein domain arrangement obtained from Bunney *et al.* (2012) (194).

To determine whether PLCγ1 mutations alter evolutionarily conserved amino acids, phylogenetic conservation analysis was performed. The PLCγ1 protein sequences from 12 vertebrates were obtained from the genome browser Ensembl (176) and aligned using the Clustal Omega multiple sequence alignment tool (265). All nine mutations were identified to alter PLCγ1 residues that are highly conserved amongst vertebrates (Figure 3. 9). Analysis of PLCγ2 residues, which correspond to the PLCγ1 residues that are altered by *PLCG1* mutations, showed that these PLCγ2 amino acids are also highly conserved amongst vertebrates (Figure 3. 9). As all nine mutations alter evolutionarily conserved residues, they are likely to influence the structure and/ or function of the PLCγ1 protein.

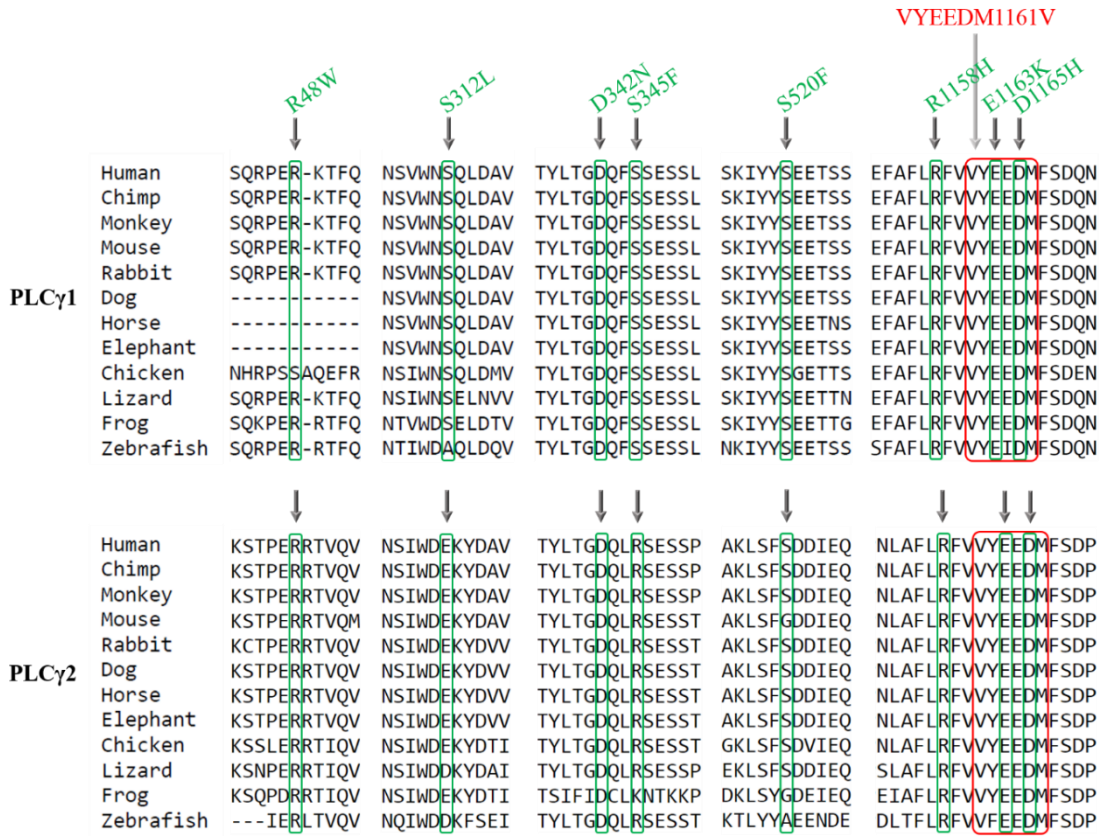

Figure 3. 9. PLCγ1 mutations alter evolutionarily conserved residues in vertebrates. The corresponding PLCγ2 residues are also highly conserved.

3.7. Mutations occur throughout the PLCG1 gene but particularly at five hotspots

PLCG1 mutations are reported in several mature T-cell lymphomas (Table 1. 3). Data from the COSMIC database confirmed that *PLCG1* is frequently mutated in ATLL, PTCL-nos, AITL, MF and SS (Figure 3. 10) (272). The COSMIC data also highlighted five hotspot mutations: p.R48W, p.S345F, p.S520F, p.E1163K and p.D1165H, with the most recurrent p.S345F mutation identified in 63 individual tumours (Figure 3. 10). Notably, all five hotspot mutations were identified by our TCS of SS tumours (147).

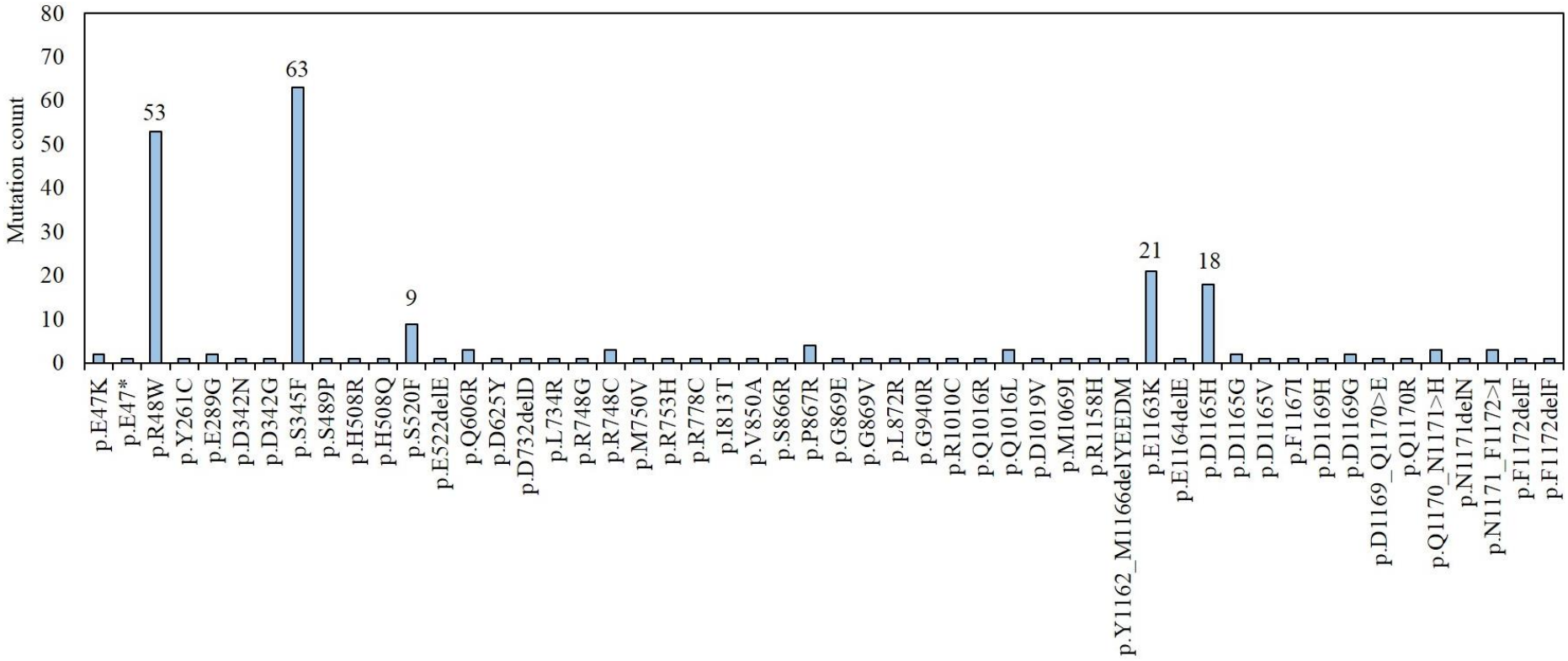

Figure 3. 10. Mature T-cell lymphomas frequently harbour *PLCG1* mutations throughout the gene. *PLCG1* is a commonly mutated gene in adult T-cell leukaemia/lymphomas, peripheral T-cell lymphomas-not otherwise specified, angioimmunoblastic T-cell lymphomas, Mycosis Fungoides and Sézary Syndrome and has five hotspot mutations. Mutation counts were obtained from the COSMIC database (version 87).

All PLCγ1 mutations identified in mature T-cell lymphomas by WES, TCS and selective sequencing studies were mapped to the protein domains to investigate mutation distribution per functional domain. Mutation frequencies were calculated by expressing the number of mutations per domain as a percentage of total *PLCG1* mutations reported. Overall, the γ1-specific array encompasses 16% of all mutations and the PLCγ1 core domains harbour 82% of the reported mutations (Figure 3. 11). Four of the five hotspot mutations map to the core domains and the p.S520F mutation maps to the γ1-specific array.

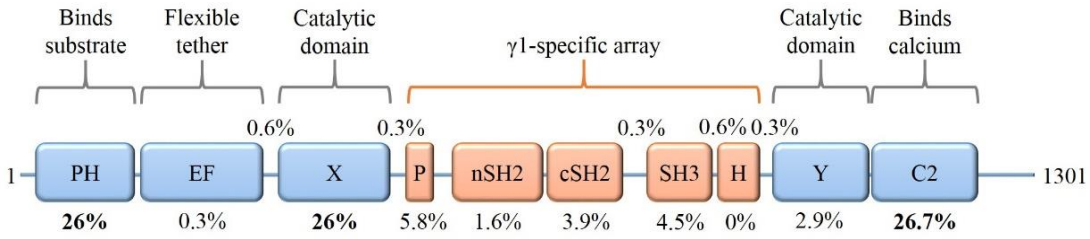

Figure 3. 11. Distribution of PLCγ1 mutations reported in mature T-cell lymphomas per functional domain. Mutation frequencies for domains are shown below and frequencies for the linker regions are shown on the upper part of the schematic.

3.8. CTCL cell lines do not harbour PLCG1 mutations

The aim of this section was to determine whether the CTCL cell lines SeAx (SS), HUT-78 (SS) and MyLa (MF) and the acute T-cell leukaemia Jurkat cell line harbour any of the nine *PLCG1* mutations of interest. Cell lines identified to harbour mutations could be used as model systems to investigate the functional effects of the mutations. cDNA from the cell lines was available in our group for analysis. PCR and Sanger sequencing primers were designed to amplify the *PLCG1* ORF and the optimal annealing temperatures of eight primer pairs were determined as described in section 3.3. PCRs were performed using cell line cDNA as templates and the reaction products were enzymatically cleaned-up and sent for Sanger sequencing.

SeAx and HUT-78 cells were identified to harbour one copy of the minor G allele at position c.A835 (p.S279G) (Figure 3. 12). The c.C2438T (p.I813T) variant was identified in all four cell lines with the SeAx, HUT-78 and MyLa cell lines having a heterozygous C/T genotype and Jurkat cells had a homozygous C/C genotype (Figure

3. 13). Both variants are common single nucleotide polymorphisms (SNPs) identified in the general population by the 1000 genomes project as determined from the dbSNP database (273). The minor alleles of the c.A835G and c.C2438T variants have a frequency of 7.9% and 26.7%, respectively. Table 3. 4 summarises the variants identified in the cell lines. As the CTCL and Jurkat cell lines do not endogenously harbour the mutations of interest, these cells would not serve as models to investigate the functional effects of *PLCG1* mutations.

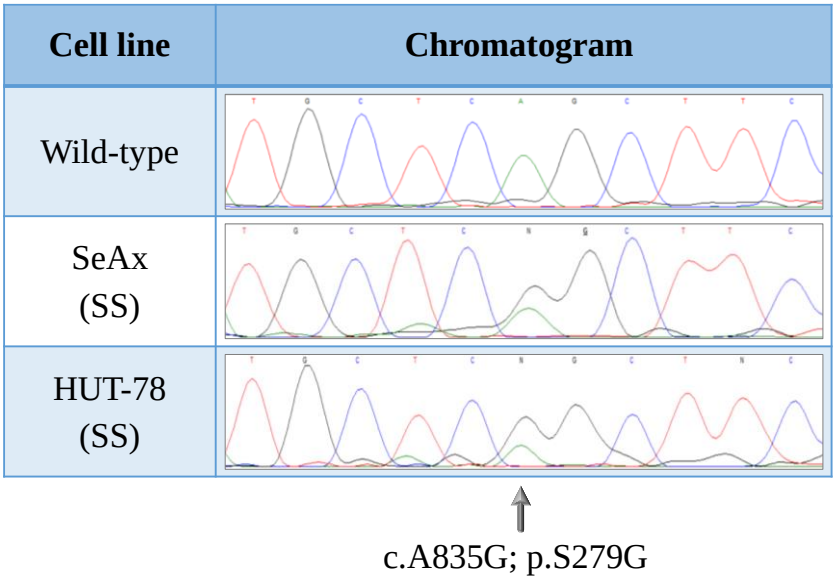

Figure 3. 12. SeAx and HUT-78 cells harbour the *PLCG1* c.A835G polymorphism.

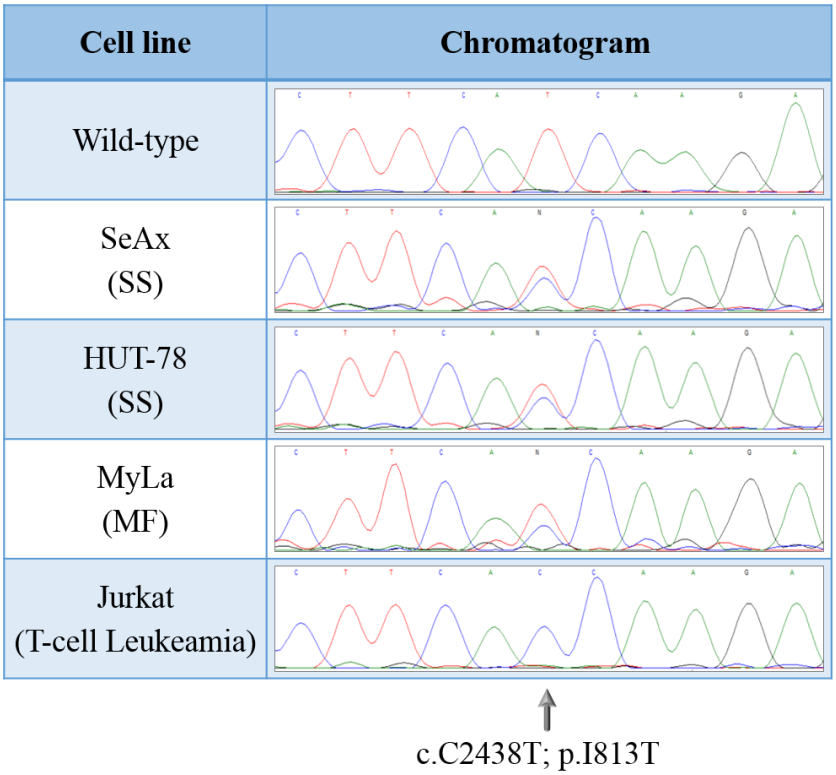

Figure 3. 13. The c.C2438T polymorphism is present in CTCL cell lines and Jurkat cells. SeAx, HUT-78 and MyLa cells have a heterozygous *PLCG1* c.C2438T polymorphism and Jurkat cells have a homozygous C/C genotype.

Table 3. 4. A summary of *PLCG1* polymorphisms identified in CTCL and adult T-cell leukaemia cell lines. Minor allele frequencies (MAF) of the general population were obtained from the 1000 genomes project via the dbSNP database.

Cell Line	Variant	Genotype	Amino Acid change	MAF	SNP I.D.
SeAx (SS)	c.A835G	A/G	p.S279G	7.9%	rs2228246
	c.C2438T	C/T	p.I813T	26.7%	rs753381
HUT 78 (SS)	c.A835G	A/G	p.S279G	7.9%	rs2228246
	c.C2438T	C/T	p.I813T	26.7%	rs753381
MyLa (MF)	c.C2438T	C/T	p.I813T	26.7%	rs753381
Jurkat (T-cell Leukaemia)	c.C2438T	C/C	p.I813T	26.7%	rs753381

3.9. Cell lines derived from aggressive ATLL tumours harbour PLCG1 mutations

The search for cell lines harbouring mutations of interest was expanded to 20 ATLL cell lines as *PLCG1* mutations frequently occur in this mature T-cell malignancy (221). The ATLL cell lines were derived from three sub-types of the disease including acute (the most aggressive form), carrier (less aggressive) and smouldering (indolent disease). Six of each of the carrier and smouldering cell lines and seven acute cell lines were analysed in addition to the MT2 cell line, which has no sub-type classification. Fourteen primer pairs were designed to amplify the 32 *PLCG1* exons. As previously described, primer pairs were optimised and the cell line gDNA was amplified by PCR and sent for Sanger sequencing.

Fifteen cell lines were identified to harbour one or both alleles of the common c.C2438T; p.I813T polymorphism as shown using representative chromatograms from the CY-6 and UR1 cell lines, respectively (Figure 3. 14 and Figure 3. 15) (Table 3. 5). This polymorphism was also detected in the CTCL and Jurkat cell lines (section 3.8). The MT2 and smouldering cell lines did not have any *PLCG1* mutations. Only one of the carrier cell lines, CY-6, harboured the rare p.E650STOP variant (Appendix Figure 16), which has not been reported in mature T-cell lymphomas.

Five (KOB, KKI, LMY1, LMY2 and LMWT5) of the seven acute cell lines were identified to have one or more *PLCG1* variants (Figure 3. 16 – Figure 3. 22), which were not reported as polymorphisms by the dbSNP database. The acute ATLL cell lines, KKI and LMY2, harboured one mutation each. The KKI cell line had the p.S345F mutation (Figure 3. 18), which frequently occurs in many mature T-cell lymphomas including ATLL, CTCL, PTCL-nos and AITL. The c.CCGGCGCGCCCTCGGACGC41del-insT; p.P14L indel was identified in the LMY2 cell line (Appendix Figure 17), an aberration not reported in mature T-cell lymphomas.

The acute cell lines KOB, LMY1 and LMWT5 harboured two heterozygous *PLCG1* mutations each. KOB cells had the p.R48W and p.M750V mutations (Figure 3. 16 and Figure 3. 17), both of which have been detected in ATLL and the p.R48W hotspot mutation is also reported in ATLL, SS and AITL. The LMY1 cell line harboured the p.N1171I and p.R1252P mutations (Figure 3. 19 and Figure 3. 20), the former of which has been reported in ATLL (221). LMWT5 cells had the p.S520F and p.R748H

mutations (Figure 3. 21 – Figure 3. 22) and the p.S520F mutation has been reported in ATLL, CTCL and AITL. The p.R748 residue has been identified to be mutated to a Cysteine or Glycine bases in ATLL (221) but not to a Histidine residue as identified in the LMWT5 cell line.

As summarised in Table 3. 5, indolent smouldering cells had no mutations, one carrier cell line had one mutation and cell lines derived from aggressive acute ATLLs harboured one or more *PLCG1* mutations. *PLCG1* mutations frequently occurred in the acute subtype of ATLL, suggesting a key role for this gene in the aggressive form of the disease. The only cell line identified to harbour a mutation of interest (p.S345F) without additional mutations was the acute KKI cell line.

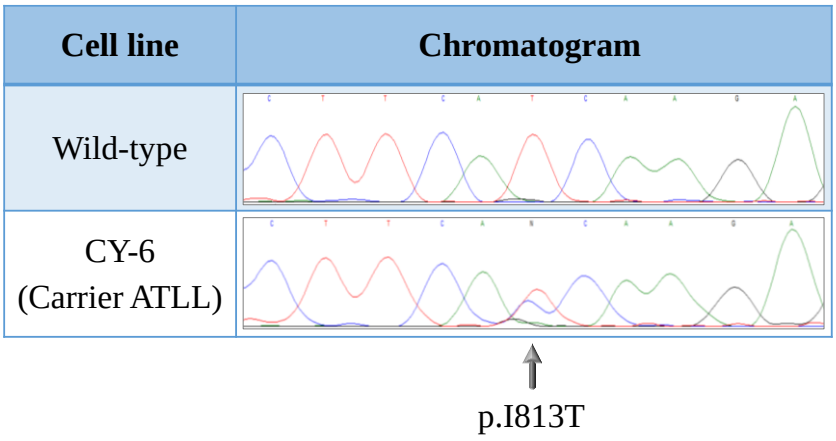

Figure 3. 14. CY-6 cells harbour a heterozygous *PLCG1* c.T2438C; p.I813T variant.

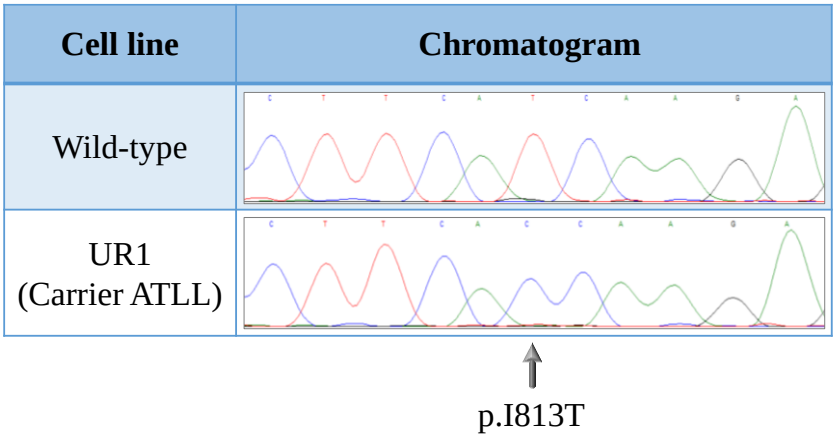

Figure 3. 15. UR1 cells have a homozygous *PLCG1* c.T2438C; p.I813T variant.

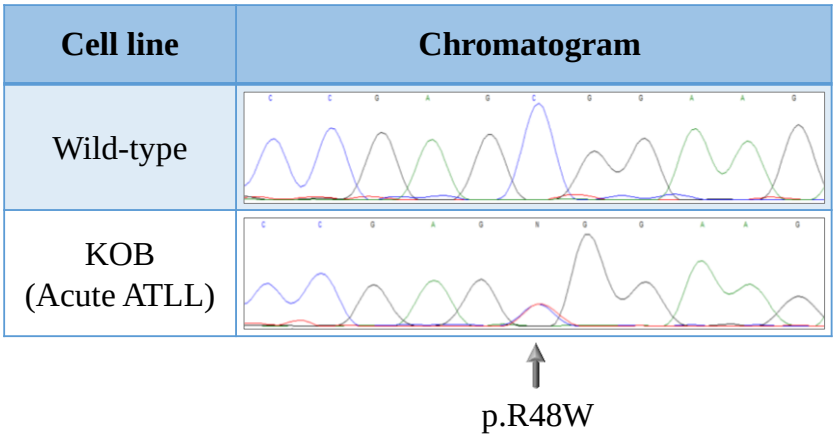

Figure 3. 16. KOB cells harbour a heterozygous *PLCG1* c.C142T; p.R48W variant.

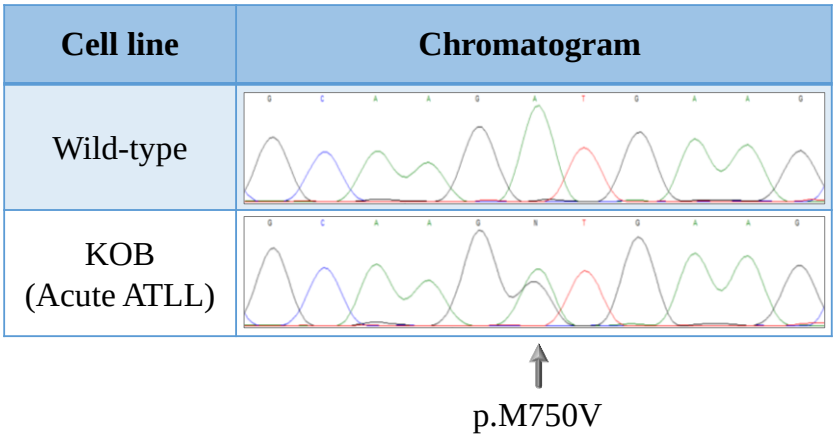

Figure 3. 17. KOB cells have a heterozygous *PLCG1* c.A2248G; p.M750V variant.

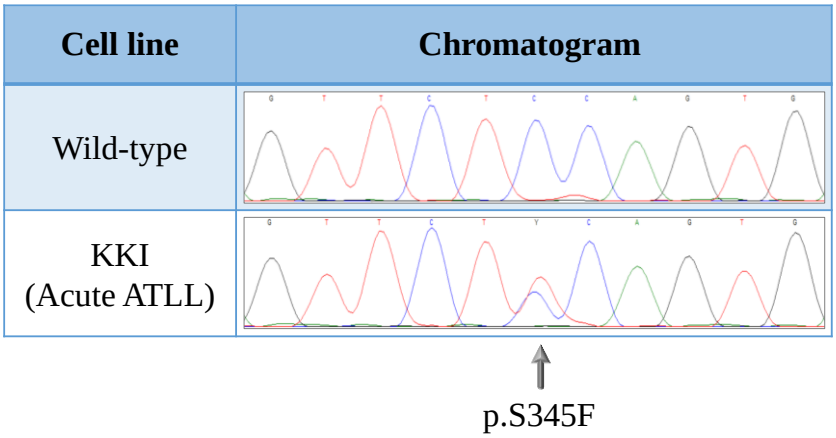

Figure 3. 18. KKI cells have a heterozygous *PLCG1* c.C1034T; p.S345F variant.

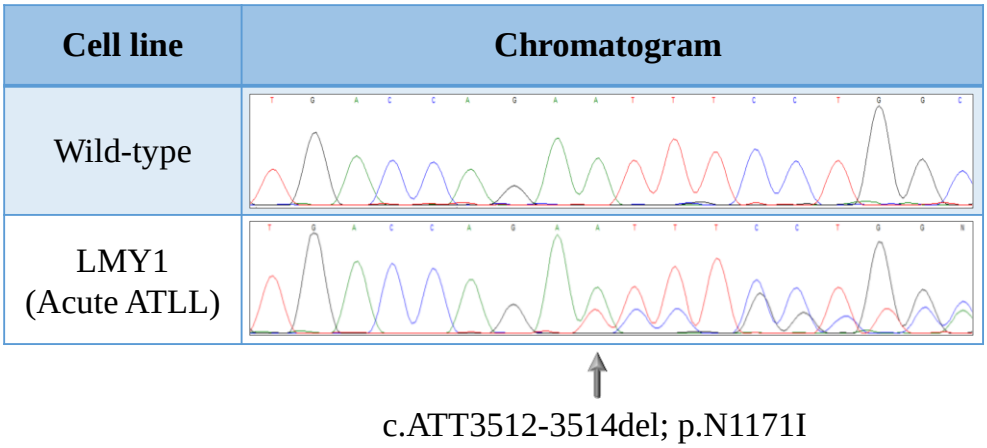

Figure 3. 19. LMY1 cells harbour a heterozygous *PLCG1* c.ATT3512-3514del; p.N1171I variant.

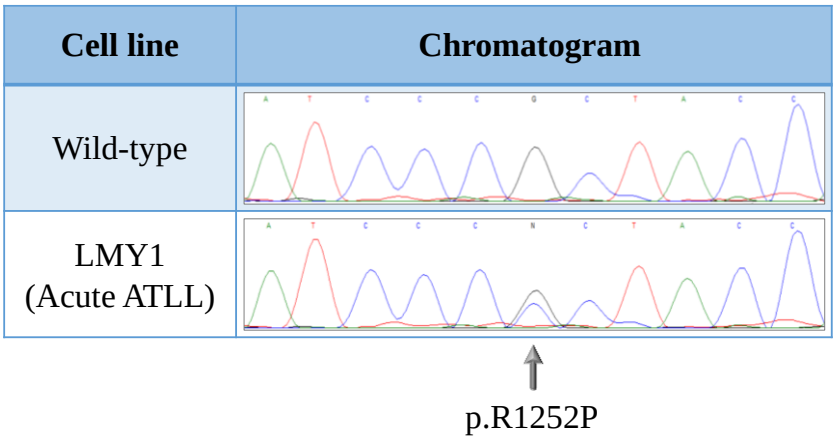

Figure 3. 20. LMY1 cells have a heterozygous *PLCG1* c.G3755C; p.R1252P variant.

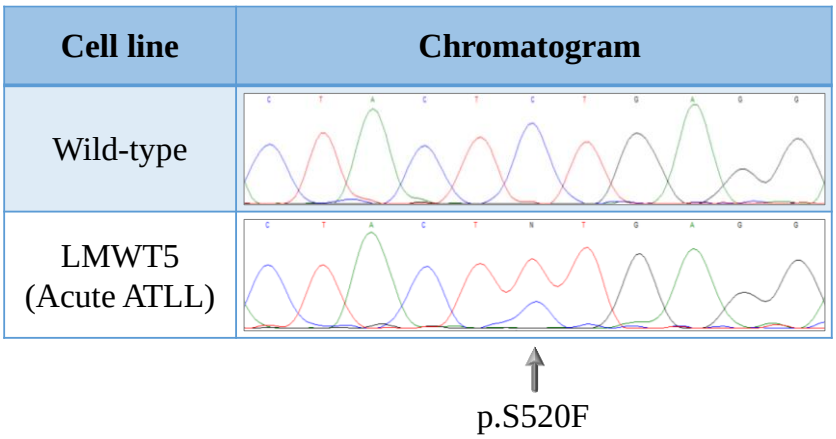

Figure 3. 21. LMWT5 cells harbour a heterozygous *PLCG1* c.C1559T; p.S520F variant.

Cell line	Chromatogram
Wild-type	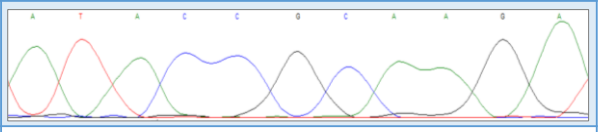
LMWT5 (Acute ATLL)	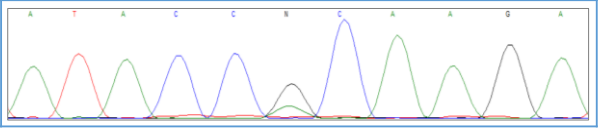

p.R748H

Figure 3. 22. LMWT5 cells harbour a heterozygous *PLCG1* c.G2243A; p.R748H variant.

Table 3. 5. A summary of the *PLCG1* variants identified in 20 ATLL cell lines. Rare variants i.e. mutations are shown in red text.

Cell line	Clinical Stage	Variant	Genotype	Amino Acid Change	MAF	SNP I.D.
MT2	-	c.T2438C	C/C	p.I813T	26.7%	rs753381
EE8	Smouldering	c.T2438C	C/C	p.I813T	26.7%	rs753381
OKA3	Smouldering	c.T2438C	T/C	p.I813T	26.7%	rs753381
YGS13	Smouldering	-	-	-	-	-
JSH4	Smouldering	c.T2438C	C/C	p.I813T	26.7%	rs753381
HAM9	Smouldering	c.T2438C	C/C	p.I813T	26.7%	rs753381
YK8	Smouldering	c.T2438C	C/C	p.I813T	26.7%	rs753381
CY-6	Carrier	c.G1948T	G/T	p.E650STOP	-	-
		c.T2438C	T/C	p.I813T	26.7%	rs753381
USH'2	Carrier	-	-	-	-	-
UR1	Carrier	c.T2438C	C/C	p.I813T	26.7%	rs753381
OGF20	Carrier	c.T2438C	C/C	p.I813T	26.7%	rs753381
MKI-1	Carrier	c.T2438C	T/C	p.I813T	26.7%	rs753381
KAW2	Carrier	-	-	-	-	-
KOB	Acute	c.C142T	C/T	p.R48W	-	-
		c.A2248G	A/G	p.M750V	-	-
KKI	Acute	c.C1034T	C/T	p.S345F	-	-
		c.T2438C	C/C	p.I813T	26.7%	rs753381
SO4	Acute	c.T2438C	C/C	p.I813T	26.7%	rs753381
LMY1	Acute	c.T2438C	C/C	p.I813T	26.7%	rs753381
		c.ATT3512-3514del	ATT/ATT del	p.N1171I	-	-
		c.G3755C	G/C	p.R1252P	-	-
LMY2	Acute	c.CCGGCGCGCCCTCGGACGC41del-insT	CCGGCGCGCCCTCGGACGC/CCGGCGCGCCCTCGGACGCdelinsT	p.P14L	-	-
		c.T2438C	C/C	p.I813T	26.7%	rs753381
LMWT5	Acute	c.C1559T	C/T	p.S520F	-	-
		c.G2243A	G/A	p.R748H	-	-
HUT102	Acute	c.T2438C	C/C	p.I813T	26.7%	rs753381

3.10. Summary

The aim of this chapter was to determine which of the nine PLCγ1 mutations (p.R48W, p.S312L, p.D342N, p.S345F, p.S520F, p.R1158H, p.E1163K, p.D1165H and p.VYEEDM1161V) identified in SS tumours should be prioritised for functional analyses. All seven mutations identified by our study were validated by Sanger sequencing. The presence of *PLCG1* mutations in diagnostic samples implicates that these are early events that may contribute to initiating tumourigenesis. Furthermore, persistence of *PLCG1* mutations in multiple tumour compartments and/ or over extended periods of time suggests that these are driver gene mutations that are positively selected by tumour cells. *PLCG1* mutations were shown to occur throughout the gene in mature T-cell lymphomas and five residues were recurrently mutated supporting the role of these hotspot mutations as drivers of oncogenesis (149).

All mutations except p.S312L were predicted to be damaging by pathogenicity prediction algorithms. The mutations alter evolutionarily conserved residues in vertebrates. The p.S312L mutation, although not predicted to be damaging, will be included in functional analyses as it alters an evolutionarily conserved residue and was detected in multiple tumour tissues at diagnosis in patient 3 (Figure 3. 4). Based on the analyses performed, all nine mutations will be taken forward for functional interrogations.

Sequencing of the *PLCG1* gene in CTCL and ATLL cell lines to identify a potential model for functional studies revealed that the KKI ATLL cell line harboured the p.S345F mutation. ATLL cell lines are derived from patients with Human T-leukaemia virus type 1 (HTLV-1) infections, therefore the KKI cell line would need to be cultured in a containment level 3 laboratory. As this facility was unavailable in our department it was not feasible to perform functional analyses to investigate the effect of one mutation of interest in a different research department.

To functionally interrogate the nine PLCγ1 mutations, mutant constructs will be made from a wild-type PLCγ1 vector. The constructs will be used to transiently transfect cell lines to assay protein expression and activity as will be described in Chapter 4.

Chapter 4 Activating PLCγ1 mutations mediate p.Y783 phosphorylation-independent signalling

4.1 Introduction

The analyses presented in Chapter 3 identified nine PLCγ1 mutations (p.R48W, p.S312L, p.D342N, p.S345F, p.S520F, p.R1158H, p.E1163K, p.D1165H and p.VYEEDM1161V) in SS tumours for functional interrogation.

To investigate the effect of the mutations, a wild-type PLCγ1 construct will be used as a template to generate mutant constructs. The constructs will be transiently transfected into HEK293 and COS-7 cells as these in addition to derivatives (HEK293T cells) are well established models used to study PLCγ1 function (160, 172, 194, 213, 218, 269, 274). IP production will be quantified and luciferase reporter assays will be utilised to analyse the effect of mutant PLCγ1 on proximal signalling and downstream transcriptional activity, respectively.

Phosphorylation of the p.Y783 tyrosine residue has been shown to be critical for proximal signalling and production of IP by PLCγ1 hydrolysis (177, 194). The requirement of p.Y783 phosphorylation in mutant PLCγ1 proteins will be assessed by mutating the tyrosine residue and analysing downstream NFκB, NFAT and AP-1 transcriptional activity. Finally, the efficacy of an IKKβ inhibitor to reduce PLCγ1-induced elevated NFκB activity will be assessed using luciferase reporter assays.

4.2 Generation of mutant PLCγ1 constructs

To investigate the effect of PLCγ1 mutations on protein expression and activity, mutant constructs were generated. The pTriEx-4 vector containing the full length human wild-type *PLCG1* cDNA and two constructs harbouring the p.S345F and p.S520F mutations were kindly provided by Professor Matilda Katan (UCL). The wild-type PLCγ1 vector was used as a template for site-directed mutagenesis to create the mutant p.R48W, p.S312L, p.D342N, p.R1158H, p.E1163K, p.D1165H and p.VYEEDM1161V constructs. The p.R1158H and p.VYEEDM1161V constructs were generated by Dr. Antoinette Yoxall (a research student under my supervision). The introduction of mutant bases was validated by Sanger sequencing (Figure 4. 1). Furthermore, the ORF and regulatory regions including the CMV enhancer and promoter and the polyA tail were analysed by Sanger sequencing and confirmed to harbour no additional mutations from the mutagenesis reactions. All constructs were routinely analysed on 0.8% agarose gels to confirm that they had not degraded (data not shown). The constructs were used to overexpress wild-type and mutant PLCγ1 in cells by transient transfection.

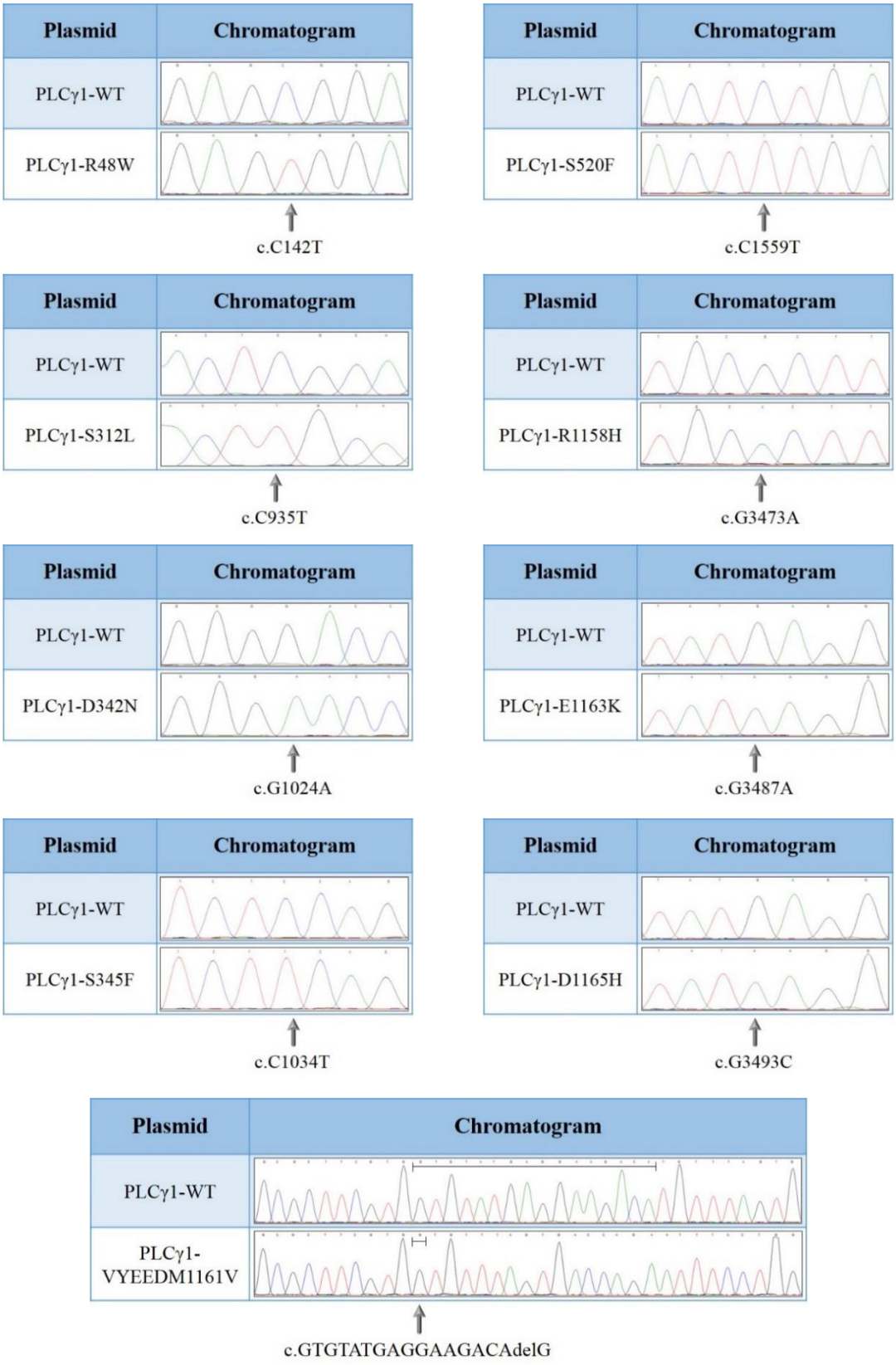

Figure 4. 1. Chromatograms confirming introduction of mutant alleles in PLCγ1 constructs by site-directed mutagenesis. Sequences from the wild-type constructs are shown in the top panels and mutant alleles in the bottom panels. The p.R1158H and p.VYEEDM1161V constructs were generated by Dr. Antoinette Yoxall.

4.3 The p.VYEEDM1161V indel alters total and phosphorylated PLCγ1 expression

Transfection of HEK293 cells with PLCγ1 constructs was optimised and the ideal antibody dilutions to be used for western blotting were determined as described in section 2.2.32. The optimised conditions were used to investigate the effect of nine PLCγ1 mutations of interest on protein expression and phosphorylation of the p.Y783 residue, which is known to activate wild-type PLCγ1. The p.Y783 residue has a more prominent role in protein activation compared to the other four tyrosine residues that are phosphorylated in PLCγ1 as described on page 67.

HEK293 cells were transfected with wild-type or mutant PLCγ1 vectors alongside a vehicle control and untreated cells. Cells were treated with pervanadate for 1 hour prior to harvesting and whole-cell lysates were probed with the following primary antibodies: anti-PLCγ1 (1:20,000), anti-p-PLCγ1 (1:50,000) and anti-β-actin (1:10,000). Eight mutant proteins that harboured a missense mutation demonstrated comparable total protein expression to wild-type PLCγ1 (Figure 4. 2). In contrast, the in-frame p.VYEEDM1161V indel mutant protein had markedly reduced total PLCγ1 expression (Figure 4. 2). PLCγ1 phosphorylation levels were similar in mutant and wild-type proteins, however the p.VYEEDM1161V protein had increased phosphorylation relative to total PLCγ1 expression (Figure 4. 2). This expression pattern was also observed in an independent repeat experiment showing that the data is reproducible.

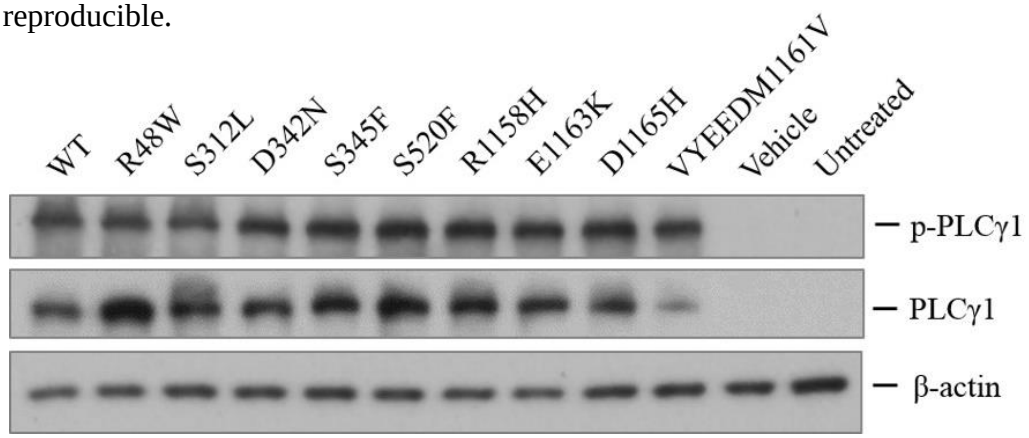

Figure 4. 2. The p.VYEEDM1161V indel reduces total PLCγ1 expression, but has relatively increased protein phosphorylation. Total (150 kDa) and phosphorylated PLCγ1 (p-PLCγ1; 155 kDa) expression was analysed in whole-cell lysates of transfected HEK293 cells, using β-actin expression (45 kDa) as a loading control. The blots shown are representative of two independent transfections and western blot analyses that demonstrate the same expression patterns.

Cells transfected with six mutant constructs (p.R48W, p.S312L, p.D342N, p.S345F, p.S520F and p.E1163K) but not treated with pervanadate also show comparable mutant and wild-type PLCγ1 expression. This demonstrates that pervanadate treatment does not influence protein stability and expression (Figure 4. 3).

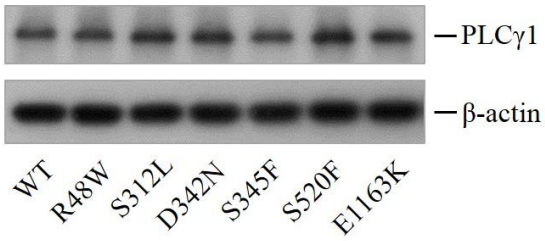

Figure 4. 3. Transfected cells not treated with pervanadate show comparable wild-type and mutant PLCγ1 expression. HEK293 cells were transfected with PLCγ1 constructs and total PLCγ1 expression (150 kDa) was analysed relative to β-actin expression (45 kDa) used as a loading control. The blots shown are representative of two independent transfections and western blot analyses.

4.4 Five PLCγ1 mutations potently activate downstream signalling

Activated PLCγ1 produces the secondary messengers IP_3 and DAG, which induce extensive signalling cascades to activate the NFAT, NFκB and AP-1 transcription factor families (Figure 1. 18). To investigate the effect of PLCγ1 mutations on downstream signalling, HEK293 cells were co-transfected with PLCγ1 plasmids and NFκB- or NFAT-luciferase constructs and transcriptional activity was measured using luciferase reporter assays. NFAT activity was analysed to interrogate the IP_3-calcineurin-NFAT pathway. Of the two DAG signalling cascades that activate NFκB and AP-1, the NFκB transcription factor was selected for analysis as it has a substantial role in the pathogenesis of CTCL.

4.4.1 Co-transfection optimisation for luciferase reporter assays

Prior to being used in experiments, the reporter constructs were confirmed by Sanger sequencing to encode the appropriate transcription factor binding elements as listed in Table 2. 31. To determine the optimal concentration of PLCγ1 plasmid DNA for transfections, cells were co-transfected with 0 µg, 0.05 µg, 0.3 µg and 1 µg of the wild-type or mutant PLCγ1 plasmids and 100 ng of the NFκB-, NFAT- and AP-1-luciferase

reporter plasmids. Four hours after transfection, cells were serum-starved overnight to remove growth factors within the serum-containing media that can activate PLCγ1 signalling. Transcriptional reporter activity was normalised to that of vehicle transfected cells. The p.R1158H and in-frame indel p.VYEEDM1161V constructs were generated at a later time in the project by Dr. Antoinette Yoxall, therefore the optimal concentrations were determined in separate experiments. Cells transfected with 1 µg of wild-type or mutant PLCγ1 constructs induced the highest levels of NFκB activity (Figure 4. 4) and also NFAT and AP-1 activity (data not shown). Therefore, 1 µg of PLCγ1 plasmid DNA was determined to be optimal for co-transfection of HEK293 cells to analyse the activity on all three transcription factors.

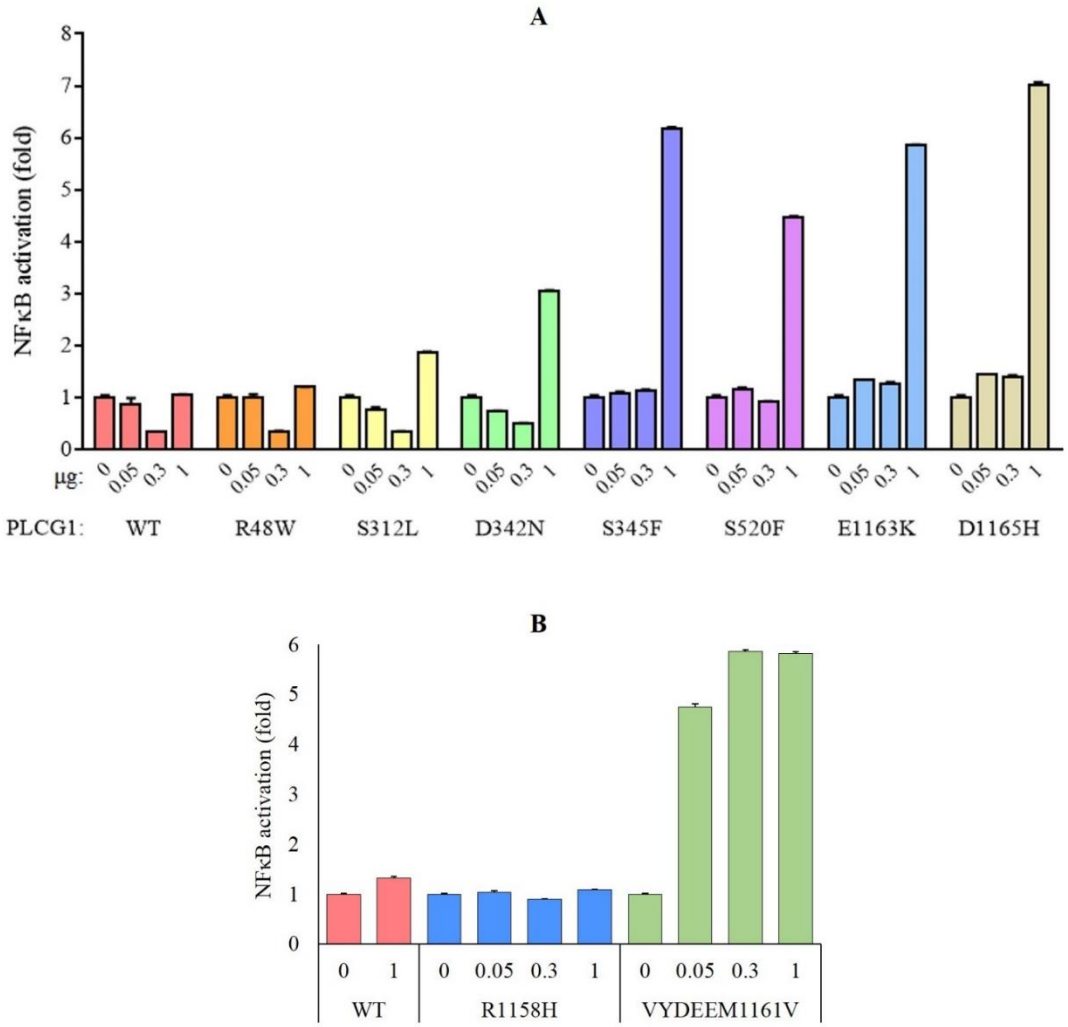

Figure 4. 4. Optimisation of HEK293 cell co-transfection with PLCγ1 constructs for NFκB-luciferase reporter assays. Cells were co-transfected with the NFκB reporter construct, vehicle control (0 μg) and increasing concentrations of wild-type or mutant PLCγ1 plasmids. Activity levels were normalised to cells transfected with a vehicle control. Data is represented as mean ± SD of n=1 assay performed in triplicate.

4.4.2 Five PLCγ1 mutations significantly elevate NFκB and NFAT activity in basal conditions

The experiments were repeated using the optimal co-transfection conditions to confirm the effect of the mutant proteins on NFκB and NFAT activity. The p.S345F, p.S520F, p.E1163K, p.D1165H and p.VYEEDM1161V mutant proteins significantly elevated NFκB activation 3.3 – 6.1 fold ($p \leq 0.03$) compared to wild-type PLCγ1 (Figure 4. 5. A). The same mutant proteins also significantly increased NFAT transcriptional activity between 3.3 – 10 fold ($p < 0.0001$) relative to wild-type PLCγ1 (Figure 4. 5. B). These data show that the p.S345F, p.S520F, p.E1163K, p.D1165H and p.VYEEDM1161V mutant proteins have potent gain-of-function properties in basal conditions, which significantly increase downstream signalling.

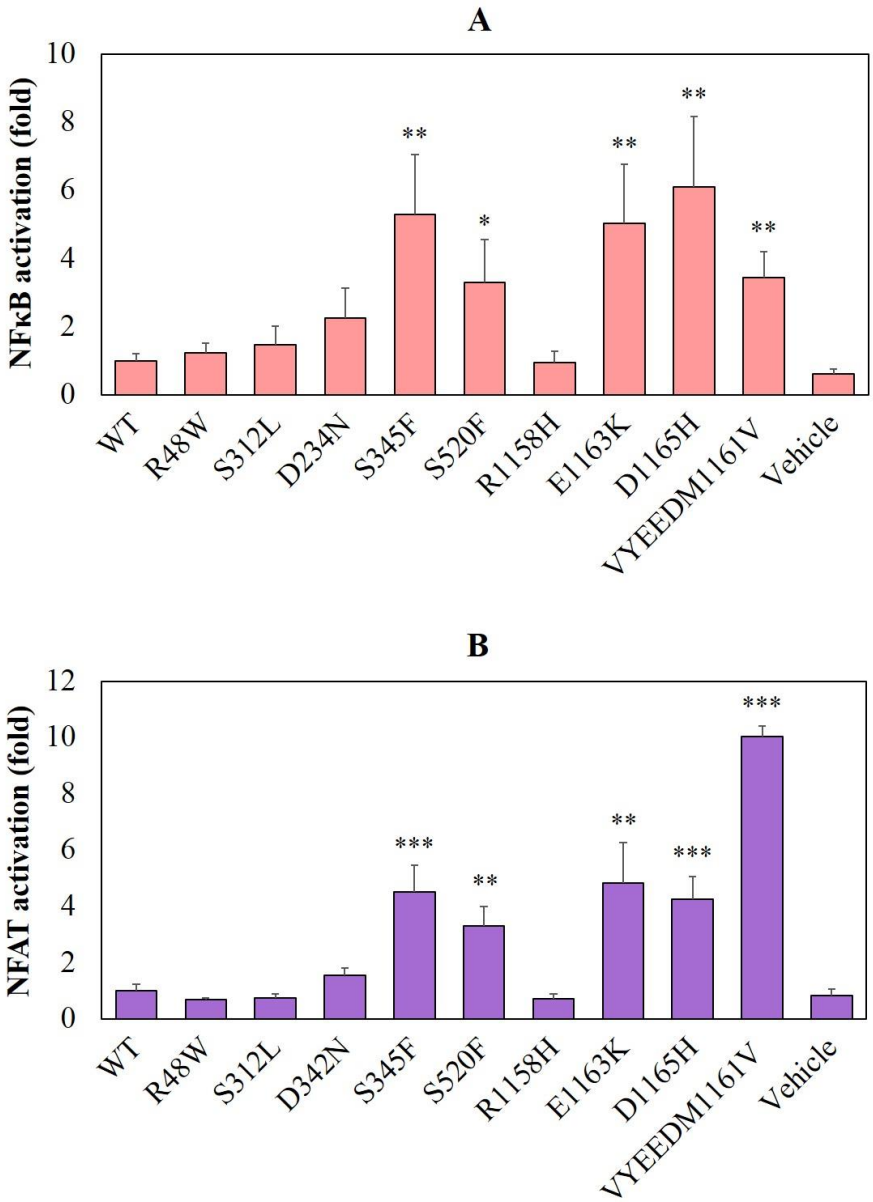

Figure 4. 5. Five mutant PLCγ1 proteins significantly increase NFκB and NFAT transcriptional activity in basal conditions. Activation fold changes were normalised to cells overexpressing wild-type PLCγ1. Data is represented as mean ± SEM. NFκB; n=4. NFAT; n=3. Student's t-test, *p<0.05, **p<0.01, ***p<0.001.

4.4.3 Optimisation of EGF stimulation for HEK293 cells

The p.R48W, p.S312L, p.D342N and p.R1158H mutant proteins did not significantly increase transcriptional activity in basal conditions. To investigate if these proteins alter NFκB activity in stimulated conditions, EGF stimulation of HEK293 cells was optimised. HEK293 cells express low levels of the EGF receptor (268), therefore the receptor was overexpressed by transfection of the pBABE-EGFR plasmid. Cells were co-transfected with increasing concentrations (100 ng, 250 ng, 500 ng, 750 ng and 1 μg) of the pBABE-EGFR vector, wild-type PLCγ1 plasmid and the NFκB-luciferase construct. After serum-starving overnight, the cells were stimulated with 100 ng/mL EGF for 8 hours. The dose and duration of EGF stimulation was optimised using conditions from the literature as a guide (data not shown). Over-expressing the EGF receptor increased NFκB activity in response to EGF stimulation (Figure 4. 6). Specifically, co-transfecting cells with 750 ng of the pBABE-EGFR vector induced a 3.11 fold increase in NFκB activity compared to unstimulated cells that did not overexpress the receptor (Figure 4. 6). Thus, 750 ng of the pBABE-EGFR plasmid was determined to be optimal for transfections in all subsequent experiments that required EGF-stimulation of HEK293 cells.

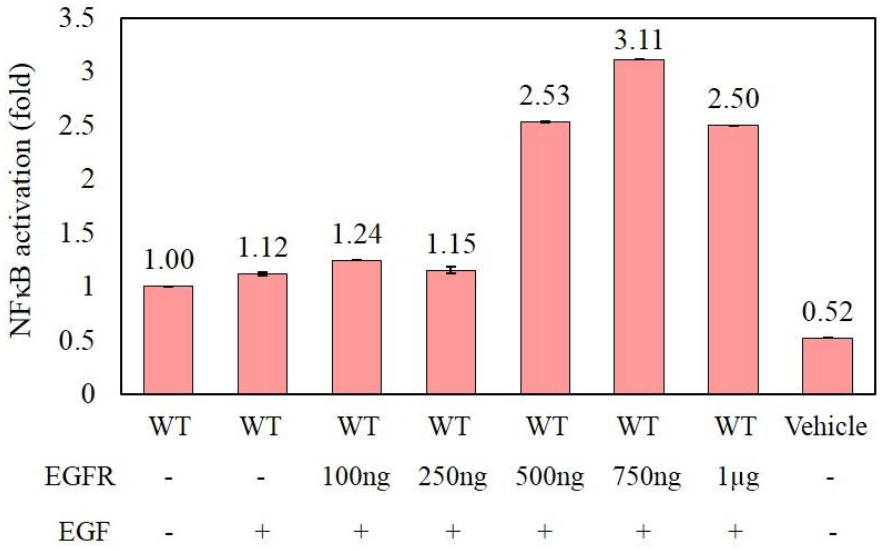

Figure 4. 6. Overexpressing the EGF receptor increases NFκB activity in response to EGF stimulation. HEK293 cells were co-transfected with increasing concentrations of the pBABE-EGFR plasmid, wild-type PLCγ1 vector and NFκB reporter construct. Following serum starvation, cells were stimulated with 100 ng/mL EGF for 8 hours. Activity levels were normalised to unstimulated cells overexpressing wild-type PLCγ1. Data is represented as mean ± SD; n=1 assay performed in triplicate.

As mentioned in section 1.12, PLCγ1 can be activated by engagement of the EGFR after which the enzyme mediates signalling to the NFκB, NFAT and AP-1 transcription factors (Figure 1. 15). To confirm that PLCγ1 mediates EGF signalling the following experiment was performed. HEK293 cells were co-transfected with either wild-type PLCγ1 plasmid or a vehicle control, the pBABE-EGFR vector and the NFκB reporter construct. Cells were serum-starved overnight and then stimulated with 100 ng/mL EGF for 8 hours. Both vehicle-transfected and PLCγ1-transfected cells demonstrated higher NFκB activity after stimulation (Figure 4. 7). Importantly, cells overexpressing wild-type PLCγ1 had 2.9 fold greater NFκB activity compared to vehicle-transfected cells in stimulated conditions, confirming that PLCγ1 mediates EGF signalling to the NFκB transcription factor.

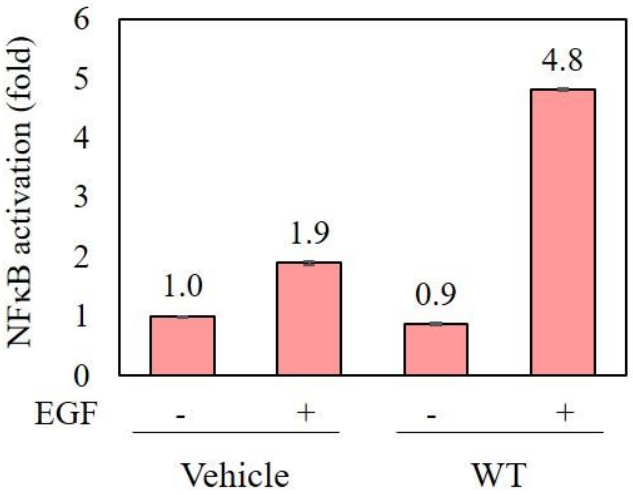

Figure 4. 7. PLCγ1 mediates EGF signalling to induce NFκB activation in HEK293 cells. Cells were co-transfected with the wild-type PLCγ1 vector or vehicle control, pBABE-EGFR plasmid and NFκB reporter construct. Following serum starvation, cells were stimulated with 100 ng/mL EGF for 8 hours. Activation levels were normalised to unstimulated vehicle-transfected cells. Data is represented as mean ± SD, n=1 assay performed in triplicate.

4.4.4 The hotspot p.R48W mutation significantly increases NFκB activity in stimulated conditions

As the p.R48W, p.S312L, p.D342N and p.R1158H proteins did not significantly increase NFκB activity in basal conditions, these mutant proteins were analysed in stimulated cells using the optimised conditions. The p.R48W, p.D342N and p.R1158H mutant proteins increased NFκB activity 0.3 – 0.5 fold compared to wild-type PLCγ1 in stimulated cells, but the p.S312L protein showed reduced protein activity (Figure 4. 8).

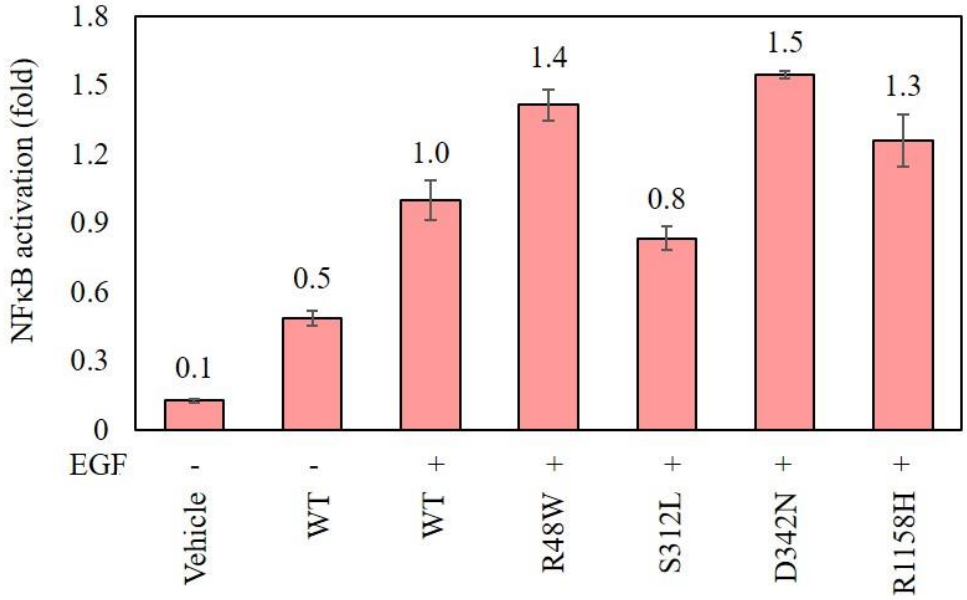

Figure 4. 8. The p.R48W, p.D342N and p.R1158H mutant proteins increase NFκB activation in stimulated cells. HEK293 cells were co-transfected with PLCγ1 vectors, the pBABE-EGFR construct and the NFκB reporter plasmid. After serum starvation overnight, cells were stimulated with 100 ng/mL EGF for 8 hours. Activation fold changes were normalised to stimulated cells overexpressing wild-type PLCγ1. Data is represented as mean ± SD, n=1 assay performed in triplicate.

The p.R48W mutation was selected for further analysis as this is a hotspot mutation that has been reported in SS, AITL and frequently in ATLL (67, 69, 70, 147, 218, 221). Co-transfection of HEK293 cells with wild-type and the p.R48W mutant construct was repeated thrice and the mutant protein was shown to significantly increase NFκB activity 1.3 fold compared to wild-type PLCγ1 in stimulated cells (p=0.0074) (Figure 4. 9).

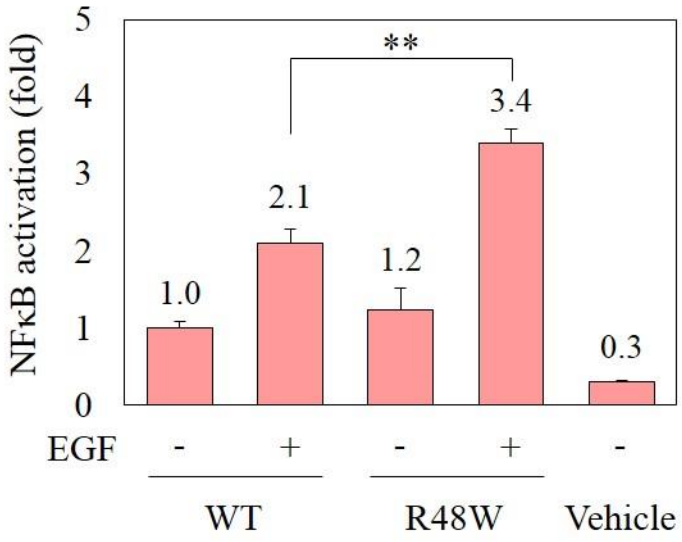

Figure 4. 9. The p.R48W mutant protein significantly increases NFκB activity in stimulated cells. HEK293 cells were co-transfected with PLCγ1 vectors, the NFκB reporter construct and the pBABE-EGFR plasmid. Following serum starvation, cells were stimulated with 100 ng/mL EGF for 8 hours. Activation fold changes were normalised to unstimulated cells overexpressing wild-type PLCγ1. Data is represented as mean ± SEM; n=3. Student's t-test, *p<0.05, **p<0.01, ***p<0.001.

4.5 Five PLCγ1 mutations directly increase IP production and proximal signalling

PLCγ1 hydrolyses PIP_2 to produce the secondary messengers IP_3 and DAG (Figure 1. 18 and Figure 1. 20). To determine the direct influence of mutations on PLCγ1 activity and proximal signalling, COS-7 cells were transfected with PLCγ1 vectors and total IP production was quantified by liquid scintillation. The IP quantification experiments presented here were performed by our collaborator, Dr. Marta Martins (Instituto de Medicina Molecular, Portugal).

Of the nine PLCγ1 mutations of interest, the p.S312L and p.R1158H mutations were excluded from the analyses as these mutant proteins did not demonstrate gain-of-function effects on downstream signalling (section 4.4.2). All IP data shown are representative of two independent experiments. The inter-assay data has not been averaged as the raw values from individual experiments vary largely, however, the same data trend was observed between experiments. This is in line with the presentation of IP data by Poulin *et al*. (2005) and Bunney *et al*. (2012) (177, 194).

The p.S345F, p.S520F, p.E1163K, p.D1165H and p.VYEEDM1161V mutant proteins elevated IP production 3.4 – 6.6 fold compared to wild-type PLCγ1 in basal conditions (Figure 4. 10). In contrast, the p.R48W and p.D342N mutants had low impact on basal PLCγ1 activity by increasing IP production 1.4 and 1.6 fold, respectively compared to wild-type. These findings support the data from section 4.4.2 and demonstrate that the p.S345F, p.S520F, p.E1163K, p.D1165H and p.VYEEDM1161V proteins are potent mediators of gain-of-function, which directly increase proximal and downstream signalling.

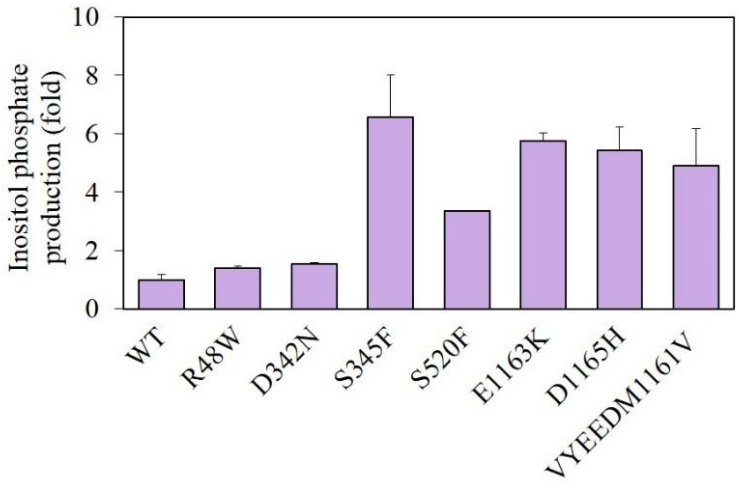

Figure 4. 10. Five mutant PLCγ1 proteins elevate IP production in basal conditions. IP production was measured by liquid scintillation of COS-7 cells transfected with PLCγ1 constructs. Data is presented as mean ± SD of internal duplicates. Representative data of two independent experiments performed by Dr. Marta Martins is shown.

The p.D342N protein has previously been shown to elevate IP production in stimulated COS-7 cells (269). To confirm these findings, COS-7 cells transfected with the PLCγ1 p.D342N vector were stimulated 100 ng/mL EGF for 1 hour and IP was quantified. Notably, COS-7 cells were not co-transfected with the pBABE-EGFR vector as these cells express higher levels (5 fold) of the EGF receptor than HEK293 cells (268). The p.D342N mutant protein increased IP production 4.8 fold compared to wild-type PLCγ1 in stimulated conditions (Figure 4. 11).

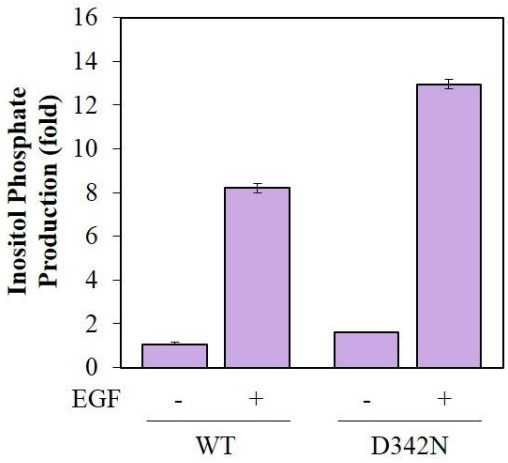

Figure 4. 11. The p.D342N mutant protein generates more IP than wild-type PLCγ1 in stimulated cells. Transfected COS-7 cells were stimulated with 100 ng/mL EGF for 1 hour and IP production was measured by liquid scintillation. Data is presented as mean ± SD of internal duplicates. Representative data of two independent experiments performed by Dr. Marta Martins is shown.

4.6 Activating PLCγ1 proteins do not require p.Y783 phosphorylation to increase downstream signalling

The PLCγ1 p.Y783 residue is critical for proximal TCR signalling *in vitro*. Abrogating the p.Y783 residue by mutating the tyrosine residue to phenylalanine (p.Y783F) has been shown to drastically reduce but not obliterate IP production in stimulated COS-7 and TV-1 cells (177, 194). The aim of this section was to determine whether the PLCγ1 mutations shown to have gain-of-function activity in sections 4.4.2 and 4.5 require phosphorylation of the p.Y783 residue to increase downstream signalling by assaying NFAT, NFκB and AP-1 transcriptional activity.

4.6.1 The rationale for selecting mutations for analysis

The PLCγ1 mutations analysed in this study were grouped based on their location in functional protein domains and a representative activating mutation from each group was selected for further analysis (Figure 4. 12). The gain-of-function p.S345F mutation was chosen from the catalytic X domain, the p.S520F mutation from the γ1-specific array and the p.E1163K mutation from the C2 domain.

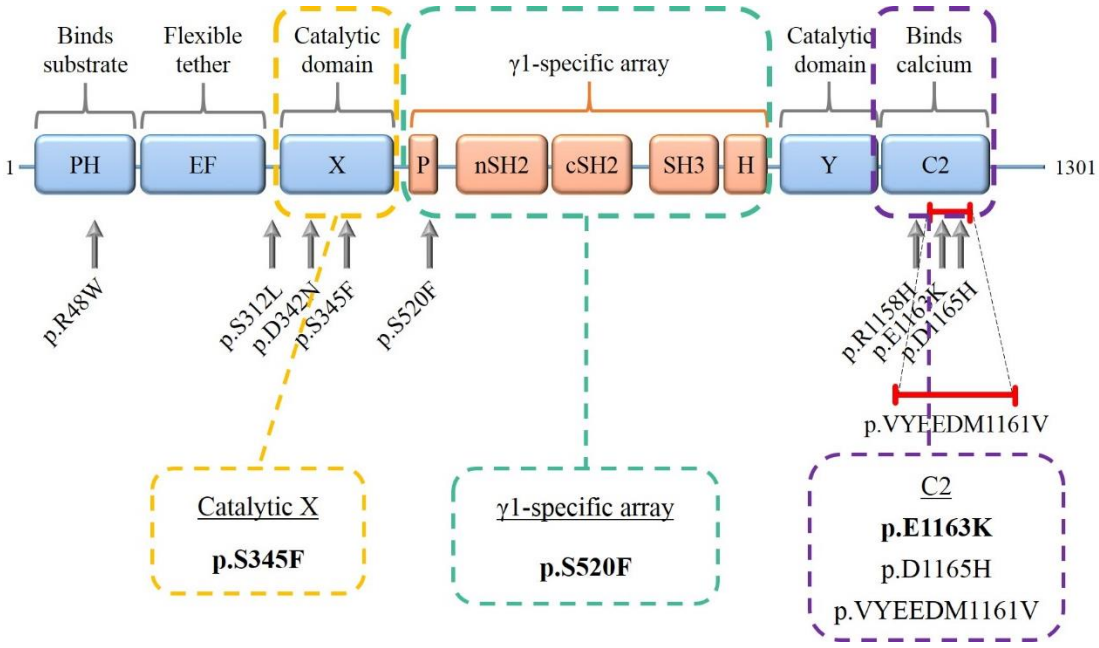

Figure 4. 12. Mutant proteins selected to investigate if p.Y783 phosphorylation is required for protein activity. PLCγ1 mutations were mapped to the functional protein domains and one activating mutation (indicated in bold) was selected per functional domain or per groups of domains that function together, namely the γ1-specific array.

4.6.2 Generation of double mutant constructs

The PLCγ1-p.Y783F construct, which encodes the mutated p.Y783F residue was a kind gift from Professor Matilda Katan (UCL). This construct was used as a template for site-directed mutagenesis to incorporate the activating p.S345F, p.S520F and p.E1163K mutations. Introduction of the gain-of-function mutations into the PLCγ1-p.Y783F vector was confirmed by Sanger sequencing (Figure 4. 13). These plasmids will henceforth be referred to as "double mutants". The double mutant vectors were further sequenced and confirmed to harbour the p.Y783F residue and no additional mutations in the *PLCG1* ORF, CMV promoter and enhancer and the polyA tail.

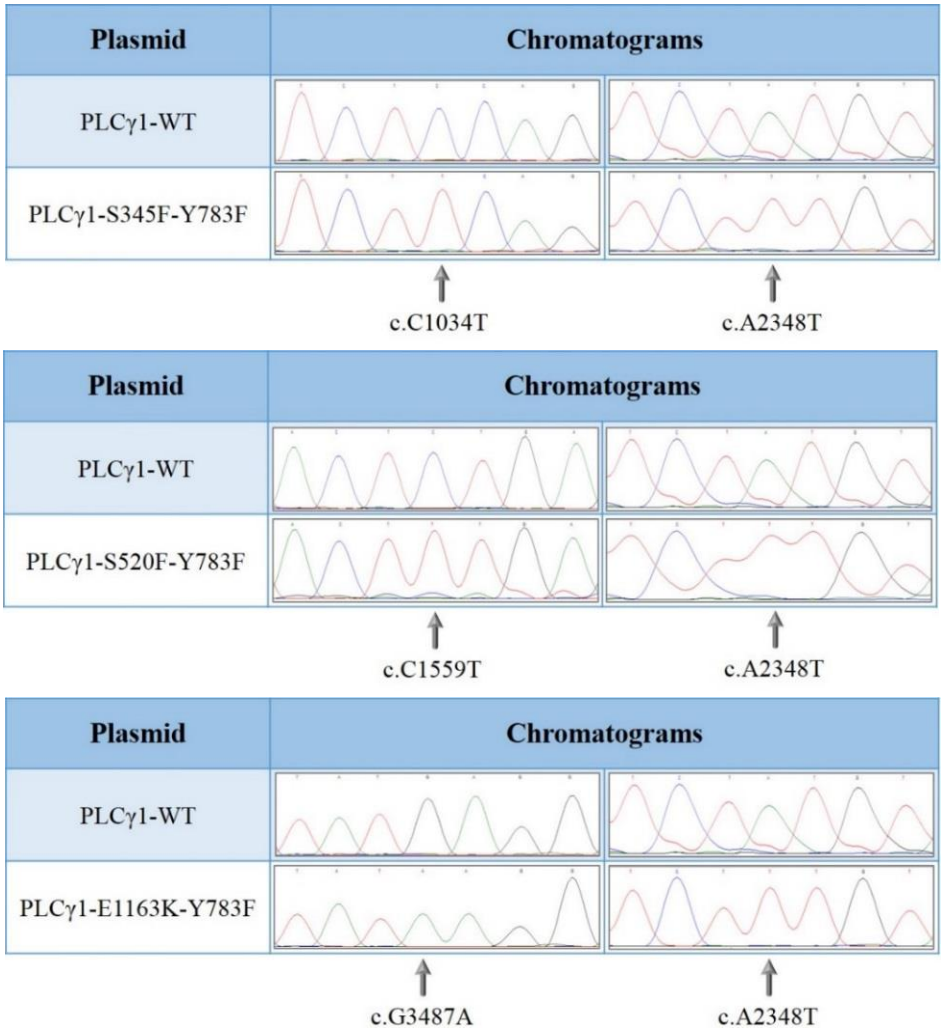

Figure 4. 13. Chromatograms confirming introduction of mutant alleles in the PLCγ1-p.Y783 construct by site-directed mutagenesis. Sequences from the wild-type constructs are shown in the top panels and mutant alleles in the bottom panels. Each mutant plasmid harboured two *PLCG1* mutations: one identified in SS tumours and the c.A2348T mutation, which abrogates the p.Y783 phosphorylation residue.

4.6.3 The PLCγ1 p.Y783F mutation abolishes phosphorylation of PLCγ1

Expression of the double mutant proteins was analysed to confirm that the mutant p.Y783F residue was not phosphorylated in basal conditions. HEK293 cells were transfected with vectors encoding wild-type PLCγ1, the p.Y783F mutation, gain-of-function mutations and double mutants. After 23 hours, the cells were treated with pervanadate for 1 hour to stabilise phosphorylation signals and then harvested. Western blotting of whole-cell lysates demonstrated total PLCγ1 expression in all cells transfected with PLCγ1 plasmids (Figure 4. 14). p-PLCγ1 expression was detected only in cells transfected with constructs encoding the tyrosine residue at position p.783 (Figure 4. 14). This data confirms that the anti-p-PLCγ1 antibody used in this assay was specific for the p.Y783 residue and also demonstrates that the phosphorylation residue had been effectively abrogated in the double mutant proteins. This expression pattern was also observed in an independent repeat experiment and also in EGF-stimulated cells (data not shown).

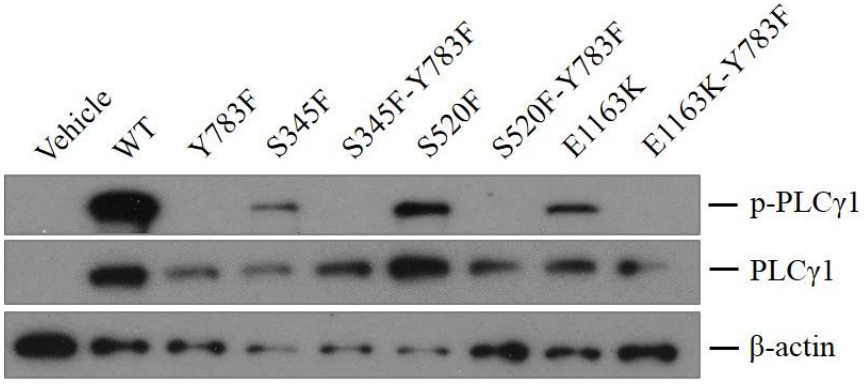

Figure 4. 14. Abrogation of the p.Y783 residue results in loss of PLCγ1 phosphorylation. Western blotting confirmed PLCγ1 (150 kDa) expression in transfected HEK293 cells and demonstrated absence of phosphorylation (p-PLCγ1; 155 kDa) in cells transfected with constructs encoding the mutated p.Y783F phosphorylation residue. Representative blot of two independent transfections.

4.6.4 Gain-of-function PLCγ1 proteins do not require phosphorylation to elevate transcriptional activity in basal conditions

The effect of abrogating the p.Y783 phosphorylation residue in the gain-of-function mutant proteins was analysed by assaying downstream NFAT, NFκB and AP-1 transcriptional activity in HEK293 cells. Cells were co-transfected with the wild-type, p.Y783F mutant, gain-of-function or double mutant PLCγ1 constructs and either of the three transcription reporter plasmids. The NFAT, NFκB and AP-1 transcriptional activity induced by the p.S345F, p.S520F, p.E1163K proteins was comparable to that of the p.S345F-Y783F, p.S520F-Y783F, p.E1163K-Y783F double mutant proteins and no statistically significant difference was determined (Figure 4. 15). These data therefore demonstrate that the gain-of-function mutant proteins do not require phosphorylation of the PLCγ1 p.Y783 residue to induce transcriptional activity in basal conditions.

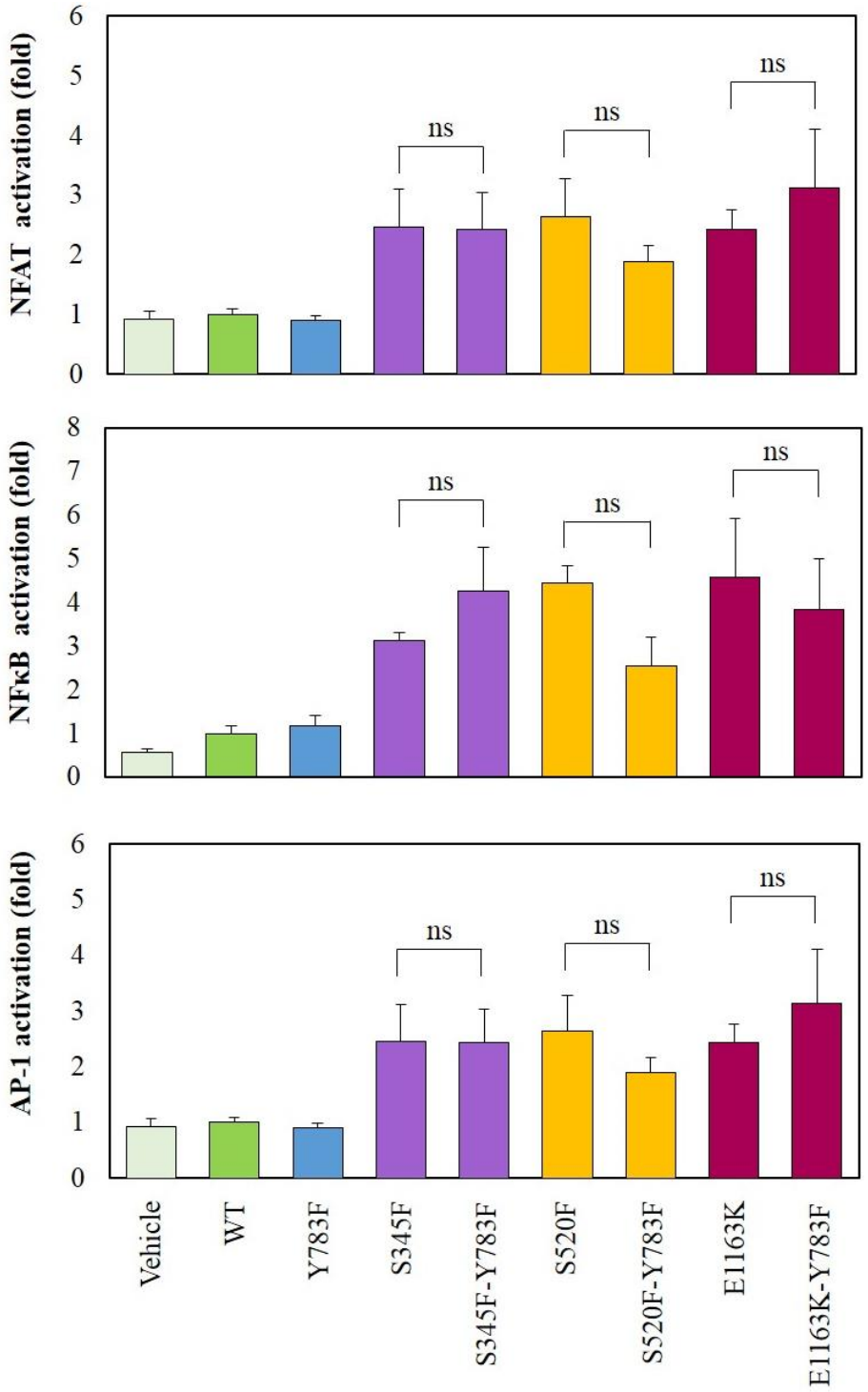

Figure 4. 15. Activating PLCγ1 proteins induce NFAT, NFκB and AP-1 activity without p.Y783 phosphorylation in basal conditions. HEK293 cells were co-transfected with wild-type, p.Y783F mutant, gain-of-function mutant or double mutant PLCγ1 vectors and luciferase reporter constructs. Activity levels were normalised to cells overexpressing wild-type PLCγ1. Data is represented as mean ± SEM, n=3 for each reporter. Student's t-test, ns=not significant.

4.6.5 Activating PLCγ1 mutant proteins induce transcriptional activity without p.Y783 phosphorylation in stimulated conditions

Notably, the p.Y783F mutant protein induced transcriptional activity at comparable levels to wild-type PLCγ1 (Figure 4. 15). These findings differ from those of Poulin *et al*. (2005) and Bunney *et al*. (2012) who demonstrated that mutating the phosphorylation residue to p.Y783F diminished IP production compared to wild-type PLCγ1 (177, 194). Importantly, previous studies analysed the influence of the p.Y783F mutant protein in stimulated cells whereas the experiments performed herein were in basal conditions.

Therefore, to determine if the levels of transcriptional activity induced by p.Y783F differ from wild-type PLCγ1 in stimulated cells, the experiments were repeated but cells were additionally co-transfected with the pBABE-EGFR vector and stimulated with 100 ng/mL EGF for 8 hours. This experimental set-up was used in parallel to determine if the gain-of-function mutant proteins and corresponding double mutant proteins differ in their ability to induce NFκB activity in stimulated conditions.

In both unstimulated and stimulated cells, the p.Y783F mutant protein induced NFκB activity but importantly to a lesser extent than wild-type PLCγ1 (Figure 4. 16). These findings are consistent with previous reports, which show that mutating the p.Y783 phosphorylation residue reduces IP production and phospholipase activity in stimulated conditions (172, 177, 194).

No significant difference was observed in the elevated NFκB activity induced by the gain-of-function proteins and corresponding double mutant proteins in stimulated cells in six biological repeat experiments (Figure 4. 16). Three of the six experiments were performed by Dr. Farrah Bakr, a fellow PhD student. Collectively, data in this section show that the gain-of-function PLCγ1 proteins do not require phosphorylation of the p.Y783 residue, which is critical for activating wild-type PLCγ1 and suggest that these activating mutations mediate downstream signalling in a phosphorylation-independent manner.

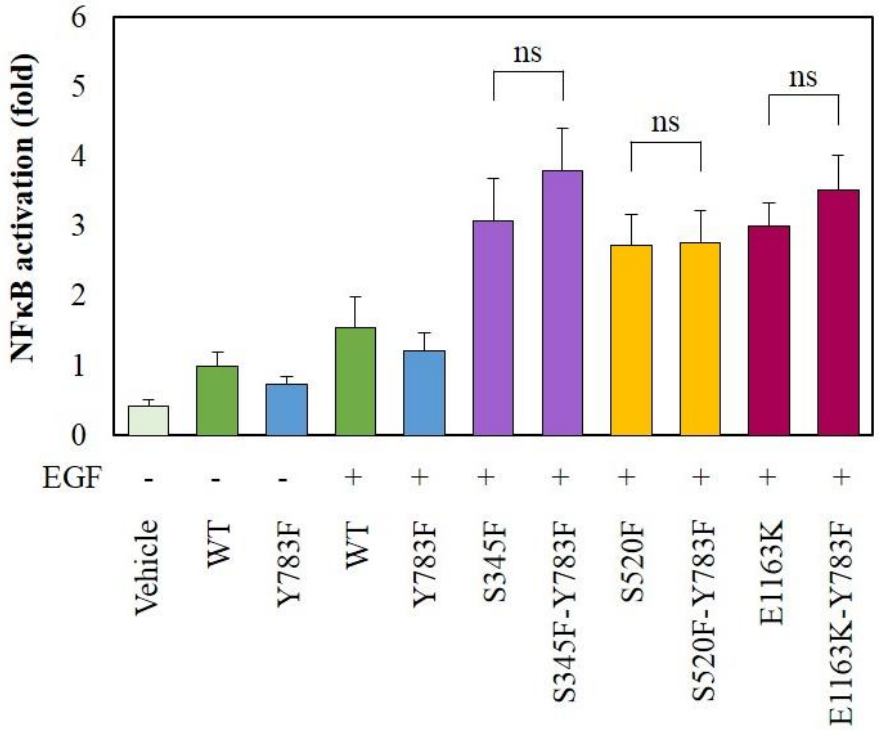

Figure 4. 16. Activating PLCγ1 proteins induce NFκB activity without p.Y783 phosphorylation in stimulated conditions. HEK293 cells were co-transfected with PLCγ1 vectors, the pBABE-EGFR construct and the NFκB reporter plasmid. After serum starvation overnight, cells were stimulated with 100 ng/mL EGF for 8 hours. Activity levels were normalised to unstimulated cells overexpressing wild-type PLCγ1. Data is represented as mean ± SEM; n=6. Student's t-test, ns=not significant. Three experimental repeats were performed by Dr. Farrah Bakr.

4.6.6 The p.R48W and p.D342N mutant proteins may require p.Y783 phosphorylation to increase downstream signalling

In stimulated conditions, the hotspot p.R48W mutant protein elevates NFκB activity (Figure 4. 9) and the p.D342N protein was confirmed to increase IP production (Figure 4. 11). Therefore, these mutant proteins were selected to investigate whether they require p.Y783 phosphorylation to elicit their gain-of-function effects on NFκB signalling in stimulated cells. The increased signalling induced by p.R48W and p.D342N in stimulated conditions suggests that these proteins require p.Y783 phosphorylation for protein activity as does wild-type PLCγ1.

As previously described in this section, the PLCγ1-p.Y783F construct was used as a template for site-directed mutagenesis to generate the p.R48W-Y783F and p.D342N-Y783F constructs. Sanger sequencing confirmed the introduction of these mutations into the vectors and also validated the presence of the p.Y783F mutation (Figure 4. 17). The *PLCG1* ORF, CMV promoter and enhancer and the polyA tails of the plasmids were sequenced and confirmed not to harbour any additional mutations.

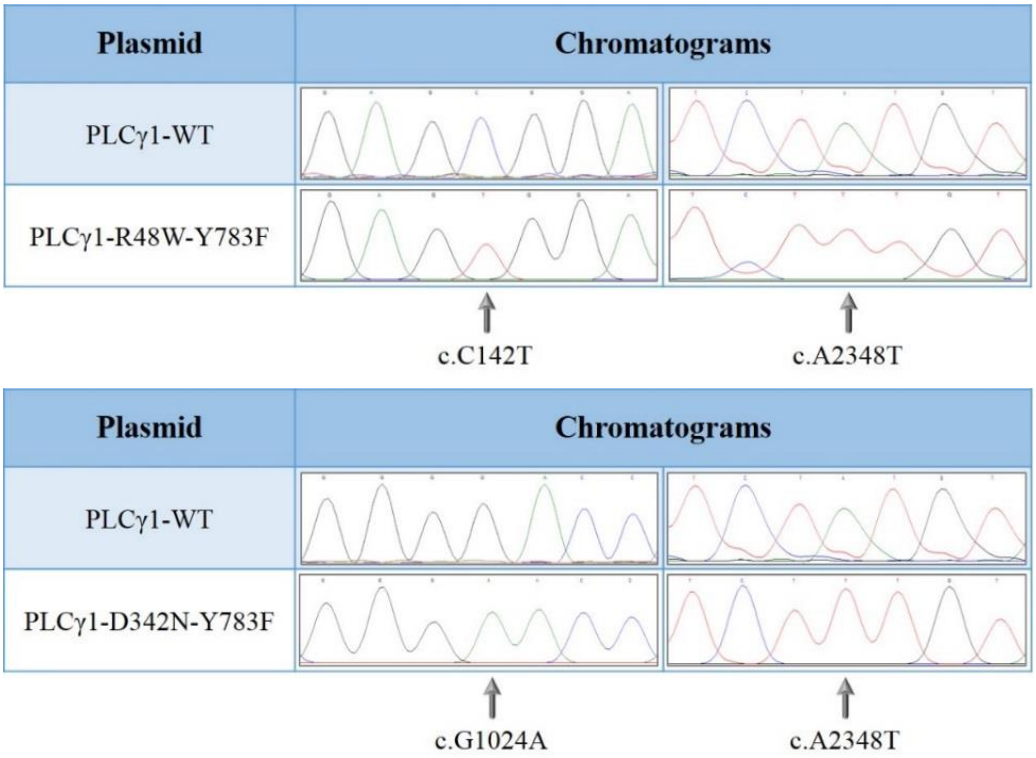

Figure 4. 17. Chromatograms confirming introduction of the p.R48W and p.D342N mutations in the PLCγ1-p.Y783F vector. Site-directed mutagenesis was used to introduce the c.C142T (p.R48W) and p.G1024A (p.D342N) mutations into the vectors harbouring the c.A2348T (p.Y783F) mutation.

HEK293 cells were co-transfected and stimulated with EGF as described in section 4.6.5. The p.E1163K and p.E1163K-p.Y783F mutant proteins were used as positive control samples. Cells expressing p.R48W-Y783F and p.D342N-Y783F demonstrate a reduction in NFκB activity compared to cells expressing p.R48W and p.D342N, respectively (Figure 4. 18). These are early findings as the experiment was performed once due to time constraints. Therefore, further biological repeat experiments are required to determine if there is a statistically significant difference in the NFκB activity induced by the p.R48W and p.D342N proteins with an intact phosphorylation residue compared to mutant proteins expressing the abrogated p.Y783F residue.

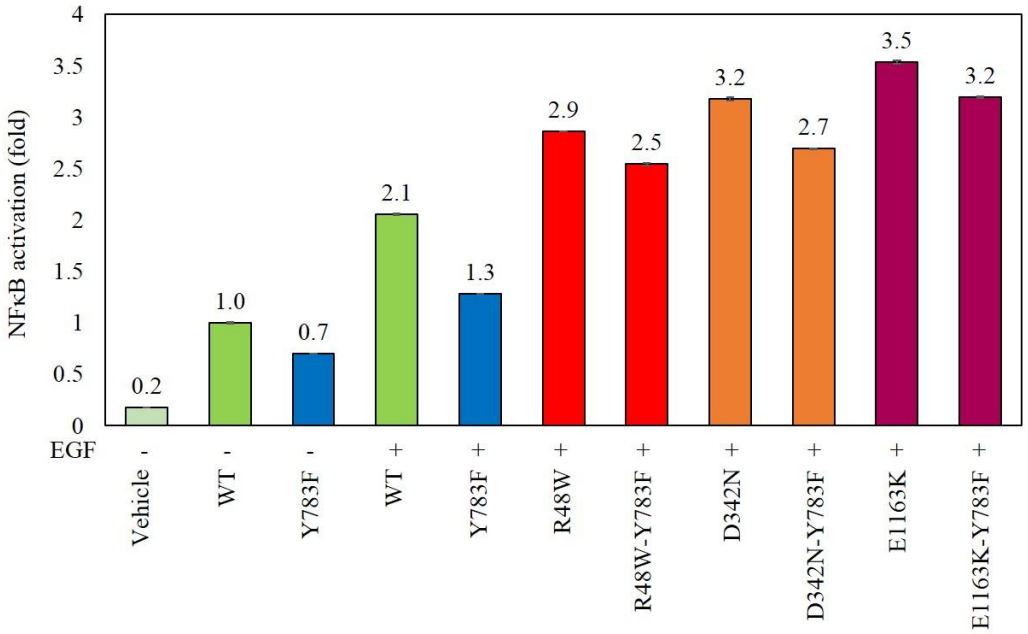

Figure 4. 18. The p.R48W and p.D342N proteins may require p.Y783 phosphorylation to induce NFκB activity in stimulated cells. HEK293 cells were co-transfected with PLCγ1 vectors, the pBABE-EGFR construct and the NFκB reporter plasmid. Following serum starvation, cells were stimulated with 100 ng/mL EGF for 8 hours. Activity levels were normalised to unstimulated cells overexpressing wild-type PLCγ1. Data is represented as mean ± SD of n=1 assay performed in triplicate.

4.7 TPCA-1 does not inhibit PLCγ1-induced NFκB activity

As shown in sections 4.4.2 and 4.5, five PLCγ1 mutations have potent gain-of-function properties. To determine if the elevated NFκB activity induced by activating mutations can be reduced, TPCA-1, an inhibitor of the IKKβ subunit of the IKK complex (Figure 1. 18) was selected for analysis. The IKK complex phosphorylates IκBα, which is degraded and unveils the NLS of the NFκB (p50/p65) heterodimer, allowing it to translocate to the nucleus and initiate transcription. As TPCA-1 inhibits the IKK complex it would be expected to inhibit activation of NFκB.

To identify the optimal concentration of TPCA-1, HEK293 cells were co-transfected with the wild-type PLCγ1 vector, pBABE-EGF construct and NFκB reporter plasmid and then serum starved overnight. Cells were pre-treated with 10 nM, 1 μM, 2.5 μM, 5 μM or 10 μM of TPCA-1 for 30 minutes and then stimulated with 100 ng/mL EGF for 8 hours to activate the signalling pathway. In this section, NFκB reporter activity is expressed as a percentage relative to stimulated or unstimulated cells that were not treated with inhibitor as having 100% transcriptional activity. This means of representation was chosen to effectively demonstrate reductions in transcriptional activity due to inhibitor treatment, which would otherwise be more complicated to interpret if expressed as relative fold changes in activity. Cells treated with increasing concentrations of TPCA-1 did not show a dose-dependent decrease in NFκB activation (Figure 4. 19). Particularly, cells treated with 10 nM, 5 μM and 10 μM demonstrated increased NFκB activity. In contrast, the intermediate TPCA-1 concentrations of 1 μM and 2.5 μM successfully reduced transcriptional activity.

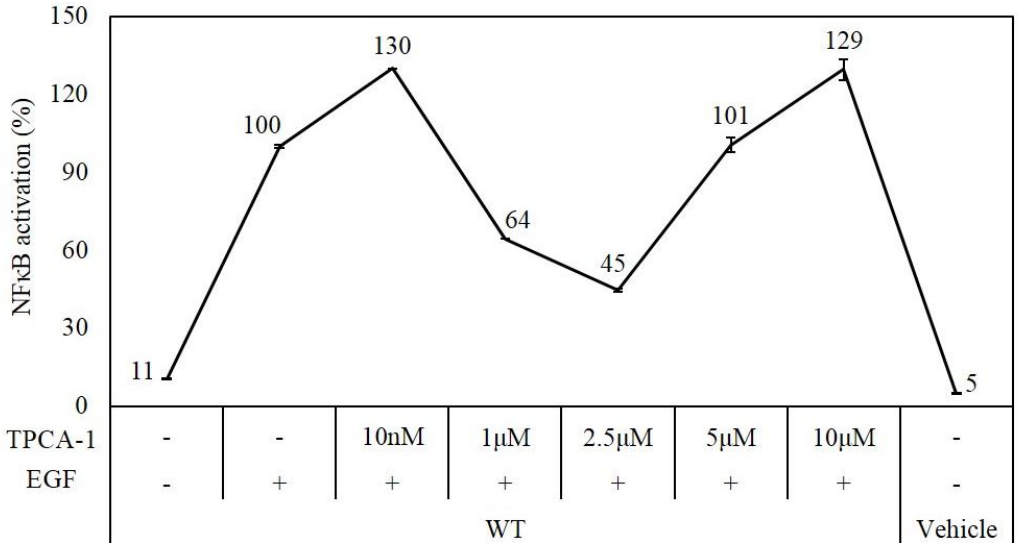

Figure 4. 19. TPCA-1 does not reduce wild-type PLCγ1-induced NFκB activity in a dose-dependent manner. Activation levels were normalised to EGF-stimulated HEK293 cells overexpressing wild-type PLCγ1 but not treated with TPCA-1. Data is represented as mean ± SD, n=1 assay performed in triplicate.

To determine if TPCA-1 inhibits the NFκB activity induced by gain-of-function mutations, the experiment was repeated by co-transfecting cells with the PLCγ1 p.E1163K construct. Cells were not transfected with the pBABE-EGFR construct nor stimulated as the mutant protein elevates transcriptional activity in basal conditions (Figure 4. 5). Treating cells with increasing doses of TPCA-1 did not result in a dose-dependent decrease in p.E1163K-induced NFκB activity (Figure 4. 20). Cells treated with 10 nM, 1 μM and 2.5 μM TPCA-1 had reduced NFκB activity compared to untreated cells expressing the p.E1163K protein. Treatment with higher concentrations, specifically 5 μM and 10 μM, increased NFκB activity. Therefore, as observed in cells overexpressing wild-type PLCγ1, TPCA-1 does not inhibit p.E1163K-induced NFκB activity in a dose-dependent manner.

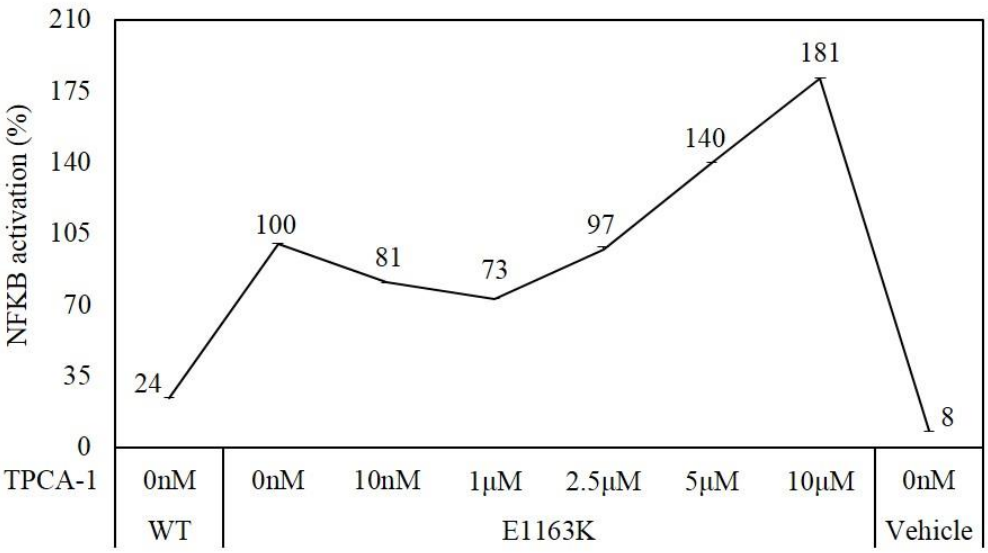

Figure 4. 20. TPCA-1 does not reduce p.E1163K-induced NFκB activity in a dose-dependent manner. Activation levels were normalised to untreated HEK293 cells expressing the p.E1163K protein. Data is represented as mean ± SD, n=1 assay performed in triplicate.

To determine if TPCA-1 treatment of cells for 8.5 hours was sub-optimal and responsible for inducing NFκB activity at particular doses, time course experiments were performed. Cells were transfected with the wild-type or p.E1163K PLCγ1 vectors and following serum starvation overnight the cells were treated with 1 μM of TPCA-1 for 4.5, 6.5 and 8.5 hours. The concentration of 1 μM was chosen as this dose effectively reduced NFκB activity in stimulated cells overexpressing wild-type PLCγ1 (Figure 4. 19) and cells expressing the p.E1163K protein (Figure 4. 20). TPCA-1 did not reduce wild-type PLCγ1-induced NFκB activity in stimulated cells at any time-point (Figure 4. 21. A) and conflict the data shown in Figure 4. 19. Treating p.E1163K-expressing cells with TPCA-1 for 6.5 and 8.5 hours reduced NFκB activity 30% and 27%, respectively compared to untreated cells (Figure 4. 21. B).

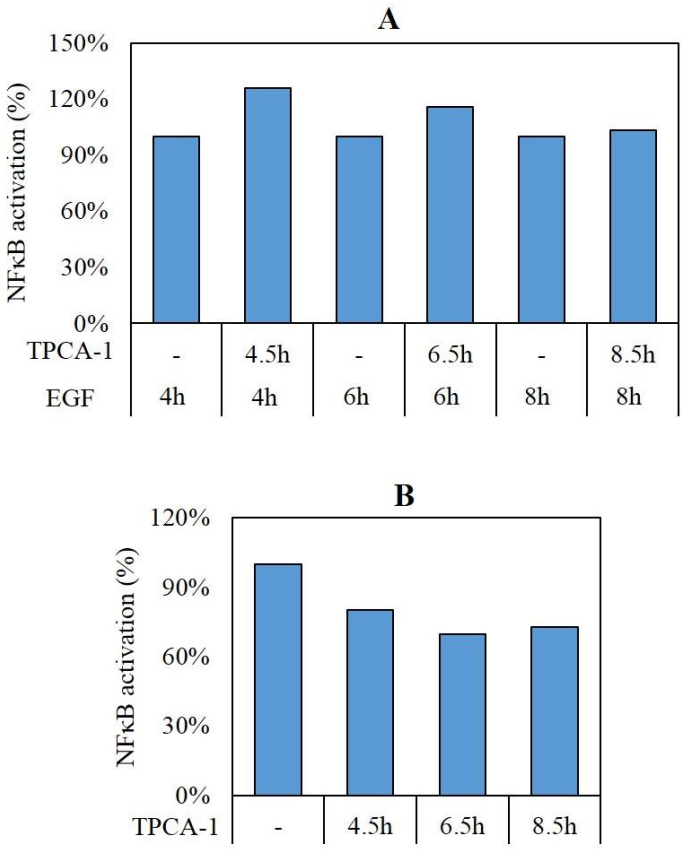

Figure 4. 21. TPCA-1 treatment time course in HEK293 cells. (A) Cells expressing wild-type PLCγ1 (and transfected with the pBABE-EGFR vector) were pre-treated with 1 μM TPCA-1 for 30 minutes and then stimulated with 100 ng/mL EGF for three time points. (B) Cells expressing the mutant p.E1163K protein were treated with 1 μM TPCA-1 for three time points. Activation levels were normalised to cells not treated with inhibitor in each experiment. Data is represented as mean ± SD, n=1 assay performed in triplicate.

To obtain a third biological repeat, cells expressing wild-type and p.E1163K protein were treated with 1 μM TPCA-1 for 8.5 hours. This dose was selected as it reduced NFκB activity in cells expressing wild-type and mutant PLCγ1 (Figure 4. 19 and Figure 4. 20). In the repeat experiments, stimulated cells expressing wild-type PLCγ1 and cells expressing the p.E1163K protein both demonstrated increased NFκB activity when treated with TPCA-1 (data not shown). These results clearly demonstrate that TPCA-1 does not consistently and effectively inhibit PLCγ1-induced NFκB activity in HEK293 cells.

To investigate if the inhibitor had become ineffective, a positive control experiment was performed as per Lu *et al*. (2014) (270), using TNFα instead of EGF to activate NFκB in HEK293 cells. Cells were transfected with the NFκB reporter plasmid and the pRL-TK renilla luciferase vector. After 24 hours, cells were pre-treated with 0 μM, 1 μM, 2.5 μM, 5 μM and 10 μM of TPCA-1 for 30 minutes and then stimulated with 10 ng/mL TNFα for 5 hours. As per the findings of Lu *et al*. (2014) (270), a dose-dependent decrease in TNFα-induced NFκB activity was observed in cells treated with 0 μM – 5 μM of TPCA-1 (Figure 4. 22). Cells treated with 10 μM TPCA-1 had marginally more NFκB activity than cells treated with 5 μM, however such variation in the same experimental system has previously been reported (275). This data confirms that TPCA-1 inhibits TNFα-induced NFκB activity.

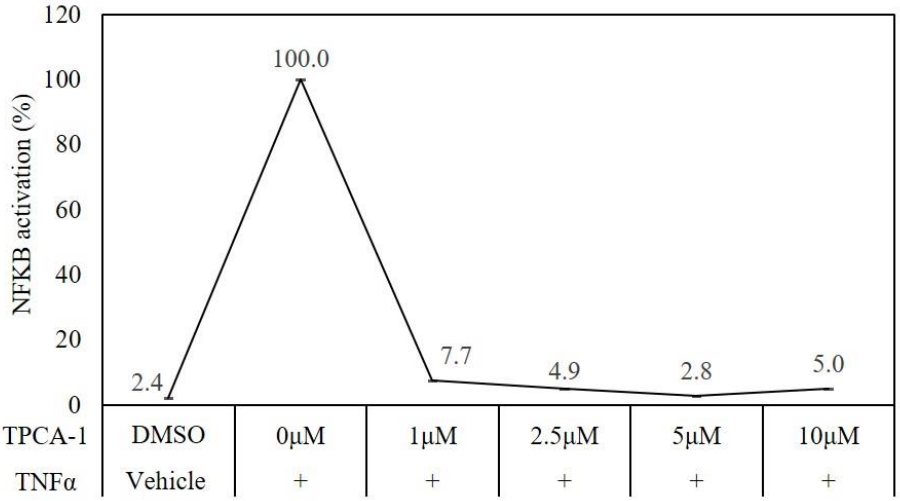

Figure 4. 22. TPCA-1 inhibits TNFα-induced NFκB activity in HEK293 cells. Cells were co-transfected with the NFκB reporter and pRL-TK transfection control plasmid. After 24 hours cells were pre-treated with TPCA-1 for 30 minutes and then stimulated with 10 ng/mL TNFα for 5 hours. Activity levels were normalised to stimulated cells not treated with inhibitor. Data is represented as mean ± SD, n=1 assay performed in triplicate.

Overall, the data presented in this section show that TPCA-1 effectively inhibits TNFα-induced but not PLCγ1-induced NFκB activity and cannot be used to reverse the gain-of-function effects of PLCγ1 mutations. It may be possible that TPCA-1 is a specific inhibitor for the TNFα but not TCR signalling pathway, which both activate NFκB. Although the TCR was not directly activated in these experiments, PLCγ1

activity was induced by engaging the EGFR in an analogous set-up based on the fact that multiple cell surface receptors can activate PLCγ1 (Figure 1. 15).

4.8 Summary

To investigate the effect of nine PLCγ1 mutations (p.R48W, p.S312L, p.D342N, p.S345F, p.S520F, p.R1158H, p.E1163K, p.D1165H and p.VYEEDM1161V) on protein expression and activity, mutant constructs were generated.

The transfection of HEK293 cells was optimised for western blot analyses and luciferase reporter assays. Protein expression analysis revealed that eight mutant proteins had comparable PLCγ1 expression to wild-type protein, but the in-frame indel p.VYEEDM1161V protein showed a marked reduction in total PLCγ1 expression and a relative increase in PLCγ1 phosphorylation. The p.S345F, p.S520F, p.E1163K, p.D1165H and p.VYEEDM1161V proteins significantly elevated downstream signalling by increasing NFκB and NFAT activity in basal conditions, making them potent gain-of-function mutant proteins. Furthermore, the hotspot p.R48W mutation significantly increased NFκB activity in stimulated conditions. The p.S345F, p.S520F, p.E1163K, p.D1165H and p.VYEEDM1161V proteins in addition to increasing downstream signalling, also enhanced IP production and directly increased proximal signalling in basal conditions.

Phosphorylation of the p.Y783 residue has been shown to be critical for PLCγ1 activation, IP production and proximal signalling (172, 177, 194). The data presented in this chapter demonstrates that three gain-of-function PLCγ1 proteins do not require p.Y783 phosphorylation to elevate downstream signalling by showing increased NFκB, NFAT and AP-1 transcriptional activity in basal conditions. The activating mutations also did not show a dependency on p.Y783 phosphorylation to induce NFκB activity in stimulated cells. Pilot data showed that the p.R48W and p.D342N mutant proteins may be partially dependent on p.Y783 phosphorylation to increase NFκB activity in stimulated cells, however this warrants further investigation.

To investigate if the elevated NFκB activity induced by gain-of-function PLCγ1 mutations can be reversed, cells were treated with the IKKβ inhibitor, TPCA-1. This inhibitor effectively reduced TNFα-induced NFκB activity in a control experiment but not PLCγ1-induced NFκB activity in HEK293 cells.

Chapter 5 Establishing a system to visualise the cellular localisation of mutant PLCγ1

5.1 Introduction

The PLCγ1 p.D342N, p.S345F and p.E1163K mutations have previously been mapped onto the structure of the PLCβ3 and/ or PLCβ2 isoforms (67, 160). The mutations were proposed to affect residues on the protein surface that is predicted to interact with the plasma membrane, where the PLC substrate PIP_2 is located.

In this chapter, the position of nine PLCγ1 mutations (including the aforementioned three) will be determined by mapping onto a composite structure of PLCγ2, an isoform that is more closely related to PLCγ1 than PLCβ3 or PLCβ2. An *in vitro* imaging system will then be set up using immunofluorescence analysis and confocal microscopy to visualise the location of the mutant proteins within cells.

5.2 Activating PLCγ1 mutations map to the protein surface that likely interacts with the plasma membrane

To gain insight into mechanisms of mutant protein activity, PLCγ1 mutations were mapped onto a composite structure of PLCγ2 using the DeepView-Swiss-PdbViewer and Pymol molecular visualisation software. PLCγ2 has high sequence homology with PLCγ1 in key functional domains (Figure 1. 14) (175). The mutations were mapped onto the PLCγ2 isoform because only the structure of the PLCγ1 SH2 and SH3 domains has been resolved. The mutation mapping was performed by Dr. Katy Everett (University of Cambridge).

The PLCγ2 model demonstrates that the p.R48W, p.D342N, p.S345F, p.E1163K, p.D1165H and p.VYEEDM1161V mutations map to the protein surface that is predicted to interact with the plasma membrane, where the PIP_2 substrate of PLC is located (Figure 5. 1). The p.S312L and p.S520F mutations orient to the opposite face of the protein and the p.R1158H locates towards the centre of PLCγ2. The ability of the p.R48W hotspot mutation and p.D342N mutant to increase PLCγ1 signalling in stimulated conditions supports their location at the surface of PLCγ2, in close proximity to the gain-of-function p.S345F, p.E1163K, p.D1165H and p.VYEEDM1161V mutations.

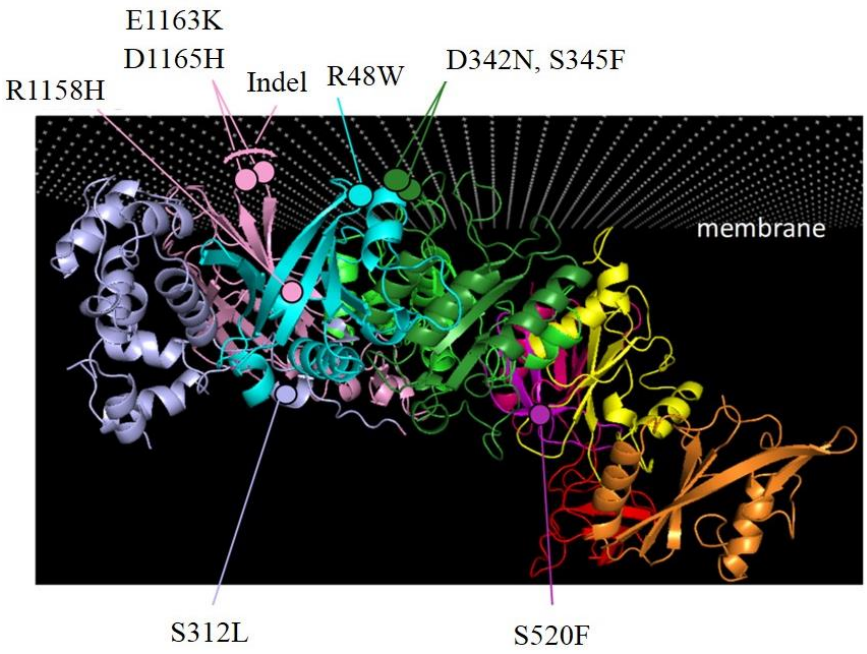

Figure 5. 1. PLCγ1 mutations mapped to the PLCγ2 crystal structure. The activating PLCγ1 mutations p.S345F, p.E1163K, p.D1165H and p.VYEEDM1161V (indel) locate to the PLCγ2 surface that is predicted to interact with the plasma membrane, where PIP_2 resides. Mutation mapping was performed by Dr. Katy Everett.

5.3 Generation of GFP-tagged mutant constructs

As the mutations that increase basal PLCγ1 activity (p.S345F, p.E1163K, p.D1165H and p.VYEEDM1161V) and the mutations that elevate signalling after stimulation (p.R48W and p.D342N) map to the PLCγ2 protein surface that likely interacts with the plasma membrane, it is postulated that these mutant proteins may elevate PIP_2 hydrolysis via increased membrane interactions, leading to amplified downstream signalling. To investigate whether the p.S345F, p.E1163K, p.D1165H and p.VYEEDM1161V proteins interact more with the plasma membrane compared to wild-type PLCγ1, immunofluorescence and confocal microscopy analyses were optimised. The p.D342N mutant was also selected for analysis as it locates in close proximity to the activating p.S345F mutation. The p.S520F mutation was included for analysis to visualise the cellular localisation of this activating protein, which does not map in the vicinity of the gain-of-function mutations in the 3D model.

The eGFP-PLCγ1 vector that encodes an eGFP tag upstream the wild-type *PLCG1* ORF was kindly provided by Professor Matilda Katan (UCL). The vector was used as a template to generate six GFP-tagged mutant PLCγ1 constructs. The introduction of mutant alleles was confirmed by Sanger sequencing (Figure 5. 2). The *PLCG1* ORF, CMV promoter and enhancer, eGFP tag, and polyA tail sequences of the plasmids were confirmed not to harbour any additional mutations.

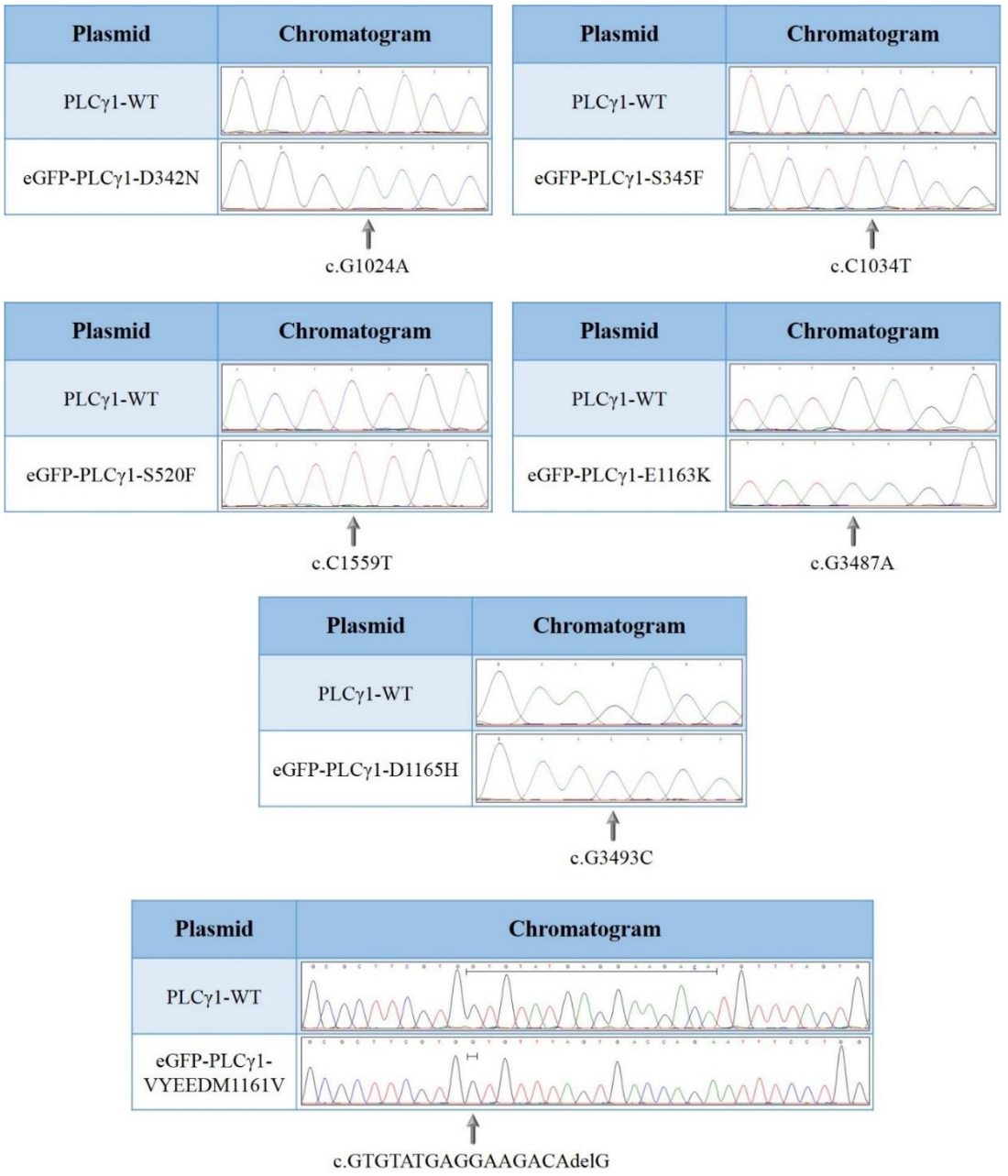

Figure 5. 2. Chromatograms confirming introduction of mutant alleles in the eGFP-PLCγ1 constructs by site-directed mutagenesis. Sequences from the wild-type constructs are shown in the top panels and mutant alleles in the bottom panels.

5.4 The GFP tag does not hinder mutant PLCγ1 activity

HeLa cells were chosen for immunofluorescence analyses as these cells have a large cytoplasm, enabling better visualisation of protein localisation. To determine whether the GFP tag interferes with the elevated transcriptional activity induced by the PLCγ1 mutations in the folded protein conformation, HeLa cells were co-transfected with wild-type or mutant GFP-tagged or untagged vectors and the NFAT-luciferase reporter plasmid. The NFAT activity induced by the GFP-tagged mutant PLCγ1 proteins was comparable to or greater than that induced by the untagged proteins (Figure 5. 3), showing that the N-terminus GFP tag does not interfere with the gain-of-function properties of mutant PLCγ1 proteins.

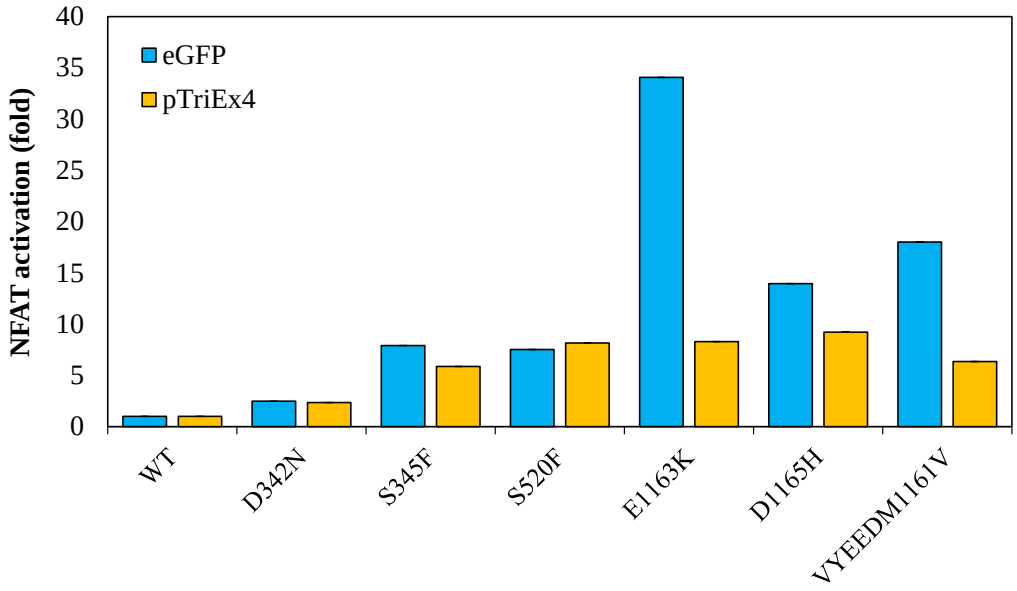

Figure 5. 3. The GFP tag in the eGFP-PLCγ1 constructs does not hinder PLCγ1 activity. GFP-tagged proteins induce comparable levels of NFAT transcriptional activity to untagged (pTriEx-4) PLCγ1 proteins in transfected HeLa cells. Activation levels induced by tagged and untagged mutant proteins were normalised to those of the corresponding wild-type proteins. Data is represented as mean ± SD; n=1 assay performed in triplicate.

5.5 Optimisation of HeLa cell transfection, staining and confocal microscopy settings

To determine whether the mutant PLCγ1 proteins localise to the plasma membrane, a model system was set up in which HeLa cells were transfected with eGFP-PLCγ1 plasmids and stained with Phalloidin and DAPI to visualise F-actin and the nucleus, respectively. Co-localisation of PLCγ1 proteins with the plasma membrane would result in yellow-orange pixels from overlapping green (PLCγ1) and red (F-actin) fluorescence. The cSH2 domain of PLCγ1 has been shown to interact with the actin-cytoskeleton, which enables the enzyme to translocate to the plasma membrane where it is activated by phosphorylation from RTKs (276). Therefore, the visualisation system would also enable investigations to determine whether mutant proteins alter the cellular structure.

The experiments will initially optimise visualisation in basal conditions as the activating mutations do not require stimulation to elicit gain-of-function. As wild-type PLCγ1 requires stimulation to induce signalling, EGF-stimulation of HeLa cells can be optimised and the cells visualised by real-time fluorescence imaging in future investigations as per Matsuda *et al*. (2012) and Wang and Wang (2003) (178, 277).

The first experiment aimed to ensure that the DAPI and Phalloidin dyes stained their specified targets within cells and to confirm that the stained features can be successfully visualised by confocal microscopy. HeLa cells (8×10^4) were transfected with 500 ng of either wild-type or mutant eGFP-PLCγ1 plasmids and stained with 1 unit of Phalloidin and 300 nM of DAPI. Cells were visualised using immersion oil and a 60X objective on a Nikon A1 inverted microscope and analysed using the NIS elements analysis software (Version 4.51) at the Nikon Imaging Centre (KCL). PLCγ1 expression was confirmed in all transfected cells (Figure 5. 4). Intra- and inter-sample variation in GFP expression was observed as some cells demonstrated more intense GFP expression. Cells were successfully stained with DAPI and Phalloidin, enabling visualisation of the nucleus and cell structure (Figure 5. 4). Imaging of the nucleus, however required higher laser power as the staining was weak. Therefore, in subsequent experiments cells were stained with a higher concentration of DAPI to avoid using high laser power that can photo-bleach the fluorophores. In the merged images of the p.S345F, p.S520F, p.E1163K and p.VYEEDM1161V samples, co-

localisation of PLCγ1 with the plasma membrane can be visualised by the orange pixels at the cell boundary, however this was not observed in cells expressing wild-type PLCγ1 (Figure 5. 4). It could not be determined if the p.D1165H mutant protein co-localises to the plasma membrane from the merged image as the F-actin staining was weak compared to GFP expression (Figure 5. 4). However, in the GFP-only channel, an increase in protein expression was observed at the periphery of a p.D1165H-transfected cell (Figure 5. 4). Elevated protein expression was also observed in the GFP-only channel in cells expressing the p.VYEEDM1161V indel (Figure 5. 4).

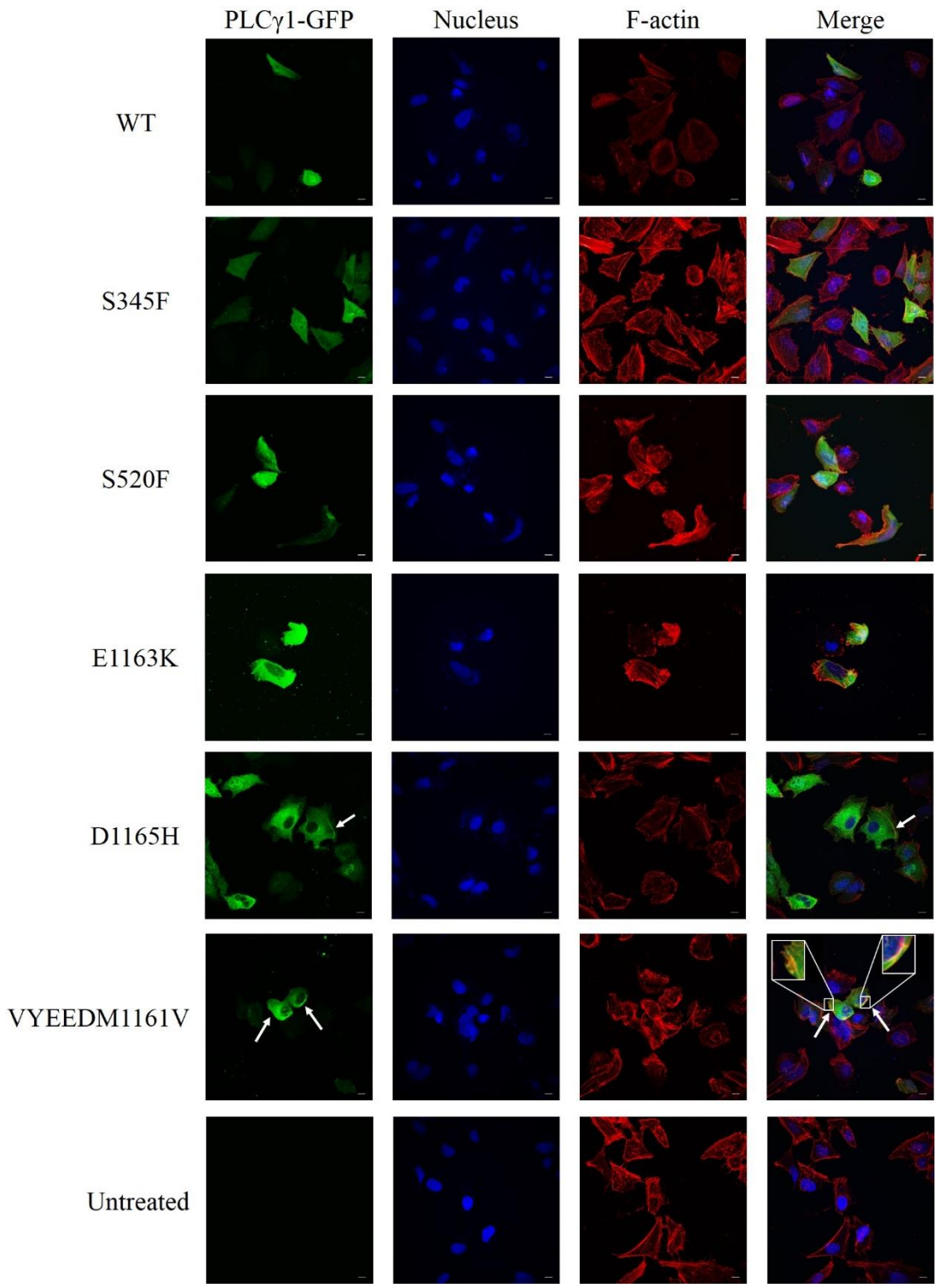

Figure 5. 4. Mutant PLCγ1 may have increased co-localisation to the plasma membrane *in vitro*. HeLa cells were transfected with eGFP-tagged PLCγ1 constructs and stained to visualise the nucleus and F-actin. Orange pixels at the cell boundary in merged images may represent increased co-localisation of PLCγ1 at the plasma membrane. Arrows indicate a potential increase in PLCγ1 localisation to the membrane in the GFP-only channel and corresponding merged images.

The high intensity GFP expression over-powered the F-actin staining, making it difficult to visualise co-localisation at the plasma membrane. Therefore, HeLa cells were transfected with decreasing concentrations of the wild-type or p.E1163K plasmids. p.E1163K was selected for analysis because cells expressing this mutant protein produced the most intense GFP signals (Figure 5. 4). HeLa cells (7×10^4) were transfected with 350 ng, 200 ng or 100 ng of the eGFP-PLCγ1 plasmids, stained with 1 unit of Phalloidin and 600 nM of DAPI and analysed using immersion oil with a 100X objective. The intensity of GFP expression was comparable within and between samples, with the exception of two cells expressing p.E1163K (Figure 5. 5). Cells transfected with 350 ng of eGFP plasmids enabled optimal visualisation of co-localisation at the plasma membrane compared to cells transfected with 200 ng or 100 ng plasmid DNA, therefore this concentration was used for subsequent immunofluorescence analyses (Figure 5. 5).

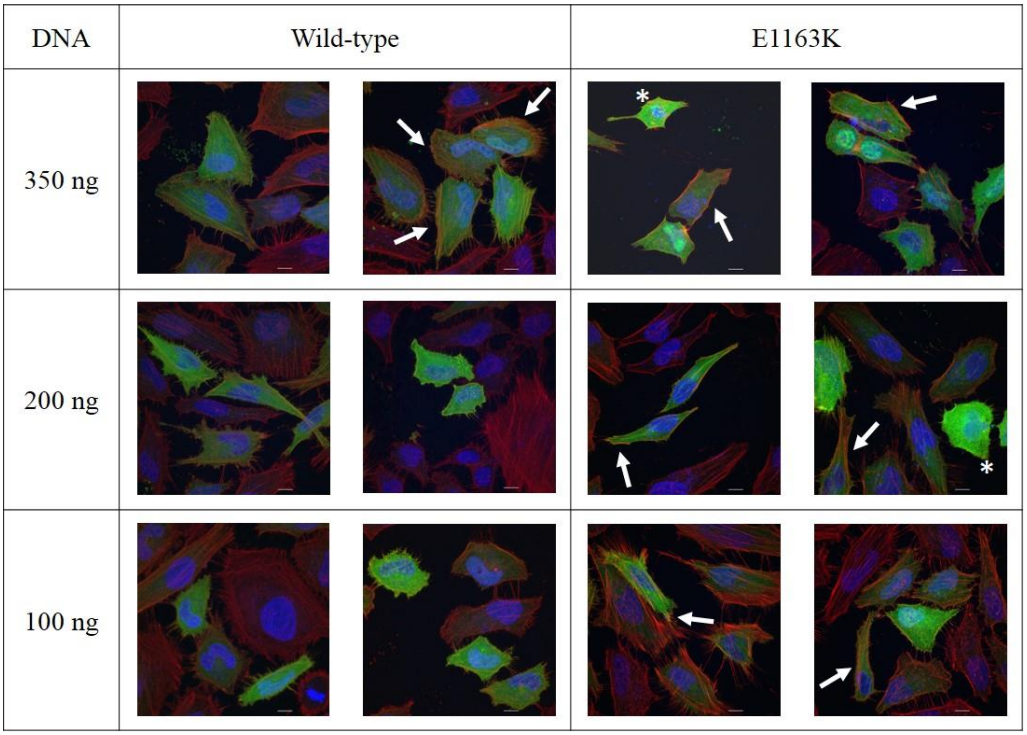

Figure 5. 5. Optimisation of HeLa cell transfection with GFP-tagged PLCγ1 constructs. Cells transfected with decreasing concentrations of wild-type and p.E1163K PLCγ1 plasmids showed comparable GFP expression. Panels show merged immunofluorescence images of two fields of view per sample. Asterisks denote cells with more intense GFP expression than other cells and arrows indicate cells that demonstrate co-localisation of PLCγ1 at the plasma membrane.

Despite increasing the objective from 60X to 100X and reducing the number of seeded cells from 8 x 10^4 to 7 x 10^4, it was difficult to visualise single cells due to high confluency. Therefore, 1 x 10^4 HeLa cells were transfected with 350 ng of wild-type or p.D1165H plasmid DNA. F-actin and DAPI staining was weak in previous experiments and required high laser power for detection. Therefore, cells were stained with higher concentrations of Phalloidin (4 units) and DAPI (1 μM) to prevent photo-bleaching and analysed using a 100X objective and oil immersion. Cells expressing GFP-tagged wild-type PLCγ1 varied greatly in shape (Figure 5. 6). Increased localisation of PLCγ1 to the cell periphery was observed in the GFP-only channel in cell 1 and 2 but not in cell 3 (Figure 5. 6). However, the increased GFP localisation in the first cell appears to be an artefact as the pattern of localisation was not observed in the other two cells in this experiment and also previous experiments. Co-localisation of PLCγ1 to the cell membrane was observed in the second cell (Figure 5. 6).

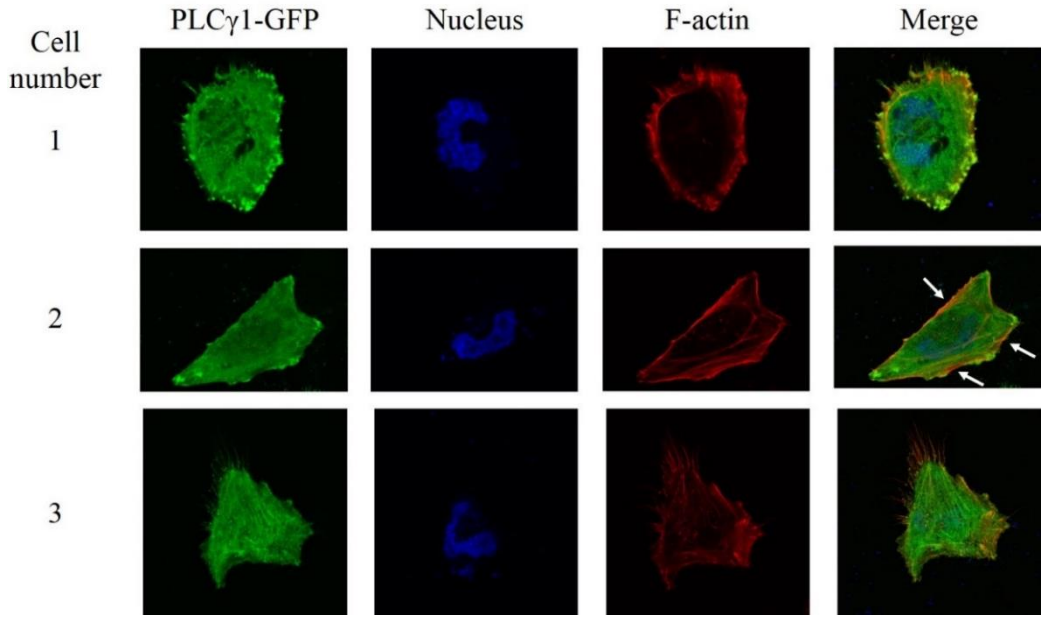

Figure 5. 6. HeLa cells expressing GFP-tagged wild-type PLCγ1 vary in cell shape. Cells were transfected and stained to enable visualisation of the nucleus and F-actin. Arrows indicate potential co-localisation of PLCγ1 with the plasma membrane.

Cells transfected with the PLCγ1 p.D1165H mutant also demonstrate variable morphology. The p.D1165H-transfected cell (expressing GFP) showed less defined F-actin organisation compared to the adjacent untransfected cell (Figure 5. 7. A). The cells shown in Figure 5. 7. B further demonstrate the variability in cell shape and also show increased PLCγ1 localisation at the membrane in both the GFP-only channel and the merged image. Figure 5. 7. C shows an amplification of the merged image from Figure 5. 7.B, which demonstrates co-localisation of the mutant p.D1165H protein with the plasma membrane in both cells.

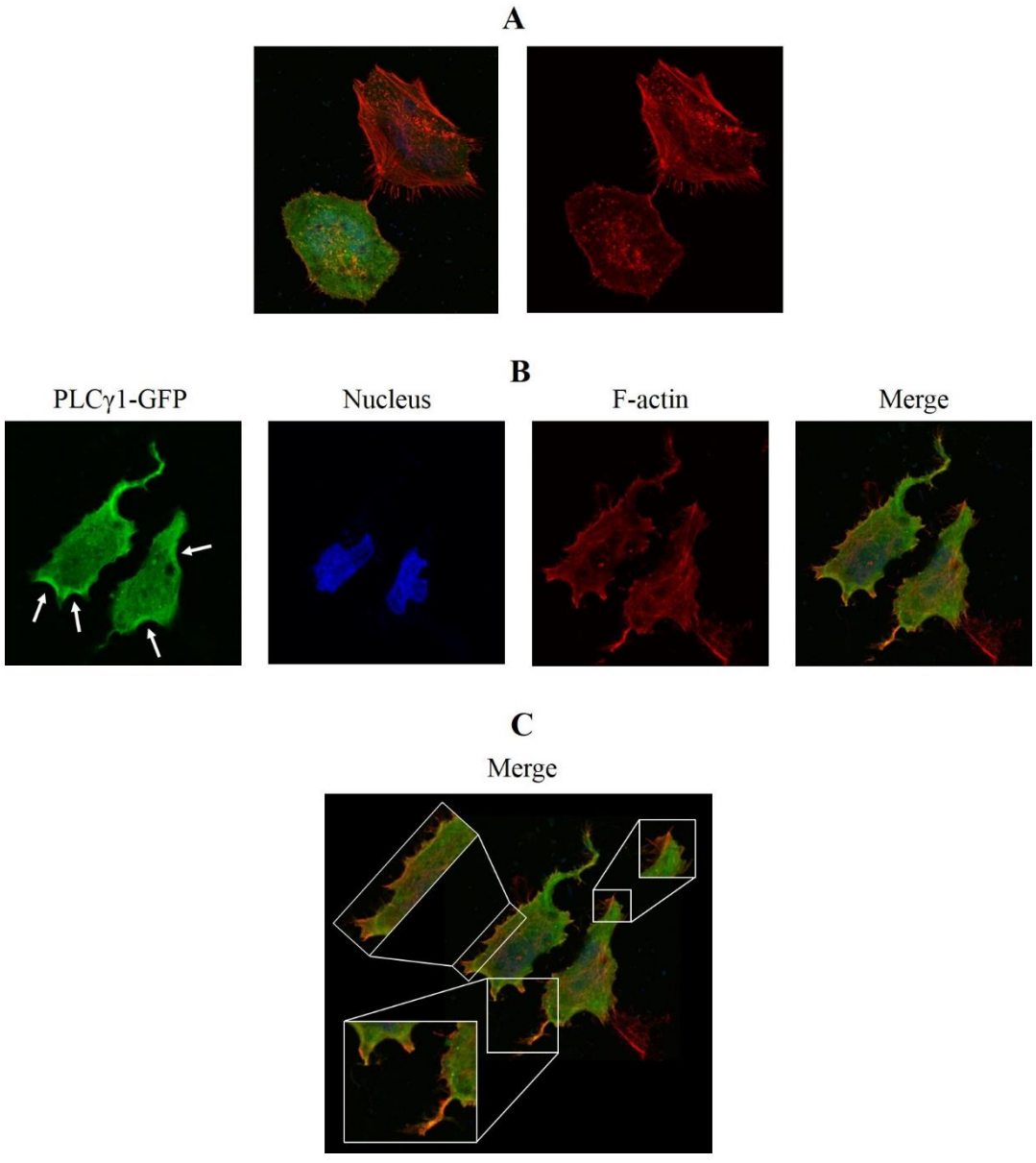

Figure 5. 7. HeLa cells expressing the GFP-tagged p.D1165H mutant protein have variable cellular morphology. Cells were transfected and stained to enable visualisation of the nucleus and F-actin. Arrows indicate potential co-localisation of mutant PLCγ1 with the plasma membrane.

Overall, clearly visualising increased co-localisation of mutant PLCγ1 to the plasma membrane compared to wild-type protein was difficult as PLCγ1 was expressed throughout the cytoplasm. Furthermore, it was challenging to determine whether the activating PLCγ1 proteins alter cellular structure because of the large variation in morphology observed. To be able to confidently quantify co-localisation and determine mutation-induced differences in cellular structure, at least 20 cells expressing wild-type and each mutant protein would need to be analysed. This was unachievable due to time constraints, however the experimental system to successfully transfect and stain HeLa cells has been established for use in future experiments.

5.6 Summary

The PLCγ1 p.S345F, p.E1163K, p.D1165H and p.VYEEDM1161V gain-of-function mutations were shown to map to the PLCγ2 protein surface that likely interacts with the plasma membrane. The p.R48W and p.D342N mutant proteins, which elevate signalling in stimulated conditions, also map to this surface. Thus, it was hypothesised that these mutant proteins may have increased interactions with the plasma membrane as a mechanism of elevating substrate hydrolysis and increasing downstream signalling. To investigate whether mutant proteins have increased membrane interactions, an imaging system was established. Firstly, mutant GFP-tagged PLCγ1 constructs were generated and the transfection and staining of HeLa cells to visualise PLCγ1 localisation was optimised for immunofluorescence analysis. Further investigations are required to quantify co-localisation of wild-type and mutant PLCγ1 with the plasma membrane and to confidently determine any mutation-induced changes in cellular morphology.

Chapter 6 Concluding remarks

6.1 Discussion

6.1.1. Novel findings presented in this study

This thesis addresses the hypothesis that PLCγ1 variants are true gain-of-function mutations that increase TCR signalling and contribute to the pathogenesis of SS. Accordingly, *PLCG1* mutations were shown to persist in multiple SS tumour compartments over extended periods of time. *PLCG1* mutations are reported in several types of mature T-cell lymphomas, which occur throughout the gene and in particular at five hotspots. This study showed that five PLCγ1 mutations potently activate proximal and downstream signalling via the DAG-PKCθ-NFκB, DAG-PKCθ-AP-1 and IP_3-calcineurin-NFAT pathways independently of cellular activation signals. Importantly, the gain-of-function mutant proteins increased downstream signalling in a p.Y783 phosphorylation-independent manner. The data presented propose a critical role of the C2 domain in regulating PLCγ1 activity. Overall, this thesis provides strong evidence for the development of novel PLCγ1 mutation-specific inhibitors as a form of targeted therapy for mature T-cell lymphoma patients harbouring *PLCG1* mutations.

6.1.2. *PLCG1* mutations occur frequently in mature T-cell lymphomas

PLCG1 is frequently mutated in numerous mature T-cell lymphomas. To determine the overall frequency of *PLCG1* mutations in different disease subsets, a comprehensive literature analysis of all WES and targeted gene sequencing studies of mature T-cell lymphoma samples was performed. This analysis was done with the help of Dr. Christine Jones (KCL). *PLCG1* was determined to be most frequently mutated in ATLL, followed by PTCL-nos, HSTL, AITL, CTCL (MF and SS) and TPLL, but not in anaplastic large cell lymphomas, enteropathy-associated T-cell lymphomas and natural killer/T-cell lymphomas, the reasons for which remain unclear (Table 6. 1). Interestingly, the mutations reported in TPLL and HSTL are disease-specific and may contribute to disease pathogenesis in a unique way. Notably, deep sequencing studies have only analysed advanced stage MF samples and investigations into early stage disease are required to determine whether *PLCG1* mutations are early events in CTCL.

Table 6. 1. Whole-exome and targeted gene sequencing studies reporting *PLCG1* mutations in mature T-cell lymphomas. ATLL: adult T-cell leukaemia/lymphomas, PTCL-nos: peripheral T-cell lymphomas-not otherwise specified, MF: Mycosis Fungoides, AITL: angioimmunoblastic T-cell lymphomas, SS: Sézary Syndrome, HSTL: hepatosplenic T-cell lymphoma, TPLL: T-cell-prolymphocytic leukaemia, ALCL: anaplastic large cell lymphoma, EATL: enteropathy-associated T-cell lymphoma, NKTCL: natural killer/T-cell lymphoma.

Malignancy	**Mutation frequency**	**References**
ATLL	**36.2%** (134/370)	(221)
PTCL-nos	**18.2%** (4/22)	(66, 218, 278)
MF	**15.1%** (8/53)	(71, 148, 160)
HSTL	**15.0%** (3/20)	(222)
AITL	**12.0%** (11/92)	(65, 66, 218, 220, 278)
SS	**11.3%** (44/388)	(67-71, 147, 160, 161)
TPLL	**5.6** (2/36)	(223)
ALCL	**0%** (0/23)	(279)
EATL	**0%** (0/89)	(66, 280-282)
NKTCL	**0%** (0/27)	(66, 283)

Two further studies performed selective sequencing of exon 11 and/ or 15 to screen for the PLCγ1 p.S345F and p.S520F mutations in mature T-cell lymphomas (Table 6. 2) (216, 217). These variants were screened for as they have been shown to be activating mutations in CTCL (160). The two studies used highly sensitive sequencing techniques that preferentially amplify low frequency mutant alleles for detection (as will be discussed later) (216, 217). Due to the different methodology used, the frequencies from the selective sequencing studies were not included in the above-mentioned analysis to determine the overall *PLCG1* mutation frequency per disease type.

Table 6. 2. *PLCG1* mutation frequencies reported by exon-specific sequencing of mature T-cell lymphomas. c-ALCL: cutaneous-anaplastic large cell lymphomas, LyP: lymphomatoid papulosis.

Malignancy	Exons sequenced	Mutation frequency	Reference
PTCL-nos	11	**14.6%** (6/41)	Manso *et al*. 2014 (217)
AITL	11	**11.7%** (7/60)	
SS	11 & 15	**5.1%** (2/39)	Caumont *et al*. 2015 (216)
MF	11 & 15	**2.7%** (1/37)	
c-ALCL	11 & 15	**0%** (0/14)	
LyP	11 & 15	**0%** (0/4)	

The analysis reported here shows that 15.1% of MF and 11.3% of SS tumours harbour *PLCG1* mutations (Table 6. 1), which negates the report by Caumont *et al*. (2015) that *PLCG1* mutations are uncommon in CTCL (Table 6. 2) (216). The low mutation frequency reported by the latter study is likely due to the sequencing of only two exons. Analysis of deep sequencing studies of mature T-cell lymphomas (Figure 1. 22) and COSMIC data both show that *PLCG1* mutations occur throughout the gene but more frequently at five hotspots. Notably, the COSMIC database was identified to consistently under-report *PLCG1* mutations compared to an in-depth analysis of all NGS studies on mature T-cell lymphomas, as demonstrated by the hotspot mutation frequencies in Table 6. 3. This data supports that comprehensive literature analyses are the most reliable method to determine the true frequency of gene mutations.

Table 6. 3. PLCγ1 hotspot mutation counts in mature T-cell lymphomas. Counts reported by the COSMIC database and analysis of deep sequencing studies are shown.

PLCγ1 mutation	COSMIC count	Literature count	Literature references
p.R48W	53	66	(67, 69, 70, 147, 218, 221)
p.S345F	63	74	(65, 67, 68, 70, 71, 147, 148, 160, 161, 216-218, 220, 221)
p.S520F	9	11	(68, 70, 147, 160, 218, 221)
p.E1163K	21	27	(67-70, 147, 218, 221)
p.D1165H	18	21	(70, 147, 218, 221)

WGS and WES studies on CTCL tumours have demonstrated a highly heterogeneous tumour mutation profile affecting genes involved in T-cell activation, JAK/STAT signalling, DNA damage response, cell fate, cell survival, chromatin modification and many more (67-71, 148, 161). Nevertheless, a meta-analysis of 220 CTCL tumours analysed by nine deep sequencing studies highlighted that the cell cycle regulation gene *TP53* and the TCR signalling gene *PLCG1*, most frequently harboured point mutations in 14% and 9% of cases, respectively (162). These findings were confirmed by another meta-analysis of 139 CTCL tumours (from seven NGS studies), which showed that *TP53* and *PLCG1* were the most frequently mutated oncogenes in 19% and 10% of cases, respectively (166). The analysis performed here reports a similar *PLCG1* mutation frequency in 11.8% of CTCL tumours (Table 6. 1). Importantly. Chang *et al*. (2018) identified that mutations in *PLCG1*, *CARD11* and *TNFRSF2B*, which are involved in NFκB signalling occur in mutual exclusivity in SS, suggesting that aberration of one gene is sufficient to disrupt this pathway and induce oncogenesis (166).

6.1.3. *PLCG1* mutations activate three signalling pathways to induce NFκB, NFAT and AP-1 transcriptional activity

This study shows that mutant PLCγ1 proteins have potent gain-of-function properties that activate three signalling cascades to induce NFκB, NFAT and AP-1 activity in basal conditions suggesting that these proteins may induce constitutive T-cell

activation independent of TCR engagement. The data presented herein is the first to show direct activation of NFκB activity by PLCγ1 mutations *in vitro*. Previous studies have shown that PLCγ1 mutations identified in PTCL elevate MALT1 activity in transfected HEK293T cells (218). Increased MALT1 activity is suggestive of elevated NFκB activity, however unlike the data presented in this thesis, Vallois *et al*. (2016) do not directly show the effect on transcriptional activity. The only reported interrogations of NFκB in relation to PLCγ1 mutations are immunohistochemical analyses of MF samples, which showed no segregation of nuclear p50 and p52 NFκB subunit expression in patients with or without PLCγ1 mutations (160). However, a significant relationship between expression of the p.S345F mutation and nuclear localisation of p50 has been reported in PTCL samples (217). Activation of NFκB by mutant PLCγ1 is significant as this transcription factor is characteristically constitutively active in CTCL, ATLL and some PTCL subtypes (112, 113, 118, 119). Elevated autocrine TNFα production in SS tumours and HUT-78 cells, increased nuclear localisation of the p65 NFκB subunit in MF and gene rearrangements in *NFKB2* in CTCL tumours and cell lines are known mechanisms that raise NFκB activity (112, 114, 117). Data presented here strongly supports that *bona fide* gain-of-function PLCγ1 mutations are a novel and additional mechanism by which NFκB is constitutively active in CTCL and other mature T-cell lymphomas.

This study is the first to report the gain-of-function effects of PLCγ1 mutations on AP-1 transcriptional activity. Our group has previously shown that copy number gain of JUNB, an AP-1 subunit, increases expression of this subunit in CTCL (121). Therefore, activating PLCγ1 mutations are an alternative mechanism by which AP-1 activity is augmented in CTCL.

This study is the first to analyse the direct effect of disease-associated PLCγ1 mutations on proximal signalling by quantifying IP production. The p.D342N mutant protein has previously been shown to increase IP production in a study that analysed the effect of mutating residues close to the active site of PLCγ1 (269). Assays that quantify IP_1 have been used to demonstrate the gain-of-function potential of the PLCγ1 p.R707Q mutation that frequently occurs in angiosarcomas (213). The assay quantifies IP_1 as a surrogate for IP_3 production as the latter is rapidly metabolised. However, the technique used in this thesis quantifies all IP species.

The data presented herein confirms and extends the findings of Vaqué *et al*. (2014) and Vallois *et al*. (2016) by showing that PLCγ1 mutations significantly enhance NFAT activation *in vitro* (160, 218). Importantly, the in-frame indel potently enhances NFAT activation and IP production, showing its gain-of-function effects on distal and proximal signalling down the IP_3-calcineurin-NFAT signalling pathway. The activating effects of mutant PLCγ1 proteins are supported by the significant relationship between the p.S345F mutation and nuclear NFAT expression in MF tumours (160). A similar pattern of nuclear NFAT expression was also reported in the same number of PTCL tumours, however the relationship failed to reach statistical significance (217). The p.S345F mutant protein has transforming properties *in vitro* as demonstrated by an increased number of foci formed compared to wild-type PLCγ1 in transfected NIH3T3 cells that co-expressed the anti-apoptotic protein BCL2, which aids foci formation (160).

The NFκB, NFAT and AP-1 transcription factors have common targets including the Th2 cytokines genes *IL-4*, *IL-5*, *IL-10* and *IL-13* and the anti-apoptotic genes *BCL-2*, *cIAP1* and *cIAP2* (123). The expression of these cytokines is elevated in CTCL and provides a Th2-dominant milieu that promotes growth of tumour cells (96-99, 102). The anti-apoptotic genes mentioned are also characteristically overexpressed in CTCL and lead to apoptosis resistance of tumour cells (123). As PLCγ1 mutations potently activate all three transcription factors, it is likely that the mutations also induce increased expression of Th2 cytokines and anti-apoptotic genes in CTCL, however this remains to be confirmed. Increased expression of anti-apoptotic genes and Th2 cytokines may also be due to constitutive MYC, STAT3 and STAT5 activity in CTCL (124).

6.1.4. *PLCG1* mutations persist over time and in multiple tumour compartments

The *PLCG1* mutations detected in SS tumours by our deep sequencing study were validated by Sanger sequencing in all 11 patients, confirming that the mutant alleles were not sequencing artefacts. The identification of *PLCG1* mutations in diagnostic samples strongly suggests that these mutations contribute to oncogenesis. Furthermore, the mutations were detected in multiple tumour tissues in 9/11 patients and shown to persist over prolonged periods of time in 6/8 patients for whom serial tumour samples were available. The persistence of *PLCG1* mutations in tumour tissues

obtained over extended periods of time and in multiple tumour compartments strongly suggests positive selection of the mutations. Some mutations could not be detected in serial tumour tissue samples due to (i) a lack of sample availability, (ii) therapeutic interventions that reduced tumour burden or (iii) diffuse tumour infiltrates in the skin and a lack of detection sensitivity by Sanger sequencing. More sensitive sequencing techniques could be used to identify mutant alleles in lesional CTCL skin. One such technique is the locked nucleic acid-clamped real-time PCR methodology that selectively amplifies mutant alleles. This method has successfully been used to detect the PLCγ1 p.S345F mutation in CTCL and nodal PTCLs (160, 217). An alternative high resolution melting technique has been used to detect mutant alleles encoding the PLCγ1 p.S345F and p.S520F mutations in CTCL and the BRAF p.V600E mutation in melanoma cases (216, 284). Furthermore, Albitar *et al*. (2017) have developed a sequencing assay that is over 100 times more sensitive than Sanger sequencing and can detect less than 1 mutant allele in a background of 1000 wild-type alleles for the BTK p.C481S and PLCγ2 p.R665W, pS707Y, p.L845F mutations in Ibrutinib-resistant CLL tumours (285). As mutations occur throughout the *PLCG1* gene, sequencing 32 exons using these highly sensitive sequencing techniques in a large number of diagnostic samples would not be feasible, justifying the more suitable approach of using targeted gene sequencing for mutation detection at diagnosis. Nevertheless, the high sensitivity techniques would be beneficial when screening several samples for specific mutations or for detecting mutant alleles in early stage disease or lesional skin in CTCL in which tumour cells may be sparse.

6.1.5. Activating PLCγ1 mutations may have increased interactions with the plasma membrane

According to a current model PLCγ1 is maintained in an inactive state by an auto-inhibitory interaction of the X-Y catalytic domains with the cSH2 domain, which blocks substrate from accessing the active site (Figure 6. 1. A) (172). When the critical p.Y783 residue is phosphorylated by RTKs and nRTKs, it interacts with the cSH2 domain and changes the protein conformation, which disrupts the auto-inhibitory interaction and makes the active site available for substrate hydrolysis (Figure 6. 1. B-C) (175). The p.S345F and p.S520F mutations are predicted to map to domains that interact with the cSH2 domain and are therefore likely to alter protein conformation

in a way that disrupts auto-inhibition and results in constitutively active mutant proteins (Figure 6. 1. D-E) (175, 194).

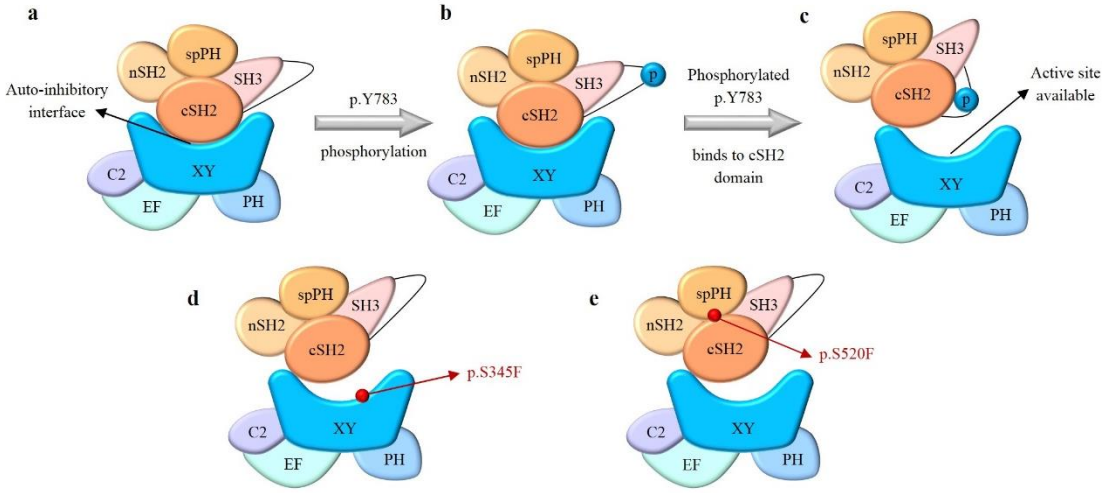

Figure 6. 1. Gain-of-function PLCγ1 mutations disrupt auto-inhibition, leading to constitutively active mutant proteins. (A) PLCγ1 activity is regulated by an auto-inhibitory interaction between the catalytic X-Y and cSH2 domains. (B, C) When the p.Y783 residue is phosphorylated it interacts with the cSH2 domain, disrupts auto-inhibition and makes the active site available for substrate hydrolysis. (D, E) The activating mutations p.S345F and p.S520F are predicted to locate to the XY-cSH2 and cSH2-split PH interaction surfaces, respectively and are likely to disrupt auto-inhibition.

The p.D342N, p.S345F and p.E1163K mutations have previously been mapped to the PLCβ3 and/ or PLCβ2 isoforms and predicted to locate to the protein surface that faces the plasma membrane (67, 160). In this study, the PLCγ1 mutations were mapped to the 3D protein structure of the PLCγ2 isoform, which is more closely related to PLCγ1 than PLCβ3 and PLCβ2, to gain insight into the potential mechanisms by which the mutations alter protein expression and activity. Four of the five activating mutations (p.S345F, p.E1163K, p.D1165H and p.VYEEDM1161V) map to the PLCγ2 protein surface that is predicted to interact with the plasma membrane where the PLCγ substrate PIP_2 resides. Therefore, it is hypothesised that these activating mutant proteins may have increased interactions with the plasma membrane to enhance PIP_2 hydrolysis and amplify downstream signalling.

The activating p.S345F hotspot mutation is predicted to have increased interactions with the plasma membrane and is also likely to disrupt protein auto-inhibition (Figure 6. 1) and thus may be acting by a dual mechanism. Such a mechanism has also been suggested for the PLCγ2 p.D993G mutation, however unlike the PLCγ1 p.S345F mutation the former mutant protein requires stimulation to induce IP production (269). The immunofluorescence system established in this thesis can be used in future studies to determine whether the p.S345F mutant protein has increased interactions with the plasma membrane. This system was optimised to address two important questions. Firstly, do gain-of-function PLCγ1 mutant proteins have increased interactions with the plasma membrane compared to wild-type protein? The imaging system enabled successful visualisation of GFP-tagged wild-type and mutant proteins and also detected co-localisation of PLCγ1 at cell boundaries, however determining a clear increase in localisation to the membrane was difficult as PLCγ1 was expressed throughout the cytoplasm. PLCγ1 interacts with the actin cytoskeleton via its cSH2 domain (276). Therefore, the second question raised was do cells expressing mutant proteins have altered cellular morphology? Using the imaging system, differences in cell shape were observed in transfected and untransfected cells. Visualisation of more cells is required to quantify co-localisation and cellular features including area and perimeter to be able to confidently determine any differences in cell shape induce by mutant PLCγ1.

6.1.6. Gain-of-function PLCγ1 mutations increase transcriptional activity in a p.Y783 phosphorylation independent manner

Phosphorylation of the p.Y783 residue is essential to activate wild-type PLCγ1 and induce IP production as demonstrated by Poulin *et al*. (2005), who showed diminished IP production in stimulated Null TV-1 cells expressing the mutant p.Y783F protein compared to cells expressing wild-type PLCγ1 (177). Subsequently, Gresset *et al*. (2010) showed using purified proteins and *in vitro* kinase assays that the mutant p.Y783F protein had drastically reduced phospholipase activity when incubated with the FGFR2K receptor which phosphorylates and activates PLCγ1 (172). Thereafter, Bunney *et al*. (2012) showed a reduction in IP production in stimulated COS-7 cells expressing the mutant p.Y783F protein (194). These studies all demonstrate that the p.Y783 residue is critical for proximal signalling. Furthermore, Serrano *et al*. (2005) analysed downstream signalling using reporter assays and showed that the p.Y783F

mutant protein reduced NFAT and AP-1 activity in PMA- and Ionomycin-stimulated Jγ1 and P10-14 cells (193), confirming that the p.Y783 residue is important for wild-type PLCγ1 activity. A similar methodology was used in this study and demonstrated that the p.Y783F mutant protein reduced NFκB activation in EGF-stimulated HEK293 cells, but to a lesser extent than the reduction in NFAT and AP-1 activity reported by Serrano *et al*. (2005). This may be due to the use of different cell lines, stimuli and reporter constructs by the two studies.

Mechanistically, this study has shown that three gain-of-function PLCγ1 proteins do not require phosphorylation of the critical p.Y783 residue to increase downstream signalling in basal and stimulated conditions. As mentioned, it is hypothesised that the mutations located at the surface of the protein (p.S345F, p.E1163K, p.D1165H and p.VYEEDM1161V) may have increased interactions with the plasma membrane and elevate PIP_2 hydrolysis to enhance downstream signalling. As the mutant proteins may increase substrate hydrolysis from increased membrane interactions, they may not need phosphorylation of p.Y783 to activate the protein as is required for wild-type PLCγ1. This thesis shows that two of the surface-oriented mutations (p.S345F and p.E1163K) enhanced transcriptional activity without p.Y783 phosphorylation. Based on the proximity of p.D1165H to p.E1163K and inclusion of both residues within the p.VYEEDM1161V indel, it may be possible that p.D1165H and the indel mutant proteins also do not require phosphorylation to induce downstream signalling but this requires functional investigations. The phosphorylation-independent nature of the activating proteins in basal conditions suggests that they do not require extracellular stimuli to induce activity and supports the notion that these proteins may constitutively activate T-cells without TCR engagement, however this remains to be confirmed.

NFκB and AP-1 are activated by the secondary messenger lipid DAG, however studies have not investigated the effect of abrogating the p.Y783 phosphorylation residue on DAG production. This may be due to the traditional techniques used namely thin layer chromatography or high performance liquid chromatography being technically challenging, inefficient and having long processing times to distinguish DAG (which remains in the plasma membrane) from other membrane lipids prior to quantification (286). However, more recent methodologies including mass spectrometry have overcome these challenges (286). Therefore, future work can analyse the effect of

mutant PLCγ1 proteins on DAG production and also PIP_2 turn over as per Haag *et al*. (2012) (287).

6.1.7. Possible explanations for four PLCγ1 mutant proteins not having gain-of-function properties

The PLCγ1 p.S312L mutant protein, as predicted by pathogenicity prediction algorithms did not influence protein expression or activity in basal conditions. This mutation maps to the opposite PLCγ2 protein surface compared to the gain-of-function proteins and is not hypothesised to facilitate increased interactions with the plasma membrane as a means of increasing protein activity. Notably, early findings presented here show that in stimulated cells, the p.S312L protein induces lower levels of NFκB activity than wild-type PLCγ1, suggesting that this may potentially be a loss-of-function protein, however this warrants further investigation. A single gene can harbour both loss- and gain-of-function mutations as demonstrated for the *RHOA* gene in ATLL tumours (271).

The p.R1158H mutation affects an evolutionarily conserved residue and was predicted to be damaging by all six pathogenicity algorithms. Nevertheless, functional analyses showed no effect on protein expression or activity in basal conditions. This mutation occurs in the C2 domain, which also harbours the gain-of-function p.E1163K, p.D1165H and p.VYEEDM1161V mutations. However, when mapped to the 3D PLCγ2 model, the p.R1158H mutation was shown to locate to the centre of the protein unlike the activating mutations, which mapped to the protein surface that likely interacts with the membrane. The p.R1158H mutant protein may therefore not have increased interactions with the plasma membrane in basal conditions. A pilot experiment demonstrated that p.R1158H increased NFκB activity in stimulated conditions, suggesting that although the mutant protein cannot drive tumourigenesis it may contribute to the process when induced by external signals, but this would need to be confirmed.

The p.R48W and p.D342N mutant proteins require stimulation to induce their activating effects. The p.R48W hotspot mutation was predicted to be damaging by all six algorithms and shown to alter a highly conserved residue in vertebrates. In the PLCγ2 model, p.R48W mapped to the protein surface that is predicted to interact with the plasma membrane and also locates in close proximity to p.D342N and the

activating p.S345F mutation. Data presented here show that p.R48W is not a true gain-of-function protein as it requires cellular stimulation to increase NFκB activity. The dependence on cellular stimuli to induce protein activity suggests that p.R48W requires phosphorylation of the p.Y783 residue as implied by early experimental data, but this requires validation. p.R48W locates to the PH domain, a domain that does not facilitate the initial translocation of PLCγ1 to the plasma membrane but plays an important role in stabilising the enzyme to the membrane in stimulated cells as a means of sustaining PLCγ1 activity (178). Therefore, the p.R48W mutant protein may enhance the function of the PH domain and stabilise mutant PLCγ1 at the plasma membrane for longer durations in stimulated cells. p.R48W is the most frequently occurring PLCγ1 mutation in ATLL tumours (14.3%; 53/370) (221) and is the second most frequent PLCγ1 hotspot mutation in mature T-cell lymphomas (Table 6. 3). ATLL is a peripheral T-cell malignancy of $CD4^+$ T-lymphocytes. Infection with the HTLV-1 oncoretrovirus is causally associated with ATLL, however accumulation of genetic aberrations over time are required for oncogenesis (288). Therefore, it may be possible that persistent HTLV-1 infections in ATLL provide the stimulated environment required for p.R48W to induce increased signalling. In HTLV-1 infected cells, the viral oncoprotein Tax binds to the IKK complex and activates NFκB (289). As PLCγ1 regulates IKK activation via the CARMA/BCL10/MALT1 signalosome, the p.R48W mutant protein may further amplify Tax-induced NFκB activity in infected cells, however this hypothesis remains to be functionally validated. *PLCG1* variations including pathogenic mutations shown to induce gain-of-function were frequently detected in ATLL cell lines derived from the aggressive acute disease stage compared to cell lines generated from the less aggressive carrier disease stage. This suggests that *PLCG1* mutations have the ability to transform HTLV-1 infected cells into aggressive tumour cells.

The p.D342N mutant protein has previously been shown to increase IP production in stimulated cells in a study that analysed the effect of mutating residues close to the active site of PLCγ1 (269). The data in this thesis confirms this finding and also shows that the mutation maps to the surface of the PLCγ2 protein that likely interacts with the plasma membrane. Early data suggests that p.D342N in addition to p.R48W, may be partially dependent on p.Y783 phosphorylation to induce increased signalling in stimulated cells, however further experiments are required to confirm this.

The functional interrogations performed demonstrate that the *in silico* pathogenicity prediction algorithms should be used only to gain insight into the effects of mutations on protein structure and function to prioritise mutations for functional analysis. Of the eight mutations predicted to be damaging by all six algorithms, five (62.5%) were identified to increase proximal and downstream signalling. The remaining three mutations did not alter protein activity or expression in basal conditions, demonstrating that only functional analyses can confirm the effect of mutations on protein function.

6.1.8. The PLCγ1 C2 domain may have a critical role in regulating protein activity

The indel p.VYEEDM1161V protein showed reduced total PLCγ1 expression compared to wild-type protein, suggesting that the indel may affect protein stability, subjecting it to degradation at a faster rate than its wild-type counterpart. Nevertheless, in its potentially shorter life span, the mutant protein strongly increased IP production and NFκB and NFAT transcriptional activity.

To date, only missense PLCγ1 mutations identified in cancer have been analysed and p.VYEEDM1161V is the first disease-associated PLCγ1 indel to be functionally interrogated. PLCγ1 deletions have previously been analysed, however these deletions were experimentally generated to gain a deeper understanding of protein activity regulation. Specifically, Gresset *et al*. (2010) used deletion mapping to show that deletion of the cSH2 domain greatly increased IP production in HEK293 cells, demonstrating that this domain is critical for regulating PLCγ1 activity by auto-inhibition (172). Interestingly, disease-associated deletions have been reported in the closely related PLCγ2 isozyme. Linkage analysis of three families affected by PLAID identified a deletion of the n-terminus of the cSH2 domain in two families and a deletion spanning the cSH2-SH3 domains in the third family (235). Quantification of IP production by COS-7 cells transfected with constructs harbouring these deletions, demonstrated that the mutant proteins augment PLCγ2 activity by disrupting protein auto-inhibition (235). Thus, the cSH2 domains in PLCγ1 and PLCγ2 are well established critical regulators of protein auto-inhibition. The data presented in this study demonstrates that the C2 domain indel has potent gain-of-function properties and proposes a novel regulatory role of the C2 domain as a critical regulator of PLCγ1 activity. The C2 domains of many signal transduction proteins bind calcium as a co-

factor and mediate interactions with the plasma membrane (290). Therefore, mutations in the C2 domain are likely to influence the interaction of PLCγ1 with PIP_2.

The p.VYEEDM1161V indel defines the critical regulatory p.V1161 – p.M1166 residues in the C2 domain, which also encompass the p.E1163K and p.D1165H gain-of-function mutations. The p.R1158 residue is unlikely to be a critical residue as the p.R1158H mutation did not influence protein activity and downstream signalling. Interestingly, ATLL tumours have been reported to harbour C2 domain deletions with deletion of the p.E1163 residue in one tumour and deletions spanning the p.1169 – p.1173 residues in 11 tumours (221). This suggests that in addition to the p.1161 – p.1166 residues shown by this thesis to be crucial for PLCγ1 regulation, the p.1169 – p.1173 residues may also be important in regulating protein activity. Based on the data presented, it is postulated that an inhibitory protein may be interacting with PLCγ1 to regulate protein activity and the C2 domain indel is likely to abolish the interaction interface between PLCγ1 and such regulatory proteins. Further studies are required to establish potential protein-protein interactions between the PLCγ1 C2 domain and negative regulatory proteins.

Based on protein sequence homology and functional analogy of PLCγ1 and PLCγ2 in TCR and BCR signalling, it is likely that the C2 domain of PLCγ2 also has regulatory functions. Frequent somatic mutations including hotspot mutations and small deletions in the C2 domains of PLCγ1 and PLCγ2 have been reported in mature T-cell lymphomas and Ibrutinib-resistant CLLs, respectively (67-70, 147, 218, 221, 238, 240, 241). The PLCγ1 C2 domain has the highest number of residues affected by mutations compared to the other protein domains (Figure 1. 22). Specifically, 59 of the 138 C2 domain residues (p.1114 – p.1173) were calculated to be altered by missense mutations, deletions or indels in 6.3% (71/1136) of all mature T-cell lymphomas by WGS, WES, TCS and selective sequencing studies. Jones *et al*. (2017) report a region of hotspot mutations affecting the highly conserved p.1140 – p.1144 residues in the C2 domain of PLCγ2 in Ibrutinib-resistant CLL tumours (240). Frequent mutations of the C2 domain residues supports the notion that this domain is a critical regulator of PLCγ activity.

Importantly, the PLCγ2 C2 mutations co-occur with BTK mutations. In contrast, PLCγ1 mutations have been shown to be mutually exclusive of mutations in gene

involved in NFκB signalling (166). Multiple PLCγ2 mutations have been reported per Ibrutinib-resistant CLL tumour (238-241). Similarly, ATLL tumours can harbour multiple PLCγ1 mutations (221), an observation not made in other types of mature T-cell lymphomas. This study showed that cell lines derived from the aggressive acute ATLL tumours also harbour more than one *PLCG1* mutation. It is likely that multiple *PLCG1* mutations in ATLL tumours and cell lines may be acting in synergy to further enhance PLCγ1 activity compared to tumours with a single *PLCG1* mutation. Such synergistic effects of multiple PLCγ2 mutations identified to co-occur in a single Ibrutinib-resistant CLL case have recently been reported (291). The gain-of-function p.R665W, p.L845F and p.S707Y PLCγ2 mutations were shown to further elevate IP production in transfected COS-7 cells compared to cells expressing each mutation individually (291). Further investigations are required to determine if co-occurring PLCγ1 mutations in ATLL also have cumulative effects on protein activity. Significantly, the KOB acute ATLL cell line was identified to harbour the PLCγ1 p.R48W and p.M750V mutations that were reported to co-occur in a single ATLL tumour by Kataoka *et al.* (2015) (221). This cell line may therefore serve as a model to interrogate the functional effect of these two PLCγ1 mutations.

6.1.9. Targeting enhanced PLCγ1 activity with inhibitors

There are currently no PLCγ1 inhibitors that could attenuate the elevated protein activity induced by the gain-of-function mutant proteins. The PLC inhibitor U73122, has been frequently used in experiments and has been shown to inhibit PLC in cellular systems (175). Vaqué *et al*. (2014) demonstrated that HEK293T cells overexpressing wild-type PLCγ1 or the activating mutant p.S345F and p.S520F proteins had reduced NFAT activity when treated with U73122, showing that the inhibitor is effective (160). Of note, the U73122 inhibitor is known to have a broad range of cellular targets including calcium channels, potassium channels, telomerase and phospholipase D and therefore lacks specificity for PLC isozymes (230, 292-295). The influx of calcium ions across the plasma membrane through calcium channels is induced by the release of calcium from intracellular stores in a process known as capacitative calcium entry (296). The reduction in NFAT activity reported by Vaqué *et al*. (2014), may not be directly attributable to inhibition of PLCγ1 as it cannot be distinguished whether U73122 inhibits PLCγ1 or capacitative calcium entry, both of which activate the NFAT transcription factor. U73122 has also been reported to reduce NFκB *in vitro* in

stimulated keratinocytes and NFκB translocation in stimulated rat osteoclasts (297, 298). The CTCL cell lines MyLa and HUT-78 show reduced cell proliferation, viability and nuclear NFAT activity in response to U73122 treatment (160). These cell lines do not harbour *PLCG1* mutations, therefore the effect of U73122 in CTCL cell lines or primary tumour cells expressing activating PLCγ1 mutations should be investigated. Paradoxically, U73122 has been shown to activate PLCγ1 (>10 fold) and also induce PLCβ3 (8 fold) and PLCβ2 (2 fold) activity in a cell-free system (230). U73122 was demonstrated to form a covalent interaction with PLCβ3, which induces the activity of this PLC isozyme (230). As this interaction was identified in a cell-free system it does not give insight into the interaction of U73122 with other cellular targets. In light of the ability of U73122 to activate PLCγ1, this inhibitor was not selected for use in this thesis.

As mutant PLCγ1 proteins trigger three signalling cascades two approaches can be taken to inhibit the elevated signalling. Firstly, targeting the signalling pathway upstream of mutant PLCγ1 to inhibit activation of all three cascades and secondly, directing inhibitors to block signalling downstream of PLCγ1 to attenuate each branch of signalling independently. Targeting individual pathways downstream of PLCγ1 have shown mixed results. NFκB is a crucial therapeutic target as this transcription factor is constitutively active in CTCL and has elevated activity in ATLL and some PTCL subtypes (118, 119). This thesis showed that the IKKβ inhibitor, TPCA-1 inhibited TNFα-induced but not PLCγ1-induced NFκB activity, making it an unsuitable inhibitor to block the elevated signalling induced by mutant PLCγ1. The TCR and TNF receptor (TNFR) activate the canonical NFκB pathway but PLCγ1 does not mediate signalling from the TNFR (299). A deeper understanding into the mechanisms by which TPCA-1 inhibits NFκB activity is therefore required. The proteasome inhibitor Bortezomib, which inhibits degradation of the NFκB inhibitor IκBα, has been shown to be well tolerated and effective in a phase II trial on relapsed or refractory CTCL (300). Bortezomib inhibits NFκB activity in HUT-78 cells by inducing translocation and accumulation of IκBα in the nucleus, which sequesters p65/p50 heterodimers (123). This inhibitor has also demonstrated anti-tumour activity in multiple myeloma (MM) but has been shown to elevate NFκB activity in tumour cells from MM patients and MM cell lines (301). This data in conjunction with the

findings presented here demonstrate that inhibitors of the NFκB pathway may further enhance or reduce elevated transcriptional activity in particular milieus.

The calcineurin inhibitor FK-506 (Tacrolimus) effectively reduces NFAT activity induced by the p.S345F and p.S520F mutations in transfected HEK293T cells (160). Tacrolimus also reduces the proliferation and viability of the MyLa, HUT-78 and HH CTCL cell lines and significantly inhibits nuclear NFAT activity in MyLa and HUT-78 cells, demonstrating that the calcineurin pathway is sensitive to inhibition (160). As mentioned, these cell lines endogenously express wild-type PLCγ1, therefore it remains to be determined if Tacrolimus would also be effective in CTCL cells that express mutant PLCγ1. The topical calcineurin inhibitors Tacrolimus and Pimecrolimus are used to treat atopic dermatitis but were marked with a 'black box warning' by the U.S. FDA due to the potential risk of developing malignancies (302). Nevertheless, a case with patch stage MF has been successfully treated with a 0.1% tacrolimus ointment (303). These findings would need to be validated in more patients to confirm that this topical therapy is effective in early stage MF. A phase two multicentre clinical trial of Pimecrolimus appears to be safe and effective for use in early stage (Ia – IIa) MF patients and the majority of patients that responded to the therapy had elevated calcineurin pathway activation (unpublished data presented by Professor Ortiz-Romero, EORTC-CLTF meeting 2018). Notably, Tacrolimus and Pimecrolimus would only be sufficient in targeting the elevated NFAT activity induced by mutant PLCγ1 and additional inhibitors would be required to inhibit the two DAG signalling pathways.

Targeting signalling upstream of PLCγ1 to inhibit the gain-of-function effects of mutant proteins is another strategy that can be investigated. Ibrutinib is an effective inhibitor that achieves remission in CLL patients (249). This inhibitor targets BTK, which activates PLCγ2 in B-lymphocytes (249). The activating BTK p.C481S and PLCγ2 p.R665W, p.L845F and p.S707Y mutations have been uniquely identified in relapsed CLL tumours but not in baseline samples suggesting that they confer resistance to Ibrutinib (238-240, 242). As PLCγ1 and PLCγ2 have homologous roles in TCR and BCR signalling and because Ibrutinib targets BTK and ITK in B- and T-cells (304), it may be plausible to hypothesise that gain-of-function PLCγ1 mutations also confer resistance to Ibrutinib. If this was true then CTCL patients could be screened for activating PLCγ1 mutations and patients that are mutation-free could be

considered for Ibrutinib treatment. Moreover, ITK expression is upregulated in CTCL and has been proposed to be used as a diagnostic marker (305, 306). Upregulated ITK expression is also associated with a poor prognosis for CTCL patients (305-307). The altered expression further supports inhibition of this kinase as a therapeutic strategy for CTCL. Ibrutinib has recently been reported to increase $CD4^+$ and $CD8^+$ activated T-cell proliferation in CLL patients (308). This would be a highly undesirable effect in CTCL, a malignancy of mature malignant skin-resident $CD4^+$ T-cells (308). Furthermore, a pilot clinical trial has shown that Ibrutinib has limited clinical efficacy in CTCL (309). Nevertheless, other small molecule ITK inhibitors such as ONO-7790500, BMS-509744 and PF-06465469 have shown promising results by reducing ITK and PLCγ1 phosphorylation, calcium flux and IL-2 and IL-21 production in Jurkat cells (310). Furthermore, the ITK inhibitor ONO-7790500 and the chemotherapy drug doxorubicin act in synergy to further reduce Jurkat cell survival compared to treatment with each agent alone (310). Therefore, the safety and efficacy of combinations of ITK inhibitors and chemotherapeutic compounds could be tested in pre-clinical and clinical trials for CTCL if deemed safe in the former.

The data presented in this study highlights that PLCγ1 is a significant therapeutic target and demonstrates that the development of novel PLCγ1-specific inhibitors to inhibit all three signalling cascades is fundamental. A potential caveat with the development of specific inhibitors is that PLCγ1 is ubiquitously expressed and the inhibitor would not only target T-cells but other tissues that express the protein at comparable levels including but not limited to the brain, ovary, prostate, bladder and colon (311). Thus, PLCγ1-specific inhibitors may result in cytotoxicity and adverse effects. Furthermore, due to the high protein sequence homology of the PLCγ1 and PLCγ2 isoforms, it would be difficult to develop PLCγ1-specific inhibitors that do not also inhibit PLCγ2 activity, leading to potential further cytotoxicity and adverse reactions. Therefore, novel mutation-specific PLCγ1 inhibitors should be developed for mature T-cell lymphomas and angiosarcomas and mutation-specific PLCγ2 inhibitors for Ibrutinib-resistant CLL, PLAID and APLAID. Generating effective mutation-specific inhibitors may be challenging as the crystal structure of PLCγ1 has not been resolved, however the PLCδ structure has been used to identify novel PLCγ-specific inhibitors by virtual high throughput screening (312). Promisingly, this screen identified that 30% of the compounds experimentally tested had fairly strong affinity

to PLCγ (312). As CTCL tumours and mature T-cell lymphomas are genetically highly heterogeneous, patients may benefit from a personalised cocktail of specific inhibitors based on their tumour mutation profiles. This would be a more targeted therapeutic approach, which may be better suited to treating individual lymphoma cases.

6.2 Conclusions

1. *PLCG1* mutations persist over time and in multiple tumour compartments in the majority of SS patients, strongly suggesting positive selection of these mutations by tumour cells.

2. The p.S345F, p.S520F, p.E1163K, p.D1165H and p.VYEEDM1161V gain-of-function proteins induce constitutive activation of PLCγ1 by directly increasing proximal signalling via IP production and significantly increase downstream signalling to the NFκB and NFAT transcription factors.

3. The mutant protein encoded by the hotspot p.R48W requires cellular stimulation to significantly induce NFκB activity.

4. The p.S345F, p.S520F and p.E1163K gain-of-function mutant proteins do not require phosphorylation of the p.Y783 residue to increase NFκB, NFAT and AP-1 transcriptional activity in basal conditions and NFκB activity in stimulated conditions.

5. The p.S345F, p.E1163K, p.D1165H and p.VYEEDM1161V activating mutations map to the PLCγ2 protein surface that is predicted to interact with the plasma membrane. The p.R48W and p.D342N mutations, which increase protein activity in stimulated conditions map in close proximity to the activating mutations.

6. The C2 domain of PLCγ1 harbours residues that are fundamental for protein activity regulation.

7. The data presented provides compelling evidence for the development of novel therapeutic inhibitors to target mutant PLCγ1 proteins.

6.3 Future work

The questions raised from this thesis are presented below and possible approaches to interrogate them are proposed. Experiments to (i) gain a deeper mechanistic understanding of mutant protein activity, (ii) investigate the ability of mutations to contribute to tumourigenesis and (iii) analyse the efficacy of novel inhibitors, have been categorised accordingly.

Mechanistic interrogations

1. Do the gain-of-function p.S345F, p.E1163K, p.D1165H and p.VYEEDM1161V proteins have increased interactions with the cell membrane compared to wild-type PLCγ1?
    - The immunofluorescence system optimised in this study can be used to obtain further cellular images and co-localisation of PLCγ1 with the plasma membrane can be quantified using the ImageJ image processing software.
2. Do the p.R48W and p.D342N mutant proteins require phosphorylation of the p.Y783F residue to induce NFκB reporter activity in stimulated cells?
    - Early experimental results indicate that these mutant proteins may be partially dependent on phosphorylation, however biological repeats are required to confirm this.
3. Do the p.R48W and p.D342N mutant proteins localise more to the plasma membrane than wild-type PLCγ1 in stimulated cells?
    - If the mutant proteins are shown to be stimulation-dependent, HeLa cells transfected with GFP-tagged PLCγ1 constructs can be analysed by real-time fluorescence imaging as per Matsuda *et al*. (2012) and Wang and Wang (2003) (178, 277), to determine if EGF stimulation induces increased or prolonged interaction of mutant proteins with the membrane.
4. Can the PLCγ1 p.Y783F phosphorylation mutant localise to the plasma membrane in basal or stimulated conditions?
    - The p.Y783 residue is phosphorylated by RTKs and non-RTKs after PLCγ1 translocates to the membrane. To determine if the p.Y783F mutant

protein has abnormal cellular localisation, HeLa cells expressing the mutant protein can be visualised using the established system for basal conditions and by real-time fluorescence imaging for EGF-stimulated cells.

5. Do gain-of-function PLCγ1 mutations affect the cell structure?
    - Differences in cellular morphology were observed in this study. To further investigate changes in cellular shape, the established imaging system can be used to visualise further cells and features including cell area, perimeter and circularity can be quantified using ImageJ.
6. Does abrogation of the p.Y783 phosphorylation residue in gain-of-function PLCγ1 proteins affect IP production?
    - COS-7 cells can be transfected with gain-of-function and double mutant constructs and IP production can be quantified by liquid scintillation to determine if the mutant proteins require protein phosphorylation to elevate proximal signalling.
7. Do negative regulatory proteins bind to the C2 domain of PLCγ1 to regulate protein activity?
    - Wild-type and the p.VYEEDM1161V mutant protein can be expressed in Jurkat cells to determine interactions between PLCγ1 and other proteins by co-immunoprecipitation and mass spectrometry. Differences in binding proteins would likely be due to abrogated interactions as a result of the indel in the C2 domain.

Tumourigenesis investigations

To investigate whether gain-of-function PLCγ1 mutations contribute to lymphomagenesis, wild-type and mutant *PLCG1* cDNA would need to be cloned into lentiviral vectors. The vectors can be used to transduce primary human $CD4^+$ T cells (i.e. serve as knock-in cells) to enable investigations into how mutant PLCγ1 proteins transform primary cells by analysing key cellular parameters including:

1. Cell viability using the CellTiter-Glo® Luminescent Cell Viability Assay (Promega), which uses ATP quantification to determine if cells expressing mutant PLCγ1 are more or less viable that those expressing wild-type PLCγ1.

2. Cell proliferation using the CyQUANT Cell Proliferation Assay Kit (Thermo Fisher) to determine cell numbers based on DNA content. This assay would establish whether PLCγ1 mutants alter the rate of cell proliferation.
3. Apoptosis using the annexin V-PE apoptosis detection kit (BD Pharmigen). Annexin V-PE is conjugated to the PE fluorochrome which binds to phosphatidylserine (PS) in apoptotic cells. PS is normally located on the inner leaflet of the plasma membrane but is exposed to the outer leaflet in cells undergoing early apoptosis. Annexin V-PE labelled can be quantified by flow cytometry. This assay would require effective and mutation-specific inhibitors to induce apoptosis, which would inform on whether cells expressing mutant PLCγ1 are more or less resistant to cell death compared to those expressing wild-type protein.

Inhibitor analyses

1. Can mutation-specific PLCγ1 inhibitors attenuate the elevated transcriptional activity induced by PLCγ1 mutations *in vitro*?
    - When novel inhibitors are developed, the mutant proteins can be expressed in HEK293 cells and treated with inhibitors to determine the effect on NFκB, NFAT and AP-1 reporter activity.
2. Can mutation-specific PLCγ1 inhibitors reduce the increased IP production induced by PLCγ1 mutations *in vitro*?
    - COS-7 cells can be transfected with PLCγ1 constructs, treated with novel inhibitors and IP production quantified by liquid scintillation.
3. Can mutation-specific PLCγ1 inhibitors reduce cell viability, proliferation and apoptosis in lymphoma cell lines and primary human $CD4^+$ T-cells transduced with PLCγ1 mutants?
    - The KKI cell line, identified in this study to harbour the activating p.S345F mutation can be used to determine the effect of inhibitor treatment on cell viability, proliferation and apoptosis.
    - Primary cells transduced with wild-type and mutant PLCγ1 constructs can be treated with specific inhibitors and key parameters that contribute to tumourigenesis can be assayed.

4. Can mutation-specific PLCγ1 inhibitors reduce cell viability, proliferation and apoptosis in primary SS tumour cells?
    - Our research group has frozen enriched $CD4^+$ T-cells from patients harbouring the gain-of-function p.S345F and p.E1163K mutations. The effect of novel mutation-specific PLCγ1 inhibitors on tumour cells can be analysed *ex vivo*.

Bibliography

1. Kim EJ, Hess S, Richardson SK, Newton S, Showe LC, Benoit BM, et al. Immunopathogenesis and therapy of cutaneous T cell lymphoma. The Journal of clinical investigation. 2005;115(4):798-812.
2. Bradford PT, Devesa SS, Anderson WF, Toro JR. Cutaneous lymphoma incidence patterns in the United States: a population-based study of 3884 cases. Blood. 2009;113(21):5064-73.
3. Hwang ST, Janik JE, Jaffe ES, Wilson WH. Mycosis fungoides and Sezary syndrome. Lancet. 2008;371(9616):945-57.
4. Willemze R, Jaffe ES, Burg G, Cerroni L, Berti E, Swerdlow SH, et al. WHO-EORTC classification for cutaneous lymphomas. Blood. 2005;105(10):3768-85.
5. Imam MH, Shenoy PJ, Flowers CR, Phillips A, Lechowicz MJ. Incidence and survival patterns of cutaneous T-cell lymphomas in the United States. Leukemia & lymphoma. 2013;54(4):752-9.
6. Swerdlow S, Campo E, Harris N, Jaffe E, Pileri S, Stein H, et al. World Health Organization Classification of Tumours of Haematopoietic and Lymphoid Tissues2017.
7. Gaide O, Emerson RO, Jiang X, Gulati N, Nizza S, Desmarais C, et al. Common clonal origin of central and resident memory T cells following skin immunization. Nature medicine. 2015;21(6):647-53.
8. Bloom T, Kuzel TM, Querfeld C, Guitart J, Rosen ST. Cutaneous T-cell lymphomas: a review of new discoveries and treatments. Current treatment options in oncology. 2012;13(1):102-21.
9. Olsen EA. Evaluation, Diagnosis, and Staging of Cutaneous Lymphoma. Dermatologic clinics. 2015;33(4):643-54.
10. Agar NS, Wedgeworth E, Crichton S, Mitchell TJ, Cox M, Ferreira S, et al. Survival outcomes and prognostic factors in mycosis fungoides/Sezary syndrome: validation of the revised International Society for Cutaneous Lymphomas/European Organisation for Research and Treatment of Cancer staging proposal. Journal of clinical oncology : official journal of the American Society of Clinical Oncology. 2010;28(31):4730-9.
11. Kim YH, Liu HL, Mraz-Gernhard S, Varghese A, Hoppe RT. Long-term outcome of 525 patients with mycosis fungoides and Sezary syndrome: clinical prognostic factors and risk for disease progression. Archives of dermatology. 2003;139(7):857-66.
12. Criscione VD, Weinstock MA. Incidence of cutaneous T-cell lymphoma in the United States, 1973-2002. Archives of dermatology. 2007;143(7):854-9.
13. Ahn CS, A AL, Sangueza OP. Mycosis fungoides: an updated review of clinicopathologic variants. The American Journal of dermatopathology. 2014;36(12):933-48; quiz 49-51.

14. Olek-Hrab K, Silny W. Diagnostics in mycosis fungoides and Sezary syndrome. Reports of practical oncology and radiotherapy : journal of Greatpoland Cancer Center in Poznan and Polish Society of Radiation Oncology. 2014;19(2):72-6.
15. Vonderheid EC, Sobel EL, Nowell PC, Finan JB, Helfrich MK, Whipple DS. Diagnostic and prognostic significance of Sezary cells in peripheral blood smears from patients with cutaneous T cell lymphoma. Blood. 1985;66(2):358-66.
16. Lutzner M, Edelson R, Schein P, Green I, Kirkpatrick C, Ahmed A. Cutaneous T-cell lymphomas: the Sezary syndrome, mycosis fungoides, and related disorders. Annals of internal medicine. 1975;83(4):534-52.
17. Willemze R, Kerl H, Sterry W, Berti E, Cerroni L, Chimenti S, et al. EORTC classification for primary cutaneous lymphomas: a proposal from the Cutaneous Lymphoma Study Group of the European Organization for Research and Treatment of Cancer. Blood. 1997;90(1):354-71.
18. Scarisbrick JJ, Whittaker S, Evans AV, Fraser-Andrews EA, Child FJ, Dean A, et al. Prognostic significance of tumor burden in the blood of patients with erythrodermic primary cutaneous T-cell lymphoma. Blood. 2001;97(3):624-30.
19. Axelrod PI, Lorber B, Vonderheid EC. Infections complicating mycosis fungoides and Sezary syndrome. Jama. 1992;267(10):1354-8.
20. Krejsgaard T, Odum N, Geisler C, Wasik MA, Woetmann A. Regulatory T cells and immunodeficiency in mycosis fungoides and Sezary syndrome. Leukemia. 2012;26(3):424-32.
21. Lutzner MA, Jordan HW. The ultrastructure of an abnormal cell in Sezary's syndrome. Blood. 1968;31(6):719-26.
22. Olsen E, Vonderheid E, Pimpinelli N, Willemze R, Kim Y, Knobler R, et al. Revisions to the staging and classification of mycosis fungoides and Sezary syndrome: a proposal of the International Society for Cutaneous Lymphomas (ISCL) and the cutaneous lymphoma task force of the European Organization of Research and Treatment of Cancer (EORTC). Blood. 2007;110(6):1713-22.
23. Kempf W, Sander CA. Classification of cutaneous lymphomas - an update. Histopathology. 2010;56(1):57-70.
24. Scheffer E, Meijer CJ, van Vloten WA, Willemze R. A histologic study of lymph nodes from patients with the Sezary syndrome. Cancer. 1986;57(12):2375-80.
25. Campbell SM, Peters SB, Zirwas MJ, Wong HK. Immunophenotypic diagnosis of primary cutaneous lymphomas: a review for the practicing dermatologist. The Journal of clinical and aesthetic dermatology. 2010;3(10):21-5.
26. Burg G, Kempf W, Cozzio A, Feit J, Willemze R, E SJ, et al. WHO/EORTC classification of cutaneous lymphomas 2005: histological and molecular aspects. Journal of cutaneous pathology. 2005;32(10):647-74.
27. Murphy M, Fullen D, Carlson JA. Low CD7 expression in benign and malignant cutaneous lymphocytic infiltrates: experience with an antibody reactive with

paraffin-embedded tissue. The American Journal of dermatopathology. 2002;24(1):6-16.

28. Dummer R, Nestle FO, Niederer E, Ludwig E, Laine E, Grundmann H, et al. Genotypic, phenotypic and functional analysis of CD4+CD7+ and CD4+CD7- T lymphocyte subsets in Sezary syndrome. Archives of dermatological research. 1999;291(6):307-11.
29. Novelli M, Fava P, Sarda C, Ponti R, Osella-Abate S, Savoia P, et al. Blood flow cytometry in Sezary syndrome: new insights on prognostic relevance and immunophenotypic changes during follow-up. American journal of clinical pathology. 2015;143(1):57-69.
30. Scarisbrick JJ, Hodak E, Bagot M, Stranzenbach R, Stadler R, Ortiz-Romero PL, et al. Blood classification and blood response criteria in mycosis fungoides and Sezary syndrome using flow cytometry: recommendations from the EORTC cutaneous lymphoma task force. European journal of cancer (Oxford, England : 1990). 2018;93:47-56.
31. Horwitz SM, Olsen EA, Duvic M, Porcu P, Kim YH. Review of the treatment of mycosis fungoides and sezary syndrome: a stage-based approach. Journal of the National Comprehensive Cancer Network : JNCCN. 2008;6(4):436-42.
32. Trautinger F, Knobler R, Willemze R, Peris K, Stadler R, Laroche L, et al. EORTC consensus recommendations for the treatment of mycosis fungoides/Sezary syndrome. European journal of cancer (Oxford, England : 1990). 2006;42(8):1014-30.
33. Contassot E, French LE. Targeting apoptosis defects in cutaneous T-cell lymphoma. The Journal of investigative dermatology. 2009;129(5):1059-61.
34. Smith BD, Wilson LD. Management of mycosis fungoides: Part 2. Treatment. Oncology (Williston Park, NY). 2003;17(10):1419-28; discussion 30, 33.
35. Zackheim HS. Treatment of patch-stage mycosis fungoides with topical corticosteroids. Dermatologic therapy. 2003;16(4):283-7.
36. Zackheim HS. Topical carmustine (BCNU) in the treatment of mycosis fungoides. Dermatol Ther. 2003;16(4):299-302.
37. Kim YH, Martinez G, Varghese A, Hoppe RT. Topical nitrogen mustard in the management of mycosis fungoides: update of the Stanford experience. Archives of dermatology. 2003;139(2):165-73.
38. Stone ML, Styles AR, Cockerell CJ, Pandya AG. Hypopigmented mycosis fungoides: a report of 7 cases and review of the literature. Cutis. 2001;67(2):133-8.
39. Diamantopoulos S, Platoni K, Kouloulias V, Pantelakos P, Dilvoi M, Papadavid E, et al. First treatment of mycosis fungoides by total skin electron beam (TSEB) therapy in Greece. Reports of practical oncology and radiotherapy : journal of Greatpoland Cancer Center in Poznan and Polish Society of Radiation Oncology. 2014;19(2):114-9.

40. Cotter GW, Baglan RJ, Wasserman TH, Mill W. Palliative radiation treatment of cutaneous mycosis fungoides--a dose response. International journal of radiation oncology, biology, physics. 1983;9(10):1477-80.
41. Photiou L, van der Weyden C, McCormack C, Miles Prince H. Systemic Treatment Options for Advanced-Stage Mycosis Fungoides and Sezary Syndrome. Current oncology reports. 2018;20(4):32.
42. Sokolowska-Wojdylo M, Lugowska-Umer H, Maciejewska-Radomska A. Oral retinoids and rexinoids in cutaneous T-cell lymphomas. Postepy dermatologii i alergologii. 2013;30(1):19-29.
43. Hymes KB. The role of histone deacetylase inhibitors in the treatment of patients with cutaneous T-cell lymphoma. Clinical lymphoma, myeloma & leukemia. 2010;10(2):98-109.
44. Zinzani PL, Bonthapally V, Huebner D, Lutes R, Chi A, Pileri S. Panoptic clinical review of the current and future treatment of relapsed/refractory T-cell lymphomas: Cutaneous T-cell lymphomas. Critical reviews in oncology/hematology. 2016;99:228-40.
45. Duvic M, Bates SE. Responses to romidepsin in patients with cutaneous T-cell lymphoma and prior treatment with systemic chemotherapy. 2018;59(4):880-7.
46. Kuzel TM, Roenigk HH, Jr., Samuelson E, Herrmann JJ, Hurria A, Rademaker AW, et al. Effectiveness of interferon alfa-2a combined with phototherapy for mycosis fungoides and the Sezary syndrome. Journal of clinical oncology : official journal of the American Society of Clinical Oncology. 1995;13(1):257-63.
47. Jin HT, Ahmed R, Okazaki T. Role of PD-1 in regulating T-cell immunity. Current topics in microbiology and immunology. 2011;350:17-37.
48. Samimi S, Benoit B, Evans K, Wherry EJ, Showe L, Wysocka M, et al. Increased programmed death-1 expression on CD4+ T cells in cutaneous T-cell lymphoma: implications for immune suppression. Archives of dermatology. 2010;146(12):1382-8.
49. Kantekure K, Yang Y, Raghunath P, Schaffer A, Woetmann A, Zhang Q, et al. Expression patterns of the immunosuppressive proteins PD-1/CD279 and PD-L1/CD274 at different stages of cutaneous T-cell lymphoma/mycosis fungoides. The American Journal of dermatopathology. 2012;34(1):126-8.
50. Querfeld C, Leung S, Myskowski PL, Curran SA, Goldman DA, Heller G, et al. Primary T Cells from Cutaneous T-cell Lymphoma Skin Explants Display an Exhausted Immune Checkpoint Profile. Cancer immunology research. 2018;6(8):900-9.
51. Dai J, Almazan T, Kim Y, Khodadoust MJAoL. Pembrolizumab in systemic and cutaneous T-cell lymphoma. 2018. 2018;2(4).
52. Scarisbrick JJ. New drugs in cutaneous T-cell lymphomas. Current opinion in oncology. 2016;28(5):384-9.

53. Leuchte K, Schlaak M, Stadler R, Theurich S, von Bergwelt-Baildon M. Innovative Treatment Concepts for Cutaneous T-Cell Lymphoma Based on Microenvironment Modulation. Oncology research and treatment. 2017;40(5):262-9.
54. Lesokhin AM, Ansell SM, Armand P, Scott EC, Halwani A, Gutierrez M, et al. Nivolumab in Patients With Relapsed or Refractory Hematologic Malignancy: Preliminary Results of a Phase Ib Study. Journal of clinical oncology : official journal of the American Society of Clinical Oncology. 2016;34(23):2698-704.
55. Xu-Monette ZY, Zhou J, Young KH. PD-1 expression and clinical PD-1 blockade in B-cell lymphomas. Blood. 2018;131(1):68-83.
56. Ogura M, Ishida T, Hatake K, Taniwaki M, Ando K, Tobinai K, et al. Multicenter phase II study of mogamulizumab (KW-0761), a defucosylated anti-cc chemokine receptor 4 antibody, in patients with relapsed peripheral T-cell lymphoma and cutaneous T-cell lymphoma. Journal of clinical oncology : official journal of the American Society of Clinical Oncology. 2014;32(11):1157-63.
57. de Masson A, Guitera P, Brice P, Moulonguet I, Mouly F, Bouaziz JD, et al. Long-term efficacy and safety of alemtuzumab in advanced primary cutaneous T-cell lymphomas. The British journal of dermatology. 2014;170(3):720-4.
58. Chen R, Hou J, Newman E, Kim Y, Donohue C, Liu X, et al. CD30 Downregulation, MMAE Resistance, and MDR1 Upregulation Are All Associated with Resistance to Brentuximab Vedotin. Molecular cancer therapeutics. 2015;14(6):1376-84.
59. Kim YH, Tavallaee M, Sundram U, Salva KA, Wood GS, Li S, et al. Phase II Investigator-Initiated Study of Brentuximab Vedotin in Mycosis Fungoides and Sezary Syndrome With Variable CD30 Expression Level: A Multi-Institution Collaborative Project. Journal of clinical oncology : official journal of the American Society of Clinical Oncology. 2015;33(32):3750-8.
60. Duvic M, Tetzlaff MT, Gangar P, Clos AL, Sui D, Talpur R. Results of a Phase II Trial of Brentuximab Vedotin for CD30+ Cutaneous T-Cell Lymphoma and Lymphomatoid Papulosis. Journal of clinical oncology : official journal of the American Society of Clinical Oncology. 2015;33(32):3759-65.
61. Phillips T, Devata S, Wilcox RA. Challenges and opportunities for checkpoint blockade in T-cell lymphoproliferative disorders. Journal for immunotherapy of cancer. 2016;4:95.
62. Snyder A, Makarov V, Merghoub T, Yuan J, Zaretsky JM, Desrichard A, et al. Genetic basis for clinical response to CTLA-4 blockade in melanoma. The New England journal of medicine. 2014;371(23):2189-99.
63. Van Allen EM, Miao D, Schilling B, Shukla SA, Blank C, Zimmer L, et al. Genomic correlates of response to CTLA-4 blockade in metastatic melanoma. Science (New York, NY). 2015;350(6257):207-11.
64. McCoy KD, Le Gros G. The role of CTLA-4 in the regulation of T cell immune responses. Immunology and cell biology. 1999;77(1):1-10.

65. Yoo HY, Sung MK, Lee SH, Kim S, Lee H, Park S, et al. A recurrent inactivating mutation in RHOA GTPase in angioimmunoblastic T cell lymphoma. Nature genetics. 2014;46(4):371-5.
66. Palomero T, Couronne L, Khiabanian H, Kim MY, Ambesi-Impiombato A, Perez-Garcia A, et al. Recurrent mutations in epigenetic regulators, RHOA and FYN kinase in peripheral T cell lymphomas. Nature genetics. 2014;46(2):166-70.
67. Choi J, Goh G, Walradt T, Hong BS, Bunick CG, Chen K, et al. Genomic landscape of cutaneous T cell lymphoma. Nature Genetics. 2015;47(9):1011-9.
68. Kiel MJ, Sahasrabuddhe AA, Rolland DCM, Velusamy T, Chung F, Schaller M, et al. Genomic analyses reveal recurrent mutations in epigenetic modifiers and the JAK-STAT pathway in Sezary syndrome. Nature communications. 2015;6:8470.
69. da Silva Almeida AC, Abate F, Khiabanian H, Martinez-Escala E, Guitart J, Tensen CP, et al. The mutational landscape of cutaneous T cell lymphoma and Sezary syndrome. Nature genetics. 2015;47(12):1465-70.
70. Wang L, Ni X, Covington KR, Yang BY, Shiu J, Zhang X, et al. Genomic profiling of Sezary syndrome identifies alterations of key T cell signaling and differentiation genes. 2015;47(12):1426-34.
71. Ungewickell A, Bhaduri A, Rios E, Reuter J, Lee CS, Mah A, et al. Genomic analysis of mycosis fungoides and Sezary syndrome identifies recurrent alterations in TNFR2. 2015;47(9):1056-60.
72. Postow MA, Manuel M, Wong P, Yuan J, Dong Z, Liu C, et al. Peripheral T cell receptor diversity is associated with clinical outcomes following ipilimumab treatment in metastatic melanoma. Journal for immunotherapy of cancer. 2015;3:23.
73. Prince HM, Querfeld C. Integrating novel systemic therapies for the treatment of mycosis fungoides and Sezary syndrome. Best practice & research Clinical haematology. 2018;31(3):322-35.
74. Vural S, Akay BN, Botsali A, Atilla E, Parlak N, Okcu Heper A, et al. Transformation of Mycosis Fungoides/Sezary Syndrome: Clinical Characteristics and Prognosis. Turkish journal of haematology : official journal of Turkish Society of Haematology. 2018;35(1):35-41.
75. Arulogun SO, Prince HM, Ng J, Lade S, Ryan GF, Blewitt O, et al. Long-term outcomes of patients with advanced-stage cutaneous T-cell lymphoma and large cell transformation. Blood. 2008;112(8):3082-7.
76. Cerroni L, Rieger E, Hodl S, Kerl H. Clinicopathologic and immunologic features associated with transformation of mycosis fungoides to large-cell lymphoma. Am J Surg Pathol. 1992;16(6):543-52.
77. Awar O, Duvic M. Treatment of transformed mycosis fungoides with intermittent low-dose gemcitabine. Oncology. 2007;73(1-2):130-5.

78. Whittaker S, Hoppe R, Prince HM. How I treat mycosis fungoides and Sezary syndrome. Blood. 2016;127(25):3142-53.
79. Hughes CF, Khot A, McCormack C, Lade S, Westerman DA, Twigger R, et al. Lack of durable disease control with chemotherapy for mycosis fungoides and Sezary syndrome: a comparative study of systemic therapy. Blood. 2015;125(1):71-81.
80. Kaye FJ, Bunn PA, Jr., Steinberg SM, Stocker JL, Ihde DC, Fischmann AB, et al. A randomized trial comparing combination electron-beam radiation and chemotherapy with topical therapy in the initial treatment of mycosis fungoides. N Engl J Med. 1989;321(26):1784-90.
81. Virmani P, Zain J, Rosen ST, Myskowski PL, Querfeld C. Hematopoietic Stem Cell Transplant for Mycosis Fungoides and Sezary Syndrome. Dermatologic clinics. 2015;33(4):807-18.
82. Cudillo L, Cerretti R, Picardi A, Mariotti B, De Angelis G, Cantonetti M, et al. Allogeneic hematopoietic stem cell transplantation in Primary Cutaneous T Cell Lymphoma. Annals of hematology. 2018;97(6):1041-8.
83. Duarte RF, Canals C, Onida F, Gabriel IH, Arranz R, Arcese W, et al. Allogeneic hematopoietic cell transplantation for patients with mycosis fungoides and Sezary syndrome: a retrospective analysis of the Lymphoma Working Party of the European Group for Blood and Marrow Transplantation. Journal of clinical oncology : official journal of the American Society of Clinical Oncology. 2010;28(29):4492-9.
84. Zhu J, Paul WE. CD4 T cells: fates, functions, and faults. Blood. 2008;112(5):1557-69.
85. King C, Tangye SG, Mackay CR. T Follicular Helper (TFH) Cells in Normal and Dysregulated Immune Responses. Annual Review of Immunology. 2008;26(1):741-66.
86. Zou W, Restifo NP. TH17 cells in tumour immunity and immunotherapy. Nature Reviews Immunology. 2011;11:565.
87. O'Shea J, Tato CM, Siegel R. 10 - Cytokines and cytokine receptors. In: Rich RR, Fleisher TA, Shearer WT, Schroeder HW, Frew AJ, Weyand CM, editors. Clinical Immunology (Third Edition). Edinburgh: Mosby; 2008. p. 139-71.
88. Eyerich K, Dimartino V, Cavani A. IL-17 and IL-22 in immunity: Driving protection and pathology. European journal of immunology. 2017;47(4):607-14.
89. Crotty S. T follicular helper cell differentiation, function, and roles in disease. Immunity. 2014;41(4):529-42.
90. O'Shea J, Gadina M, Siegel R. Clinical Immunology (4th edition)2013. 108-35 p.
91. Sallusto F, Geginat J, Lanzavecchia A. Central memory and effector memory T cell subsets: function, generation, and maintenance. Annu Rev Immunol. 2004;22:745-63.

92. Mahnke YD, Brodie TM, Sallusto F, Roederer M, Lugli E. The who's who of T-cell differentiation: human memory T-cell subsets. Eur J Immunol. 2013;43(11):2797-809.
93. Pennock ND, White JT, Cross EW, Cheney EE, Tamburini BA, Kedl RM. T cell responses: naive to memory and everything in between. Advances in physiology education. 2013;37(4):273-83.
94. Mami-Chouaib F, Blanc C, Corgnac S, Hans S, Malenica I, Granier C, et al. Resident memory T cells, critical components in tumor immunology. 2018;6(1):87.
95. Campbell JJ, Clark RA, Watanabe R, Kupper TS. Sezary syndrome and mycosis fungoides arise from distinct T-cell subsets: a biologic rationale for their distinct clinical behaviors. Blood. 2010;116(5):767-71.
96. Vowels BR, Lessin SR, Cassin M, Jaworsky C, Benoit B, Wolfe JT, et al. Th2 cytokine mRNA expression in skin in cutaneous T-cell lymphoma. The Journal of investigative dermatology. 1994;103(5):669-73.
97. Asadullah K, Docke WD, Haeussler A, Sterry W, Volk HD. Progression of mycosis fungoides is associated with increasing cutaneous expression of interleukin-10 mRNA. The Journal of investigative dermatology. 1996;107(6):833-7.
98. Vowels BR, Cassin M, Vonderheid EC, Rook AH. Aberrant cytokine production by Sezary syndrome patients: cytokine secretion pattern resembles murine Th2 cells. The Journal of investigative dermatology. 1992;99(1):90-4.
99. Geskin LJ, Viragova S, Stolz DB, Fuschiotti P. Interleukin-13 is overexpressed in cutaneous T-cell lymphoma cells and regulates their proliferation. Blood. 2015;125(18):2798-805.
100. Wu X, Hsu DK, Wang KH, Huang Y, Mendoza L, Zhou Y, et al. IL-10 is overexpressed in human cutaneous T-cell lymphoma and is required for maximal tumor growth in a mouse model. Leukemia & lymphoma. 2018:1-9.
101. Guenova E, Watanabe R, Teague JE, Desimone JA, Jiang Y, Dowlatshahi M, et al. TH2 cytokines from malignant cells suppress TH1 responses and enforce a global TH2 bias in leukemic cutaneous T-cell lymphoma. Clin Cancer Res. 2013;19(14):3755-63.
102. Miyagaki T, Sugaya M. Immunological milieu in mycosis fungoides and Sezary syndrome. The Journal of dermatology. 2014;41(1):11-8.
103. Querfeld C, Curran SA, Leung S, Myskowski PL, Horwitz SM, Halpern AC, et al. T Cells in CTCL Have an Exhausted Phenotype While Cutaneous Dendritic Cells Display a Normally Activated Mature Phenotype. 2014;124(21):1695-.
104. Ingram JT, Yi JS, Zajac AJ. Exhausted CD8 T cells downregulate the IL-18 receptor and become unresponsive to inflammatory cytokines and bacterial co-infections. PLoS pathogens. 2011;7(9):e1002273.
105. Gaulard P, de Leval L. Follicular helper T cells: implications in neoplastic hematopathology. Semin Diagn Pathol. 2011;28(3):202-13.

106. Bosisio FM, Cerroni L. Expression of T-follicular helper markers in sequential biopsies of progressive mycosis fungoides and other primary cutaneous T-cell lymphomas. Am J Dermatopathol. 2015;37(2):115-21.
107. Çetinözman F, Jansen PM, Vermeer MH, Willemze R. Differential Expression of Programmed Death-1 (PD-1) in Sézary Syndrome and Mycosis Fungoides. JAMA Dermatology. 2012;148(12):1379-85.
108. Battistella M, Beylot-Barry M, Bachelez H, Rivet J, Vergier B, Bagot M. Primary Cutaneous Follicular Helper T-cell Lymphoma: A New Subtype of Cutaneous T-cell Lymphoma Reported in a Series of 5 CasesCutaneous Follicular Helper T-cell Lymphoma. JAMA Dermatology. 2012;148(7):832-9.
109. Nedoszytko B, Lange M, Sokolowska-Wojdylo M, Renke J, Trzonkowski P, Sobjanek M, et al. The role of regulatory T cells and genes involved in their differentiation in pathogenesis of selected inflammatory and neoplastic skin diseases. Part II: The Treg role in skin diseases pathogenesis. Postepy dermatologii i alergologii. 2017;34(5):405-17.
110. Tiemessen MM, Mitchell TJ, Hendry L, Whittaker SJ, Taams LS, John S. Lack of suppressive CD4+CD25+FOXP3+ T cells in advanced stages of primary cutaneous T-cell lymphoma. The Journal of investigative dermatology. 2006;126(10):2217-23.
111. Gjerdrum LM, Woetmann A, Odum N, Burton CM, Rossen K, Skovgaard GL, et al. FOXP3+ regulatory T cells in cutaneous T-cell lymphomas: association with disease stage and survival. Leukemia. 2007;21(12):2512-8.
112. O'Connell MA, Cleere R, Long A, O'Neill LA, Kelleher D. Cellular proliferation and activation of NF kappa B are induced by autocrine production of tumor necrosis factor alpha in the human T lymphoma line HuT 78. The Journal of biological chemistry. 1995;270(13):7399-404.
113. Giri DK, Aggarwal BB. Constitutive activation of NF-kappaB causes resistance to apoptosis in human cutaneous T cell lymphoma HuT-78 cells. Autocrine role of tumor necrosis factor and reactive oxygen intermediates. The Journal of biological chemistry. 1998;273(22):14008-14.
114. Izban KF, Ergin M, Qin JZ, Martinez RL, Pooley RJ, Saeed S, et al. Constitutive expression of NF-kappa B is a characteristic feature of mycosis fungoides: implications for apoptosis resistance and pathogenesis. Human pathology. 2000;31(12):1482-90.
115. Sors A, Jean-Louis F, Pellet C, Laroche L, Dubertret L, Courtois G, et al. Down-regulating constitutive activation of the NF-kappaB canonical pathway overcomes the resistance of cutaneous T-cell lymphoma to apoptosis. Blood. 2006;107(6):2354-63.
116. Sors A, Jean-Louis F, Begue E, Parmentier L, Dubertret L, Dreano M, et al. Inhibition of IkappaB kinase subunit 2 in cutaneous T-cell lymphoma down-regulates nuclear factor-kappaB constitutive activation, induces cell death, and potentiates the apoptotic response to antineoplastic chemotherapeutic agents.

Clinical cancer research : an official journal of the American Association for Cancer Research. 2008;14(3):901-11.

117. Thakur S, Lin HC, Tseng WT, Kumar S, Bravo R, Foss F, et al. Rearrangement and altered expression of the NFKB-2 gene in human cutaneous T-lymphoma cells. Oncogene. 1994;9(8):2335-44.
118. Yamagishi M, Watanabe T. Molecular hallmarks of adult T cell leukemia. Frontiers in microbiology. 2012;3:334.
119. Martinez-Delgado B, Cuadros M, Honrado E, Ruiz de la Parte A, Roncador G, Alves J, et al. Differential expression of NF-kappaB pathway genes among peripheral T-cell lymphomas. Leukemia. 2005;19(12):2254-63.
120. Packham G. The role of NF-kappaB in lymphoid malignancies. British journal of haematology. 2008;143(1):3-15.
121. Mao X, Orchard G, Mitchell TJ, Oyama N, Russell-Jones R, Vermeer MH, et al. A genomic and expression study of AP-1 in primary cutaneous T-cell lymphoma: evidence for dysregulated expression of JUNB and JUND in MF and SS. Journal of cutaneous pathology. 2008;35(10):899-910.
122. Nakayama T, Higuchi T, Oiso N, Kawada A, Yoshie O. Expression and function of FRA2/JUND in cutaneous T-cell lymphomas. Anticancer research. 2012;32(4):1367-73.
123. Juvekar A, Manna S, Ramaswami S, Chang TP, Vu HY, Ghosh CC, et al. Bortezomib induces nuclear translocation of IkappaBalpha resulting in gene-specific suppression of NF-kappaB--dependent transcription and induction of apoptosis in CTCL. Molecular cancer research : MCR. 2011;9(2):183-94.
124. Chang TP, Vancurova I. NFkappaB function and regulation in cutaneous T-cell lymphoma. American journal of cancer research. 2013;3(5):433-45.
125. Carpenter RL, Lo HW. STAT3 Target Genes Relevant to Human Cancers. Cancers. 2014;6(2):897-925.
126. Zeller KI, Jegga AG, Aronow BJ, O'Donnell KA, Dang CV. An integrated database of genes responsive to the Myc oncogenic transcription factor: identification of direct genomic targets. Genome biology. 2003;4(10):R69.
127. Vermeer MH, van Doorn R, Dijkman R, Mao X, Whittaker S, van Voorst Vader PC, et al. Novel and highly recurrent chromosomal alterations in Sezary syndrome. Cancer research. 2008;68(8):2689-98.
128. Jones CL, Wain EM, Chu CC, Tosi I, Foster R, McKenzie RC, et al. Downregulation of Fas gene expression in Sezary syndrome is associated with promoter hypermethylation. The Journal of investigative dermatology. 2010;130(4):1116-25.
129. van Doorn R, van Kester MS, Dijkman R, Vermeer MH, Mulder AA, Szuhai K, et al. Oncogenomic analysis of mycosis fungoides reveals major differences with Sezary syndrome. Blood. 2009;113(1):127-36.

130. Sommer VH, Clemmensen OJ, Nielsen O, Wasik M, Lovato P, Brender C, et al. In vivo activation of STAT3 in cutaneous T-cell lymphoma. Evidence for an antiapoptotic function of STAT3. Leukemia. 2004;18(7):1288-95.
131. Eriksen KW, Kaltoft K, Mikkelsen G, Nielsen M, Zhang Q, Geisler C, et al. Constitutive STAT3-activation in Sezary syndrome: tyrphostin AG490 inhibits STAT3-activation, interleukin-2 receptor expression and growth of leukemic Sezary cells. Leukemia. 2001;15(5):787-93.
132. Nielsen M, Kaltoft K, Nordahl M, Ropke C, Geisler C, Mustelin T, et al. Constitutive activation of a slowly migrating isoform of Stat3 in mycosis fungoides: tyrphostin AG490 inhibits Stat3 activation and growth of mycosis fungoides tumor cell lines. Proceedings of the National Academy of Sciences of the United States of America. 1997;94(13):6764-9.
133. Netchiporouk E, Litvinov IV, Moreau L, Gilbert M, Sasseville D, Duvic M. Deregulation in STAT signaling is important for cutaneous T-cell lymphoma (CTCL) pathogenesis and cancer progression. Cell cycle (Georgetown, Tex). 2014;13(21):3331-5.
134. Qin JZ, Dummer R, Burg G, Dobbeling U. Constitutive and interleukin-7/interleukin-15 stimulated DNA binding of Myc, Jun, and novel Myc-like proteins in cutaneous T-cell lymphoma cells. Blood. 1999;93(1):260-7.
135. Bromberg J, Darnell JE, Jr. The role of STATs in transcriptional control and their impact on cellular function. Oncogene. 2000;19(21):2468-73.
136. Laharanne E, Chevret E, Idrissi Y, Gentil C, Longy M, Ferrer J, et al. CDKN2A-CDKN2B deletion defines an aggressive subset of cutaneous T-cell lymphoma. Modern pathology : an official journal of the United States and Canadian Academy of Pathology, Inc. 2010;23(4):547-58.
137. Woollard WJ, Kalaivani NP, Jones CL, Roper C, Tung L, Lee JJ, et al. Independent Loss of Methylthioadenosine Phosphorylase (MTAP) in Primary Cutaneous T-Cell Lymphoma. The Journal of investigative dermatology. 2016;136(6):1238-46.
138. Navas IC, Ortiz-Romero PL, Villuendas R, Martinez P, Garcia C, Gomez E, et al. p16(INK4a) gene alterations are frequent in lesions of mycosis fungoides. The American journal of pathology. 2000;156(5):1565-72.
139. Laharanne E, Oumouhou N, Bonnet F, Carlotti M, Gentil C, Chevret E, et al. Genome-wide analysis of cutaneous T-cell lymphomas identifies three clinically relevant classes. The Journal of investigative dermatology. 2010;130(6):1707-18.
140. Karenko L, Kahkonen M, Hyytinen ER, Lindlof M, Ranki A. Notable losses at specific regions of chromosomes 10q and 13q in the Sezary syndrome detected by comparative genomic hybridization. The Journal of investigative dermatology. 1999;112(3):392-5.
141. Kiessling MK, Oberholzer PA, Mondal C, Karpova MB, Zipser MC, Lin WM, et al. High-throughput mutation profiling of CTCL samples reveals KRAS and

NRAS mutations sensitizing tumors toward inhibition of the RAS/RAF/MEK signaling cascade. Blood. 2011;117(8):2433-40.

142. Hanahan D, Weinberg RA. The hallmarks of cancer. Cell. 2000;100(1):57-70.
143. Hanahan D, Weinberg RA. Hallmarks of cancer: the next generation. Cell. 2011;144(5):646-74.
144. Stratton MR, Campbell PJ, Futreal PA. The cancer genome. Nature. 2009;458(7239):719-24.
145. Dutt P, Stambolic V. The Basic Science of Oncology, 5e.

Chapter 7: Oncogenes and Tumor-Suppressor Genes. 5 ed: McGraw-Hill Education 2013.

146. Alexandrov LB, Nik-Zainal S, Wedge DC, Aparicio SA, Behjati S, Biankin AV, et al. Signatures of mutational processes in human cancer. Nature. 2013;500(7463):415-21.
147. Woollard WJ, Pullabhatla V, Lorenc A, Patel VM, Butler RM, Bayega A, et al. Candidate driver genes involved in genome maintenance and DNA repair in Sezary syndrome. Blood. 2016;127(26):3387-97.
148. McGirt LY, Jia P, Baerenwald DA, Duszynski RJ, Dahlman KB, Zic JA, et al. Whole-genome sequencing reveals oncogenic mutations in mycosis fungoides. Blood. 2015;126(4):508-19.
149. Vogelstein B, Papadopoulos N, Velculescu VE, Zhou S, Diaz LA, Jr., Kinzler KW. Cancer genome landscapes. Science (New York, NY). 2013;339(6127):1546-58.
150. Cheng L, Lopez-Beltran A, Massari F, MacLennan GT, Montironi R. Molecular testing for BRAF mutations to inform melanoma treatment decisions: a move toward precision medicine. Modern pathology : an official journal of the United States and Canadian Academy of Pathology, Inc. 2018;31(1):24-38.
151. Fuentes Fajardo KV, Adams D, Mason CE, Sincan M, Tifft C, Toro C, et al. Detecting false-positive signals in exome sequencing. Human mutation. 2012;33(4):609-13.
152. Lawrence MS, Stojanov P, Polak P, Kryukov GV, Cibulskis K, Sivachenko A, et al. Mutational heterogeneity in cancer and the search for new cancer-associated genes. Nature. 2013;499(7457):214-8.
153. Kumar P, Henikoff S, Ng PC. Predicting the effects of coding non-synonymous variants on protein function using the SIFT algorithm. Nature protocols. 2009;4(7):1073-81.
154. Choi Y, Chan AP. PROVEAN web server: a tool to predict the functional effect of amino acid substitutions and indels. Bioinformatics (Oxford, England). 2015;31(16):2745-7.
155. Adzhubei I, Jordan DM, Sunyaev SR. Predicting functional effect of human missense mutations using PolyPhen-2. Current protocols in human genetics. 2013;Chapter 7:Unit7.20.

156. Schwarz JM, Cooper DN, Schuelke M, Seelow D. MutationTaster2: mutation prediction for the deep-sequencing age. Nature methods. 2014;11(4):361-2.
157. Li B, Krishnan VG, Mort ME, Xin F, Kamati KK, Cooper DN, et al. Automated inference of molecular mechanisms of disease from amino acid substitutions. Bioinformatics (Oxford, England). 2009;25(21):2744-50.
158. Kircher M, Witten DM, Jain P, O'Roak BJ, Cooper GM. A general framework for estimating the relative pathogenicity of human genetic variants. 2014;46(3):310-5.
159. Brash DE. UV signature mutations. Photochemistry and photobiology. 2015;91(1):15-26.
160. Vaque JP, Gomez-Lopez G, Monsalvez V, Varela I, Martinez N, Perez C, et al. PLCG1 mutations in cutaneous T-cell lymphomas. Blood. 2014;123(13):2034-43.
161. Prasad A, Rabionet R, Espinet B, Zapata L, Puiggros A, Melero C, et al. Identification of Gene Mutations and Fusion Genes in Patients with Sezary Syndrome. The Journal of investigative dermatology. 2016;136(7):1490-9.
162. Park J, Yang J. Genomic analysis of 220 CTCLs identifies a novel recurrent gain-of-function alteration in RLTPR (p.Q575E). 2017;130(12):1430-40.
163. Perez C, Gonzalez-Rincon J, Onaindia A, Almaraz C, Garcia-Diaz N, Pisonero H, et al. Mutated JAK kinases and deregulated STAT activity are potential therapeutic targets in cutaneous T-cell lymphoma. Haematologica. 2015;100(11):e450-3.
164. Roncagalli R, Cucchetti M, Jarmuzynski N, Gregoire C, Bergot E, Audebert S, et al. The scaffolding function of the RLTPR protein explains its essential role for CD28 co-stimulation in mouse and human T cells. The Journal of experimental medicine. 2016;213(11):2437-57.
165. Quintas-Cardama A, Cortes J. Molecular biology of bcr-abl1-positive chronic myeloid leukemia. Blood. 2009;113(8):1619-30.
166. Chang LW, Patrone CC, Yang W, Rabionet R, Gallardo F, Espinet B, et al. An Integrated Data Resource for Genomic Analysis of Cutaneous T-Cell Lymphoma. The Journal of investigative dermatology. 2018.
167. Qiu L, Liu F, Yi S, Li X, Liu X, Xiao C, et al. Loss of 5-Hydroxymethylcytosine Is an Epigenetic Biomarker in Cutaneous T-Cell Lymphoma. The Journal of investigative dermatology. 2018;138(11):2388-97.
168. Shewan A, Eastburn DJ, Mostov K. Phosphoinositides in cell architecture. Cold Spring Harbor perspectives in biology. 2011;3(8):a004796.
169. Lemmon MA. Membrane recognition by phospholipid-binding domains. Nature reviews Molecular cell biology. 2008;9(2):99-111.
170. Park JB, Lee CS, Jang JH, Ghim J, Kim YJ, You S, et al. Phospholipase signalling networks in cancer. Nature reviews Cancer. 2012;12(11):782-92.

171. Hicks SN, Jezyk MR, Gershburg S, Seifert JP, Harden TK, Sondek J. General and versatile autoinhibition of PLC isozymes. Molecular cell. 2008;31(3):383-94.
172. Gresset A, Hicks SN, Harden TK, Sondek J. Mechanism of phosphorylation-induced activation of phospholipase C-gamma isozymes. The Journal of biological chemistry. 2010;285(46):35836-47.
173. Nakamura Y, Fukami K. Regulation and physiological functions of mammalian phospholipase C. Journal of biochemistry. 2017;161(4):315-21.
174. Nomikos M, Elgmati K, Theodoridou M, Georgilis A, Gonzalez-Garcia JR, Nounesis G, et al. Novel regulation of PLCzeta activity via its XY-linker. The Biochemical journal. 2011;438(3):427-32.
175. Koss H, Bunney TD, Behjati S, Katan M. Dysfunction of phospholipase Cgamma in immune disorders and cancer. Trends in biochemical sciences. 2014;39(12):603-11.
176. Zerbino DR, Achuthan P, Akanni W, Amode M R, Barrell D, Bhai J, et al. Ensembl 2018. Nucleic acids research. 2018;46(D1):D754-D61.
177. Poulin B, Sekiya F, Rhee SG. Intramolecular interaction between phosphorylated tyrosine-783 and the C-terminal Src homology 2 domain activates phospholipase C-gamma1. Proceedings of the National Academy of Sciences of the United States of America. 2005;102(12):4276-81.
178. Wang Y, Wang Z. Regulation of EGF-induced phospholipase C-gamma1 translocation and activation by its SH2 and PH domains. Traffic (Copenhagen, Denmark). 2003;4(9):618-30.
179. Lattanzio R, Piantelli M, Falasca M. Role of phospholipase C in cell invasion and metastasis. Advances in biological regulation. 2013;53(3):309-18.
180. Smith-Garvin JE, Koretzky GA, Jordan MS. T cell activation. Annual review of immunology. 2009;27:591-619.
181. Fu G, Chen Y, Schuman J, Wang D, Wen R. Phospholipase Cgamma2 plays a role in TCR signal transduction and T cell selection. Journal of immunology (Baltimore, Md : 1950). 2012;189(5):2326-32.
182. Schmidt T, Samaras P, Frejno M, Gessulat S, Barnert M, Kienegger H, et al. ProteomicsDB. Nucleic acids research. 2018;46(D1):D1271-d81.
183. Zheng Y, Adams T, Zhi H, Yu M, Wen R, Newman PJ, et al. Restoration of responsiveness of phospholipase Cgamma2-deficient platelets by enforced expression of phospholipase Cgamma1. PloS one. 2015;10(3):e0119739.
184. Chaplin DD. Overview of the immune response. The Journal of allergy and clinical immunology. 2010;125(2 Suppl 2):S3-23.
185. Birnbaum ME, Berry R, Hsiao YS, Chen Z, Shingu-Vazquez MA, Yu X, et al. Molecular architecture of the alphabeta T cell receptor-CD3 complex. Proceedings of the National Academy of Sciences of the United States of America. 2014;111(49):17576-81.

186. Jahan AS, Lestra M, Swee LK, Fan Y, Lamers MM, Tafesse FG, et al. Usp12 stabilizes the T-cell receptor complex at the cell surface during signaling. Proceedings of the National Academy of Sciences of the United States of America. 2016;113(6):E705-14.
187. Brownlie RJ, Zamoyska R. T cell receptor signalling networks: branched, diversified and bounded. Nature reviews Immunology. 2013;13(4):257-69.
188. Bubeck Wardenburg J, Fu C, Jackman JK, Flotow H, Wilkinson SE, Williams DH, et al. Phosphorylation of SLP-76 by the ZAP-70 protein-tyrosine kinase is required for T-cell receptor function. The Journal of biological chemistry. 1996;271(33):19641-4.
189. Hajicek N, Charpentier TH, Rush JR, Harden TK, Sondek J. Autoinhibition and Phosphorylation-Induced Activation of Phospholipase C-γ Isozymes. Biochemistry. 2013;52(28):4810-9.
190. Yablonski D, Kadlecek T, Weiss A. Identification of a phospholipase C-gamma1 (PLC-gamma1) SH3 domain-binding site in SLP-76 required for T-cell receptor-mediated activation of PLC-gamma1 and NFAT. Molecular and cellular biology. 2001;21(13):4208-18.
191. Bogin Y, Ainey C, Beach D, Yablonski D. SLP-76 mediates and maintains activation of the Tec family kinase ITK via the T cell antigen receptor-induced association between SLP-76 and ITK. Proceedings of the National Academy of Sciences of the United States of America. 2007;104(16):6638-43.
192. Gresset A, Sondek J, Harden TK. The phospholipase C isozymes and their regulation. Sub-cellular biochemistry. 2012;58:61-94.
193. Serrano CJ, Graham L, DeBell K, Rawat R, Veri MC, Bonvini E, et al. A new tyrosine phosphorylation site in PLC gamma 1: the role of tyrosine 775 in immune receptor signaling. Journal of immunology (Baltimore, Md : 1950). 2005;174(10):6233-7.
194. Bunney TD, Esposito D, Mas-Droux C, Lamber E, Baxendale RW, Martins M, et al. Structural and functional integration of the PLCgamma interaction domains critical for regulatory mechanisms and signaling deregulation. Structure (London, England : 1993). 2012;20(12):2062-75.
195. Hogan PG, Chen L, Nardone J, Rao A. Transcriptional regulation by calcium, calcineurin, and NFAT. Genes & development. 2003;17(18):2205-32.
196. Macian F, Lopez-Rodriguez C, Rao A. Partners in transcription: NFAT and AP-1. Oncogene. 2001;20(19):2476-89.
197. Li L, Zhao GD, Shi Z, Qi LL, Zhou LY, Fu ZX. The Ras/Raf/MEK/ERK signaling pathway and its role in the occurrence and development of HCC. Oncology letters. 2016;12(5):3045-50.
198. Karin M, Liu Z, Zandi E. AP-1 function and regulation. Current opinion in cell biology. 1997;9(2):240-6.

199. Qiao Q, Yang C, Zheng C, Fontan L, David L, Yu X, et al. Structural architecture of the CARMA1/Bcl10/MALT1 signalosome: nucleation-induced filamentous assembly. Molecular cell. 2013;51(6):766-79.
200. Oeckinghaus A, Ghosh S. The NF-kappaB family of transcription factors and its regulation. Cold Spring Harbor perspectives in biology. 2009;1(4):a000034.
201. Roche MI, Ramadas RA, Medoff BD. The role of CARMA1 in T cells. Critical reviews in immunology. 2013;33(3):219-43.
202. Treanor B. B-cell receptor: from resting state to activate. Immunology. 2012;136(1):21-7.
203. Seda V, Mraz M. B-cell receptor signalling and its crosstalk with other pathways in normal and malignant cells. European journal of haematology. 2015;94(3):193-205.
204. Watanabe D, Hashimoto S, Ishiai M, Matsushita M, Baba Y, Kishimoto T, et al. Four tyrosine residues in phospholipase C-gamma 2, identified as Btk-dependent phosphorylation sites, are required for B cell antigen receptor-coupled calcium signaling. The Journal of biological chemistry. 2001;276(42):38595-601.
205. Rodriguez R, Matsuda M, Perisic O, Bravo J, Paul A, Jones NP, et al. Tyrosine residues in phospholipase Cgamma 2 essential for the enzyme function in B-cell signaling. The Journal of biological chemistry. 2001;276(51):47982-92.
206. Ozdener F, Dangelmaier C, Ashby B, Kunapuli SP, Daniel JL. Activation of phospholipase Cgamma2 by tyrosine phosphorylation. Molecular pharmacology. 2002;62(3):672-9.
207. Kim YJ, Sekiya F, Poulin B, Bae YS, Rhee SG. Mechanism of B-cell receptor-induced phosphorylation and activation of phospholipase C-gamma2. Molecular and cellular biology. 2004;24(22):9986-99.
208. Abbas A, Lichtman A, Pillai S. Cellular and Molecular Immunology

Chapter 7: Immune Receptors and Signal Transduction. 9th ed2017.

209. Efremov DG, Wiestner A, Laurenti L. Novel Agents and Emerging Strategies for Targeting the B-Cell Receptor Pathway in CLL. Mediterranean journal of hematology and infectious diseases. 2012;4(1):e2012067.
210. Kapoor A, Singh P, Beniwal S, Singhal M, Nirban R, Kumar H. Ibrutinib: A comprehensive review of a promising drug. Clinical Cancer Investigation Journal. 2016;5(3):203-7.
211. Young RJ, Brown NJ, Reed MW, Hughes D, Woll PJ. Angiosarcoma. The Lancet Oncology. 2010;11(10):983-91.
212. Behjati S, Tarpey PS, Sheldon H, Martincorena I, Van Loo P. Recurrent PTPRB and PLCG1 mutations in angiosarcoma. 2014;46(4):376-9.
213. Kunze K, Spieker T, Gamerdinger U, Nau K, Berger J, Dreyer T, et al. A recurrent activating PLCG1 mutation in cardiac angiosarcomas increases apoptosis resistance and invasiveness of endothelial cells. Cancer research. 2014;74(21):6173-83.

214. Huang SC, Zhang L, Sung YS, Chen CL, Kao YC, Agaram NP, et al. Recurrent CIC Gene Abnormalities in Angiosarcomas: A Molecular Study of 120 Cases With Concurrent Investigation of PLCG1, KDR, MYC, and FLT4 Gene Alterations. The American journal of surgical pathology. 2016;40(5):645-55.
215. Murali R, Chandramohan R, Moller I, Scholz SL, Berger M, Huberman K, et al. Targeted massively parallel sequencing of angiosarcomas reveals frequent activation of the mitogen activated protein kinase pathway. Oncotarget. 2015;6(34):36041-52.
216. Caumont C, Gros A, Boucher C, Melard P, Prochazkova-Carlotti M, Laharanne E, et al. PLCG1 Gene Mutations Are Uncommon in Cutaneous T-Cell Lymphomas. The Journal of investigative dermatology. 2015;135(9):2334-7.
217. Manso R, Rodriguez-Pinilla SM, Gonzalez-Rincon J, Gomez S, Monsalvo S, Llamas P, et al. Recurrent presence of the PLCG1 S345F mutation in nodal peripheral T-cell lymphomas. Haematologica. 2015;100(1):e25-7.
218. Vallois D, Dobay MP, Morin RD, Lemonnier F, Missiaglia E, Juilland M, et al. Activating mutations in genes related to TCR signaling in angioimmunoblastic and other follicular helper T-cell-derived lymphomas. Blood. 2016;128(11):1490-502.
219. Manso R, Gonzalez-Rincon J, Rodriguez-Justo M, Roncador G, Gomez S, Sanchez-Beato M, et al. Overlap at the molecular and immunohistochemical levels between angioimmunoblastic T-cell lymphoma and a subgroup of peripheral T-cell lymphomas without specific morphological features. Oncotarget. 2018;9(22):16124-33.
220. Wang M, Zhang S, Chuang SS, Ashton-Key M, Ochoa E, Bolli N, et al. Angioimmunoblastic T cell lymphoma: novel molecular insights by mutation profiling. Oncotarget. 2017;8(11):17763-70.
221. Kataoka K, Nagata Y, Kitanaka A, Shiraishi Y, Shimamura T, Yasunaga J, et al. Integrated molecular analysis of adult T cell leukemia/lymphoma. 2015;47(11):1304-15.
222. McKinney M, Moffitt AB, Gaulard P, Travert M, De Leval L, Nicolae A, et al. The Genetic Basis of Hepatosplenic T-cell Lymphoma. Cancer discovery. 2017;7(4):369-79.
223. Kiel MJ, Velusamy T, Rolland D, Sahasrabuddhe AA, Chung F, Bailey NG, et al. Integrated genomic sequencing reveals mutational landscape of T-cell prolymphocytic leukemia. Blood. 2014;124(9):1460-72.
224. Prenen H, Smeets D, Mazzone M, Lambrechts D, Sagaert X, Sciot R, et al. Phospholipase C gamma 1 (PLCG1) R707Q mutation is counterselected under targeted therapy in a patient with hepatic angiosarcoma. Oncotarget. 2015;6(34):36418-25.
225. Waugh MG. Chromosomal Instability and Phosphoinositide Pathway Gene Signatures in Glioblastoma Multiforme. Molecular neurobiology. 2016;53(1):621-30.

226. Arteaga CL, Johnson MD, Todderud G, Coffey RJ, Carpenter G, Page DL. Elevated content of the tyrosine kinase substrate phospholipase C-gamma 1 in primary human breast carcinomas. Proceedings of the National Academy of Sciences of the United States of America. 1991;88(23):10435-9.
227. Lattanzio R, Marchisio M, La Sorda R, Tinari N, Falasca M, Alberti S, et al. Overexpression of activated phospholipase Cgamma1 is a risk factor for distant metastases in T1-T2, N0 breast cancer patients undergoing adjuvant chemotherapy. International journal of cancer. 2013;132(5):1022-31.
228. Nomoto K, Tomita N, Miyake M, Xhu DB, LoGerfo PR, Weinstein IB. Expression of phospholipases gamma 1, beta 1, and delta 1 in primary human colon carcinomas and colon carcinoma cell lines. Molecular carcinogenesis. 1995;12(3):146-52.
229. Li X, Hua L, Deng F, Bai X, Zeng W, Lu D, et al. NF-kappaB and Hsp70 are involved in the phospholipase Cgamma1 signaling pathway in colorectal cancer cells. Life sciences. 2005;77(22):2794-803.
230. Klein RR, Bourdon DM, Costales CL, Wagner CD, White WL, Williams JD, et al. Direct activation of human phospholipase C by its well known inhibitor u73122. The Journal of biological chemistry. 2011;286(14):12407-16.
231. Oliveira DM, Santamaria G, Laudanna C, Migliozzi S, Zoppoli P, Quist M, et al. Identification of copy number alterations in colon cancer from analysis of amplicon-based next generation sequencing data. Oncotarget. 2018;9(29):20409-25.
232. Xie Z, Chen Y, Liao EY, Jiang Y, Liu FY, Pennypacker SD. Phospholipase C-gamma1 is required for the epidermal growth factor receptor-induced squamous cell carcinoma cell mitogenesis. Biochemical and biophysical research communications. 2010;397(2):296-300.
233. Zhu D, Tan Y, Yang X, Qiao J, Yu C, Wang L, et al. Phospholipase C gamma 1 is a potential prognostic biomarker for patients with locally advanced and resectable oral squamous cell carcinoma. International journal of oral and maxillofacial surgery. 2014;43(12):1418-26.
234. Ma LW, Zhou ZT, He QB, Jiang WW. Phospholipase C-gamma1 expression correlated with cancer progression of potentially malignant oral lesions. Journal of oral pathology & medicine : official publication of the International Association of Oral Pathologists and the American Academy of Oral Pathology. 2013;42(1):47-52.
235. Ombrello MJ, Remmers EF, Sun G, Freeman AF, Datta S, Torabi-Parizi P, et al. Cold urticaria, immunodeficiency, and autoimmunity related to PLCG2 deletions. The New England journal of medicine. 2012;366(4):330-8.
236. Zhou Q, Lee GS, Brady J, Datta S, Katan M, Sheikh A, et al. A hypermorphic missense mutation in PLCG2, encoding phospholipase Cgamma2, causes a dominantly inherited autoinflammatory disease with immunodeficiency. American journal of human genetics. 2012;91(4):713-20.

237. Zhou Q, Lee GS, Brady J, Datta S, Katan M, Sheikh A, et al. A hypermorphic missense mutation in PLCG2, encoding phospholipase Cγ2, causes a dominantly inherited autoinflammatory disease with immunodeficiency. Am J Hum Genet. 2012;91:713.
238. Maddocks KJ, Ruppert AS, Lozanski G, Heerema NA, Zhao W, Abruzzo L, et al. Etiology of Ibrutinib Therapy Discontinuation and Outcomes in Patients With Chronic Lymphocytic Leukemia. JAMA oncology. 2015;1(1):80-7.
239. Woyach JA, Furman RR, Liu TM, Ozer HG, Zapatka M, Ruppert AS, et al. Resistance mechanisms for the Bruton's tyrosine kinase inhibitor ibrutinib. The New England journal of medicine. 2014;370(24):2286-94.
240. Jones D, Woyach JA, Zhao W, Caruthers S, Tu H, Coleman J, et al. PLCG2 C2 domain mutations co-occur with BTK and PLCG2 resistance mutations in chronic lymphocytic leukemia undergoing ibrutinib treatment. Leukemia. 2017;31(7):1645-7.
241. Burger JA, Landau DA, Taylor-Weiner A, Bozic I, Zhang H, Sarosiek K. Clonal evolution in patients with chronic lymphocytic leukaemia developing resistance to BTK inhibition. 2016;7:11589.
242. Walliser C, Hermkes E, Schade A, Wiese S, Deinzer J, Zapatka M, et al. The Phospholipase Cgamma2 Mutants R665W and L845F Identified in Ibrutinib-resistant Chronic Lymphocytic Leukemia Patients Are Hypersensitive to the Rho GTPase Rac2 Protein. The Journal of biological chemistry. 2016;291(42):22136-48.
243. Liu TM, Woyach JA, Zhong Y, Lozanski A, Lozanski G, Dong S, et al. Hypermorphic mutation of phospholipase C, gamma2 acquired in ibrutinib-resistant CLL confers BTK independency upon B-cell receptor activation. Blood. 2015;126(1):61-8.
244. Kadri S, Lee J. Clonal evolution underlying leukemia progression and Richter transformation in patients with ibrutinib-relapsed CLL. 2017;1(12):715-27.
245. Xu L, Tsakmaklis N, Yang G, Chen JG, Liu X, Demos M, et al. Acquired mutations associated with ibrutinib resistance in Waldenstrom macroglobulinemia. Blood. 2017;129(18):2519-25.
246. Furman RR, Cheng S, Lu P, Setty M, Perez AR, Guo A, et al. Ibrutinib resistance in chronic lymphocytic leukemia. The New England journal of medicine. 2014;370(24):2352-4.
247. Landau DA, Sun C. The evolutionary landscape of chronic lymphocytic leukemia treated with ibrutinib targeted therapy. 2017;8(1):2185.
248. Herishanu Y, Perez-Galan P, Liu D, Biancotto A, Pittaluga S, Vire B, et al. The lymph node microenvironment promotes B-cell receptor signaling, NF-kappaB activation, and tumor proliferation in chronic lymphocytic leukemia. Blood. 2011;117(2):563-74.
249. Pal Singh S, Dammeijer F, Hendriks RW. Role of Bruton's tyrosine kinase in B cells and malignancies. Molecular cancer. 2018;17(1):57.

250. Treon SP, Tripsas CK, Meid K, Warren D, Varma G, Green R, et al. Ibrutinib in previously treated Waldenstrom's macroglobulinemia. The New England journal of medicine. 2015;372(15):1430-40.
251. Wang ML, Rule S, Martin P, Goy A, Auer R, Kahl BS, et al. Targeting BTK with ibrutinib in relapsed or refractory mantle-cell lymphoma. The New England journal of medicine. 2013;369(6):507-16.
252. Wilson WH, Young RM, Schmitz R, Yang Y, Pittaluga S, Wright G, et al. Targeting B cell receptor signaling with ibrutinib in diffuse large B cell lymphoma. Nature medicine. 2015;21(8):922-6.
253. Cheah CY, Chihara D, Romaguera JE, Fowler NH, Seymour JF, Hagemeister FB, et al. Patients with mantle cell lymphoma failing ibrutinib are unlikely to respond to salvage chemotherapy and have poor outcomes. Annals of oncology : official journal of the European Society for Medical Oncology. 2015;26(6):1175-9.
254. Zhang SQ, Smith SM, Zhang SY, Lynn Wang Y. Mechanisms of ibrutinib resistance in chronic lymphocytic leukaemia and non-Hodgkin lymphoma. British journal of haematology. 2015;170(4):445-56.
255. Lampson BL, Brown JR. Are BTK and PLCG2 mutations necessary and sufficient for ibrutinib resistance in chronic lymphocytic leukemia? Expert review of hematology. 2018;11(3):185-94.
256. Ahn IE, Underbayev C, Albitar A, Herman SE, Tian X, Maric I, et al. Clonal evolution leading to ibrutinib resistance in chronic lymphocytic leukemia. Blood. 2017;129(11):1469-79.
257. Thorvaldsdottir H, Robinson JT, Mesirov JP. Integrative Genomics Viewer (IGV): high-performance genomics data visualization and exploration. Briefings in bioinformatics. 2013;14(2):178-92.
258. Untergasser A, Cutcutache I, Koressaar T, Ye J, Faircloth BC, Remm M, et al. Primer3--new capabilities and interfaces. Nucleic acids research. 2012;40(15):e115.
259. Ye J, Coulouris G, Zaretskaya I, Cutcutache I, Rozen S, Madden TL. Primer-BLAST: a tool to design target-specific primers for polymerase chain reaction. BMC bioinformatics. 2012;13:134.
260. Winship PR. An improved method for directly sequencing PCR amplified material using dimethyl sulphoxide. Nucleic acids research. 1989;17(3):1266.
261. Comeau SR, Gatchell DW, Vajda S, Camacho CJ. ClusPro: an automated docking and discrimination method for the prediction of protein complexes. Bioinformatics (Oxford, England). 2004;20(1):45-50.
262. Comeau SR, Gatchell DW, Vajda S, Camacho CJ. ClusPro: a fully automated algorithm for protein-protein docking. Nucleic acids research. 2004;32(Web Server issue):W96-9.

263. Guex N, Peitsch MC. SWISS-MODEL and the Swiss-PdbViewer: an environment for comparative protein modeling. Electrophoresis. 1997;18(15):2714-23.
264. Schrodinger, LLC. The PyMOL Molecular Graphics System, Version 1.8. 2015.
265. Larkin MA, Blackshields G, Brown NP, Chenna R, McGettigan PA, McWilliam H, et al. Clustal W and Clustal X version 2.0. Bioinformatics (Oxford, England). 2007;23(21):2947-8.
266. van Kuppeveld FJ, Johansson KE, Galama JM, Kissing J, Bolske G, van der Logt JT, et al. Detection of mycoplasma contamination in cell cultures by a mycoplasma group-specific PCR. Applied and environmental microbiology. 1994;60(1):149-52.
267. Uhlen M, Fagerberg L, Hallstrom BM, Lindskog C, Oksvold P, Mardinoglu A, et al. Proteomics. Tissue-based map of the human proteome. Science (New York, NY). 2015;347(6220):1260419.
268. Yavas S, Machan R, Wohland T. The Epidermal Growth Factor Receptor Forms Location-Dependent Complexes in Resting Cells. Biophysical journal. 2016;111(10):2241-54.
269. Everett KL, Bunney TD, Yoon Y, Rodrigues-Lima F, Harris R, Driscoll PC, et al. Characterization of phospholipase C gamma enzymes with gain-of-function mutations. The Journal of biological chemistry. 2009;284(34):23083-93.
270. Lu H, Lu Q, Gaddipati S, Kasetti RB, Wang W, Pasparakis M, et al. IKK2 inhibition attenuates laser-induced choroidal neovascularization. PloS one. 2014;9(1):e87530.
271. Nagata Y, Kontani K, Enami T, Kataoka K, Ishii R, Totoki Y, et al. Variegated RHOA mutations in adult T-cell leukemia/lymphoma. Blood. 2016;127(5):596-604.
272. Forbes SA, Beare D, Boutselakis H, Bamford S, Bindal N, Tate J, et al. COSMIC: somatic cancer genetics at high-resolution. Nucleic acids research. 2017;45(D1):D777-d83.
273. Sherry ST, Ward MH, Kholodov M, Baker J, Phan L, Smigielski EM, et al. dbSNP: the NCBI database of genetic variation. Nucleic acids research. 2001;29(1):308-11.
274. Bunney TD, Opaleye O, Roe SM, Vatter P, Baxendale RW, Walliser C, et al. Structural insights into formation of an active signaling complex between Rac and phospholipase C gamma 2. Molecular cell. 2009;34(2):223-33.
275. Shi J, Chen J, Serradji N, Xu X, Zhou H, Ma Y, et al. PMS1077 sensitizes TNF-alpha induced apoptosis in human prostate cancer cells by blocking NF-kappaB signaling pathway. PloS one. 2013;8(4):e61132.
276. Pei Z, Yang L, Williamson JR. Phospholipase C-gamma 1 binds to actin-cytoskeleton via its C-terminal SH2 domain in vitro. Biochemical and biophysical research communications. 1996;228(3):802-6.

277. Matsuda M, Paterson HF, Rodriguez R, Fensome AC, Ellis MV, Swann K, et al. Real time fluorescence imaging of PLC gamma translocation and its interaction with the epidermal growth factor receptor. The Journal of cell biology. 2001;153(3):599-612.
278. Sakata-Yanagimoto M, Enami T, Yoshida K, Shiraishi Y, Ishii R, Miyake Y, et al. Somatic RHOA mutation in angioimmunoblastic T cell lymphoma. Nature genetics. 2014;46(2):171-5.
279. Crescenzo R, Abate F, Lasorsa E, Tabbo F, Gaudiano M, Chiesa N, et al. Convergent mutations and kinase fusions lead to oncogenic STAT3 activation in anaplastic large cell lymphoma. Cancer cell. 2015;27(4):516-32.
280. Roberti A, Dobay MP, Bisig B, Vallois D, Boechat C, Lanitis E, et al. Type II enteropathy-associated T-cell lymphoma features a unique genomic profile with highly recurrent SETD2 alterations. Nature communications. 2016;7:12602.
281. Nairismagi ML, Tan J, Lim JQ, Nagarajan S, Ng CC, Rajasegaran V, et al. JAK-STAT and G-protein-coupled receptor signaling pathways are frequently altered in epitheliotropic intestinal T-cell lymphoma. Leukemia. 2016;30(6):1311-9.
282. Moffitt AB, Ondrejka SL. Enteropathy-associated T cell lymphoma subtypes are characterized by loss of function of SETD2. 2017;214(5):1371-86.
283. Jiang L, Gu ZH, Yan ZX, Zhao X, Xie YY, Zhang ZG, et al. Exome sequencing identifies somatic mutations of DDX3X in natural killer/T-cell lymphoma. Nature genetics. 2015;47(9):1061-6.
284. Boursault L, Haddad V, Vergier B, Cappellen D, Verdon S, Bellocq JP, et al. Tumor homogeneity between primary and metastatic sites for BRAF status in metastatic melanoma determined by immunohistochemical and molecular testing. PloS one. 2013;8(8):e70826.
285. Albitar A, Ma W, DeDios I, Estella J, Ahn I, Farooqui M, et al. Using high-sensitivity sequencing for the detection of mutations in BTK and PLCgamma2 genes in cellular and cell-free DNA and correlation with progression in patients treated with BTK inhibitors. Oncotarget. 2017;8(11):17936-44.
286. Blachnio-Zabielska AU, Zabielski P, Jensen MD. Intramyocellular diacylglycerol concentrations and [U-(1)(3)C]palmitate isotopic enrichment measured by LC/MS/MS. Journal of lipid research. 2013;54(6):1705-11.
287. Haag M, Schmidt A, Sachsenheimer T, Brugger B. Quantification of Signaling Lipids by Nano-Electrospray Ionization Tandem Mass Spectrometry (Nano-ESI MS/MS). Metabolites. 2012;2(1):57-76.
288. Swerdlow S, Campo E, Harris N, Jaffe E, Pileri S, Stein H, et al. WHO Classification of Tumours of Haematopoietic and Lymphoid Tissues. 4th ed2008.
289. Franchini G. Molecular mechanisms of human T-cell leukemia/lymphotropic virus type I infection. Blood. 1995;86(10):3619-39.
290. Murray D, Honig B. Electrostatic control of the membrane targeting of C2 domains. Molecular cell. 2002;9(1):145-54.

291. Walliser C, Wist M, Hermkes E, Zhou Y, Schade A, Haas J, et al. Functional characterization of phospholipase C-gamma2 mutant protein causing both somatic ibrutinib resistance and a germline monogenic autoinflammatory disorder. Oncotarget. 2018;9(76):34357-78.
292. Pulcinelli FM, Gresele P, Bonuglia M, Gazzaniga PP. Evidence for separate effects of U73122 on phospholipase C and calcium channels in human platelets. Biochemical pharmacology. 1998;56(11):1481-4.
293. Klose A, Huth T, Alzheimer C. 1-[6-[[(17beta)-3-methoxyestra-1,3,5(10)-trien-17-yl]amino]hexyl]-1H-pyrrole-2,5- dione (U73122) selectively inhibits Kir3 and BK channels in a phospholipase C-independent fashion. Molecular pharmacology. 2008;74(5):1203-14.
294. Chen YJ, Sheng WY, Huang PR, Wang TC. Potent inhibition of human telomerase by U-73122. Journal of biomedical science. 2006;13(5):667-74.
295. Burgdorf C, Schafer U, Richardt G, Kurz T. U73122, an aminosteroid phospholipase C inhibitor, is a potent inhibitor of cardiac phospholipase D by a PIP2-dependent mechanism. Journal of cardiovascular pharmacology. 2010;55(6):555-9.
296. Putney JW. Origins of the concept of store-operated calcium entry. Frontiers in bioscience (Scholar edition). 2011;3:980-4.
297. Kanda N, Mitsui H, Watanabe S. Prostaglandin E(2) suppresses CCL27 production through EP2 and EP3 receptors in human keratinocytes. The Journal of allergy and clinical immunology. 2004;114(6):1403-9.
298. Komarova SV, Pilkington MF, Weidema AF, Dixon SJ, Sims SM. RANK ligand-induced elevation of cytosolic Ca2+ accelerates nuclear translocation of nuclear factor kappa B in osteoclasts. The Journal of biological chemistry. 2003;278(10):8286-93.
299. Hayden MS, Ghosh S. Regulation of NF-kappaB by TNF family cytokines. Seminars in immunology. 2014;26(3):253-66.
300. Zinzani PL, Musuraca G, Tani M, Stefoni V, Marchi E, Fina M, et al. Phase II Trial of Proteasome Inhibitor Bortezomib in Patients With Relapsed or Refractory Cutaneous T-Cell Lymphoma. 2007;25(27):4293-7.
301. Hideshima T, Ikeda H, Chauhan D, Okawa Y, Raje N, Podar K, et al. Bortezomib induces canonical nuclear factor-kappaB activation in multiple myeloma cells. Blood. 2009;114(5):1046-52.
302. Fonacier L, Spergel J, Charlesworth EN, Weldon D, Beltrani V, Bernhisel-Broadbent J, et al. Report of the Topical Calcineurin Inhibitor Task Force of the American College of Allergy, Asthma and Immunology and the American Academy of Allergy, Asthma and Immunology. The Journal of allergy and clinical immunology. 2005;115(6):1249-53.
303. Rallis E, Economidi A, Verros C, Papadakis P. Successful treatment of patch type mycosis fungoides with tacrolimus ointment 0.1%. Journal of drugs in dermatology : JDD. 2006;5(9):906-7.

304. Dubovsky JA, Beckwith KA, Natarajan G, Woyach JA, Jaglowski S, Zhong Y, et al. Ibrutinib is an irreversible molecular inhibitor of ITK driving a Th1-selective pressure in T lymphocytes. Blood. 2013;122(15):2539-49.
305. Litvinov IV, Netchiporouk E, Cordeiro B, Dore MA, Moreau L, Pehr K, et al. The Use of Transcriptional Profiling to Improve Personalized Diagnosis and Management of Cutaneous T-cell Lymphoma (CTCL). Clin Cancer Res. 2015;21(12):2820-9.
306. Litvinov IV, Tetzlaff MT, Thibault P, Gangar P, Moreau L, Watters AK, et al. Gene expression analysis in Cutaneous T-Cell Lymphomas (CTCL) highlights disease heterogeneity and potential diagnostic and prognostic indicators. Oncoimmunology. 2017;6(5):e1306618.
307. Netchiporouk E, Gantchev J, Tsang M, Thibault P, Watters AK, Hughes JM, et al. Analysis of CTCL cell lines reveals important differences between mycosis fungoides/Sezary syndrome vs. HTLV-1(+) leukemic cell lines. Oncotarget. 2017;8(56):95981-98.
308. Long M, Beckwith K, Do P, Mundy BL, Gordon A, Lehman AM, et al. Ibrutinib treatment improves T cell number and function in CLL patients. The Journal of clinical investigation. 2017;127(8):3052-64.
309. Kumar A, Vardhana S, Moskowitz AJ, Porcu P, Dogan A, Dubovsky JA, et al. Pilot trial of ibrutinib in patients with relapsed or refractory T-cell lymphoma. Blood advances. 2018;2(8):871-6.
310. Mamand S, Allchin RL, Ahearne MJ, Wagner SD. Comparison of interleukin-2-inducible kinase (ITK) inhibitors and potential for combination therapies for T-cell lymphoma. Scientific reports. 2018;8(1):14216.
311. Stelzer G, Rosen N, Plaschkes I, Zimmerman S, Twik M, Fishilevich S, et al. The GeneCards Suite: From Gene Data Mining to Disease Genome Sequence Analyses. Current protocols in bioinformatics. 2016;54:1.30.1-1..3.
312. Reynisson J, Court W, O'Neill C, Day J, Patterson L, McDonald E, et al. The identification of novel PLC-gamma inhibitors using virtual high throughput screening. Bioorganic & medicinal chemistry. 2009;17(8):3169-76.
313. Canellada A, Ramirez BG, Minami T, Redondo JM, Cano E. Calcium/calcineurin signaling in primary cortical astrocyte cultures: Rcan1-4 and cyclooxygenase-2 as NFAT target genes. Glia. 2008;56(7):709-22.
314. Oum JH, Han J, Myung H, Hleb M, Sharma S, Park J. Molecular mechanism of NFAT family proteins for differential regulation of the IL-2 and TNF-alpha promoters. Molecules and cells. 2002;13(1):77-84.
315. Elgueta R, Benson MJ, de Vries VC, Wasiuk A, Guo Y, Noelle RJ. Molecular mechanism and function of CD40/CD40L engagement in the immune system. Immunological reviews. 2009;229(1):152-72.
316. Tabbekh M, Mokrani-Hammani M, Bismuth G, Mami-Chouaib F. T-cell modulatory properties of CD5 and its role in antitumor immune responses. Oncoimmunology. 2013;2(1):e22841.

317. Pan MG, Xiong Y, Chen F. NFAT gene family in inflammation and cancer. Current molecular medicine. 2013;13(4):543-54.
318. Rao A, Luo C, Hogan PG. Transcription factors of the NFAT family: regulation and function. Annual review of immunology. 1997;15:707-47.
319. Eferl R, Wagner EF. AP-1: a double-edged sword in tumorigenesis. Nature reviews Cancer. 2003;3(11):859-68.
320. Shaulian E, Karin M. AP-1 as a regulator of cell life and death. Nature cell biology. 2002;4(5):E131-6.
321. Samten B, Townsend JC, Weis SE, Bhoumik A, Klucar P, Shams H, et al. CREB, ATF, and AP-1 Transcription Factors Regulate IFN-γ Secretion by Human T Cells in Response to Mycobacterial Antigen. 2008;181(3):2056-64.
322. Grimm T, Schneider S, Naschberger E, Huber J, Guenzi E, Kieser A, et al. EBV latent membrane protein-1 protects B cells from apoptosis by inhibition of BAX. Blood. 2005;105(8):3263-9.
323. Catz SD, Johnson JL. Transcriptional regulation of bcl-2 by nuclear factor kappa B and its significance in prostate cancer. Oncogene. 2001;20(50):7342-51.
324. Brocke-Heidrich K, Ge B, Cvijic H, Pfeifer G, Loffler D, Henze C, et al. BCL3 is induced by IL-6 via Stat3 binding to intronic enhancer HS4 and represses its own transcription. Oncogene. 2006;25(55):7297-304.
325. Wu K, Jiang SW, Thangaraju M, Wu G, Couch FJ. Induction of the BRCA2 promoter by nuclear factor-kappa B. The Journal of biological chemistry. 2000;275(45):35548-56.
326. Yu L, Mohamed AJ, Simonson OE, Vargas L, Blomberg KE, Bjorkstrand B, et al. Proteasome-dependent autoregulation of Bruton tyrosine kinase (Btk) promoter via NF-kappaB. Blood. 2008;111(9):4617-26.
327. Schauvliege R, Vanrobaeys J, Schotte P, Beyaert R. Caspase-11 gene expression in response to lipopolysaccharide and interferon-gamma requires nuclear factor-kappa B and signal transducer and activator of transcription (STAT) 1. The Journal of biological chemistry. 2002;277(44):41624-30.
328. Toth CR, Hostutler RF, Baldwin AS, Jr., Bender TP. Members of the nuclear factor kappa B family transactivate the murine c-myb gene. The Journal of biological chemistry. 1995;270(13):7661-71.
329. Duyao MP, Buckler AJ, Sonenshein GE. Interaction of an NF-kappa B-like factor with a site upstream of the c-myc promoter. Proceedings of the National Academy of Sciences of the United States of America. 1990;87(12):4727-31.
330. Hannink M, Temin HM. Structure and autoregulation of the c-rel promoter. Oncogene. 1990;5(12):1843-50.
331. Guttridge DC, Albanese C, Reuther JY, Pestell RG, Baldwin AS, Jr. NF-kappaB controls cell growth and differentiation through transcriptional regulation of cyclin D1. Molecular and cellular biology. 1999;19(8):5785-99.
332. Hinz M, Krappmann D, Eichten A, Heder A, Scheidereit C, Strauss M. NF-kappaB function in growth control: regulation of cyclin D1 expression and

G0/G1-to-S-phase transition. Molecular and cellular biology. 1999;19(4):2690-8.

333. Iwanaga R, Ozono E, Fujisawa J, Ikeda MA, Okamura N, Huang Y, et al. Activation of the cyclin D2 and cdk6 genes through NF-kappaB is critical for cell-cycle progression induced by HTLV-I Tax. Oncogene. 2008;27(42):5635-42.
334. Nishi H, Neta G, Nishi KH, Akers LM, Rikiyama T, Proctor KN, et al. Analysis of the epidermal growth factor receptor promoter: the effect of nuclear factor-kappaB. International journal of molecular medicine. 2003;11(1):49-55.
335. Thornburg NJ, Raab-Traub N. Induction of epidermal growth factor receptor expression by Epstein-Barr virus latent membrane protein 1 C-terminal-activating region 1 is mediated by NF-kappaB p50 homodimer/Bcl-3 complexes. Journal of virology. 2007;81(23):12954-61.
336. Chan H, Bartos DP, Owen-Schaub LB. Activation-dependent transcriptional regulation of the human Fas promoter requires NF-kappaB p50-p65 recruitment. Molecular and cellular biology. 1999;19(3):2098-108.
337. Singh NP, Nagarkatti M, Nagarkatti PS. Role of dioxin response element and nuclear factor-kappaB motifs in 2,3,7,8-tetrachlorodibenzo-p-dioxin-mediated regulation of Fas and Fas ligand expression. Molecular pharmacology. 2007;71(1):145-57.
338. Matsui K, Fine A, Zhu B, Marshak-Rothstein A, Ju ST. Identification of two NF-kappa B sites in mouse CD95 ligand (Fas ligand) promoter: functional analysis in T cell hybridoma. Journal of immunology (Baltimore, Md : 1950). 1998;161(7):3469-73.
339. Corn RA, Hunter C, Liou HC, Siebenlist U, Boothby MR. Opposing roles for RelB and Bcl-3 in regulation of T-box expressed in T cells, GATA-3, and Th effector differentiation. Journal of immunology (Baltimore, Md : 1950). 2005;175(4):2102-10.
340. Sica A, Tan TH, Rice N, Kretzschmar M, Ghosh P, Young HA. The c-rel protooncogene product c-Rel but not NF-kappa B binds to the intronic region of the human interferon-gamma gene at a site related to an interferon-stimulable response element. Proceedings of the National Academy of Sciences of the United States of America. 1992;89(5):1740-4.
341. Sica A, Dorman L, Viggiano V, Cippitelli M, Ghosh P, Rice N, et al. Interaction of NF-kappaB and NFAT with the interferon-gamma promoter. The Journal of biological chemistry. 1997;272(48):30412-20.
342. Hoyos B, Ballard DW, Bohnlein E, Siekevitz M, Greene WC. Kappa B-specific DNA binding proteins: role in the regulation of human interleukin-2 gene expression. Science (New York, NY). 1989;244(4903):457-60.
343. Xu LG, Shu HB. TNFR-associated factor-3 is associated with BAFF-R and negatively regulates BAFF-R-mediated NF-kappa B activation and IL-10 production. Journal of immunology (Baltimore, Md : 1950). 2002;169(12):6883-9.

344. Cao S, Zhang X, Edwards JP, Mosser DM. NF-kappaB1 (p50) homodimers differentially regulate pro- and anti-inflammatory cytokines in macrophages. The Journal of biological chemistry. 2006;281(36):26041-50.
345. Hinz M, Lemke P, Anagnostopoulos I, Hacker C, Krappmann D, Mathas S, et al. Nuclear factor kappaB-dependent gene expression profiling of Hodgkin's disease tumor cells, pathogenetic significance, and link to constitutive signal transducer and activator of transcription 5a activity. The Journal of experimental medicine. 2002;196(5):605-17.
346. Brown RT, Ades IZ, Nordan RP. An acute phase response factor/NF-kappa B site downstream of the junB gene that mediates responsiveness to interleukin-6 in a murine plasmacytoma. The Journal of biological chemistry. 1995;270(52):31129-35.
347. Ten RM, Paya CV, Israel N, Le Bail O, Mattei MG, Virelizier JL, et al. The characterization of the promoter of the gene encoding the p50 subunit of NF-kappa B indicates that it participates in its own regulation. The EMBO journal. 1992;11(1):195-203.
348. Lombardi L, Ciana P, Cappellini C, Trecca D, Guerrini L, Migliazza A, et al. Structural and functional characterization of the promoter regions of the NFKB2 gene. Nucleic acids research. 1995;23(12):2328-36.
349. Haskill S, Beg AA, Tompkins SM, Morris JS, Yurochko AD, Sampson-Johannes A, et al. Characterization of an immediate-early gene induced in adherent monocytes that encodes I kappa B-like activity. Cell. 1991;65(7):1281-9.
350. Sun SC, Ganchi PA, Ballard DW, Greene WC. NF-kappa B controls expression of inhibitor I kappa B alpha: evidence for an inducible autoregulatory pathway. Science (New York, NY). 1993;259(5103):1912-5.
351. Tian B, Nowak DE, Jamaluddin M, Wang S, Brasier AR. Identification of direct genomic targets downstream of the nuclear factor-kappaB transcription factor mediating tumor necrosis factor signaling. The Journal of biological chemistry. 2005;280(17):17435-48.
352. Collart MA, Baeuerle P, Vassalli P. Regulation of tumor necrosis factor alpha transcription in macrophages: involvement of four kappa B-like motifs and of constitutive and inducible forms of NF-kappa B. Molecular and cellular biology. 1990;10(4):1498-506.
353. Wu H, Lozano G. NF-kappa B activation of p53. A potential mechanism for suppressing cell growth in response to stress. The Journal of biological chemistry. 1994;269(31):20067-74.
354. Schumm K, Rocha S, Caamano J, Perkins ND. Regulation of p53 tumour suppressor target gene expression by the p52 NF-kappaB subunit. The EMBO journal. 2006;25(20):4820-32.

Appendices

Appendix Table 1. Next-generation sequencing studies performed on advanced stage MF and SS tumours. WGS: whole-genome sequencing, WES: whole-exome sequencing, TCS: targeted capture sequencing, CNV: copy number variation analysis, RNA: whole-transcriptome analysis.

Malignancy	Reference	WGS	WES	TCS	CNV	RNA
MF	Vaqué *et al.* 2014 (160)			✓		
MF	McGirt *et al*. 2015 (148)	✓		✓		
MF	Ungewickell *et al*. 2015 (71)		✓	✓	✓	
MF	da Silva Almeida *et al*. 2015 (69)		✓		✓	
SS	Vaqué *et al.* 2014 (160)			✓		
SS	Choi *et al*. 2015 (67)	✓	✓	✓	✓	✓
SS	Kiel *et al.* 2015 (68)	✓	✓		✓	
SS	Wang *et al*. 2015 (70)		✓	✓		✓
SS	da Silva Almeida *et al*. 2015 (69)		✓		✓	
SS	Prasad *et al*. 2016 (161)		✓		✓	✓
SS	Woollard *et al*. 2016 (147)		✓	✓	✓	

Appendix Table 2. NFAT target genes and functions.

Gene	Target gene function	References
BDNF	Stimulates neuronal growth and differentiation	(313)
CD40LG	Co-stimulatory T-cell ligand	(196, 314, 315)
CD5	Regulates anti-tumour immune responses of T-cells	(196, 316)
c-myc	Proto-oncogene, stimulates proliferation	(317)
CSF2	Stimulates proliferation	(196)
EGR-1	Transcriptional regulator	(313)
FASLG	Stimulates apoptosis	(196, 314)
IFNG	Cytokine produced by Th1 cells	(196, 314)
IGF1	Stimulates proliferation	(313)
IL10	Cytokine produced by Th2 cells	(313)
IL12	Th1-inducing cytokine	(313)
IL13	Cytokine produced by Th2 cells	(196, 313)
IL1b	Pro-inflammatory cytokine	(318)
IL2	Cytokine secreted by T-cells	(196, 313, 314)
IL2RA	CD25; IL-2 receptor α-chain; mediates IL-2 signalling in T-cells	(196)
IL4	Th2-inducing cytokine	(314, 317)
IL5	Cytokine produced by Th2 cells	(196, 318)
IL6	Th17-inducing cytokine	(313)
IP3R1	IP_3 receptor	(313)
NFKB1	DNA binding subunit of the NFκB	(318)
RCAN1-4	Negative regulators of calcineurin	(313)
REL	Proto-oncogene, stimulates survival and proliferation	(318)
TGFB1	Regulates growth, proliferation, differentiation and apoptosis	(313)
TNF	Regulates proliferation and apoptosis	(196, 313, 314)

Appendix Table 3. AP-1 target genes and functions.

Gene	Target gene function	References
BCL2	Inhibits apoptosis	(319)
BCL2L1	Inhibits apoptosis	(319)
BCL2L11	Stimulates apoptosis	(319)
BCL3	Inhibits apoptosis	(319)
CCND1	Cyclin D1; cell cycle progression regulator	(319)
CDKN1A	Inhibits proliferation	(319)
CDKN2A	Tumour suppressor, inhibits proliferation, stimulates apoptosis	(319)
CSF2	Stimulates proliferation	(319)
DNMT1	Epigenetic regulator	(319)
EGFR	Stimulates proliferation	(319)
FAS	Cell surface death receptor	(319)
FASLG	Stimulates apoptosis	(320)
FGF7	Stimulates proliferation	(319)
HBEGF	Stimulates proliferation	(319)
IFNG	Cytokine produced by Th1 cells	(321)
IL13	Cytokine produced by Th2 cells	(196)
IL2RA	CD25; IL-2 receptor α-chain; mediates IL-2 signalling in T-cells	(196)
IL4	Th2-inducing cytokine	(196)
IL5	Cytokine produced by Th2 cells	(196)
TP53	Inhibits proliferation, stimulates apoptosis	(319)
VEGFD	Stimulates proliferation	(319)

Appendix Table 4. NFκB target genes and functions.

Genes	Target gene function	References
Bax	Stimulates apoptosis	(322)
BCL-2	Inhibits apoptosis	(323)
BCL-3	Inhibits apoptosis	(324)
BRCA2	Tumour suppressor	(325)
BTK	Stimulates proliferation	(326)
CASP4	Apoptosis regulator	(327)
c-myb	Proto-oncogene	(328)
c-myc	Proto-oncogene	(329)
c-rel	Proto-oncogene	(330)
CCND1	Cyclin D1; cell cycle progression regulator	(331, 332)
CCND2	Cyclin D2; cell cycle progression regulator	(333)
EGFR	Stimulates proliferation	(334, 335)
FAS	Cell surface death receptor	(336, 337)
FASLG	Stimulates apoptosis	(337, 338)
GATA3	T-cell differentiation	(339)
IFNG	Cytokine produced by Th1 cells	(340, 341)
IL2	Cytokine produced by Th1 cells	(342)
IL10	Cytokine produced by Th2 cells	(343, 344)
IL13	Cytokine produced by Th2 cells	(345)
JUNB	Proto-oncogene	(346)
NFKB1	NFkB p105 subunit precursor	(347)
NFKB2	NFkB p100 subunit precursor	(348)
NFKBIA	IkB-α; NFkB inhibitor	(349, 350)
NFKBIE	IkB-ε: NFkB inhibitor	(351)
STAT5A	Stimulates proliferation	(345)
TNF	Regulates proliferation and apoptosis	(352)
TP53	Tumour suppressor, inhibits proliferation, stimulates apoptosis	(353, 354)

Sample	Sample no.	Chromatogram
Wild-type	-	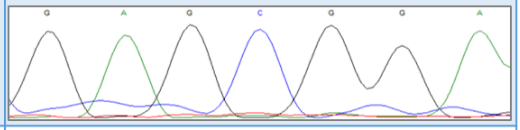
Blood	8004B	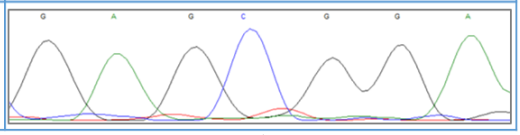

c.C142T; p.R48W

Appendix Figure 1. The *PLCG1* c.C142T; p.R48W mutation in patient 2.

Sample	Sample no.	Chromatogram
Wild-type	-	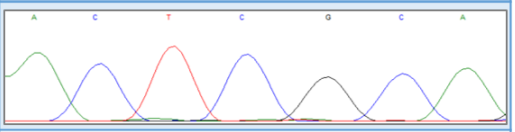
Blood	L11_0158B	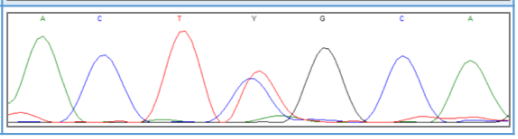

c.C935T; p.S312L

Appendix Figure 2. The *PLCG1* c.C935T; p.S312L mutation in patient 3.

Sample	Sample no.	Chromatogram
Wild-type	-	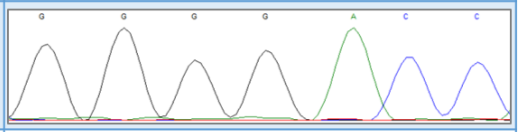
Blood	3297B	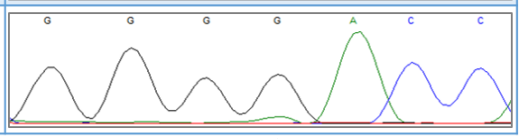

c.G1024A; p.D342N

Appendix Figure 3. The *PLCG1* c.G1024A; p.D342N mutation in patient 4. Sequencing and analysis were performed by Dr. Begum.

Sample	Sample no.	Chromatogram
Wild-type	-	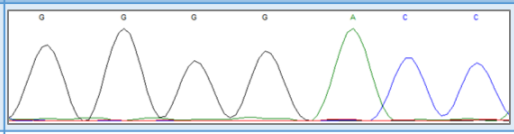
Blood	8344b	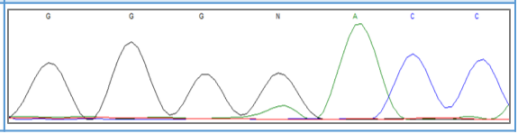

c.G1024A; p.D342N

Appendix Figure 4. The *PLCG1* c.G1024A; p.D342N mutation in patient 5. Sequencing and analysis were performed by Dr. Begum.

Sample	Sample no.	Chromatogram
Wild-type	-	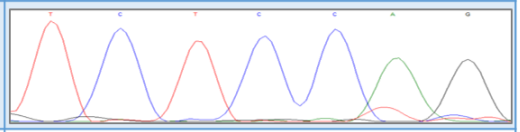
Blood	3451B	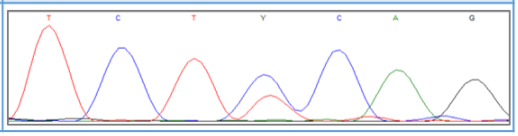

c.C1034T; p.S345F

Appendix Figure 5. The *PLCG1* c.C1034T; p.S345F mutation in patient 6. Sequencing and analysis were performed by Dr. Begum.

Sample	Sample no.	Chromatogram
Wild-type	-	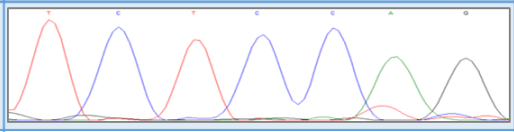
Blood	9308B	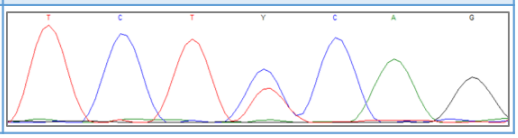

c.C1034T; p.S345F

Appendix Figure 6. The *PLCG1* c.C1034T; p.S345F mutation in patient 7. Sequencing and analysis were performed by Dr. Begum.

Sample	Sample no.	Chromatogram
Wild-type	-	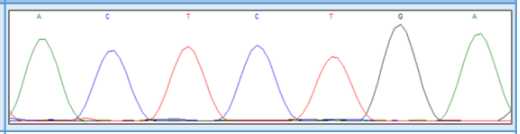
Blood	4736B	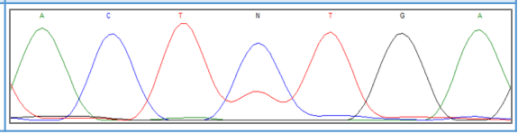

c.C1559T; p.S520F

Appendix Figure 7. The *PLCG1* c.C1559T; p.S520F mutation in patient 8.

Sample	Sample no.	Chromatogram
Wild-type	-	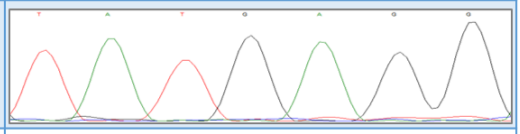
Blood	L12_0697B	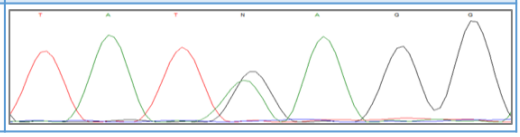

c.G3487A; p.E1163K

Appendix Figure 8. The *PLCG1* c.G3487A; p.E1163K mutation in patient 9.

Sample	Sample no.	Chromatogram
Wild-type	-	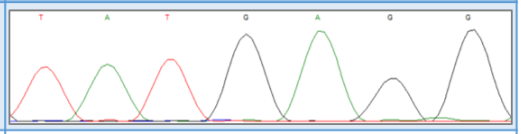
Blood	4142B	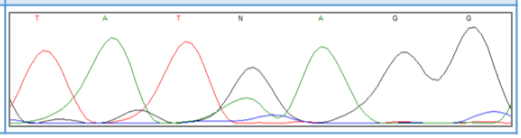

c.G3487A; p.E1163K

Appendix Figure 9. The *PLCG1* c.G3487A; p.E1163K mutation in patient 10.

Sample	Sample no.	Chromatogram
Wild-type	-	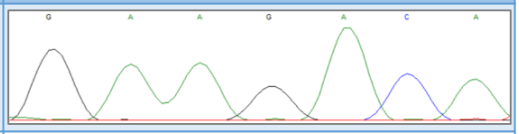
Blood	4346B	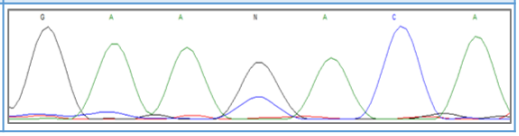

c.G3493C; p.D1165H

Appendix Figure 10. The *PLCG1* c.G3493C; p.D1165H mutation in patient 11.

Tumour compartment	Enriched CD4+ cells?	Template	Months post diagnosis	Chromatogram
Healthy control	x	DNA	-	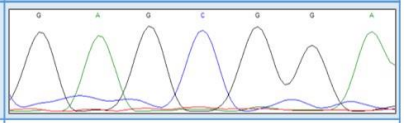
Peripheral blood	x	DNA	2	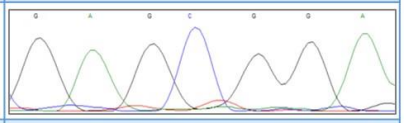
Lesional skin	x	DNA	2	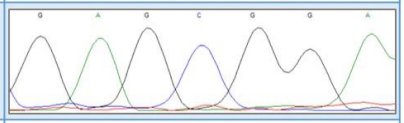
Peripheral blood	x	DNA	12	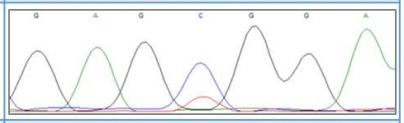
Peripheral blood	✓	cDNA	12	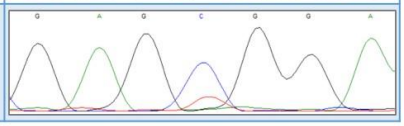

c.C142T; p.R48W

Appendix Figure 11. The *PLCG1* c.C142T; p.R48W mutation persists in multiple tumour compartments for 1 year in patient 2. DNA from a healthy control individual was sequenced to show the wild-type allele in the top panel.

Tumour compartment	Enriched CD4+ cells?	Template	Months post diagnosis	Chromatogram
Healthy control	x	DNA	-	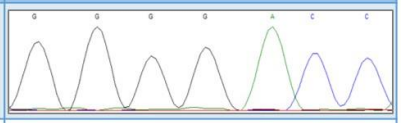
Peripheral blood	x	DNA	0	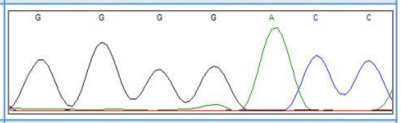
Lesional skin	x	DNA	0	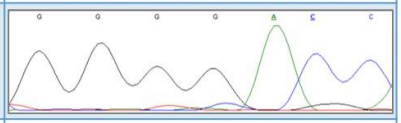
Peripheral blood	x	DNA	4	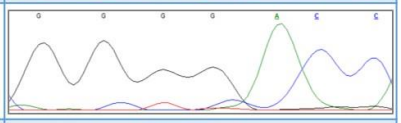
Peripheral blood	x	DNA	9	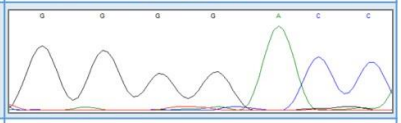
Peripheral blood	x	DNA	23	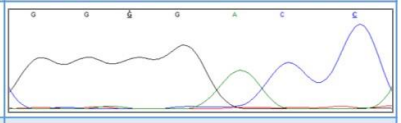
Lesional skin	x	DNA	82	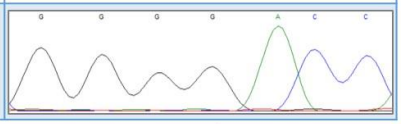

c.G1024A; p.D342N

Appendix Figure 12. The *PLCG1* c.G1024A; p.D342N mutation in a diagnostic blood sample from patient 4. The mutation was absent thereafter as the patient developed lymphopenia from multiple therapies including chemotherapy, biologics and retinoids and Campath monoclonal antibody therapy. DNA from a healthy control individual was sequenced to show the wild-type allele in the top panel.

Tumour compartment	Enriched CD4+ cells?	Template	Months post diagnosis	Chromatogram
Healthy control	x	DNA	-	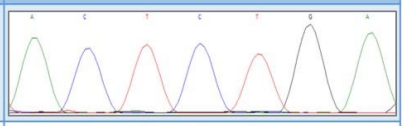
Peripheral blood	x	DNA	4	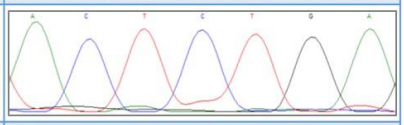
Peripheral blood	x	DNA	18	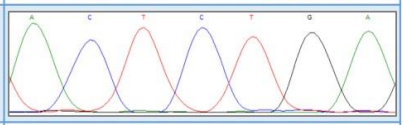
Peripheral blood	x	DNA	24	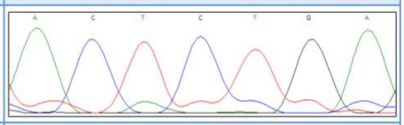
Peripheral blood	x	DNA	35	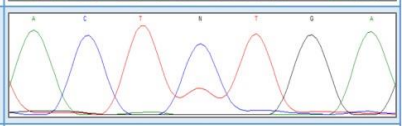
Peripheral blood	x	DNA	81	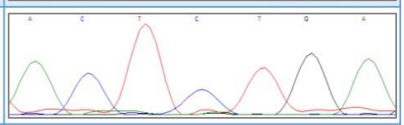
Peripheral blood	✓	cDNA	106	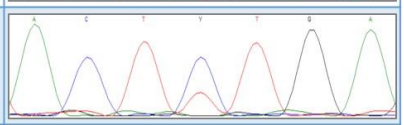
Peripheral blood	x	DNA	181	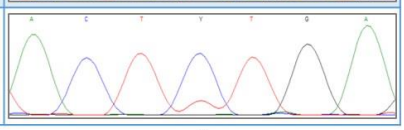

Appendix Figure 13. The *PLCG1* c.C1559T; p.S520F mutation persists for 15 years in patient 8. Fluctuations in the tumour burden may account for the variable intensity of the mutant allele detected. DNA from a healthy control individual was sequenced to show the wild-type allele in the top panel.

Tumour compartment	Enriched CD4+ cells?	Template	Months post diagnosis	Chromatogram
Healthy control	x	DNA	-	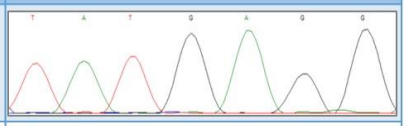
Peripheral blood	x	DNA	0	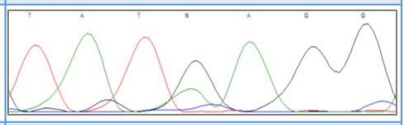
Lesional skin	x	DNA	0	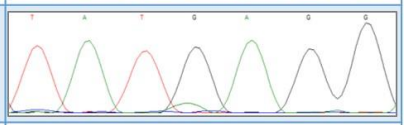
Lymph node	x	DNA	0	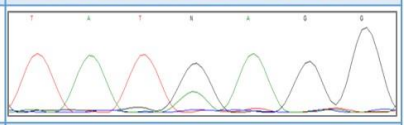
Lesional skin	x	DNA	6	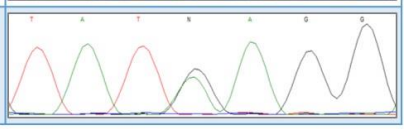

c.G3487A; p.E1163K

Appendix Figure 14. The *PLCG1* c.G3487A; p.E1163K mutation in multiple tumour compartments in patient 10. DNA from a healthy control individual was sequenced to show the wild-type allele in the top panel.

Tumour compartment	Enriched CD4+ cells?	Template	Months post diagnosis	Chromatogram
Healthy control	x	DNA	-	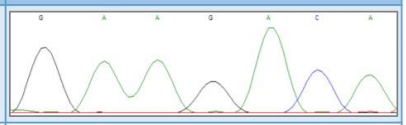
Peripheral blood	x	DNA	0	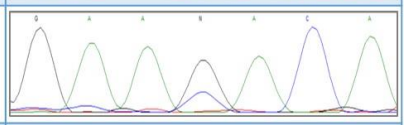
Peripheral blood	x	DNA	1	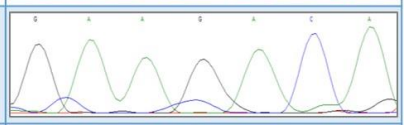
Peripheral blood	x	DNA	4	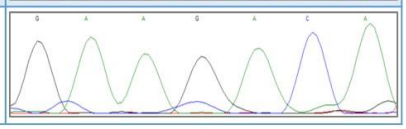

c.G3493C; p.D1165H

Appendix Figure 15. The *PLCG1* c.G3493C; p.D1165H mutation persists in patient 11. DNA from a healthy control individual was sequenced to show the wild-type allele in the top panel.

Cell line	Chromatogram
Wild-type	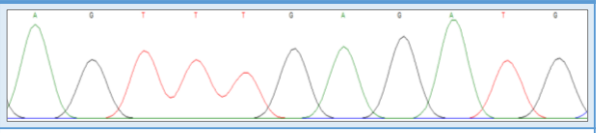
CY-6 (Carrier ATLL)	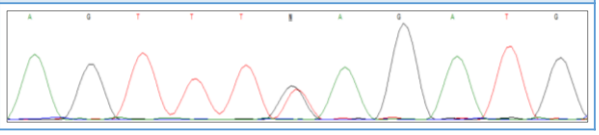

E650STOP

Appendix Figure 16. The heterozygous *PLCG1* c.G1948T; p.E650STOP variant in the CY-6 cell line.

Cell line	Chromatogram
Wild-type	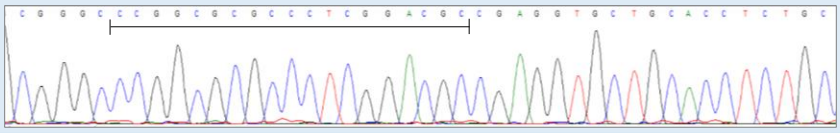
LMY2 (Acute ATLL) Forward	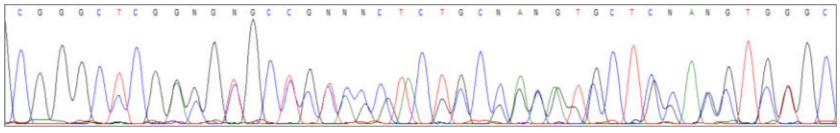
LMY2 (Acute ATLL) Reverse	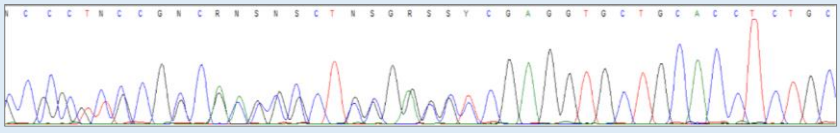

c.CCGGCGCGCCCTCGGACGC41del-insT; p.P14L

Appendix Figure 17. The heterozygous PLCγ1 p.P14L indel in the LMY2 cell line.

Publication

Frequent and Persistent *PLCG1* Mutations in Sézary Cells Directly Enhance PLCγ1 Activity and Stimulate NFκB, AP-1, and NFAT Signaling

Varsha M. Patel[1,4], Charlotte E. Flanagan[1,4], Marta Martins[2], Christine L. Jones[1], Rosie M. Butler[1], Wesley J. Woollard[1], Farrah S. Bakr[1], Antoinette Yoxall[1], Nelema Begum[1], Matilda Katan[3], Sean J. Whittaker[1] and Tracey J. Mitchell[1]

Phospholipase C Gamma 1 (*PLCG1*) is frequently mutated in primary cutaneous T-cell lymphoma (CTCL). This study functionally interrogated nine *PLCG1* mutations (p.R48W, p.S312L, p.D342N, p.S345F, p.S520F, p.R1158H, p.E1163K, p.D1165H, and the in-frame indel p.VYEEDM1161V) identified in Sézary Syndrome, the leukemic variant of CTCL. The mutations were demonstrated in diagnostic samples and persisted in multiple tumor compartments over time, except in patients who achieved a complete clinical remission. In basal conditions, the majority of the mutations confer PLCγ1 gain-of-function activity through increased inositol phosphate production and the downstream activation of NFκB, AP-1, and NFAT transcriptional activity. Phosphorylation of the p.Y783 residue is essential for the proximal activity of wild-type PLCγ1, but we provide evidence that activating mutations do not require p.Y783 phosphorylation to stimulate downstream NFκB, NFAT, and AP-1 transcriptional activity. Finally, the gain-of-function effects associated with the p.VYEEDM1161V indel suggest that the C2 domain may have a role in regulating PLCγ1 activity. These data provide compelling evidence to support the development of therapeutic strategies targeting mutant PLCγ1.

Journal of Investigative Dermatology (2019) ■, ■–■; doi:10.1016/j.jid.2019.07.693

INTRODUCTION

Cutaneous T-cell lymphoma (CTCL) is an extra-nodal mature T-cell lymphoma derived from skin-homing memory $CD4^+$ T-cells (Kim et al., 2005). Sézary Syndrome (SS) is a rare leukemic subtype of CTCL, closely related to Mycosis Fungoides (MF), and is associated with a dismal prognosis and an urgent need for effective therapies (Swerdlow, 2017).

Recent next generation sequencing (NGS) studies, including our own work, have identified the dysregulation of T-cell signaling and differentiation pathways as a defining feature of mature T-cell lymphomas, including CTCL (Choi et al., 2015; da Silva Almeida et al., 2015; Kataoka et al., 2015; Kiel et al., 2015; Kiel et al., 2014; McGirt et al., 2015; McKinney et al., 2017; Palomero et al., 2014; Prasad et al., 2016; Sakata-Yanagimoto et al., 2014; Simpson et al., 2015; Ungewickell et al., 2015; Vallois et al., 2016; Vaqué et al., 2014; Wang et al., 2015; Wang et al., 2017; Woollard et al., 2016; Yoo et al., 2014). After *TP53*, the PLCγ1 gene *PLCG1,* has been identified as the second most commonly mutated gene in SS (Chang et al., 2018; Park et al., 2017) and is also frequently mutated in advanced stage MF (McGirt et al., 2015; Ungewickell et al., 2015; Vaqué et al., 2014), and adult T-cell leukemia/lymphoma (Kataoka et al., 2015). PLCγ1 plays a pivotal role in T-cell receptor (TCR) signaling and is activated by receptor and non-receptor tyrosine kinases, which trigger signaling cascades to activate the transcription factors NFκB, NFAT, and AP-1 (Smith-Garvin et al., 2009). These transcription factors regulate the expression of genes involved in cell proliferation, survival, differentiation, and death (Smith-Garvin et al., 2009). Nuclear accumulation and constitutive activation of NFκB signaling has been consistently reported in Sézary cells and CTCL cell lines, but the underlying mechanism remains unexplained (Giri and Aggarwal, 1998; O'Connell et al., 1995; Sors et al., 2006). Increased NFκB activity is also a key feature of other mature T-cell lymphomas, including adult T-cell leukemia/lymphoma and sub-types of peripheral T-cell lymphomas (Martínez-Delgado et al., 2005; Yamagishi and Watanabe, 2012). Elevated NFκB activation induces the expression of anti-apoptotic genes, including *BCL-2*, leading to apoptosis resistance, another hallmark of CTCL (Juvekar et al., 2011).

This study investigates the functional effects of nine *PLCG1* mutations reported in SS patients on PLCγ1 activity. We show that 5 of 9 variants confer the constitutive activation of PLCγ1 as demonstrated by the significant induction of downstream NFκB, NFAT, and AP-1 transcriptional activity and increased proximal activity in basal conditions, as well as confirming previous findings showing the induction of NFAT transcriptional activity. Furthermore, we provide evidence that these

[1]St. John's Institute of Dermatology, School of Basic & Medical Biosciences, King's College London, Guy's Hospital, London, United Kingdom; [2]Insituto de Medicina Molecular- João Lobo Antunes, Faculdade de Medicina, Universidade de Lisboa, Lisboa, Portugal; and [3]Structural and Molecular Biology, Division of Biosciences, University College London, United Kingdom

[4]These authors contributed equally to this work.

Correspondence: Tracey Mitchell. St. John's Institute of Dermatology, School of Basic & Medical Biosciences, King's College London, Guy's Hospital, London, SE1 9RT, United Kingdom. E-mail: tracey.mitchell@kcl.ac.uk

Abbreviations: CTCL, cutaneous T-cell lymphoma; IP, inositol phosphate; MF, Mycosis Fungoides; NGS, next generation sequencing; SS, Sézary Syndrome; TCR, T-cell receptor

Received 24 December 2018; revised 17 June 2019; accepted 1 July 2019; accepted manuscript published online 31 July 2019; corrected proof published online XXX

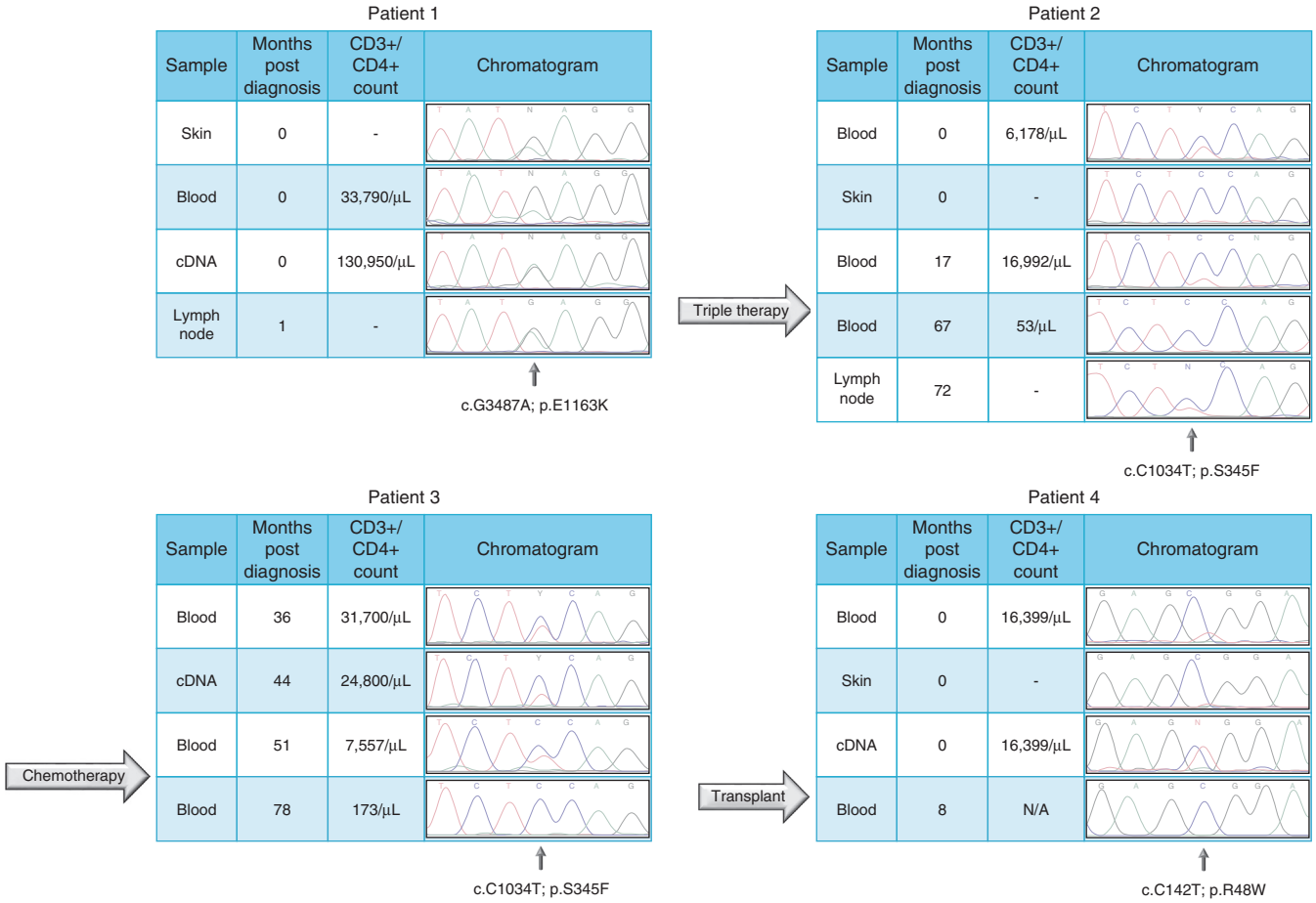

Figure 1. Persistence of mutant *PLCG1* alleles in multiple tumor compartments in SS patients. Sanger sequencing of the DNA extracted from PBMCs, lesional skin biopsies and involved lymph nodes. RNA was isolated from enriched $CD4^+$ tumor cells and reverse transcribed into cDNA. The chromatograms were analyzed using the FinchTV software. $CD3^+/CD4^+$ counts/µl are shown as a proxy for tumor burden. N/A, but no diagnostic TCR clonal gene rearrangement was detected in the post-transplant sample. N/A, $CD3^+/CD4^+$ unavailable; PBMC, peripheral blood mononuclear cells; TCR, T-cell receptors.

gain-of-function mutations increase downstream signaling without phosphorylation of the PLCγ1 p.Y783 residue. We also propose a role for C2 domain residues in the regulation of PLCγ1 activity, and our findings suggest that mutant PLCγ1 proteins represent potential therapeutic targets in CTCL.

RESULTS

Persistence of *PLCG1* mutations in multiple SS tumor compartments

Our recent NGS study identified seven coding *PLCG1* mutations in tumor cells from 11 SS patients, including four recurrent aberrations (p.R48W, p.D342N, p.S345F, and p.E1163K) (Woollard et al., 2016). In this study, Sanger sequencing confirmed all 11 mutations in DNA from diagnostic blood samples and demonstrated persistence in different tumor compartments, including serial blood samples, lesional skin, involved lymph nodes, and RNA extracted from tumor-enriched peripheral blood $CD4^+$ T-cells. Using four representative cases, we demonstrate that *PLCG1* mutations persist several years after diagnosis in multiple tumor compartments, strongly implicating their role as driver mutations (Figure 1). In Sézary cells from patient 1, the p.E1163K mutation was detected in all four tumor compartments at diagnosis. In patient 2, the p.S345F mutation persisted in the blood for 17 months after diagnosis but was not detected after triple therapy (interferon-α, photopheresis, and bexarotene) led to resolution of the leukemic disease. Subsequently, the mutation was detected in an involved lymph node when the patient developed nodal progression at 72 months. In patient 3, the p.S345F mutation was detected in the blood and Sézary cell-derived RNA up to 51 months after diagnosis but was absent in the blood 78 months post diagnosis at the time of a complete clinical remission following chemotherapy. Finally, in patient 4, the p.R48W mutation was detected in the blood and at the transcriptional level at diagnosis but not in lesional skin, which is likely attributed to a lack of detection sensitivity associated with a sparse cutaneous tumor cell infiltrate. The mutant allele and clonal TCR rearrangement were absent in the blood after the patient achieved complete remission following allogeneic hematopoietic stem cell transplantation.

PLCG1 mutations are frequent in CTCL and other mature T-cell lymphomas

To identify the most frequent *PLCG1* mutations and those to prioritize for functional studies, we performed a comprehensive analysis of previously published NGS studies (whole-exome and targeted gene sequencing) on CTCL and other

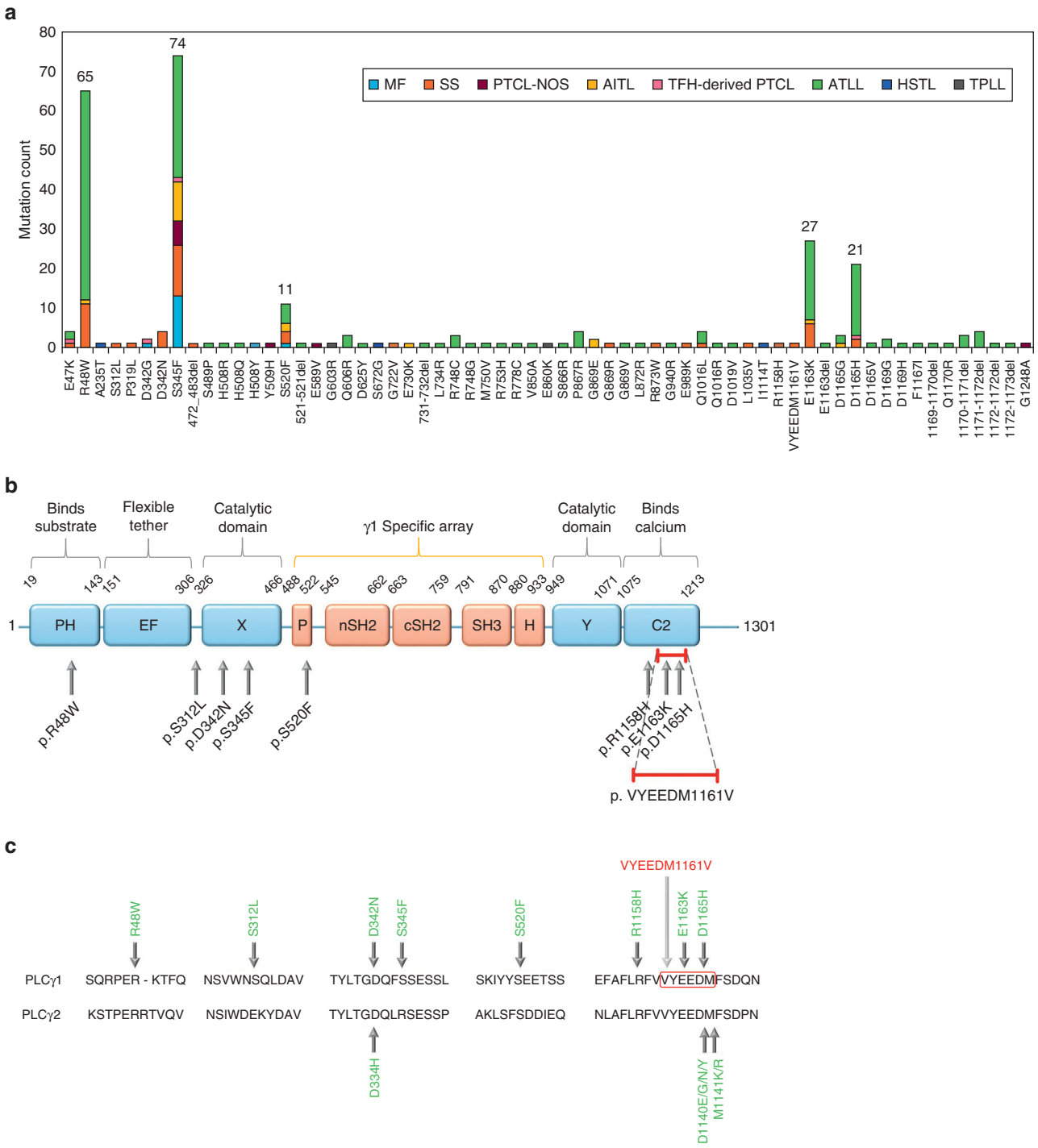

Figure 2. *PLCG1* is frequently mutated in mature T-cell lymphomas. (**a**) PLCγ1 mutations identified by next generation sequencing of different mature T-cell lymphomas were plotted to determine the incidence of each mutation per disease type. (**b**) Schematic representation of the eight missense mutations and one in-frame indel (p.VYEEDM1161V) examined in this study mapped to the PLCγ1 functional protein domains. (**c**) PLCγ1 and PLCγ2 residues were aligned using the Clustal Omega software. PLCγ1 mutations analyzed in this study and the corresponding PLCγ2 mutations reported in B-cell ibrutinib-resistant chronic lymphocytic leukemia are shown. AITL, angioimmunoblastic T-cell lymphomas; ATLL, adult T-cell leukemia/lymphoma; HSTL, hepatosplenic T-cell lymphoma; MF, Mycosis Fungoides; SS, Sézary Syndrome; PTCL-nos, peripheral T-cell lymphomas-not otherwise specified; TFH-derived PTCL, follicular helper T-cell-derived lymphomas; TPLL, T-cell-prolymphocytic leukemia.

mature T-cell lymphomas (Supplementary Table S1). *PLCG1* mutations were found in 36.2% of adult T-cell leukemia/lymphomas, 18.2% of peripheral T-cell lymphomas-not otherwise specified, 15% of hepatosplenic T-cell lymphomas, 12% of angioimmunoblastic T-cell lymphomas, 11.8% of CTCLs (MF and SS), and 5.6% of T-cell-prolymphocytic leukemias but not identified in anaplastic large cell lymphomas, enteropathy-associated T-cell lymphomas, and natural killer/T-cell lymphomas. Collating all the mutations reported by NGS studies demonstrated that *PLCG1* harbors five hotspot

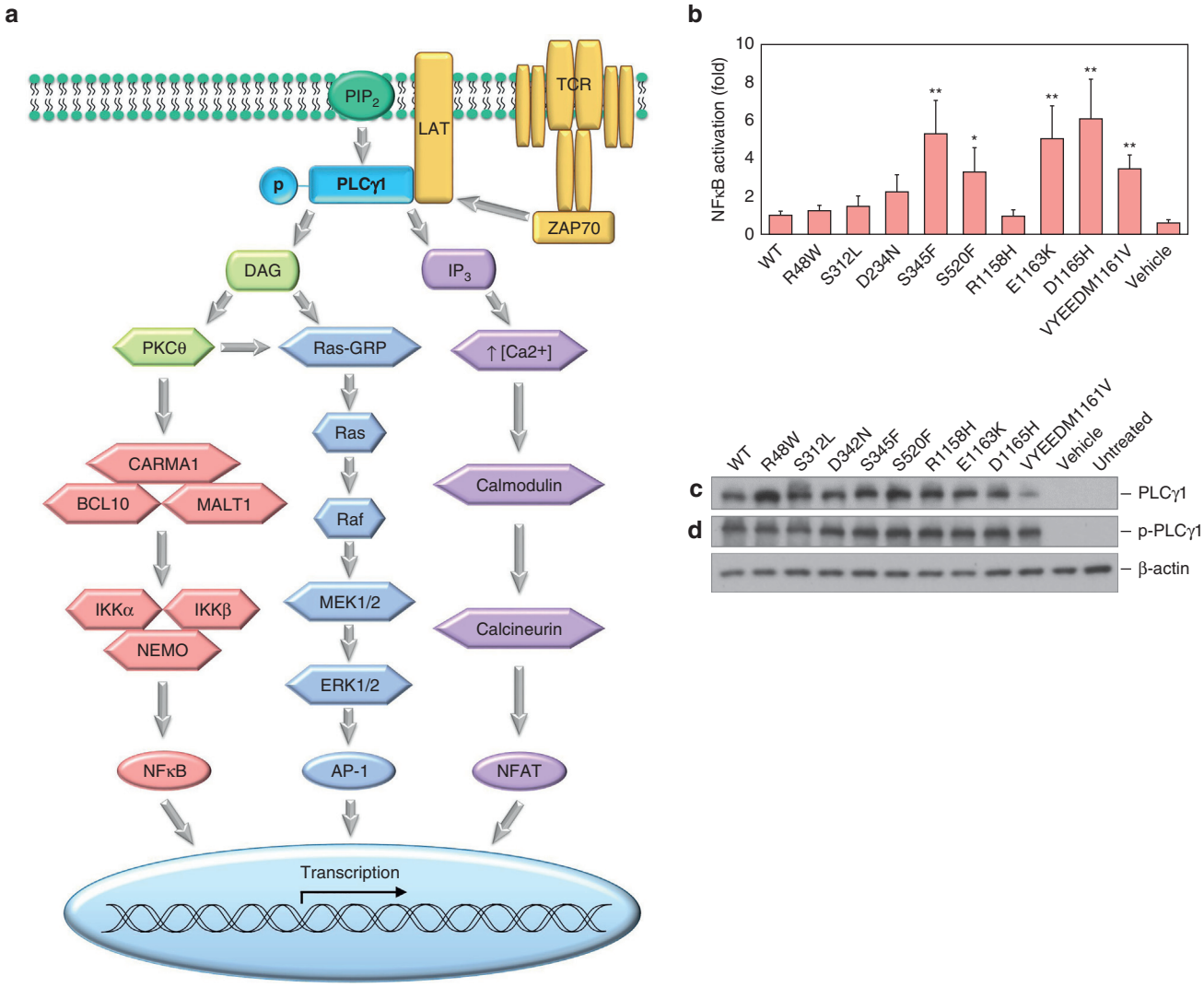

Figure 3. PLCγ1 mutations increase NFκB transcriptional activity. (**a**) Schematic representation of PLCγ1 mediating TCR signaling via IP_3 and DAG to the NFκB, AP-1, and NFAT transcription factors. (**b**) HEK293 cells were co-transfected with PLCγ1-pTriEx-4, pRL-TK Renilla-luciferase, and NFκB-firefly-luciferase plasmids. Cells were starved overnight, and their transcriptional activity was analyzed. Activation fold changes were normalized to cells overexpressing wild-type PLCγ1. Data is represented as the mean ± the standard error of the mean; $n = 4$. Student's *t*-test, $^{*}P < 0.05$, $^{**}P < 0.01$, $^{***}P < 0.001$. (**c, d**) HEK293 cells were transfected with PLCγ1-pTriEx-4 vectors and treated with 100 μM pervanadate before they were harvested. Lysates were probed with (**c**) an anti-PLCγ1 antibody and (**d**) an anti-p-PLCγ1 antibody to analyze the total and phosphorylated protein expression, respectively, relative to β-actin expression as a loading control. DAG, diacylglycerol; IP_3, inositol trisphosphate; TCR, T-cell receptors; WT, wild-type.

mutations (p.R48W, p.S345F, p.S520F, p.E1163K, and p.D1165H) (Figure 2a) with p.S345F being the most frequently reported in 74 individual tumors. All five mutations were detected in the SS tumors in our NGS study (Woollard et al., 2016). The seven *PLCG1* mutations (p.R48W, p.S345F, p.S520F, p.E1163K, p.D1165H, p.S312L, and p.D342N) confirmed by Sanger sequencing and two additional variants reported in SS (p.R1158H and the p.VYEEDM1161V indel) (Kiel et al., 2015) were selected for further analyses (Figure 2b). Pathogenicity predictions suggested that all but one of these mutations (p.S312L) are predicted to be damaging by a consensus drawn from 5 of 6 algorithms for missense mutations and 3 of 4 algorithms for the indel (see Supplementary Table S2). PLCγ2 is an isozyme of PLCγ1, and both have high protein sequence identity in all critical functional domains (Koss et al., 2014). PLCγ2 has an analogous role to PLCγ1 and is a critical mediator of B-cell receptor signaling (Koss et al., 2014). Aligning the isozyme sequences revealed that the PLCγ1 p.D342N, p.D1165H, and p.M1166 (deleted in p.VYEEDM1161V) mutant residues correspond to the PLCγ2 p.D334H, p.D1140E/G/N/Y, and p.M1141K/R mutations somatically acquired in B-cell ibrutinib-resistant chronic lymphocytic leukemia (Figure 2c) (Burger et al., 2016; Jones et al., 2017; Maddocks et al., 2015).

Gain-of-function PLCγ1 mutations drive NFκB transcriptional activation

We generated mutant constructs for the nine PLCγ1 mutations and compared activity and expression with the wild-type PLCγ1 using an NFκB luciferase reporter assay and western blotting in HEK293 cells. In basal conditions, 5 of 9

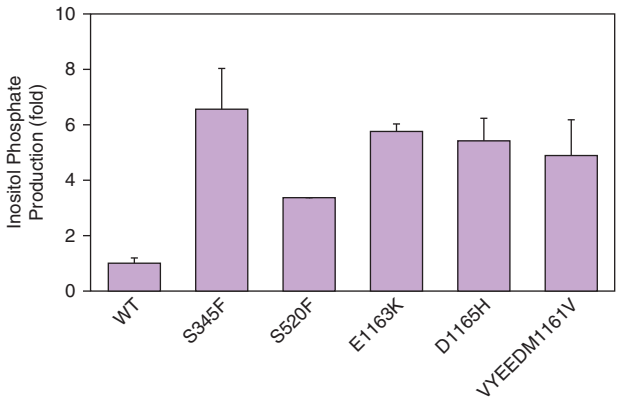

Figure 4. PLCγ1 mutations elevate proximal signaling. COS-7 cells were transfected with PLCγ1-pTriEx-4 vectors, and IP production was quantified by liquid scintillation counting. The IP production was normalized to cells overexpressing wild-type PLCγ1. The data are represented as the mean ± standard deviation and are representative of two independent experiments. IP, inositol phosphate; WT, wild-type.

mutant PLCγ1 proteins (p.S345F, p.S520F, p.E1163K, p.D1165H, and p.VYEEDM1161V) significantly increased NFκB transcriptional activity 3.3 − 6.1-fold relative to the wild-type protein ($P \leq 0.03$), suggesting that they represent gain-of-function mutations (Figure 3b).

Next, we sought to confirm previous reports showing that PLCγ1 mutations can activate NFAT transcriptional activity in basal conditions. Our data is entirely consistent with published findings (Vallois et al., 2016; Vaqué et al., 2014) and confirm that the p.S345F, p.S520F, p.E1163K, and p.D1165H mutations significantly elevate NFAT transcriptional activity 3.3 − 4.8-fold relative to the wild-type ($P \leq 0.0013$; Supplementary Figure S1). However, in addition, we found that the p.VYEEDM1161V indel was the most potent activator (10-fold; $P < 0.0001$) of the NFAT transcriptional activity compared to the other mutant proteins. Interestingly and consistent with a published report (Vallois et al., 2016), in HEK293T cells, p.R48W had no significant effect on NFAT transcriptional activity compared to the wild-type protein.

Western blotting detected a reduction in the total mutant PLCγ1 expression associated with the p.VYEEDM1161V indel, while all other mutant proteins had expression comparable to that of the wild-type protein (Figure 3c). However, a PLCγ1 p.Y783 phosphorylation-specific (p-PLCγ1) antibody revealed that the p.VYEEDM1161V indel is associated with increased protein phosphorylation relative to total PLCγ1 expression, while the other mutations showed levels of phosphorylation similar to that of the wild-type protein (Figure 3d).

PLCγ1 mutations activate proximal signaling in basal conditions through a direct increase in inositol phosphate production

To confirm the observed gain-of-function in transcriptional activity associated with the five PLCγ1 mutations in basal conditions, proximal PLCγ1 signaling was investigated. PLCγ1 hydrolyzes phosphatidylinositol 4,5-bisphosphate to produce IP_3 and diacylglycerol. IP_3 releases intracellular calcium to activate calmodulin/calcineurin signaling and drive NFAT activation (Hogan et al., 2003). We used our previously published method (Everett et al., 2009) to assay inositol phosphate (IP) production in COS-7 cells transfected with PLCγ1 gain-of-function mutants (p.S345F, p.S520F, p.E1163K, p.D1165H, and p.VYEEDM1161V) and wild-type constructs. Consistent with the transcriptional activation data, all five mutations were associated with a 3.4 − 6.6-fold increase in IP production than that of the wild-type PLCγ1 in basal conditions (Figure 4).

PLCγ1 p.R48W is activating in a T-cell line

Given the high incidence rate of p.R48W in SS (Figure 2a), it was surprising that this variant lacked gain-of-function properties. Therefore, to exclude the possibility that our findings were cell line-specific, we tested the two most common variants reported in CTCL (p.R48W and p.S345F) in T-cell lines. Overexpression of PLCγ1 in the SS-derived cell line SeAx and Jurkat cell lines was associated with high cytotoxicity (data not shown), which has also been reported in other lymphoid cell lines (Vaqué et al., 2014). Therefore, we used the J.gamma1 T-cell lymphoma line (Irvin et al., 2000), which is a *PLCG1* null line derived from Jurkat cells. The absence of PLCγ1 expression in the J.gamma1 cells compared with the parent Jurkat cell line was confirmed by western blotting (Figure 5a). In basal conditions, p.R48W significantly increased NFAT and AP-1 transcriptional activity 2.47- and 2.35-fold, respectively, relative to the wild-type ($P \leq 0.001$; Figure 5b and c). NFκB activity was also increased (Figure 5d). However, this finding was not statistically significant, which may be attributed to the high levels of endogenous NFκB activity in this cell line (data not shown). In addition, p.S345F significantly activated NFκB, AP-1 (both $P \leq 0.05$), and NFAT ($P \leq 0.001$), consistent with the data in the HEK293 cells.

Phosphorylation of p.Y783 is not essential for transcriptional activation by gain-of-function PLCγ1 mutations

In normal physiological conditions, activation of the wild-type PLCγ enzymes is associated with the phosphorylation of specific tyrosine residues in the highly conserved PLCγ-specific array domains by receptor and non-receptor tyrosine kinases (Koss et al., 2014). Moreover, studies have shown that mutating the PLCγ1 p.Y783 residue (to p.Y783F) drastically reduces but does not obliterate IP production in vitro (Bunney et al., 2012; Poulin et al., 2005). To determine whether the activating mutations require p.Y783 phosphorylation to increase downstream transcriptional activity, the phosphorylation residue was mutated to p.Y783F in plasmids harboring the p.S345F, p.S520F, and p.E1163K mutations. These mutations were chosen to represent bona fide gain-of-function mutations in specific PLCγ1 domains, namely the catalytic X-box domain (p.S345F), the PLCγ-specific array (p.S520F), and the C2 domain (p.E1163K). The absence of p-PLCγ1 was shown in cells transfected with vectors harboring the mutated p.Y783F residue (Figure 6a). In cells transfected with either the p.S345F, p.S520F, and p.E1163K plasmids, or the p.S345F-Y783F, p.S520F-Y783F, and p.E1163K-Y783F vectors, there was no significant difference between the single and double mutants in NFAT, NFκB, and AP-1 transcriptional activity (Figure 6b–d). To exclude the possibility that these observations were cell type-specific, we also tested p.S345F and the double mutant p.S345F-Y783F in the J.gamma1

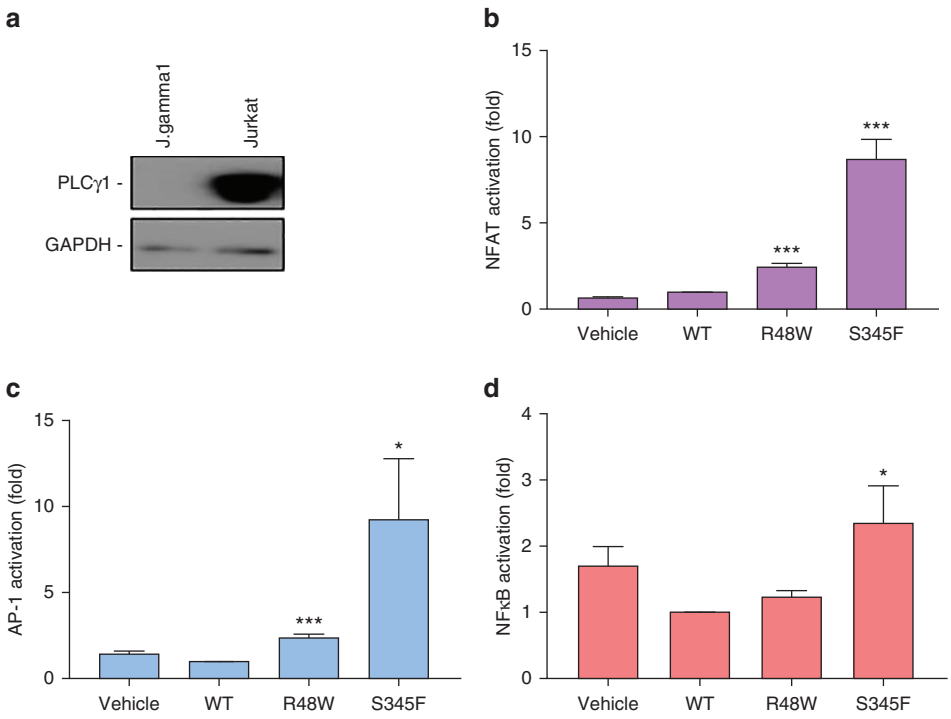

Figure 5. PLCγ1 p.R48W is activating in a T-cell lymphoma cell line. (**a**) Whole cell lysates from J.gamma1 and Jurkat cells were probed with an anti-PLCγ1 antibody to analyze the total protein expression using GAPDH expression as a loading control. (**b-d**) J.gamma1 cells were co-transfected with PLCγ1-pTriEx-4, pRL-TK Renilla-luciferase, and pGL3-NFAT-firefly-luciferase, pGL3-AP-1-luciferase, or NFκB-firefly-luciferase vectors. Cells were starved overnight and then lysed; $n = 3$ for each assay. Activation fold changes were normalized to cells overexpressing wild-type PLCγ1. Data are represented as the mean ± standard error of the mean; $n = 3$. Student's t-test, $^{*}P < 0.05$, $^{**}P < 0.01$, $^{***}P < 0.001$. GAPDH, glyceraldehyde-3-phosphate dehydrogenase; WT, wild-type.

T-cell lymphoma line. These data confirm the findings in HEK293 cells and suggest that phosphorylation of the PLCγ1 p.Y783 residue is not essential for the PLCγ1 activity associated with gain-of-function mutations (Figure 6e–g).

DISCUSSION

This study has demonstrated that the majority of PLCγ1 variants identified in SS act as gain-of-function mutations by significant induction of both NFκB and AP-1 transcriptional activity and increased proximal activity in basal conditions. In addition, we have confirmed previous studies showing that PLCγ1 mutations activate NFAT transcriptional activity. Importantly, our results indicate that these gain-of-function mutations can increase downstream signaling without phosphorylation of the PLCγ1 p.Y783 residue.

We have also shown that identical *PLCG1* mutations are present in multiple tumor compartments and persist several years after diagnosis, suggesting that these are probably driver gene mutations, which are positively selected. Our review of the published literature also confirms a high prevalence of *PLCG1* mutations in CTCL (MF 15% and SS 11%) and other mature T-cell malignancies, notably adult T-cell leukemia/lymphoma.

In CTCL, several genes involved in TCR signaling harbor mutations, including *CARD11, CD28,* and *TNFRSF1B*, as well as *PLCG1* (Chang et al., 2018; Choi et al., 2015; da Silva Almeida et al., 2015; Park et al., 2017; Ungewickell et al., 2015; Vaqué et al., 2014; Wang et al., 2015; Woollard et al., 2016). Although one study reported that *PLCG1* mutations were uncommon in CTCL, occurring in only 3-5% of cases (Caumont et al., 2015), our data and other reports suggest that *PLCG1* mutations are among the most common mutations in CTCL, occurring in approximately 10% of tumors (Chang et al., 2018; Park et al., 2017; Woollard et al., 2016). This apparent inconsistency is likely attributable to the selective sequencing of only two *PLCG1* exons harboring hotspot mutations by Caumont et al. (2015), whereas *PLCG1* mutations occur throughout the gene. Importantly, a recent study analyzing integrated NGS datasets from 139 CTCL (MF and SS) cases identified *PLCG1* as the most frequently mutated gene involved in the NFκB pathway (Chang et al., 2018). Furthermore, analysis of the mutations within the NFκB pathway revealed that mutations in *PLCG1*, *CARD11*, and *TNFRSF1B* were mutually exclusive in SS. Our study demonstrates that gain-of-function PLCγ1 mutations in SS can activate both proximal IP and distal NFκB pathway signaling in the absence of p.Y783 phosphorylation and stimulation, which to our knowledge is previously unreported. This is a potentially crucial mechanism driving the hyperactivation of TCR signaling. Interestingly, in B-cell malignancies, approved therapies, such as ibrutinib, target B-cell receptor activation, but resistance can emerge owing to the acquisition of downstream activating *PLCG2* mutations (Liu et al., 2015).

Our data also extends to previous reports showing that recurrent PLCγ1 mutations in CTCL and angioimmunoblastic T-cell lymphoma increase NFAT activation (Vallois et al., 2016; Vaqué et al., 2014). These studies used the canonical human embryonic kidney cell line HEK293T, and consistent with our findings, show that p.R48W is not activating in basal conditions. However, given the high frequency of p.R48W in SS, suggesting that this mutation is positively selected, it seemed unlikely that it would not be associated with PLCγ1 gain-of-function. Reassuringly, our data demonstrates that in a T-cell line, p.R48W is associated with increased NFAT and AP-1 transcriptional activity, and it could be argued that this is more biologically relevant to CTCL than the findings in the HEK293 cells.

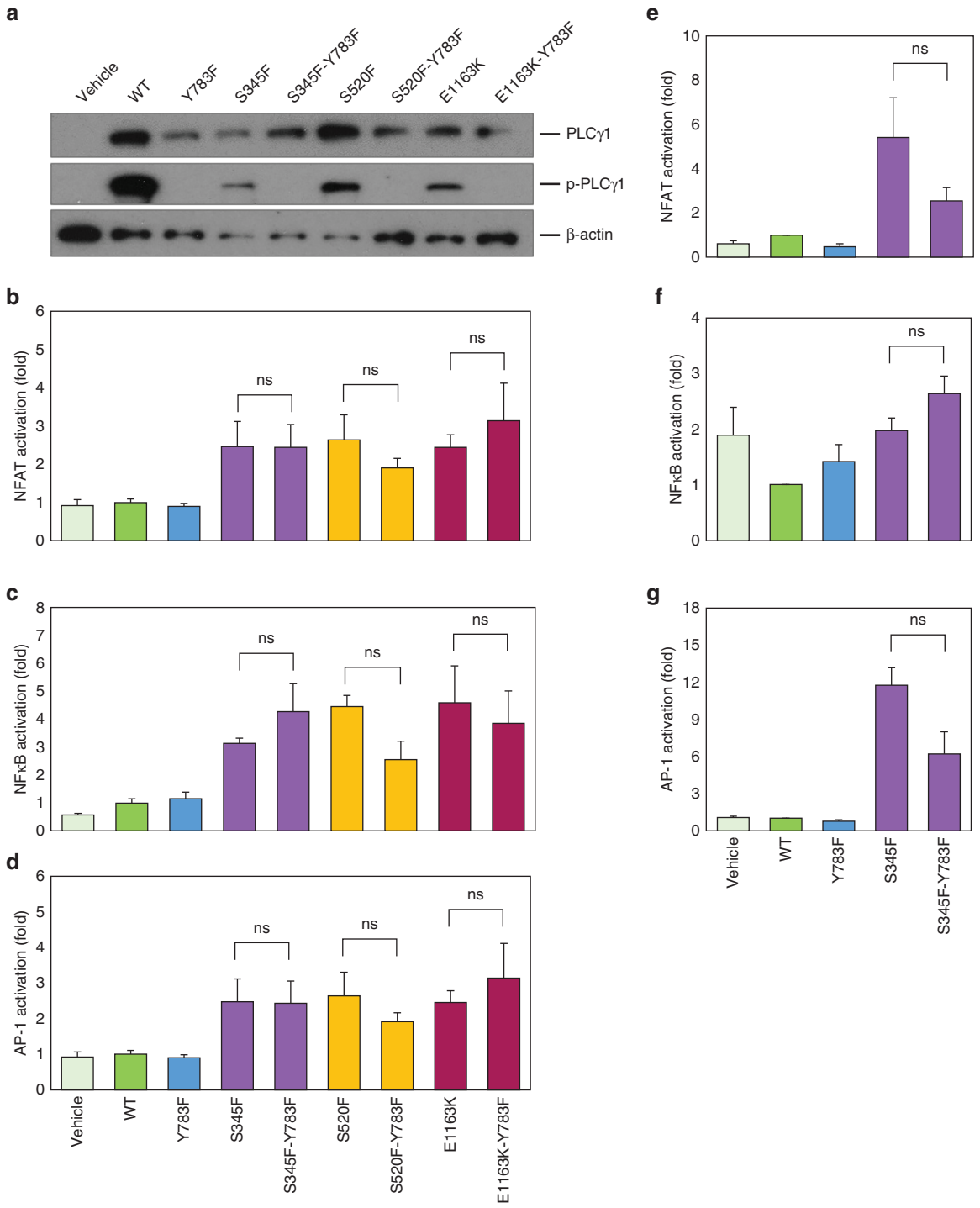

Figure 6. Mutant proteins mediate gain-of-function effects without PLCγ1 phosphorylation. (**a**) HEK293 cells transfected with PLCγ1-pTriEx-4 vectors were treated with 100 μM pervanadate before they were harvested. The lysates were probed with anti-PLCγ1 and anti-p-PLCγ1 antibodies to analyze the total and phosphorylated protein expression using β-actin expression as a loading control. (**b-d**) HEK293 and (**e-g**) J.gamma1 cells were co-transfected with PLCγ1-pTriEx-4, pRL-TK Renilla-luciferase and pGL3-NFAT-firefly-luciferase, NFκB-firefly-luciferase, or pGL3-AP-1-luciferase vectors. Cells were starved overnight and then lysed; $n = 3$ for each assay. Activation fold changes were normalized to cells overexpressing wild-type PLCγ1. Data are represented as the mean ± standard error of the mean. Student's *t*-test. ns, not significant; WT, wild-type.

Interestingly, functional studies of *CARD11* mutations reported in CTCL have also demonstrated the activation of NFκB signaling (da Silva Almeida et al., 2015). Enhanced NFκB, NFAT, and AP-1 activity may contribute to increased T helper type 2 cytokine expression in CTCL, inhibiting the anti-tumor effects of the T helper type 1 cytokines IL-2 and IFNγ, thereby providing an advantageous microenvironment for tumor cells (Miyagaki and Sugaya, 2014). Further study is required to determine the effect of specific *PLCG1* mutations on key parameters, such as T-cell survival and the proliferation of tumor cells.

PLCγ1 is maintained in an inactive state by an auto-inhibitory interaction between the catalytic X-Y domains and the cSH2 domain (Supplementary Figure S2) (Gresset et al., 2010; Koss et al., 2014). The phosphorylated p.Y783 residue interacts with the cSH2 domain to disrupt the auto-inhibitory interface and renders the active site available for substrate hydrolysis (Poulin et al., 2005) and subsequent activation of the wild-type PLCγ1 to produce IP (Bunney et al., 2012; Poulin et al., 2005). Germline deletions of the PLCγ2 cSH2 and cSH2-SH3 domains disrupt auto-inhibition and elevate protein activity in rare inherited conditions, such as phospholipase Cγ2—Associated Antibody Deficiency and Immune Dysregulation (Ombrello et al., 2012). The p.S345F and p.S520F mutations have also been proposed to act via the disruption of auto-inhibition (Koss et al., 2014). The p.S345F and p.E1163K mutations are predicted to be located at the protein surface that faces the plasma membrane, based on a 3-dimensional PLCβ2/3 model (Choi et al., 2015; Vaqué et al., 2014). Similarly, using our PLCγ2 model, we suggest that p.R48W, p.S345F, p.E1163K, p.D1165H, and p.VYEEDM1161V mutations are also likely to interact with the plasma membrane where the PLCγ substrate, phosphatidylinositol 4,5-bisphosphate, resides (Supplementary Figure S3). We hypothesize that these mutant proteins may have increased affinity for the plasma membrane and therefore could enhance phosphatidylinositol 4,5-bisphosphate hydrolysis, leading to amplified downstream signaling. Furthermore, this may also explain why these gain-of-function mutations appear to act independently of p.Y783 phosphorylation. However, the hotspot p.S345F mutation is also predicted to disrupt auto-inhibition (Koss et al., 2014) and may therefore act by a dual mechanism, as suggested for the PLCγ2 Ali5 (p.D993G) mutation (Everett et al., 2009).

Importantly, we have shown that the p.VYEEDM1161V indel in the PLCγ1 C2 domain is also a potent mediator of gain-of-function and therefore conclude that, in addition to the cSH2 domain, the C2 domain is fundamental for regulating PLCγ1 activity. The C2 domains in PLCγ1 and PLCγ2 harbor somatic hotspot mutations in mature T-cell lymphomas and ibrutinib-resistant chronic lymphocytic leukemia, respectively, (Choi et al., 2015; da Silva Almeida et al., 2015; Jones et al., 2017; Kataoka et al., 2015; Kiel et al., 2015; Vallois et al., 2016; Wang et al., 2015; Woollard et al., 2016) and based on protein sequence homology and functional analogy of PLCγ1 and PLCγ2, it is likely that the PLCγ2 C2 domain also has regulatory functions. Notably, the p.VYEEDM1161V indel reduced the total PLCγ1 protein expression, suggesting that it affects protein stability and may be subjected to degradation faster than the wild-type PLCγ1. Further functional work is now required to determine if the p.VYEEDM1161V indel harbors key regulatory residues that control PLCγ1 activity. U73122, is an inhibitor of phospholipase C, which has been shown to reduce elevated NFAT activity in HEK293T cells transfected with wild-type and mutant PLCγ1 (Vaqué et al., 2014), but U73122 paradoxically activates the PLCβ3 isozyme, highlighting the lack of specific PLCγ1 inhibitors (Klein et al., 2011).

In summary, this comprehensive study has shown that the PLCγ1 mutations reported in CTCL represent bona fide gain-of-function mutations that drive constitutive activation of proximal and distal PLCγ1 signaling cascades. These data provide further evidence that PLCγ enzymes are potentially important therapeutic targets.

MATERIALS AND METHODS

Patient samples

All patients fulfilled the WHO-EORTC diagnostic criteria for SS and were classified as blood stage B2 (Swerdlow, 2017). An identical clonal TCR rearrangement was demonstrated in peripheral blood and lesional skin. Tumor samples were obtained with written informed consent from a nationally approved research tissue bank (IRAS Project ID: 238203).

Polymerase chain reaction and Sanger sequencing

PCR, reverse transcriptase—PCR, and Sanger sequencing (Bioscience, Cambridge, United Kingdom) were used to validate the mutations in tumor-derived DNA and RNA and to confirm the introduction of mutant bases into the PLCγ1-pTriEx-4 vectors. Sequencing chromatograms were analyzed using FinchTV (Geospiza Incorporation, Seattle, WA).

Mutation mapping to protein domains

PLCγ1 mutations were mapped to the functional protein domains based on the amino acid numbering and protein domain schematic presented by Bunney et al. (2012).

Protein sequence alignment

Human PLCγ1 and PLCγ2 protein sequences were obtained from the Genome browser Ensembl (Zerbino et al., 2018) and aligned using the multiple sequence alignment software Clustal Omega (Sievers et al., 2011).

Site-directed mutagenesis

The PLCγ1-pTriEx-4 vector was used to generate mutant constructs with the QuikChange Lightning Site-Directed Mutagenesis Kit (Agilent Technologies, Santa Clara, CA).

Cell lines

HEK293 and COS-7 cells were obtained from the ECACC (Salisbury, United Kingdom). Jurkat cells were obtained from Public Health England (Salisbury, United Kingdom). J.gamma1 cells were obtained from the ATCC (Manassas, VA) and SeAx cells were a gift from Professor M. Vermeer (Leiden University Medical Centre, Leiden, Netherlands). Adherent cells were cultured in DMEM, and non-adherent cells were maintained in RPMI 1640 Medium (both Life Technologies, Carlsbad, CA). Cultures were supplemented with 10% (v/v) Fetal bovine serum (Biosera, Nuaille, France), 100 units/ml penicillin and 100 μg/ml streptomycin (Life Technologies). SeAx cells were supplemented with 3 ng/ml rhIL-2 (R&D systems, Minneapolis, MN). Cultures were routinely tested for Mycoplasma contamination using PCR (van Kuppeveld et al., 1994).

Dual-luciferase reporter assays

HEK293 cells were co-transfected with 1 μg PLCγ1-pTriEx-4 vectors, 0.05 μg pRL-TK Renilla-luciferase construct, and 0.1 μg of NFκB-firefly-luciferase, pGL3-NFAT-firefly-luciferase, or pGL3-AP-1-luciferase reporter plasmids as described by Vaqué et al. (2014). J.gamma1 cells were co-transfected with 0.5-5 μg PLCγ1-pTriEx-4 vectors, 0.5-1 μg pRL-TK Renilla-luciferase construct, and 1 μg of NFκB-firefly-luciferase, or 5 μg pGL3-NFAT-firefly luciferase/pGL3-AP-1-luciferase reporter plasmids. Transfections were performed by

electroporation as per the manufacturer's instructions (Lonza, Basel, Switzerland). Lysates were analyzed using the dual-luciferase reporter assay system (Promega, Madison, WI). The assays were repeated at least three times.

Western blotting

HEK293 cells were transfected with 2 μg PLCγ1-pTriEx-4 plasmids and 6 μl FuGene HD Transfection Reagent (Promega). After 23 hours, the cells were treated with 100 μM pervanadate (protein-tyrosine phosphatase inhibitor) for 1 hour to stabilize the PLCγ1 phosphorylation (Kunze et al., 2014) and then harvested. HEK293, Jurkat, and J.gamma1 whole cell lysates were probed with antibodies listed in Supplementary Table S3. The experiments were repeated twice.

Inositol phosphate quantification assay

IP production was quantified in counts per minute in COS-7 cells transfected with 2.5 μg PLCγ1-pTriEx-4 vectors (Everett et al., 2009). The assays were repeated at least twice. IP levels were normalized to the wild-type PLCγ1 activity.

Data availability statement

No data sets were generated or analyzed during the current study.

ORCIDs

Varsha M. Patel: https://orcid.org/0000-0001-6760-9310
Charlotte E. Flanagan: https://orcid.org/0000-0002-5913-9192
Marta Martins: https://orcid.org/0000-0003-0429-9380
Christine L. Jones: https://orcid.org/0000-0001-9539-7458
Rosie M. Butler: https://orcid.org/0000-0003-1063-9097
Wesley J. Woollard: https://orcid.org/0000-0001-5567-8765
Farrah S. Bakr: https://orcid.org/0000-0002-2753-8586
Antoinette Yoxall: https://orcid.org/0000-0003-3918-1307
Nelema Begum: https://orcid.org/0000-0001-7351-0085
Matilda Katan: https://orcid.org/0000-0001-9992-8375
Sean J. Whittaker: https://orcid.org/0000-0003-0972-2600
Tracey J. Mitchell: https://orcid.org/0000-0001-8892-0642

CONFLICT OF INTEREST

The authors state no conflicts of interest.

ACKNOWLEDGMENTS

The authors would like to thank the National Institute for Health Research (NIHR) Biomedical Research Centre at the Guy's and St Thomas' NHS Foundation Trust and King's College London for funding this independent research. The views expressed are those of the author(s) and not necessarily those of the NHS, the NIHR, or the Department of Health. RMB and CEF were supported by the King's Bioscience Institute and the Guy's and St Thomas' Charity Prize PhD Programme in Biomedical and Translational Science. We thank Katy Everett for the structure-based 3D modeling. We also acknowledge the support from Cancer Research UK and MRC to MK's laboratory.

AUTHOR CONTRIBUTIONS

Conceptualization: VMP, CEF, SJW, TJM; Data Curation: VMP, CEF, CLJ, WJW; Formal Analysis: VMP, CEF, CLJ, WJW, SJW, TJM; Funding Acquisition: SJW, TJM; Investigation: VMP, CEF, MM, CLJ, RMB, WJW, FSB, AY; Methodology: VMP, CEF, MM, CLJ, SJW, TJM; Project Administration: SJW, TJM; Resources: SJW, TJM; Software: VMP, CEF, CLJ, WJW, SJW, TJM; Supervision: MK, SJW, TJM; Validation: VMP, CLJ, WJW, NB; Visualization: VMP, CEF, CLJ, TJM; Writing - Original Draft Preparation: VMP, CEF, CLJ, SJW, TJM; Writing - Review and Editing: VMP, CEF, TJM.

SUPPLEMENTARY MATERIAL

Supplementary material is linked to the online version of the paper at www.jidonline.org, and at https://doi.org/10.1016/j.jid.2019.07.693.

REFERENCES

Bunney TD, Esposito D, Mas-Droux C, Lamber E, Baxendale RW, Martins M, et al. Structural and functional integration of the PLCgamma interaction domains critical for regulatory mechanisms and signaling deregulation. Structure 2012;20:2062–75.

Burger JA, Landau DA, Taylor-Weiner A, Bozic I, Zhang H, Sarosiek K, et al. Clonal evolution in patients with chronic lymphocytic leukaemia developing resistance to BTK inhibition. Nat Commun 2016;7:11589.

Caumont C, Gros A, Boucher C, Mélard P, Prochazkova-Carlotti M, Laharanne E, et al. PLCG1 gene mutations are uncommon in cutaneous T-cell lymphomas. J Invest Dermatol 2015;135:2334–7.

Chang LW, Patrone CC, Yang W, Rabionet R, Gallardo F, Espinet B, et al. An integrated data resource for genomic analysis of cutaneous T-cell lymphoma. J Invest Dermatol 2018;138:2681–3.

Choi J, Goh G, Walradt T, Hong BS, Bunick CG, Chen K, et al. Genomic landscape of cutaneous T cell lymphoma. Nat Genet 2015;47:1011–9.

da Silva Almeida AC, Abate F, Khiabanian H, Martinez-Escala E, Guitart J, Tensen CP, et al. The mutational landscape of cutaneous T cell lymphoma and Sezary syndrome. Nat Genet 2015;47:1465–70.

Everett KL, Bunney TD, Yoon Y, Rodrigues-Lima F, Harris R, Driscoll PC, et al. Characterization of phospholipase Cγ enzymes with gain-of-function mutations. J Biol Chem 2009;284:23083–93.

Giri DK, Aggarwal BB. Constitutive activation of NF-kappaB causes resistance to apoptosis in human cutaneous T cell lymphoma HuT-78 cells. Autocrine role of tumor necrosis factor and reactive oxygen intermediates. J Biol Chem 1998;273:14008–14.

Gresset A, Hicks SN, Harden TK, Sondek J. Mechanism of phosphorylation-induced activation of phospholipase C-gamma isozymes. J Biol Chem 2010;285:35836–47.

Hogan PG, Chen L, Nardone J, Rao A. Transcriptional regulation by calcium, calcineurin, and NFAT. Genes Dev 2003;17:2205–32.

Irvin BJ, Williams BL, Nilson AE, Maynor HO, Abraham RT. Pleiotropic contributions of phospholipase C-gamma1 (PLC-gamma1) to T-cell antigen receptor-mediated signaling: reconstitution studies of a PLC-gamma1-deficient Jurkat T-cell line. Mol Cell Biol 2000;20:9149–61.

Jones D, Woyach JA, Zhao W, Caruthers S, Tu H, Coleman J, et al. PLCG2 C2 domain mutations co-occur with BTK and PLCG2 resistance mutations in chronic lymphocytic leukemia undergoing ibrutinib treatment. Leukemia 2017;31:1645–7.

Juvekar A, Manna S, Ramaswami S, Chang TP, Vu HY, Ghosh CC, et al. Bortezomib induces nuclear translocation of Iκßα resulting in gene-specific suppression of NF- κß–dependent transcription and induction of apoptosis in CTCL. Mol Cancer Res MCR 2011;9:183–94.

Kataoka K, Nagata Y, Kitanaka A, Shiraishi Y, Shimamura T, Yasunaga J, et al. Integrated molecular analysis of adult T cell leukemia/lymphoma. Nat Genet 2015;47:1304–15.

Kiel MJ, Sahasrabuddhe AA, Rolland DCM, Velusamy T, Chung F, Schaller M, et al. Genomic analyses reveal recurrent mutations in epigenetic modifiers and the JAK-STAT pathway in Sezary syndrome. Nat Commun 2015;6:8470.

Kiel MJ, Velusamy T, Rolland D, Sahasrabuddhe AA, Chung F, Bailey NG, et al. Integrated genomic sequencing reveals mutational landscape of T-cell prolymphocytic leukemia. Blood 2014;124:1460–72.

Kim EJ, Hess S, Richardson SK, Newton S, Showe LC, Benoit BM, et al. Immunopathogenesis and therapy of cutaneous T cell lymphoma. J Clin Invest 2005;115:798–812.

Klein RR, Bourdon DM, Costales CL, Wagner CD, White WL, Williams JD, et al. Direct activation of human phospholipase C by its well known inhibitor U73122. J Biol Chem 2011;286:12407–16.

Koss H, Bunney TD, Behjati S, Katan M. Dysfunction of phospholipase Cgamma in immune disorders and cancer. Trends Biochem Sci 2014;39:603–11.

Kunze K, Spieker T, Gamerdinger U, Nau K, Berger J, Dreyer T, et al. A recurrent activating PLCG1 mutation in cardiac angiosarcomas increases apoptosis resistance and invasiveness of endothelial cells. Cancer Res 2014;74:6173–83.

Liu TM, Woyach JA, Zhong Y, Lozanski A, Lozanski G, Dong S, et al. Hypermorphic mutation of phospholipase C, gamma 2 acquired in ibrutinib-resistant CLL confers BTK independency upon B-cell receptor activation. Blood 2015;126:61–8.

Maddocks KJ, Ruppert AS, Lozanski G, Heerema NA, Zhao W, Abruzzo L, et al. Etiology of ibrutinib therapy discontinuation and

outcomes in patients with chronic lymphocytic leukemia. JAMA Oncol 2015;1:80–7.

Martínez-Delgado B, Cuadros M, Honrado E, Ruiz de la Parte A, Roncador G, Alves J, et al. Differential expression of NF-kappaB pathway genes among peripheral T-cell lymphomas. Leukemia 2005;19:2254–63.

McGirt LY, Jia P, Baerenwald DA, Duszynski RJ, Dahlman KB, Zic JA, et al. Whole-genome sequencing reveals oncogenic mutations in mycosis fungoides. Blood 2015;126:508–19.

McKinney M, Moffitt AB, Gaulard P, Travert M, De Leval L, Nicolae A, et al. The genetic basis of hepatosplenic T-cell lymphoma. Cancer Discov 2017;7:369–79.

Miyagaki T, Sugaya M. Immunological milieu in mycosis fungoides and Sezary syndrome. J Dermatol 2014;41:11–8.

O'Connell MA, Cleere R, Long A, O'Neill LA, Kelleher D. Cellular proliferation and activation of NF kappa B are induced by autocrine production of tumor necrosis factor alpha in the human T lymphoma line HuT 78. J Biol Chem 1995;270:7399–404.

Ombrello MJ, Remmers EF, Sun G, Freeman AF, Datta S, Torabi-Parizi P, et al. Cold urticaria, immunodeficiency, and autoimmunity related to PLCG2 deletions. N Engl J Med 2012;366:330–8.

Palomero T, Couronné L, Khiabanian H, Kim MY, Ambesi-Impiombato A, Perez-Garcia A, et al. Recurrent mutations in epigenetic regulators, RHOA and FYN kinase in peripheral T cell lymphomas. Nat Genet 2014;46:166–70.

Park J, Yang J, Wenzel AT, Ramachandran A, Lee WJ, Daniels JC, et al. Genomic analysis of 220 CTCLs identifies a novel recurrent gain-of-function alteration in RLTPR. Blood 2017;130:1430–40.

Poulin B, Sekiya F, Rhee SG. Intramolecular interaction between phosphorylated tyrosine-783 and the C-terminal Src homology 2 domain activates phospholipase C-gamma1. Proc Natl Acad Sci USA 2005;102:4276–81.

Prasad A, Rabionet R, Espinet B, Zapata L, Puiggros A, Melero C, et al. Identification of gene mutations and fusion genes in patients with Sezary syndrome. J Invest Dermatol 2016;136:1490–9.

Sakata-Yanagimoto M, Enami T, Yoshida K, Shiraishi Y, Ishii R, Miyake Y, et al. Somatic RHOA mutation in angioimmunoblastic T cell lymphoma. Nat Genet 2014;46:171–5.

Sievers F, Wilm A, Dineen D, Gibson TJ, Karplus K, Li W, et al. Fast, scalable generation of high-quality protein multiple sequence alignments using Clustal Omega. Mol Syst Biol 2011;7:539.

Simpson HM, Khan RZ, Song C, Sharma D, Sadashivaiah K, Furusawa A, et al. Concurrent Mutations in ATM and Genes Associated with common gamma chain Signaling in peripheral T cell Lymphoma. PLOS ONE 2015;10:e0141906.

Smith-Garvin JE, Koretzky GA, Jordan MS. T cell activation. Annu Rev Immunol 2009;27:591–619.

Sors A, Jean-Louis F, Pellet C, Laroche L, Dubertret L, Courtois G, et al. Down-regulating constitutive activation of the NF-kappaB canonical pathway overcomes the resistance of cutaneous T-cell lymphoma to apoptosis. Blood 2006;107:2354–63.

Swerdlow SH, editor. WHO classification of tumours of haematopoietic and lymphoid tissues (revised 4th edition. Lyon: International Agency for Research on Cancer; 2017.

Ungewickell A, Bhaduri A, Rios E, Reuter J, Lee CS, Mah A, et al. Genomic analysis of mycosis fungoides and Sezary syndrome identifies recurrent alterations in TNFR2. Nat Genet 2015;47:1056–60.

Vallois D, Dobay MP, Morin RD, Lemonnier F, Missiaglia E, Juilland M, et al. Activating mutations in genes related to TCR signaling in angioimmunoblastic and other follicular helper T-cell-derived lymphomas. Blood 2016;128:1490–502.

van Kuppeveld FJ, Johansson KE, Galama JM, Kissing J, Bölske G, van der Logt JT, et al. Detection of mycoplasma contamination in cell cultures by a mycoplasma group-specific PCR. Appl Environ Microbiol 1994;60:149–52.

Vaqué JP, Gómez-López G, Monsálvez V, Varela I, Martínez N, Pérez C, et al. PLCG1 mutations in cutaneous T-cell lymphomas. Blood 2014;123:2034–43.

Wang L, Ni X, Covington KR, Yang BY, Shiu J, Zhang X, et al. Genomic profiling of Sezary syndrome identifies alterations of key T cell signaling and differentiation genes. Nat Genet 2015;47:1426–34.

Wang M, Zhang S, Chuang SS, Ashton-Key M, Ochoa E, Bolli N, et al. Angioimmunoblastic T cell lymphoma: novel molecular insights by mutation profiling. Oncotarget 2017;8:17763–70.

Woollard WJ, Pullabhatla V, Lorenc A, Patel VM, Butler RM, Bayega A, et al. Candidate driver genes involved in genome maintenance and DNA repair in Sezary syndrome. Blood 2016;127:3387–97.

Yamagishi M, Watanabe T. Molecular hallmarks of adult T cell leukemia. Front Microbiol 2012;3:334.

Yoo HY, Sung MK, Lee SH, Kim S, Lee H, Park S, et al. A recurrent inactivating mutation in RHOA GTPase in angioimmunoblastic T cell lymphoma. Nat Genet 2014;46:371–5.

Zerbino DR, Achuthan P, Akanni W, Amode MR, Barrell D, Bhai J, et al. Ensembl 2018. Nucleic Acids Res 2018;46:D754–61.

SUPPLEMENTARY METHODS AND MATERIALS

Comprehensive literature analysis

The PubMed database was used to identify publications incorporating the World Health Organization classification of T-cell lymphomas (T-cell prolymphocytic leukemia, T-cell large granular lymphocyte leukemia, adult T-cell leukemia/lymphoma, extra-nodal natural killer/T-cell lymphoma (nasal type), enteropathy-associated T-cell lymphoma, hepatosplenic T-cell lymphoma, Mycosis Fungoides / Sézary Syndrome, primary cutaneous CD30-positive T cell lymphoproliferative disorders, primary cutaneous anaplastic large cell lymphoma, lymphomatoid papulosis, peripheral T-cell lymphoma-not otherwise specified, angioimmunoblastic T-cell lymphoma, and anaplastic large cell lymphoma) in combination with either the term "whole-exome sequencing" or "next-generation sequencing". The resulting publications and the corresponding supplementary data were interrogated for *PLCG1* mutations. Mutations identified by subsequent targeted gene sequencing were also included to obtain the overall frequency of *PLCG1* mutations per disease subtype.

Pathogenicity prediction

SIFT, Provean, PolyPhen2, Mutation Taster2, MutPred2 and CADD were used to predict the potential effect of the *PLCG1* variants on the protein level (Adzhubei et al., 2013; Choi and Chan, 2015; Kircher et al., 2014; Kumar et al., 2009; Li et al., 2009; Schwarz et al., 2014). A consensus prediction was determined using the criteria of 5 of 6 algorithms having the same result for missense mutations. The PolyPhen2 and MutPred2 algorithms only predict the effect of point mutations, therefore the criteria of 3 of 4 algorithms having the same result was used to predict the effect of the indel.

3-dimensional protein modeling

The 3-dimensional model of the full length PLCγ protein was generated by using the structure of PLCγ2 to represent the PLCγ core. PLCγ2 structures from the Protein Data Bank were used for modeling; spPH (PDB: 2K2J), nSH2 (PDB: 2DX0), cSH2 (PDB: 2EOB), and SH3 (PDB: 2EQI). First, the structure of the tandem SH2 domains from PLCγ1 (PDB: 3GQI) was used to arrange these domains relative to each other. Docking of the domains to the triosephosphate isomerase barrel was carried out using the ClusPro web-server (Comeau et al., 2004a, 2004b). The two SH2 domains were docked with the catalytic domain, and the spPH domain was docked to this complex, followed by the SH3 domain. At each stage, the most likely conformation was chosen based on biochemical data. The models were analyzed using DeepView-Swiss-PDBViewer (Guex and Peitsch, 1997) and Pymol version 1.8 (Schrodinger LLC, New York, NY). *PLCG1* mutations were subsequently mapped to this model.

SUPPLEMENTARY REFERENCES

Adzhubei I, Jordan DM, Sunyaev SR. Predicting functional effect of human missense mutations using PolyPhen-2. Curr Protoc Hum Genet 2013;76:7–20.

Choi Y, Chan AP. PROVEAN web server: a tool to predict the functional effect of amino acid substitutions and indels. Bioinformatics 2015;31:2745–7.

Comeau SR, Gatchell DW, Vajda S, Camacho CJ. ClusPro: a fully automated algorithm for protein-protein docking. Nucleic Acids Res 2004a;32(Web Server Issue):W96–9.

Comeau SR, Gatchell DW, Vajda S, Camacho CJ. ClusPro: an automated docking and discrimination method for the prediction of protein complexes. Bioinformatics 2004b;20:45–50.

Guex N, Peitsch MC. SWISS-MODEL and the Swiss-PdbViewer: an environment for comparative protein modeling. Electrophoresis 1997;18:2714–23.

Kircher M, Witten DM, Jain P, O'Roak BJ, Cooper GM, Shendure J. A general framework for estimating the relative pathogenicity of human genetic variants. Nat Genet 2014;46:310–5.

Kumar P, Henikoff S, Ng PC. Predicting the effects of coding non-synonymous variants on protein function using the SIFT algorithm. Nat Protoc 2009;4:1073–81.

Li B, Krishnan VG, Mort ME, Xin F, Kamati KK, Cooper DN, et al. Automated inference of molecular mechanisms of disease from amino acid substitutions. Bioinformatics 2009;25:2744–50.

Schwarz JM, Cooper DN, Schuelke M, Seelow D. MutationTaster2: mutation prediction for the deep-sequencing age. Nat Methods 2014;11:361–2.

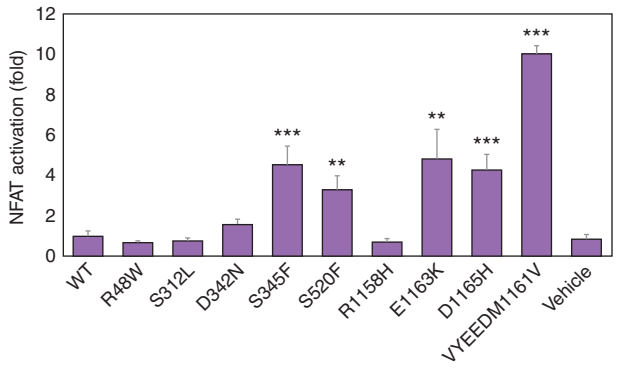

Supplementary Figure S1. PLCγ1 mutations significantly increase NFAT transcriptional activity. Five mutations significantly enhance NFAT activity in basal conditions in HEK293 cells. Transcriptional activity was analyzed using dual-luciferase reporter assays. Data is represented as the mean ± standard error of the mean; $n = 3$ Student's *t*-test, $^{*}P < 0.05$, $^{**}P < 0.01$, $^{***}P < 0.001$. WT, wild-type.

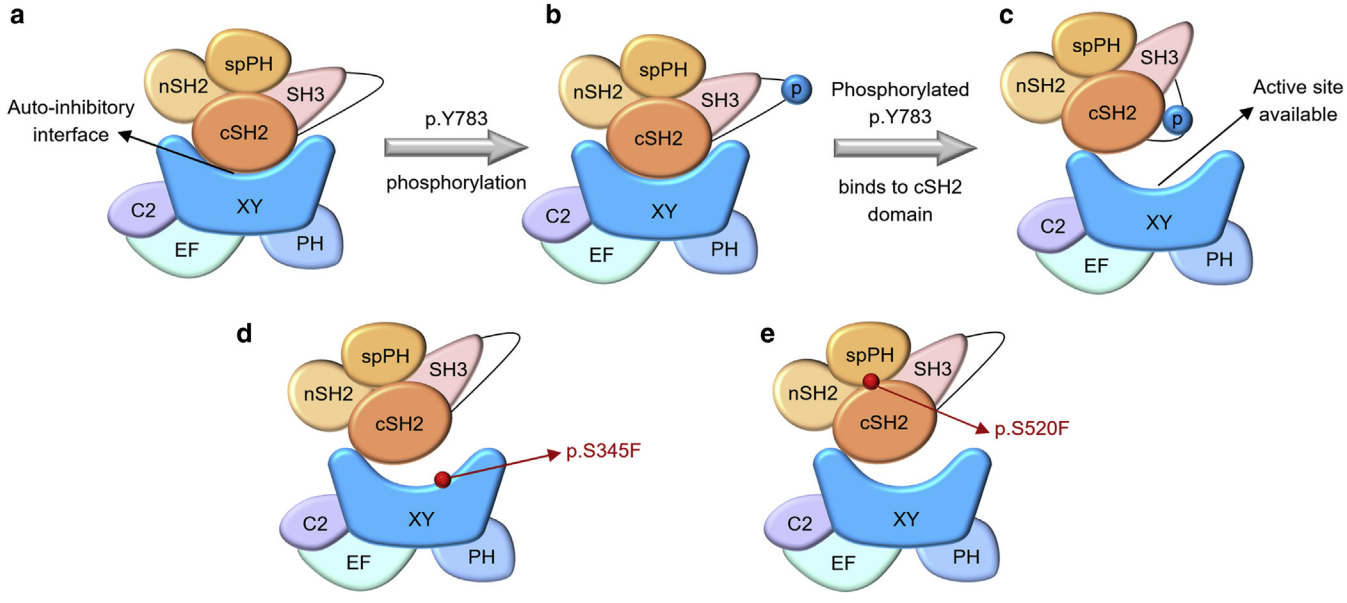

Supplementary Figure S2. Gain-of-function PLCγ1 mutations disrupt auto-inhibition, leading to constitutively active mutant proteins. (**a**) PLCγ1 is maintained in an inactive state by an auto-inhibitory interaction between the X-Y catalytic domains and the cSH2 domain, which blocks the substrate from accessing the active site. (**b, c**) Receptor and non-receptor tyrosine kinases phosphorylate the p.Y783 residue, which interacts with the cSH2 domain and disrupts the auto-inhibitory interface, making the active site available for substrate hydrolysis. (**d, e**) The activating mutations p.S345F and p.S520F are predicted to be located on the surface of the catalytic X domain and at the cSH2-split PH domain interaction surface, respectively, and are likely to disrupt auto-inhibition.

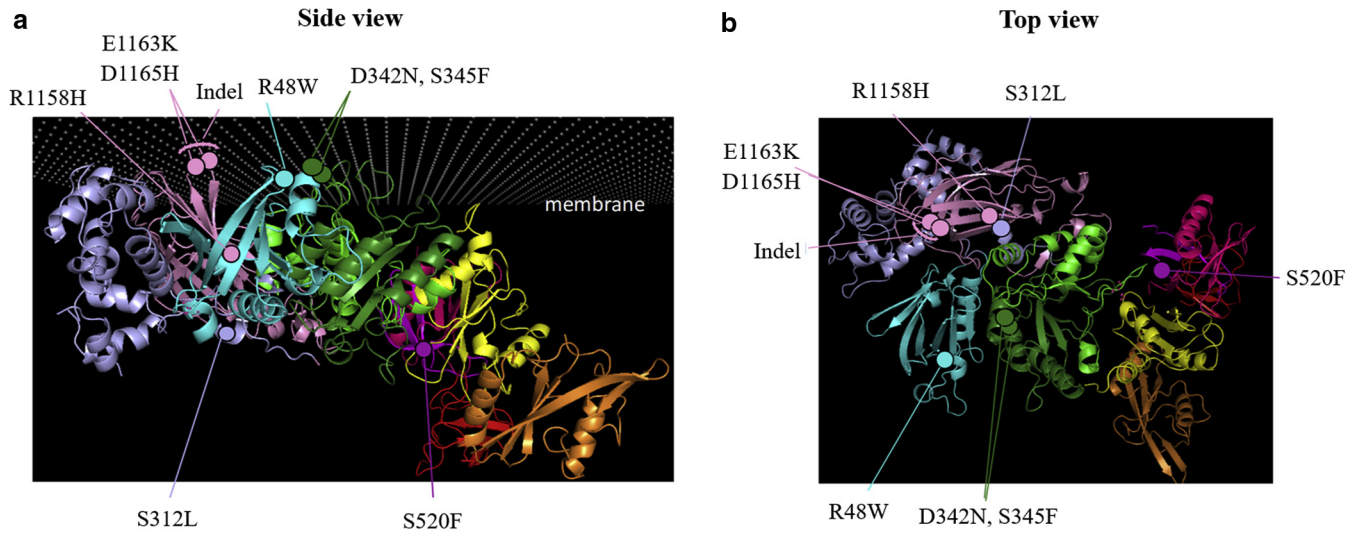

Supplementary Figure S3. Bona fide activating PLCγ1 mutations p.R48W, p.S345F, p.E1163K, p.D1165H, and the indel p.VYEEDM1161V map to the surface of the protein that is predicted to interact with the plasma membrane. (**a**) Side and (**b**) top view of the PLCγ1 mutations mapped to the PLCγ2 protein structure.

Supplementary Table S1. Whole-exome and targeted gene sequencing studies reporting *PLCG1* mutations in mature T-cell lymphomas

Malignancy	Mutation frequency	References
ATLL	36.2% (134/370)	(Kataoka et al., 2015)
PTCL-nos	18.2% (4/22)	(Palomero et al., 2014; Sakata-Yanagimoto et al., 2014; Vallois et al., 2016)
MF	15.1% (8/53)	(McGirt et al., 2015; Ungewickell et al., 2015; Vaqué et al., 2014)
HSTL	15.0% (3/20)	(McKinney et al., 2017)
AITL	12.0% (11/92)	(Palomero et al., 2014; Sakata-Yanagimoto et al., 2014; Vallois et al., 2016; Wang et al., 2017; Yoo et al., 2014)
SS	11.3% (44/388)	(Choi and Goh, 2015; da Silva Almeida et al., 2015; Kiel et al., 2015; Prasad et al., 2016; Ungewickell et al., 2015; Vaqué et al., 2014; Wang et al., 2015; Woollard et al., 2016)
TPLL	5.6 (2/36)	(Kiel et al., 2014)
ALCL	0% (0/23)	(Crescenzo et al., 2015)
EATL	0% (0/89)	(Moffitt and Ondrejka, 2017; Nairismagi et al., 2016; Palomero et al., 2014; Roberti et al., 2016)
NKTCL	0% (0/27)	(Jiang et al., 2015; Palomero et al., 2014)

Abbreviations: AITL, angioimmunoblastic T-cell lymphoma; ALCL, anaplastic large cell lymphoma; ATLL, adult T-cell leukemia/lymphoma; EATL, enteropathy-associated T-cell lymphoma; HSTL, hepatosplenic T-cell lymphoma; MF, Mycosis Fungoides; NKTCL, natural killer/T-cell lymphoma; PTCL-nos, peripheral T-cell lymphoma-not otherwise specified; SS,: Sézary Syndrome; TPLL, T-cell-prolymphocytic leukemia. Refer to the main manuscript for references.

Supplementary Table S2. Pathogenicity predictions performed using multiple algorithms for nine SS-associated PLCγ1 variants. Consensus criteria for missense mutations: 5 of 6 algorithms. Consensus criteria for indel: 3 of 4 algorithms

Nucleotide substitution	Amino acid change	SIFT	Provean	PolyPhen2	MutationTaster	MutPred2	CADD	Consensus
c.C142T	p.R48W	Damaging	Deleterious	Probably damaging	Disease causing	Damaging	Deleterious	**Damaging**
c.C935T	p.S312L	Tolerated	Deleterious	Benign	Disease causing	Neutral	Deleterious	Inconclusive
c.G1024A	p.D342N	Tolerated	Deleterious	Probably damaging	Disease causing	Damaging	Deleterious	**Damaging**
c.C1034T	p.S345F	Damaging	Deleterious	Probably damaging	Disease causing	Damaging	Deleterious	**Damaging**
c.C1559T	p.S520F	Damaging	Deleterious	Probably damaging	Disease causing	Damaging	Deleterious	**Damaging**
c.G3473A	p.R1158H	Damaging	Deleterious	Probably damaging	Disease causing	Damaging	Deleterious	**Damaging**
c.G3487A	p.E1163K	Damaging	Deleterious	Probably damaging	Disease causing	Damaging	Deleterious	**Damaging**
c.G3493C	p.D1165H	Damaging	Deleterious	Probably damaging	Disease causing	Damaging	Deleterious	**Damaging**
c.GTGTATGAG GAAGACAdelG	p.VYEEDM1161V	Damaging	Deleterious	N/A	Disease causing	N/A	Deleterious	**Damaging**

Abbreviation: N/A, Not applicable.

Supplementary Table S3. Antibodies used for western blotting

Antibody	Product code	Dilution
Rabbit monoclonal anti-PLCγ1	5690	1:20,000
Rabbit polyclonal anti-p-PLCγ1	2821	1:50,000
Rabbit polyclonal anti-β-Actin	4967	1:10,000
Rabbit monoclonal anti-GAPDH	2118	1:2,000

All antibodies listed were manufactured by Cell Signaling Technology (Danver, MA).